SANDIA REPORT
SAND2014-0560
Unlimited Release
Printed February 2014

Susceptibility Study of Audio Recording Devices to Electromagnetic Stimulations

Matthew S. Halligan, Daryl G. Beetner, and Steven L. Grant

Prepared by
Sandia National Laboratories
Albuquerque, New Mexico 87185 and Livermore, California 94550

Sandia National Laboratories

Issued by Sandia National Laboratories, operated for the United States Department of Energy by Sandia Corporation.

Available to DOE and DOE contractors from

U.S. Department of Energy
Office of Scientific and Technical Information
P.O. Box 62
Oak Ridge, TN 37831

Telephone:	(865) 576-8401
Facsimile:	(865) 576-5728
E-Mail:	reports@adonis.osti.gov
Online ordering:	http://www.osti.gov/bridge

Available to the public from

U.S. Department of Commerce
National Technical Information Service
5285 Port Royal Rd.
Springfield, VA 22161

Telephone:	(800) 553-6847
Facsimile:	(703) 605-6900
E-Mail:	orders@ntis.fedworld.gov
Online order:	http://www.ntis.gov/help/ordermethods.asp?loc=7-4-0#online

SAND2014-0560
Unlimited Release
Printed February 2014

Susceptibility Study of Audio Recording Devices to Electromagnetic Stimulations

Matthew S. Halligan
Power Systems, Cables, and EMI Department
Sandia National Laboratories
P.O. Box 5800
Albuquerque, New Mexico 87185-0402

Daryl G. Beetner and Steven L. Grant
Electrical and Computer Engineering Department
Missouri University of Science and Technology
Rolla, Missouri 65401

Abstract

Little research has been performed to study how intentional electromagnetic signals may couple into recording devices. An electromagnetic susceptibility study was performed on an analog tape recorder, a digital video camera, a wired computer microphone, and a wireless microphone system to electromagnetic interference. Devices were subjected to electromagnetic stimulations in the frequency range of 1-990 MHz and field strengths up to 4.9 V/m. Carrier and message frequencies of the stimulation signals were swept, and the impacts of device orientation and antenna polarization were explored. Message signals coupled into all devices only when amplitude modulated signals were used as stimulation signals. Test conditions that produced maximum sensitivity were highly specific to each device. Only narrow carrier frequency ranges could be used for most devices to couple messages into recordings. A basic detection technique using cross-correlation demonstrated the need for messages to be as long as possible to maximize message detection and minimize detection error. Analysis suggests that detectable signals could be coupled to these recording devices under realistic ambient conditions.

ACKNOWLEDGMENTS

This work was funded in full by the Missouri University of Science and Technology Electromagnetic Compatibility Laboratory.

CONTENTS

FIGURES

TABLES

NOMENCLATURE

AM	amplitude modulation
dB	decibel
DC	direct current
DOE	Department of Energy
DUT	device under test
EM	electromagnetic
EMI	electromagnetic interference
FM	frequency modulation
PSD	power spectral density
SNL	Sandia National Laboratories
SNR	signal-to-noise ratio

1. INTRODUCTION

The widespread use of wireless electronics and commercial electronics in recent years has created a harsher ambient electromagnetic (EM) environment than in years past. This harsher ambient EM environment represents an increased risk for electronic failures and operational incompatibilities for both modern and legacy electronic systems. To mitigate this risk, most electronics are put through a series of immunity tests to quantify device susceptibility. Electronics are placed in environments with variable EM field strengths to qualify a device for use in an anticipated worst-case ambient EM environment [1]. Immunity tests can range from electro-static discharge tests to those exposing a device to high level EM fields from a nearby transmitting antenna [1].

One class of devices whose susceptibility properties to EM fields is of interest to many communities is audio recording devices. Most audio recordings are taken in an ambient environment that is not electromagnetically “quiet”, where signals from strong radio frequency transmitters such as radio stations, television stations, and even commercial electronics are often present. Susceptibilities in audio recording devices can result in unintentional signals in audio recordings that degrade the quality of a recording. One common example is a “buzzing” sound created in a recording due to a nearby active cell phone to an audio recording device. Susceptibilities can also result in coupled signals in a recording, while not detectable audibly by the user. Signal processing techniques can be used to determine the sensitivity of audio recording devices to an ambient EM environment even when coupled signals fall below the noise floor of a recording.

The focus of this research was to characterize the electromagnetic susceptibility of audio recording devices and the audio recording portion of video recording equipment. Four different devices were tested, including a General Electric micro-cassette player model 3-5385B (analog tape recorder), a Dell wired computer microphone (computer microphone), a Sony DCR-DVD105 DVD Handycam® Camcorder (digital video camera), and a Nady Systems DKW-8U single-channel UHF wireless microphone system with a BT-8U transmitter (wireless microphone system). In the following section a general discussion of the testing methodology used for each of these devices is presented. Next, the coupling results for each device is given, and then the results are summarized. A discussion then follows about how the message coupling is related to the electric field strength at a recording device. Theoretical equations for the electric field at the recording devices are developed, and then compared to electric field measurements. Following this, field strength conditions are correlated to signal coupling levels for each recording device, and a discussion of basic signal processing for optimal signal detection of coupled signals is presented. Lastly, the results from the entire susceptibility study are summarized.

2. ELECTROMAGNETIC COUPLING CHARACTERIZATION

2.1. Testing Methodology

A variety of signal frequency sweeps were performed to determine coupling parameters for each device. All tests were performed in a semi-anechoic chamber where a Sunol Sciences JB5 biconilog antenna was used. Recording devices were placed on a wooden table about three meters away from the biconilog antenna. Both the antenna and device were at a height of one meter. The instrumentation feeding the biconilog antenna was located outside of the chamber and consisted of a direct current (DC) power supply and two signal generators. The specific instruments used for testing and their purposes are given in Table 2.1. A block diagram of the general testing setup is shown in Figure 2.1.

Initial testing involved sweeping an un-modulated sine wave at the antenna feed to stimulate interference in the recording device. Other tests involved modulated signals with amplitude modulation (AM) and frequency modulation (FM) where both the carrier frequency and message signal frequency were swept simultaneously. Data was taken for both vertical and horizontal transmitting antenna polarizations and four turntable positions: 0°, 90°, 180°, and 270°. In all cases the modulation source signal generator was set to a maximum power output of 13 dBm, and the carrier frequency was swept over 1-990 MHz. For sweeps involving modulation (AM or FM), the message signal was swept discretely in the range of 25 Hz-25 kHz which was the input message signal frequency limits of the modulation source. All audio recordings were analyzed with MatLab® software by creating spectrograms or power spectral density (PSD) estimate plots using Welch's method. All plots were created with a log scale on the y-axis. Tests involving frequency sweeps were carefully timed so that a correlation could be made between time and the frequency of the carrier signal or the message signal as appropriate.

After performing general testing with a variety of signal sweeps, the data gathered from these tests was used to perform additional testing to determine specific coupling parameters for each device. This specific testing consisted of narrower sweeps in frequency for the carrier and message signals, and longer time intervals at the carrier and message signal frequencies. The coupling parameters explored in this susceptibility study for coupling were: carrier frequency limits, message frequency limits, turntable position, antenna polarization, and signal power. Complete testing details for each device can be found in the testing tables of Appendix A.

Table 2.1. Measurement Instrumentation List

Instrument Name	Purpose
HP 8656A Signal Generator	Modulation Source
Metex MXG-9802 Function Generator	Message Source (Modulation Tests Only)
Agilent E3648A DC Power Supply	Message Source Frequency Control

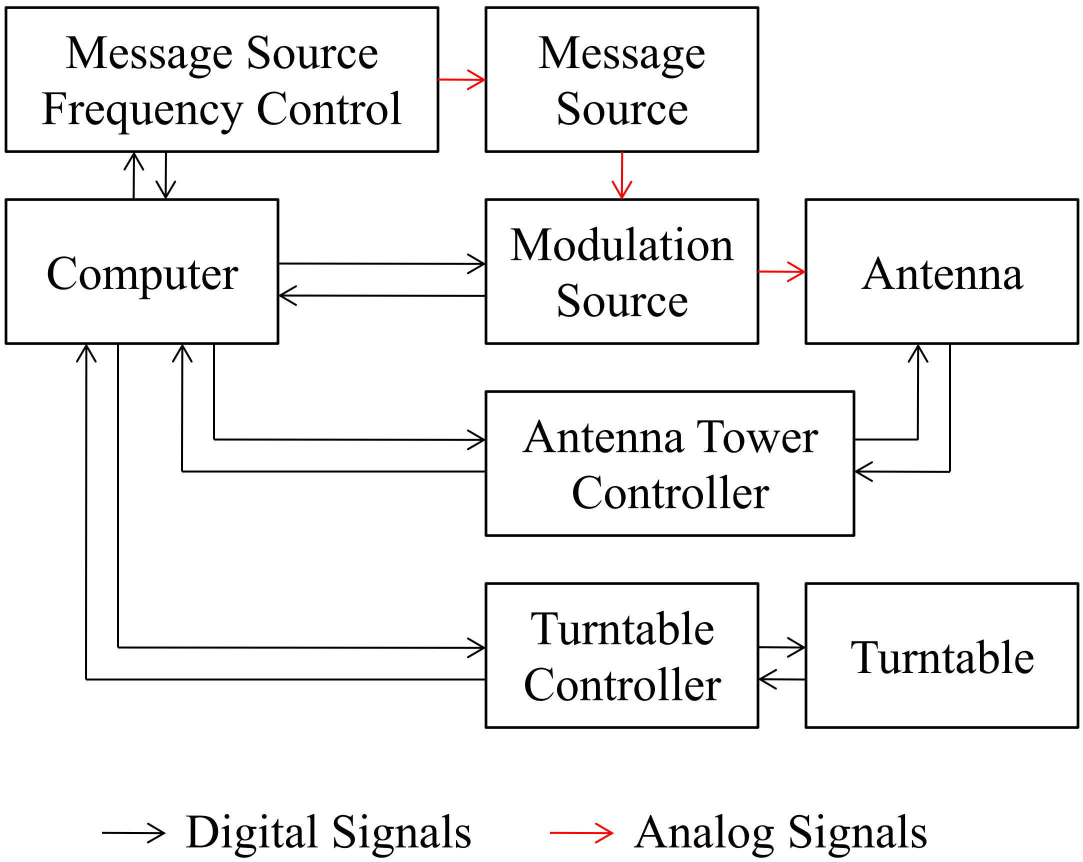

Figure 2.1. General Testing Setup Block Diagram.

The following sections indicate the coupling parameters for each device. A summary of testing results is given at the end of this section.

2.2. Device Susceptibility

2.2.1. Analog Tape Recorder

Figure 2.2 shows the testing setup for the analog tape recorder at a 0° turntable position.

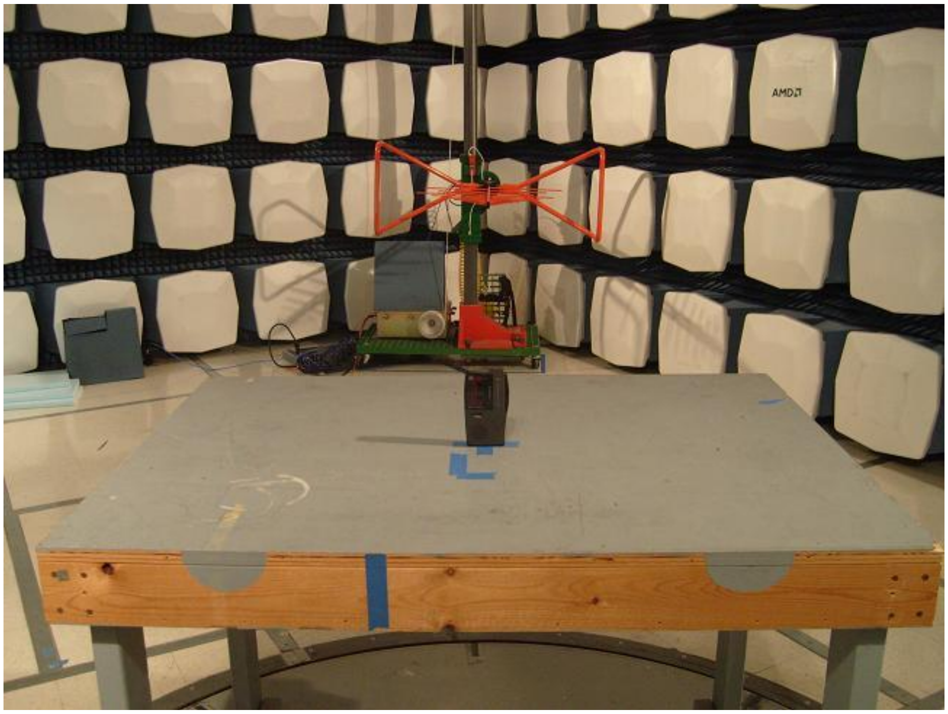

Figure 2.2. Analog Tape Recorder Chamber Testing Setup.

Although sweep tests were performed with a pure sine wave signal and with FM signals, these did not yield any coupled messages onto recordings with the analog tape recorder. Tests involving AM signals, however, did produce coupled messages in the recordings. Figures 2.3-2.5 show spectrogram plots produced under equivalent test conditions (same device orientation and antenna polarization) when a pure sine wave, an AM signal, and an FM signal was applied to the transmitting antenna.

The message coupling can be seen in Figure 2.3, represented by the vertical, dark red lines in the spectrogram plot. In addition, the message coupling can easily be heard. The message signal was ramped over a two second interval from 45 Hz to 15.5 kHz. Due to the scaling of the plot, the lines representing the ramping message appear vertically oriented. These lines are dotted because the message signal was swept discretely in frequency with a DC power supply. No lines representing the frequency ramping message appear in Figure 2.2 and Figure 2.4. The carrier frequency was ramping from 506 MHz to 591 MHz in the plots during the time interval shown.

Specific testing with this device revealed two carrier frequency coupling ranges that produced measureable signals in the recordings: 510-600 MHz and 803-855 MHz. Within these

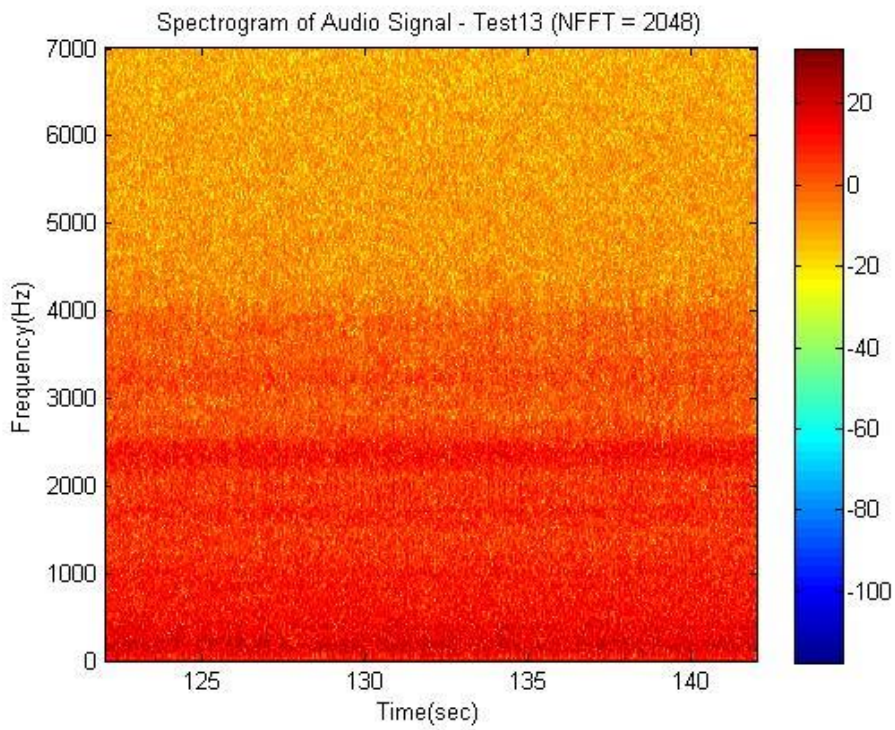

Figure 2.3. Analog Tape Recorder: Sine Wave Sweep.

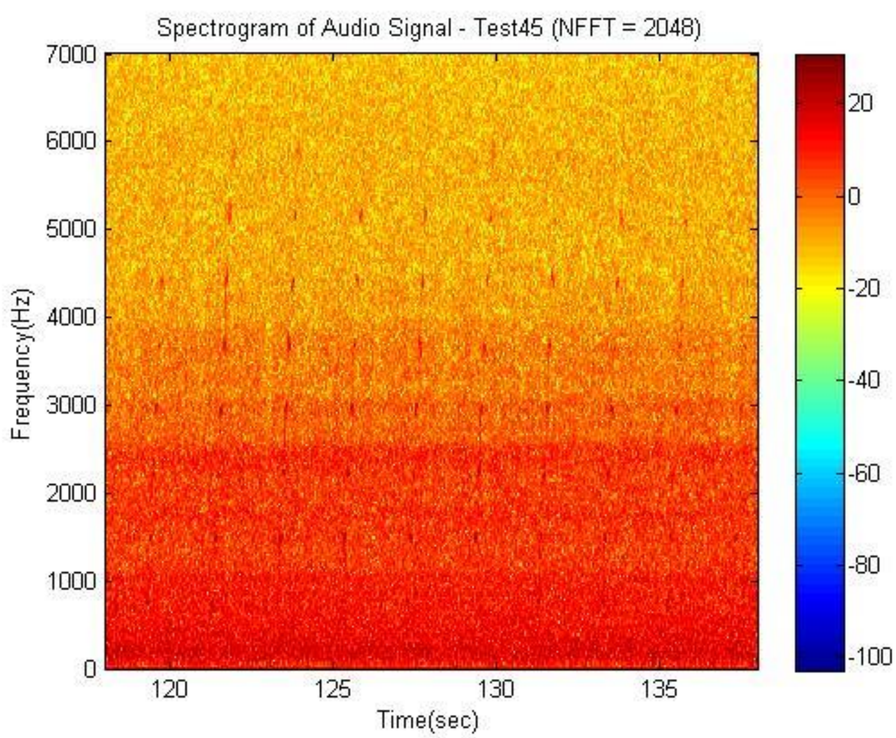

Figure 2.4. Analog Tape Recorder: AM with Simultaneous Carrier Sweep and Message Sweep.

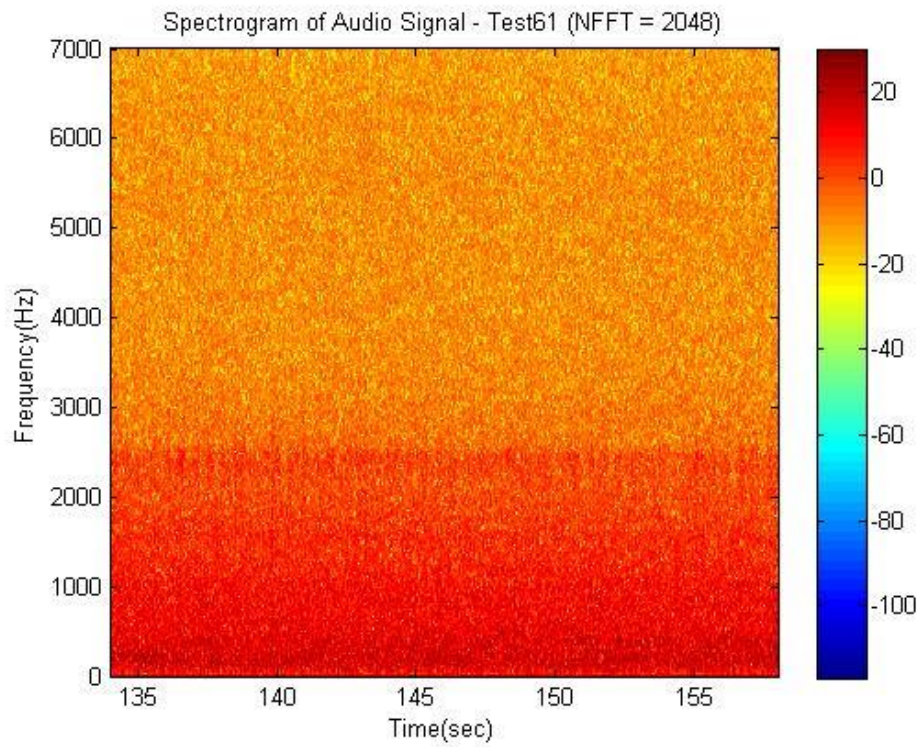

Figure 2.5. Analog Tape Recorder: FM with Simultaneous Carrier Sweep and Message Sweep.

frequency ranges, the coupling was strongest for carrier frequencies between 512-568 MHz and 823-845 MHz. Figure 2.6 and Figure 2.7 show examples of message coupling in each of the strongest carrier frequency ranges, respectively. These figures show that when the carrier frequency was set to a frequency within either strong coupling range, the messages can easily be seen above the noise floor.

To determine the message signal frequency limits, the carrier frequency was set to one of two different strong coupling carrier frequencies and the message signal was swept in frequency over the range 45 Hz-15 kHz in one instance, and 25 Hz-500 Hz in another. The message frequency limits for the analog tape recorder were approximately 300 Hz-6 kHz. The limits were not carrier frequency dependent as long as the carrier frequency was within one of the strong coupling ranges. Figures 2.8-2.11 display the results from these experiments. Although Figure 2.8 and Figure 2.9 suggest that the upper limit for message coupling should be larger than 6 kHz, further testing revealed that messages above 6 kHz were not easily detectable.

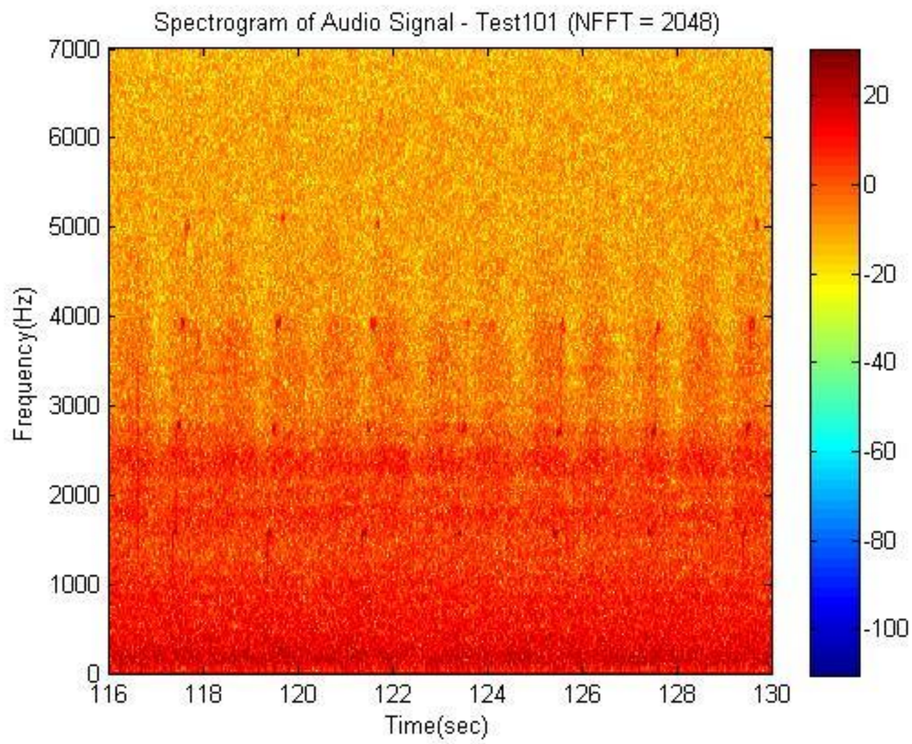

Figure 2.6. Analog Tape Recorder: Strong Coupling Range #1.

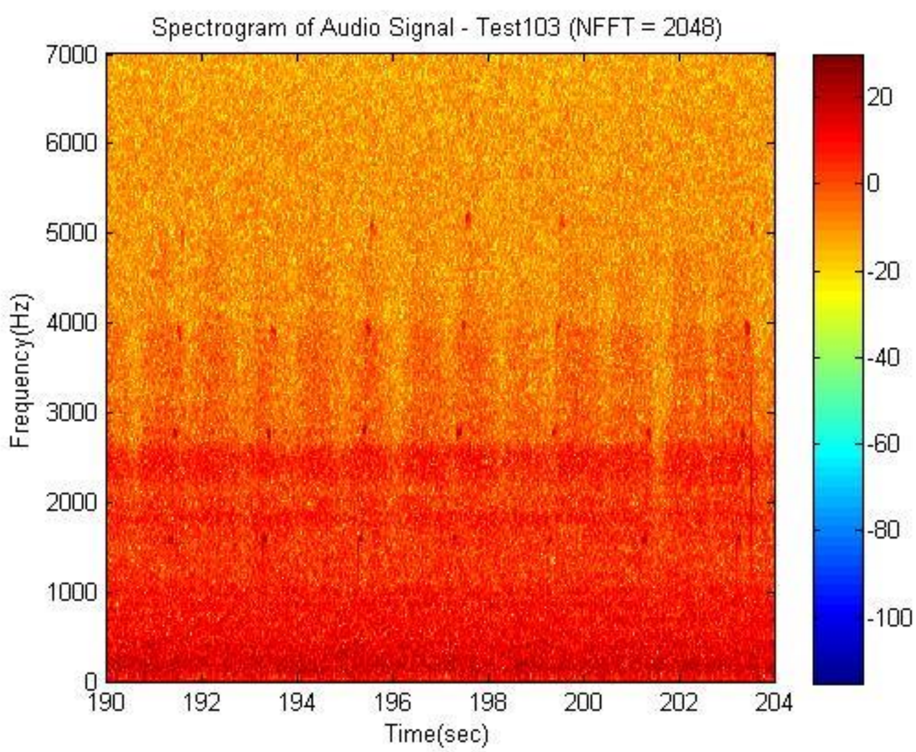

Figure 2.7. Analog Tape Recorder: Strong Coupling Range #2.

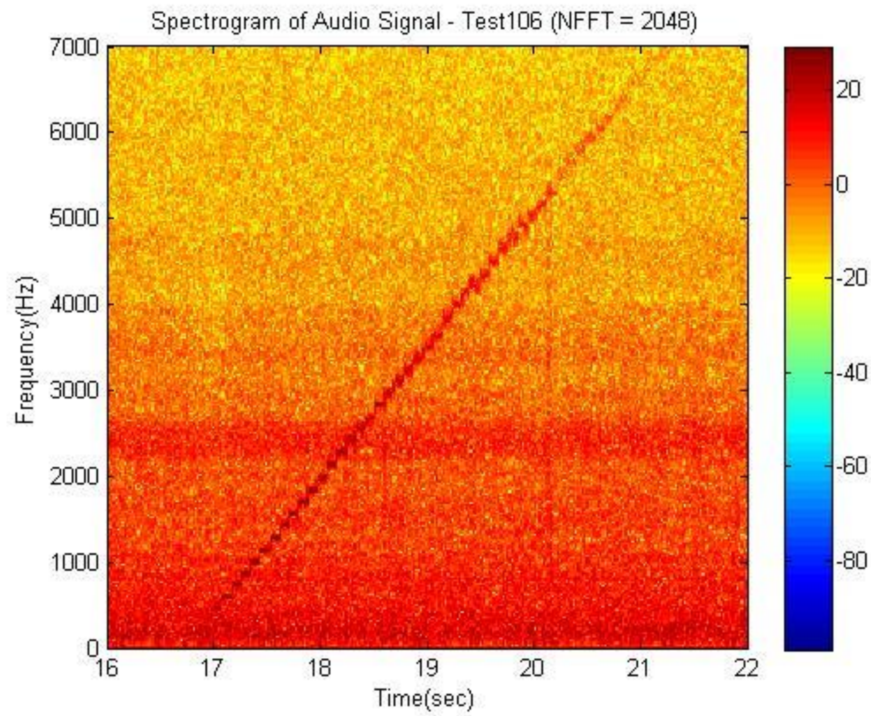

Figure 2.8. Analog Tape Recorder: Message Frequency Total Limits Testing with 547 MHz Carrier Frequency.

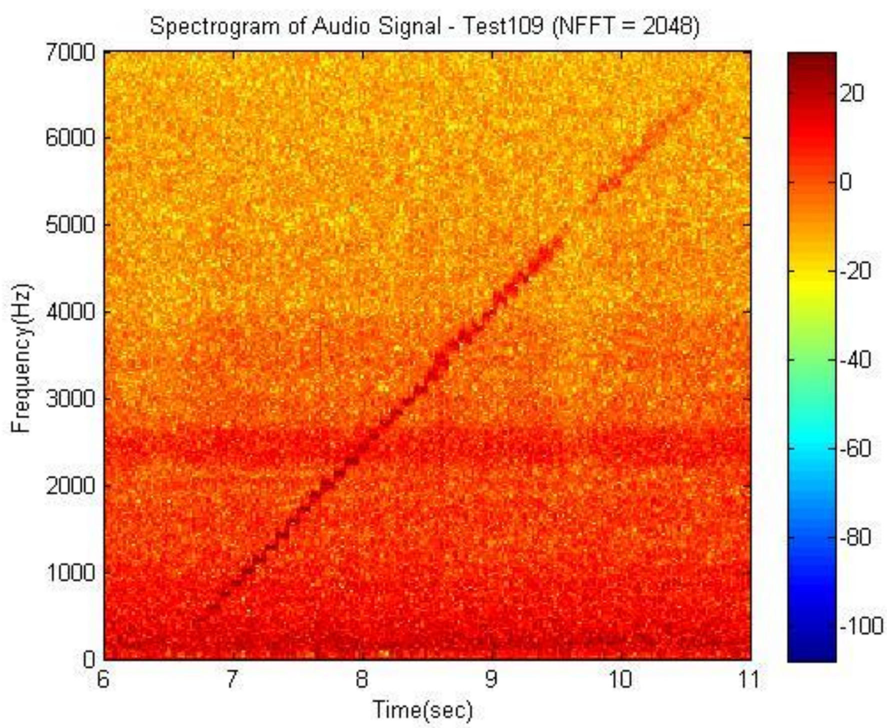

Figure 2.9. Analog Tape Recorder: Message Frequency Total Limits Testing with 831 MHz Carrier Frequency.

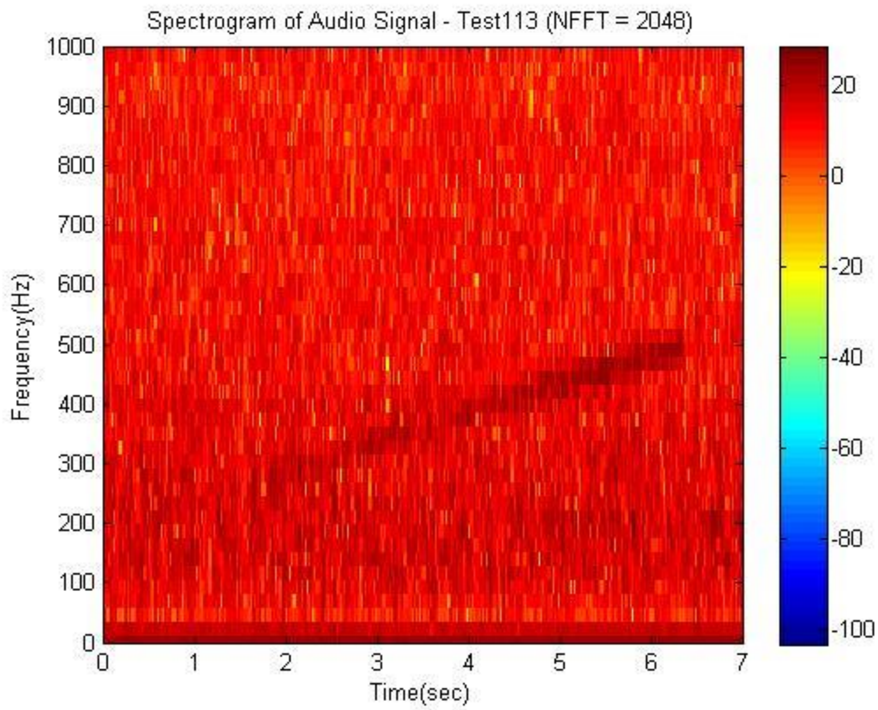

Figure 2.10. Analog Tape Recorder: Message Frequency Lower Limit Testing with 547 MHz Carrier Frequency.

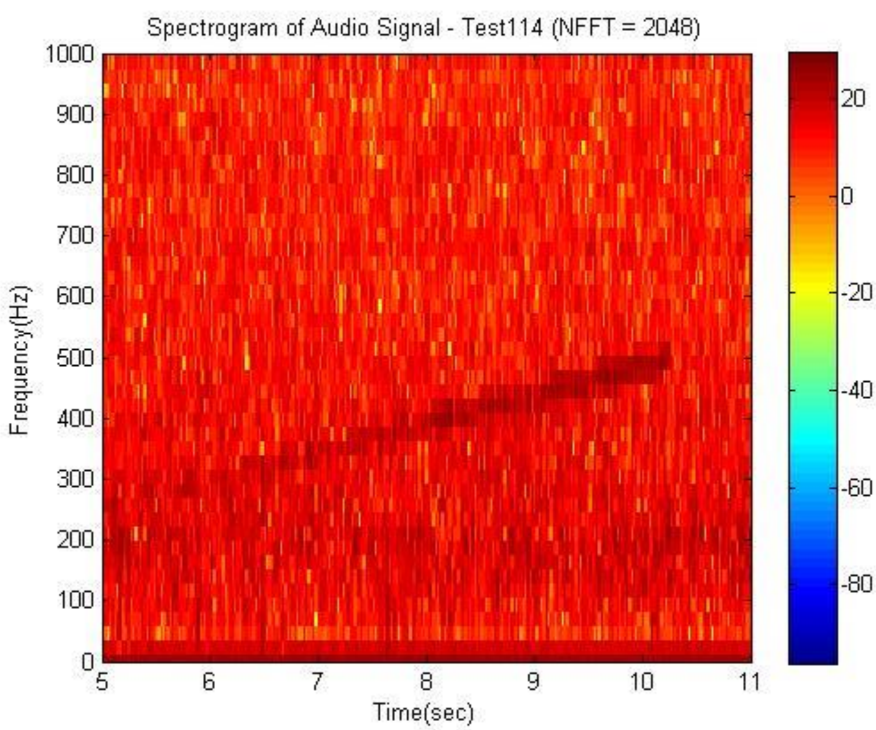

Figure 2.11. Analog Tape Recorder: Message Frequency Lower Limit Testing with 831 MHz Carrier Frequency.

Figure 2.10 and Figure 2.11 show that the lower limit for message coupling was around 300 Hz because it was at this frequency that the dark red line representing the swept frequency message vanishes.

Additional testing was performed to show that the coupled messages in the recordings were the same as the messages created by the signal generators. The carrier frequency was fixed, and messages were transmitted at a few fixed frequencies. The recordings were analyzed by creating a PSD estimate plot using Welch's method. Figures 2.12-2.15 show a few of the results from these experiments. Additional plots can also be found in Appendix B.

The message signal spikes in the PSD plots show a strong correlation between the messages seen in the recordings and the messages input to the modulation source. For example, for the data shown in Figure 2.13, a 300 Hz message was applied to the modulation source while a recording was made. Spectral analysis of the recording made under these test conditions revealed a coupled message at 300 Hz, showing that the coupled message was equivalent to the original message applied to the modulation source. Figure 2.12 provides a PSD plot of the full frequency spectrum of an example recording so that it may be compared to previous spectrogram plots.

In order to couple a message into the analog tape recorder, the antenna polarization must be vertically polarized with respect to the recorder position in Figure 2.2. The picture shown in Figure 2.2, for instance, would not result in any message coupling in the audio recording due to the horizontal polarization of the transmitting antenna. For tests with horizontal antenna polarization, no detectable coupling occurred. Figure 2.4 and Figure 2.16 show results from two identical tests where the carrier frequency and message signals were swept, but the antenna polarizations were different. The message signal was ramping over a two second interval from 45 Hz to 15.5 kHz, and the carrier frequency was ramping from 506 MHz to 591 MHz. Recall that the message frequency limits for the analog tape recorder were approximately 300 Hz-6 kHz. The data shown in Figure 2.4 was taken with a vertical antenna polarization. The data shown in Figure 2.16 was taken with a horizontal antenna polarization.

Figure 2.16 illustrates that no coupling occurred for horizontal antenna polarization by the lack of dark red vertical lines representing the swept frequency message signal. In contrast, Figure 2.4 shows message coupling with the presence of dark red vertical lines representing the swept frequency message signal.

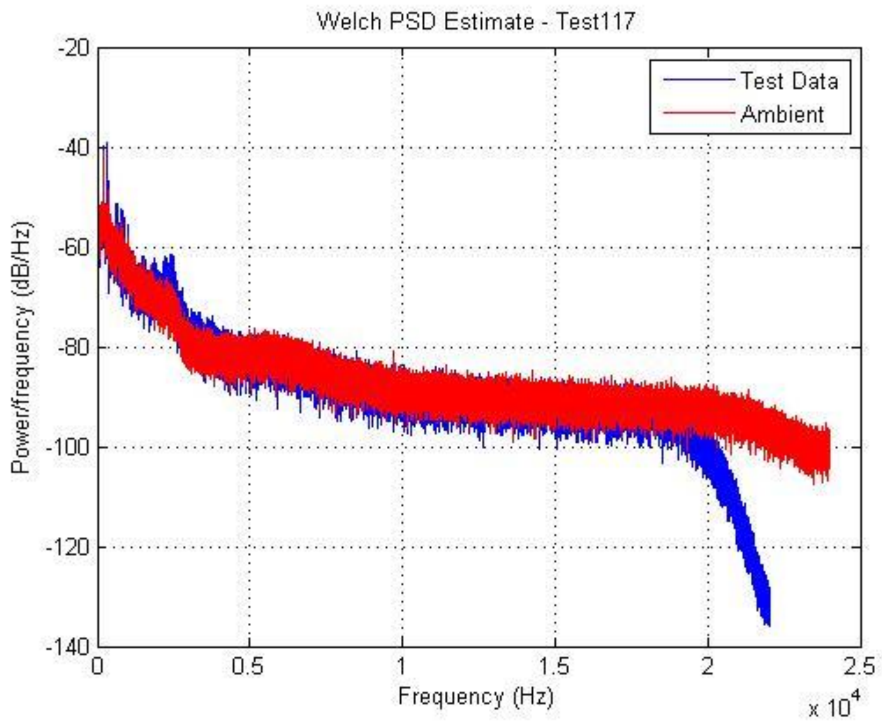

Figure 2.12. Analog Tape Recorder: PSD Estimate with 547 MHz Carrier Frequency and 300 Hz Message (Full Frequency Range).

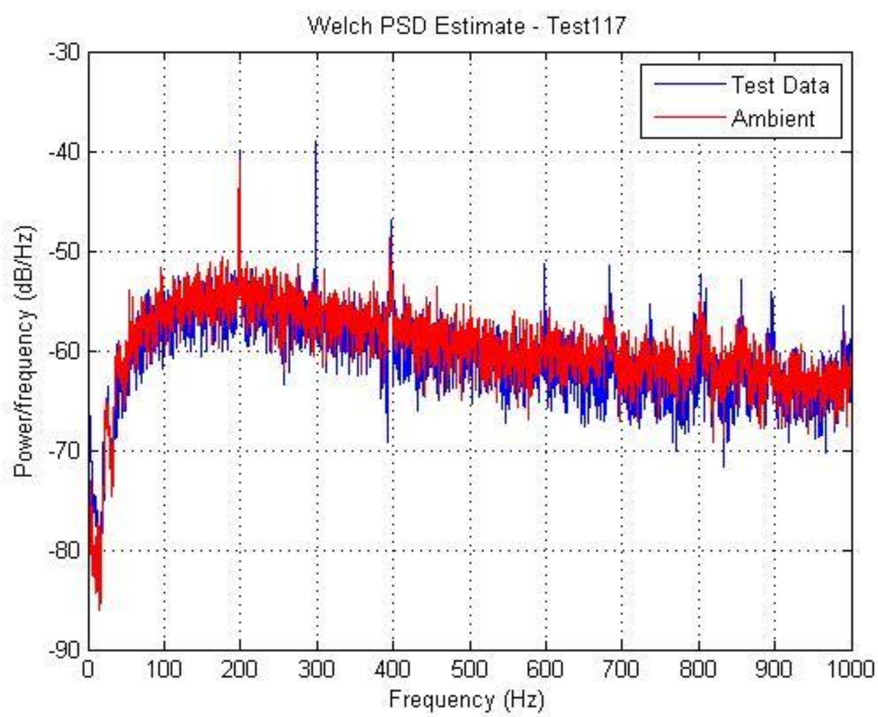

Figure 2.13. Analog Tape Recorder: PSD Estimate with 547 MHz Carrier Frequency and 300 Hz Message (Expanded Near 300 Hz).

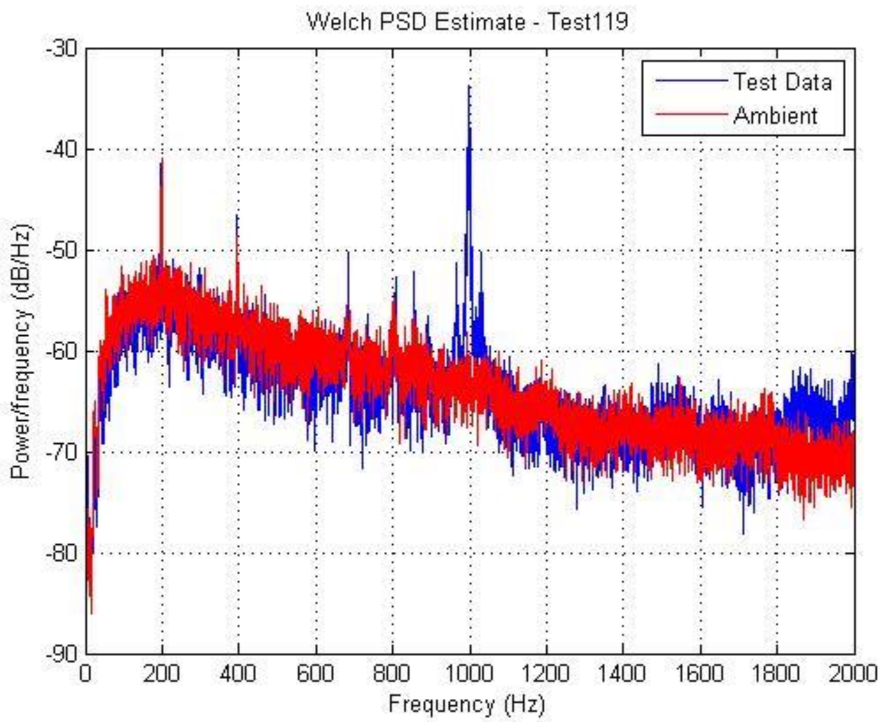

Figure 2.14. Analog Tape Recorder: PSD Estimate with 547 MHz Carrier Frequency and 1 kHz Message (Expanded Near 1 kHz).

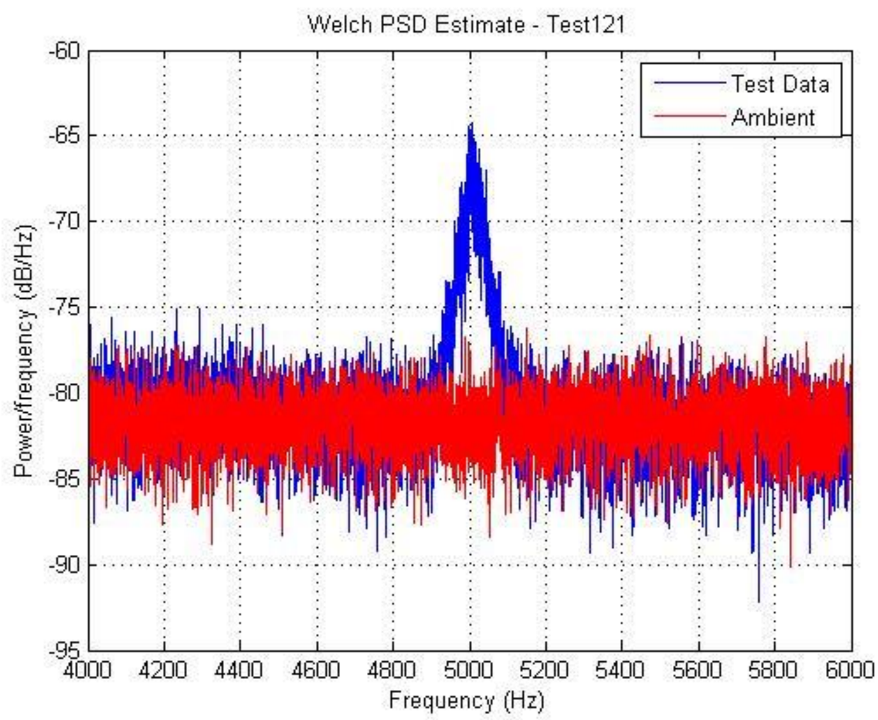

Figure 2.15. Analog Tape Recorder: PSD Estimate with 547 MHz Carrier Frequency and 5 kHz Message (Expanded Near 5 kHz).

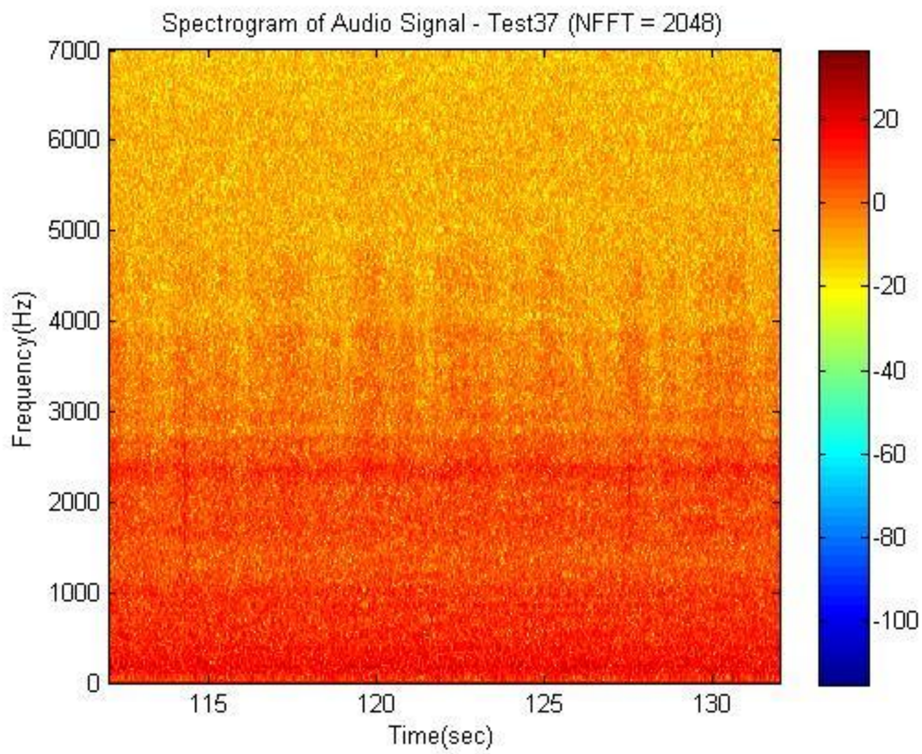

Figure 2.16. Analog Tape Recorder: Horizontal Antenna Polarization.

Two tests were performed to determine the signal strength needed to produce a measureable message in the recording. In the first test, the carrier frequency and message frequency were fixed while the input power (-127 dBm to 13 dBm) into the transmitting antenna was varied. In the second test, the same signal frequencies were used while the percent modulation was varied (1-99%). The message frequency was fixed at 1 kHz. Without any additional signal processing than that used to generate the plots, it was found that the message signal could be detected with a minimum of 3 dBm of carrier frequency input power and a 50% modulation depth for input power sweep testing. Similarly for modulation depth sweep testing, the minimum modulation depth for detection was about 15% with 11 dBm carrier frequency input power. Figure 2.17 and Figure 2.18 show the results from these experiments. These figures show the general trend that as either the carrier frequency power or the percent modulation of the message signal becomes larger, the message couples better into the audio recordings. This increase in coupling is represented by the horizontal red line at 1 kHz that darkens in color over time.

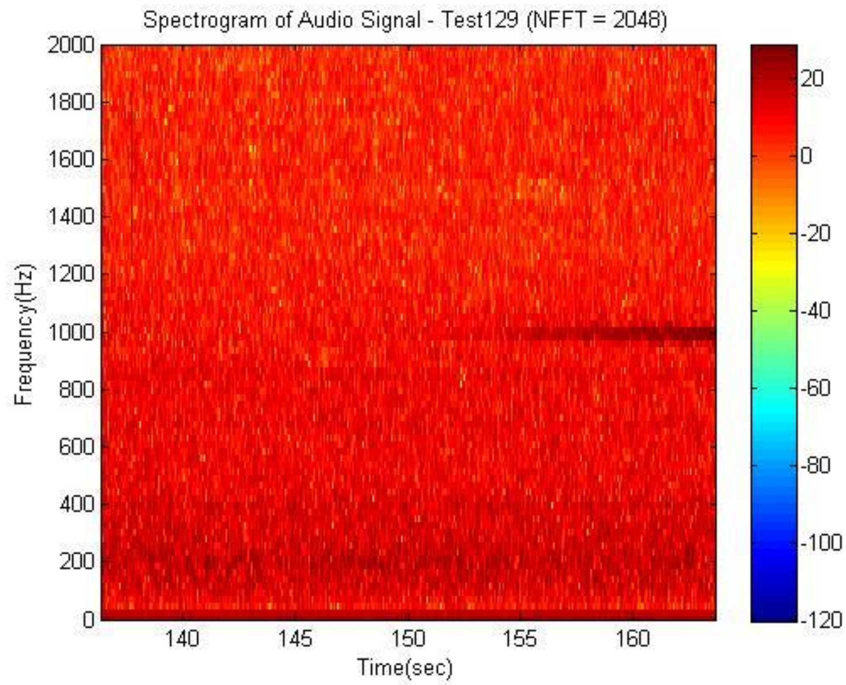

Figure 2.17. Analog Tape Recorder: Carrier Frequency Input Power Sweep.

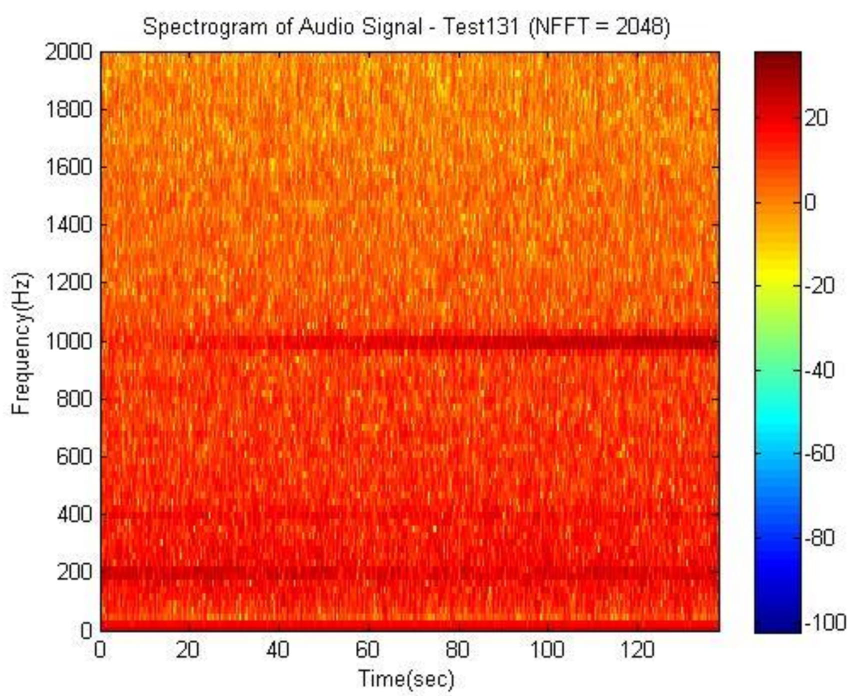

Figure 2.18. Analog Tape Recorder: Modulation Depth Sweep.

To determine how the orientation of the tape recorder impacted testing, recordings were taken with turntable positions ranging from 0° to 355° at 5° increments while using a fixed coupling carrier frequency and message frequency. The recordings for each turntable position were nearly 10 seconds long. A PSD estimate was calculated for each recording, and the value at the message frequency was stored in a data array. This data array was then normalized with respect to the largest value and graphed in a polar plot as shown in Figure 2.19 and Figure 2.20. Message frequencies of 500 Hz, 3 kHz, and 5 kHz were tested in three separate sets of experiments. The polar plots generated for these messages were all similar in shape as verified by the additional plots in Appendix B.

Compared to the noise, coupled messages were fairly independent of turntable position. Figure 2.19 illustrates this independence, where one sees only a 10 dB difference between the minimum and maximum coupling among turntable positions. Comparing the coupled data to itself, a general trend can be seen that increased coupling occurred when the face of the analog tape recorder was facing towards the antenna. The susceptibility pattern of the analog tape recorder shown in Figure 2.20 is similar to the E-plane cut of a pyramidal horn antenna radiation pattern [2].

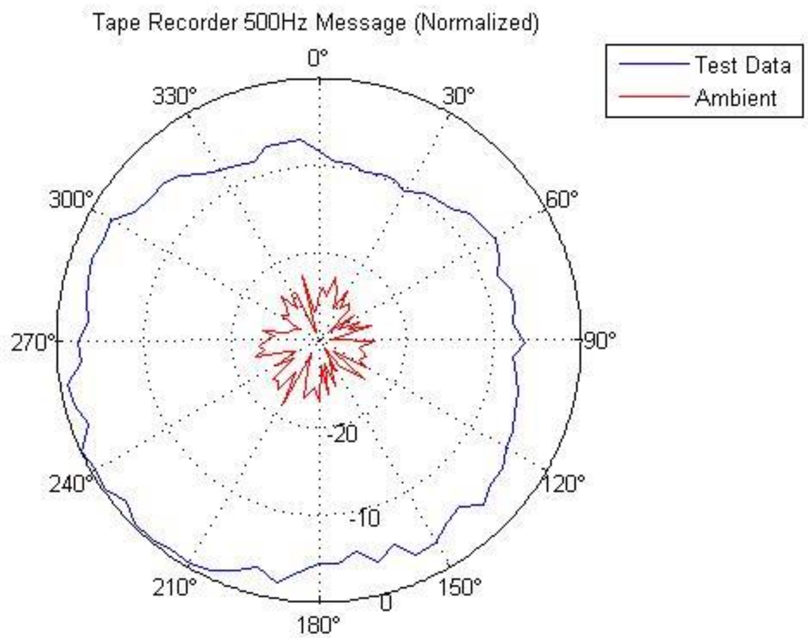

Figure 2.19. Analog Tape Recorder: PSD Estimate Comparison Polar Plot for Message Frequency 500 Hz.

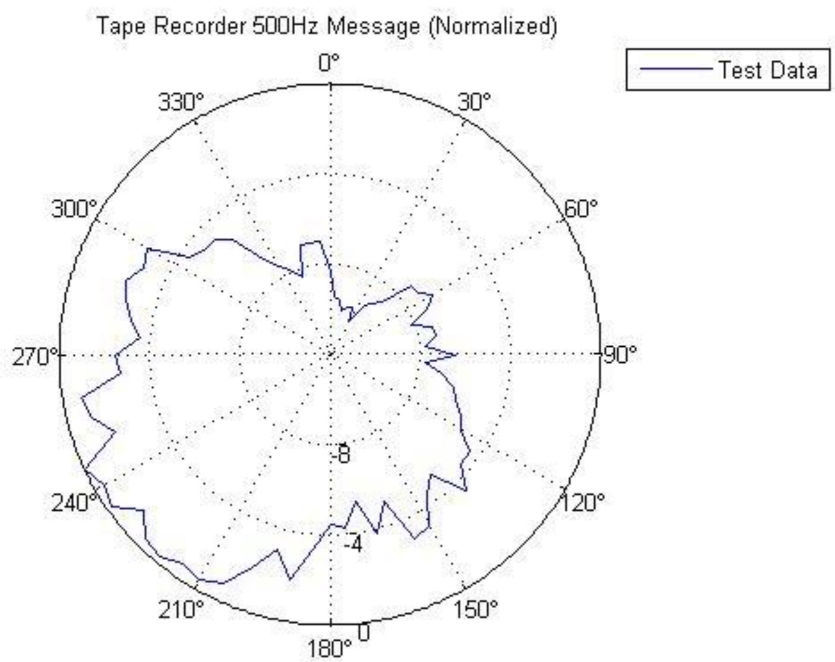

Figure 2.20. Analog Tape Recorder: PSD Estimate Single Polar Plot for Message Frequency 500 Hz.

2.2.2. Computer Microphone

Figure 2.21 shows the testing setup for the computer microphone at a 0° turntable position.

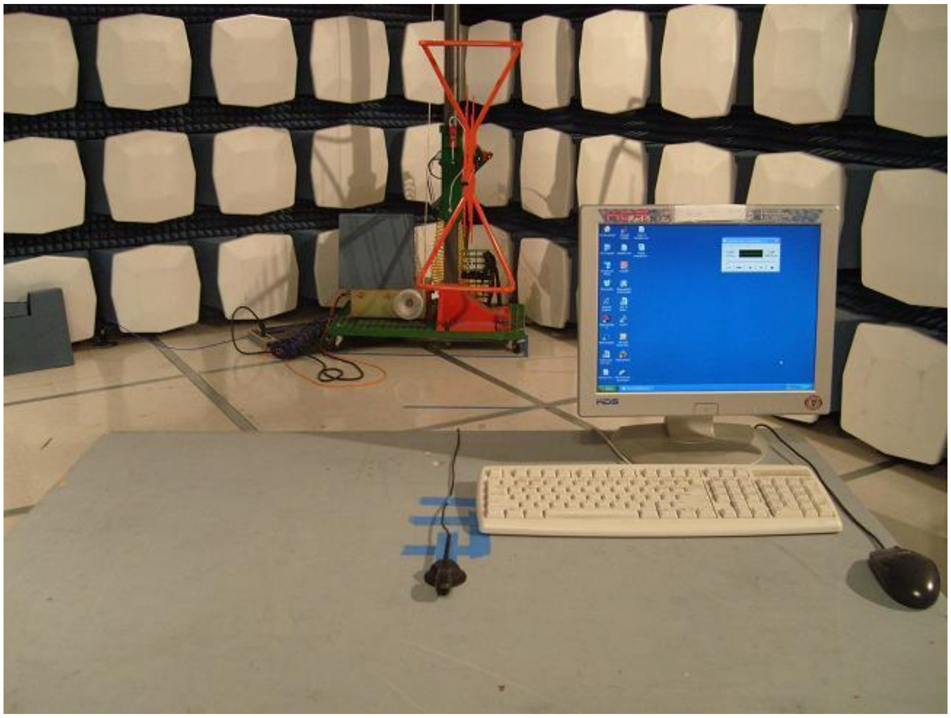

Figure 2.21. Computer Microphone Chamber Testing Setup.

Although sweep tests were performed with a pure sine wave signal and with FM signals, these did not yield any coupled messages onto recordings with the computer microphone. Tests involving AM signals, however, did produce coupled messages in the recordings. Figures 2.22-2.24 show spectrogram plots produced under equivalent test conditions (same device orientation and antenna polarization) when a pure sine wave, an AM signal, and an FM signal was applied to the transmitting antenna.

The message coupling can be seen in Figure 2.23, represented by the vertical, yellow lines in the spectrogram plot. In addition, the message coupling can easily be heard. The message signal was ramped over a two second interval from 440 Hz to 25 kHz. This ramped sweep can clearly be seen in the plot shown in Figure 2.23. The lines are dotted because the message signal was swept discretely in frequency with a DC power supply. No lines representing the frequency ramping message appear in Figure 2.22 and Figure 2.24. The carrier frequency was ramping from 206 MHz to 228 MHz in the plots below during the time interval shown.

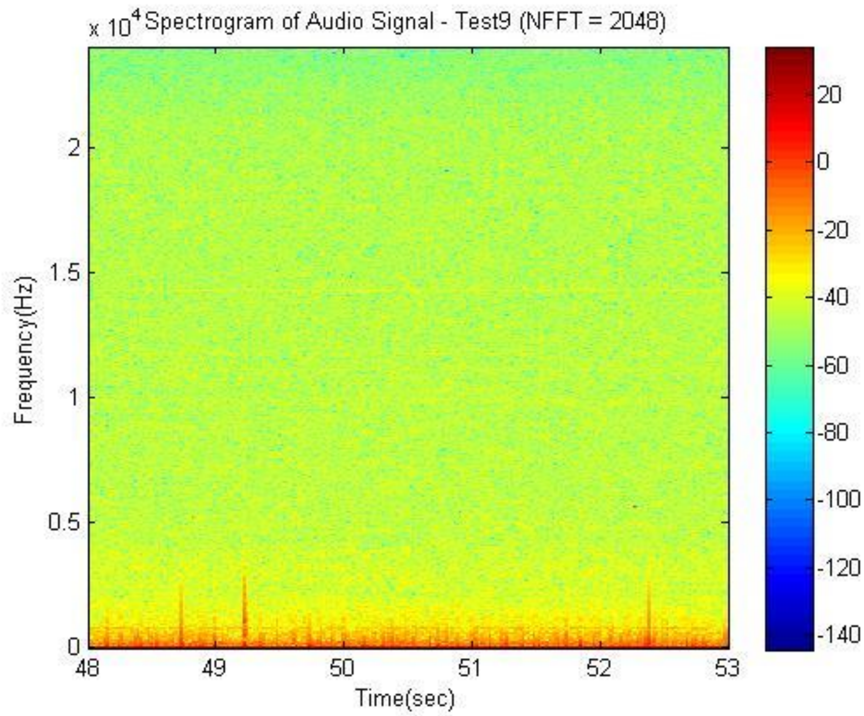

Figure 2.22. Computer Microphone: Sine Wave Sweep.

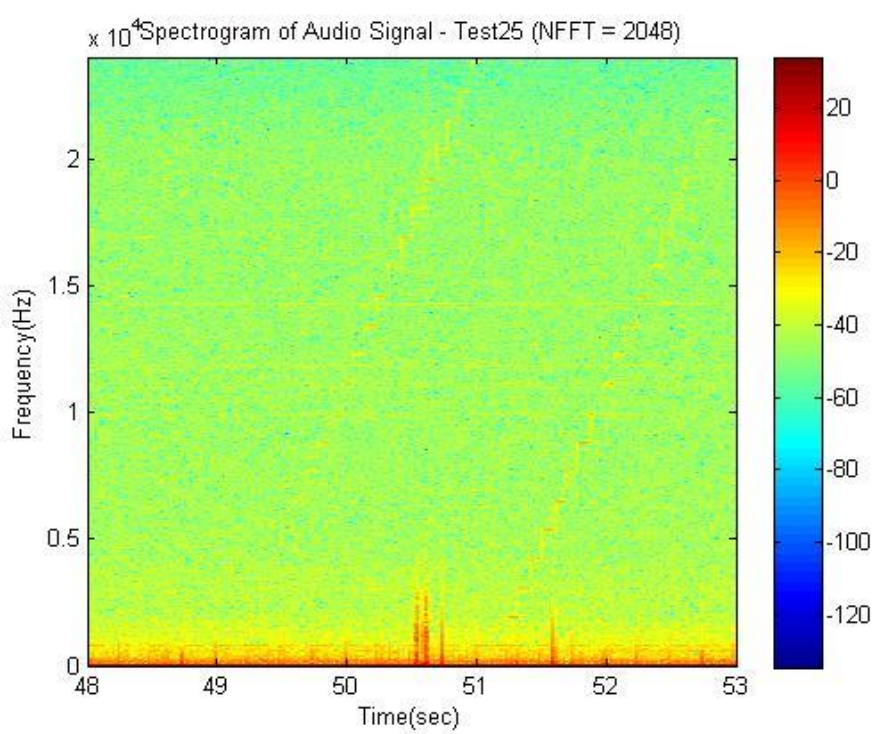

Figure 2.23. Computer Microphone: AM with Simultaneous Carrier Sweep and Message Sweep.

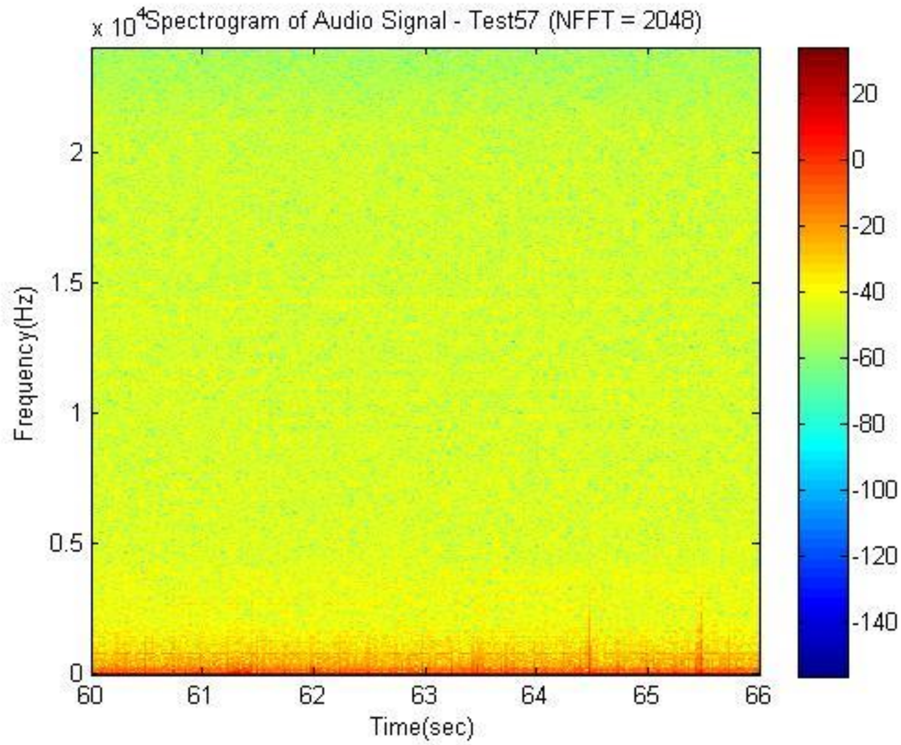

Figure 2.24. Computer Microphone: FM with Simultaneous Carrier Sweep and Message Sweep.

General testing showed that there were many different carrier frequencies that coupled to the computer microphone. The coupling was orientation and polarization sensitive depending on the coupling frequency. The two best coupling ranges that produced measureable signals in the recordings were 215-227 MHz and 425-437 MHz. Within these frequency ranges, the coupling was strongest for carrier frequencies between 216-223 MHz and 427-434 MHz. Figure 2.25 and Figure 2.26 show examples of message coupling in each of the strongest carrier frequency ranges, respectively. These figures show that when the carrier frequency was set to a frequency within either strong coupling range, the messages can easily be seen above the noise floor.

To determine the message signal frequency limits, the carrier frequency was set to one of two different strong coupling carrier frequencies and the message signal was swept in frequency over the range 470 Hz-25 kHz in one instance, and 25 Hz-1.5 kHz in another. The message frequency limits for the computer microphone were approximately 400 Hz-24 kHz. The limits were not carrier frequency dependent as long as the carrier frequency was within one of the strong coupling ranges. Figures 2.27-2.30 display the results from these experiments. The

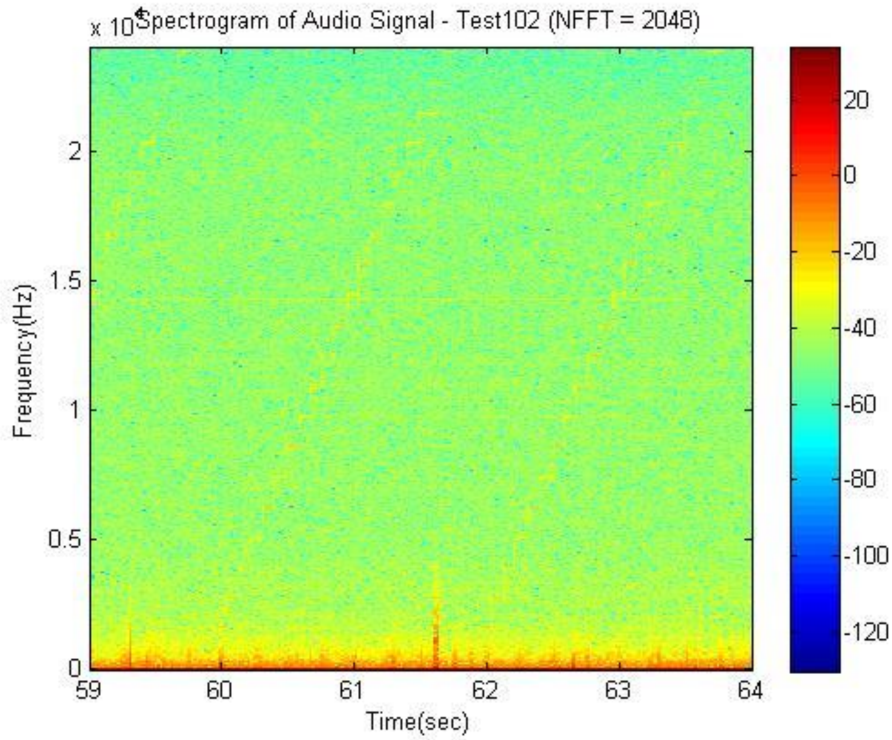

Figure 2.25. Computer Microphone: Strong Coupling Range #1.

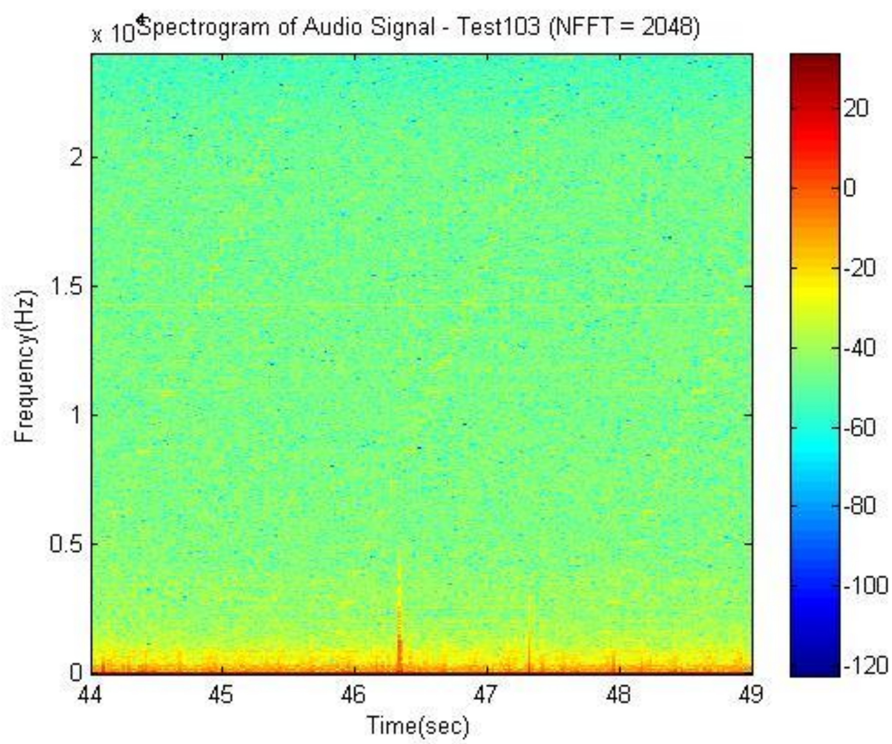

Figure 2.26. Computer Microphone: Strong Coupling Range #2.

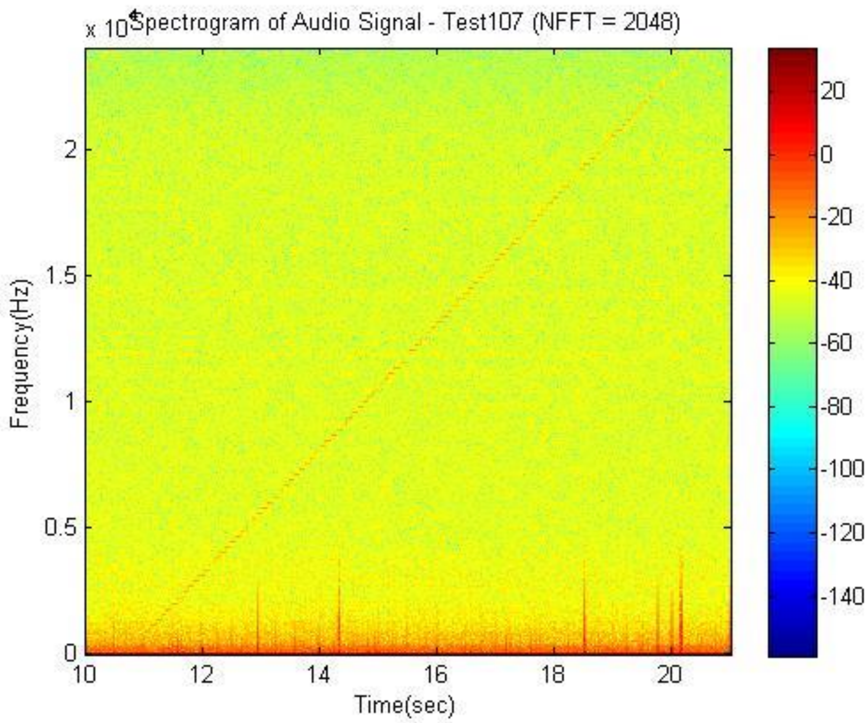

Figure 2.27. Computer Microphone: Message Frequency Total Limits Testing with 220 MHz Carrier Frequency.

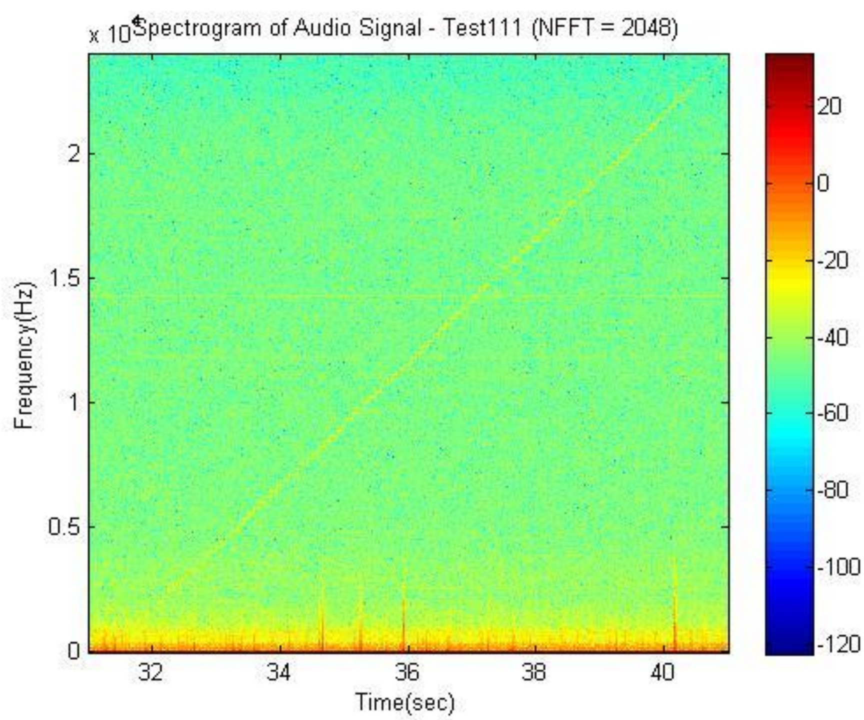

Figure 2.28. Computer Microphone: Message Frequency Total Limits Testing with 430 MHz Carrier Frequency.

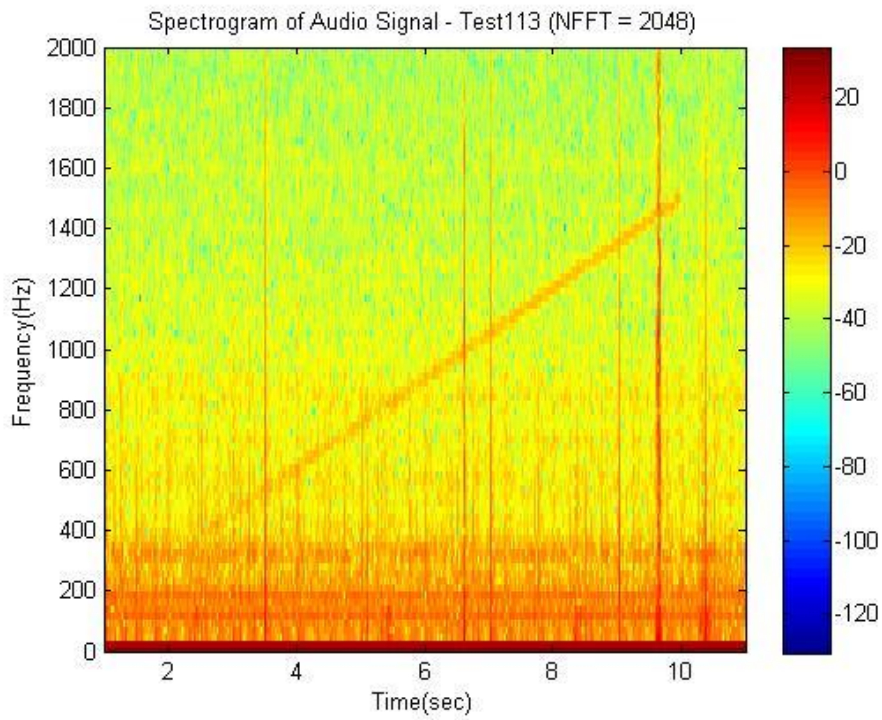

Figure 2.29. Computer Microphone: Message Frequency Lower Limit Testing with 220 MHz Carrier Frequency.

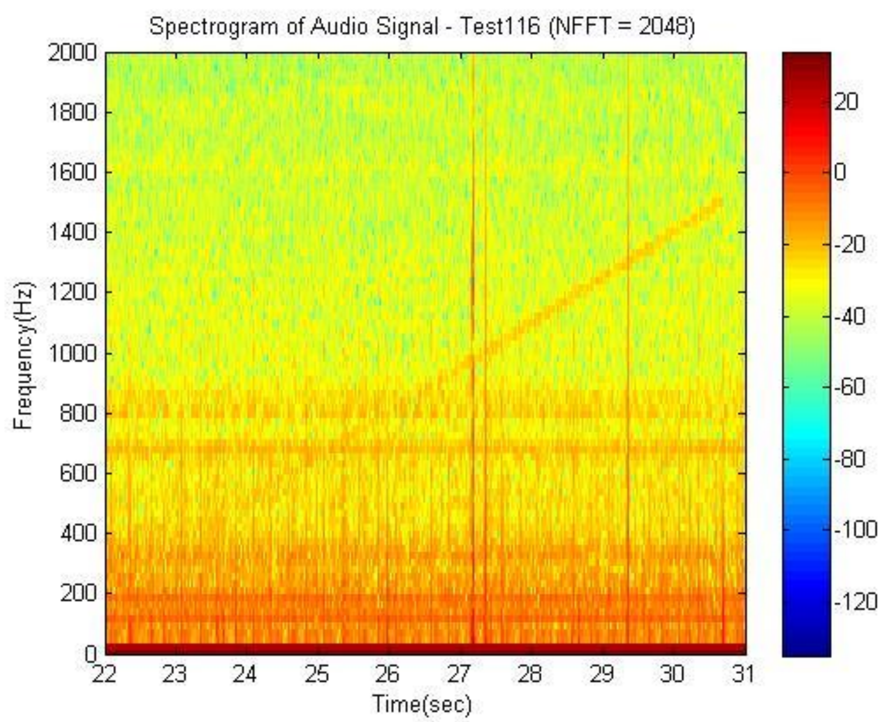

Figure 2.30. Computer Microphone: Message Frequency Lower Limit Testing with 430 MHz Carrier Frequency.

upper limit to message coupling was 24 kHz since Figure 2.27 and Figure 2.28 show the swept message signal without bound up to this frequency. Figure 2.29 and Figure 2.30 illustrate that the lower limit for the message coupling was around 400 Hz because it is at this frequency that the red line representing the swept frequency message vanishes.

Additional testing was performed to show that the coupled messages in the recordings were the same as the messages created by the signal generators. The carrier frequency was fixed, and messages were transmitted at a few fixed frequencies. The recordings were analyzed by creating a PSD estimate plot using Welch's method. Figures 2.31-2.34 show a few of the results from these experiments. Additional plots can also be found in Appendix B.

The message signal spikes in the PSD plots show a strong correlation between messages seen in the recordings and the messages input to the modulation source. For example, for the data shown in Figure 2.33, a 10 kHz message was applied to the modulation source while a recording was made. Spectral analysis of the recording made under these test conditions revealed a coupled message at 10 kHz, showing that the coupled message was equivalent to the original message applied to the modulation source. Figure 2.31 provides a PSD plot of the full frequency spectrum of an example recording so that is may be compared to previous spectrogram plots.

In order to couple a message into the computer microphone, the antenna polarization should be vertically polarized with respect to the computer microphone position in Figure 2.21. Message coupling could occur for horizontal antenna polarization, but in general the coupling strength was much lower than that of test cases with vertical antenna polarization. Figure 2.23 and Figure 2.35 show results from two identical tests where the carrier frequency and message signals were swept, but the antenna polarizations were different. The message signal was ramping over a two second interval from 440 Hz to 25 kHz, and the carrier frequency was ramping from 206 MHz to 228 MHz. Recall that the message frequency limits for the computer microphone were approximately 400 Hz-24 kHz. The data shown in Figure 2.23 was taken with a vertical antenna polarization. The data shown in Figure 2.35 was taken with a horizontal antenna polarization.

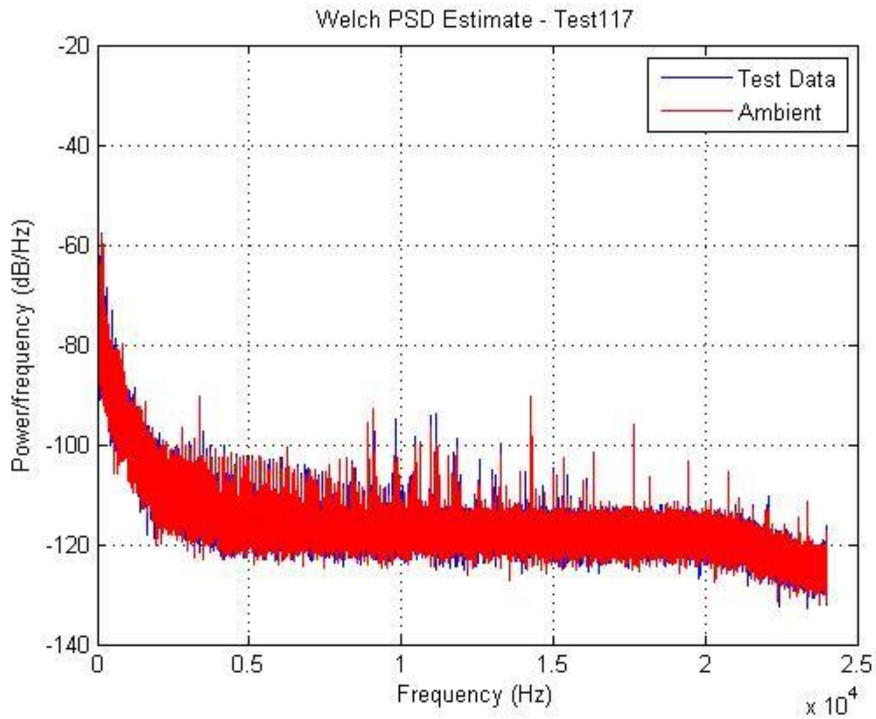

Figure 2.31. Computer Microphone: PSD Estimate with 220 MHz Carrier Frequency and 500 Hz Message (Full Frequency Range).

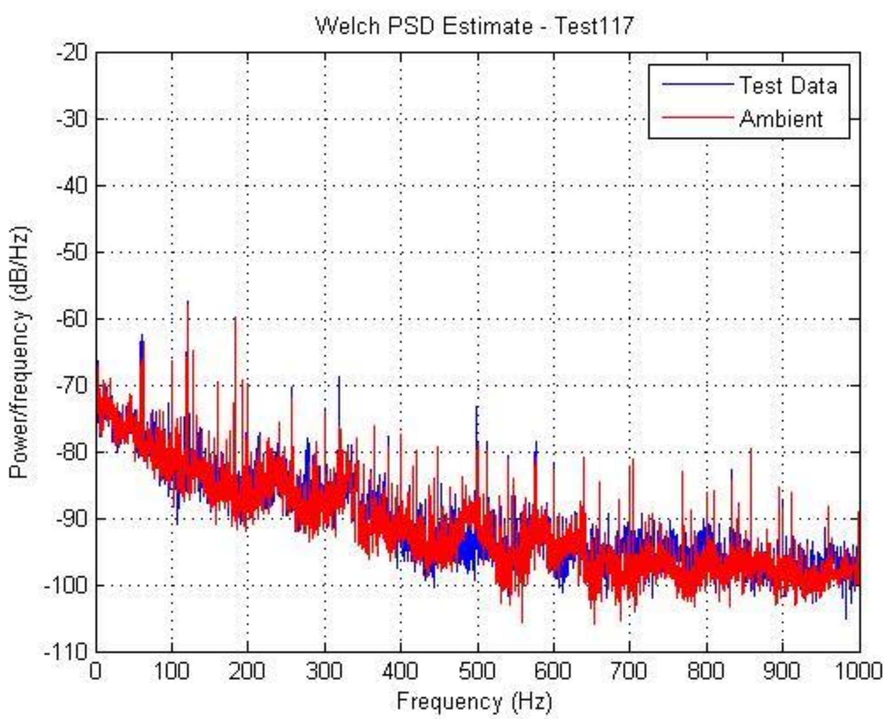

Figure 2.32. Computer Microphone: PSD Estimate with 220 MHz Carrier Frequency and 500 Hz Message (Expanded Near 500 Hz).

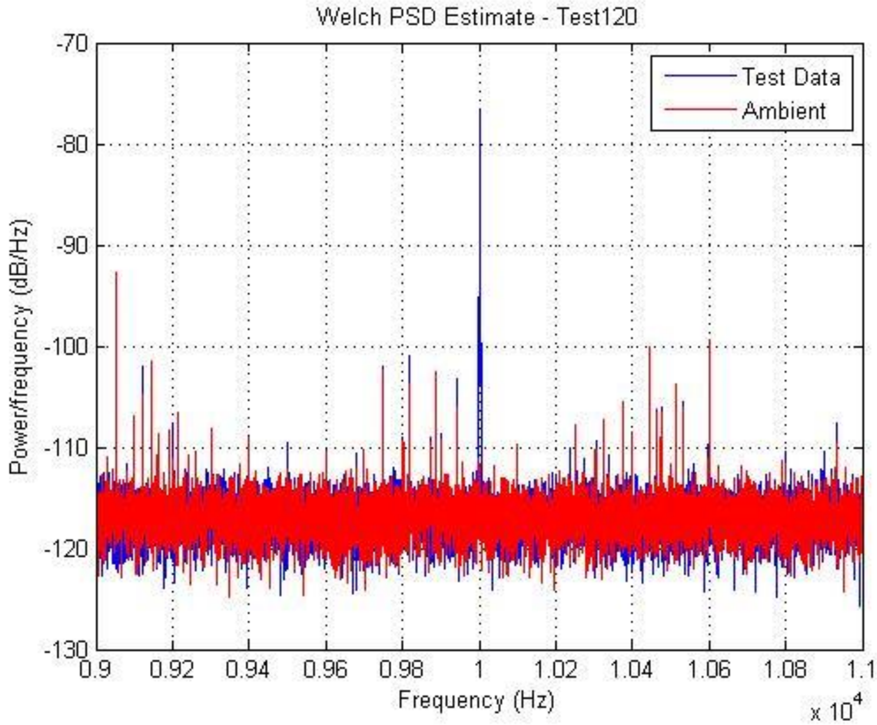

Figure 2.33. Computer Microphone: PSD Estimate with 220 MHz Carrier Frequency and 10 kHz Message (Expanded Near 10 kHz).

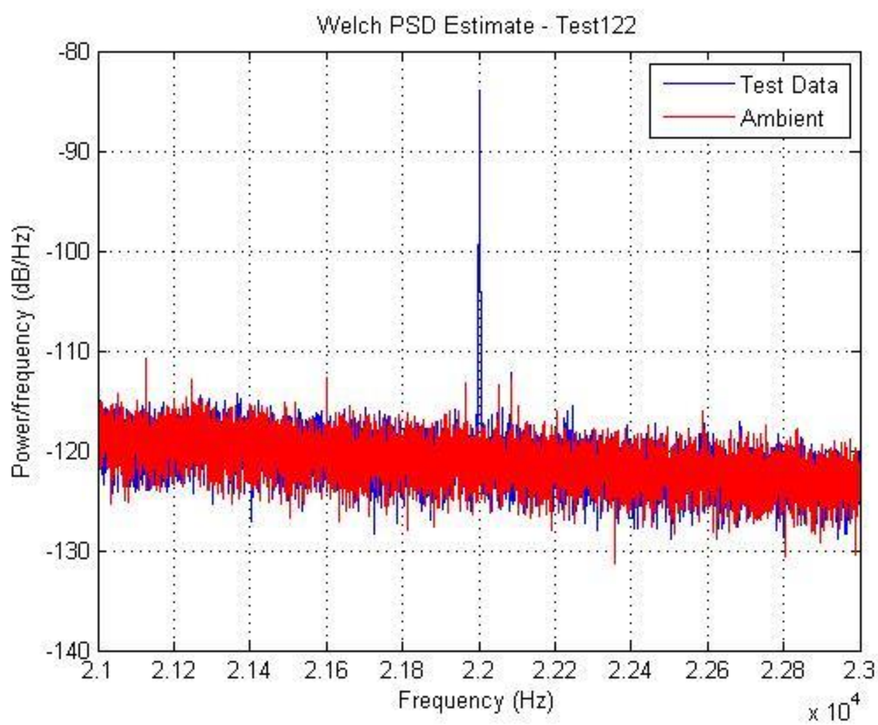

Figure 2.34. Computer Microphone: PSD Estimate with 220 MHz Carrier Frequency and 22 kHz Message (Expanded Near 22 kHz).

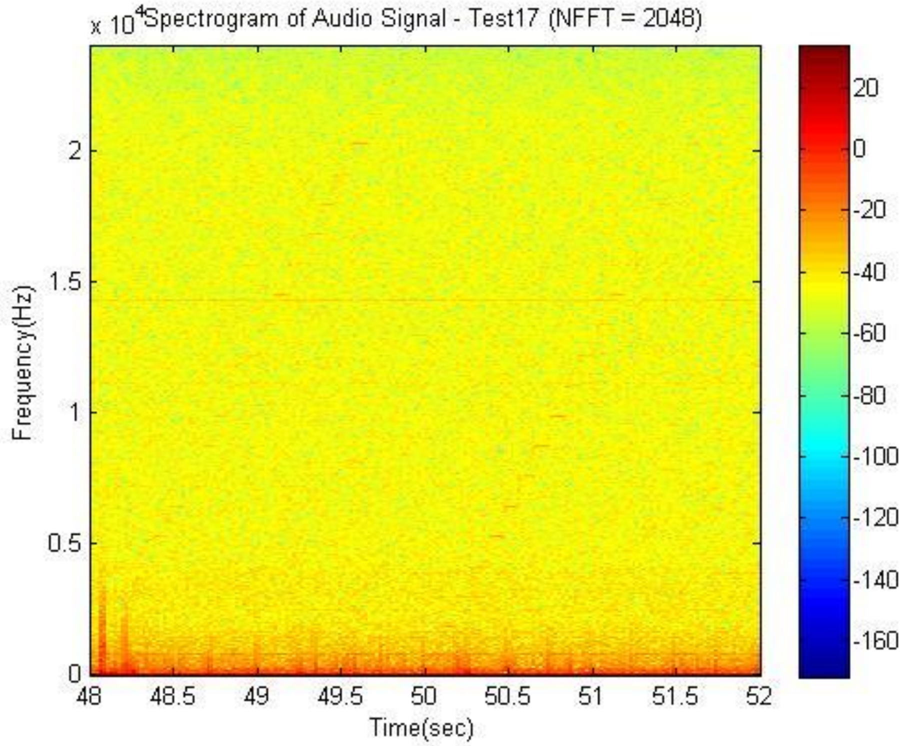

Figure 2.35. Computer Microphone: Horizontal Antenna Polarization.

Figure 2.35 illustrates that weak coupling occurred for horizontal antenna polarization, with the orange vertical lines representing the swept frequency message signal. In contrast, Figure 2.23 shows message coupling that was much stronger, with a higher visibility above the noise floor.

Two tests were performed to determine the signal strength needed to produce a measureable message in the recording. In the first test, the carrier frequency and message frequency were fixed while the input power (-127 dBm to 13 dBm) into the transmitting antenna was varied. In the second test, the same signal frequencies were used while the percent modulation was varied (1-99%). The message frequency was fixed at 10 kHz. Without any additional signal processing than that used to generate the plots, it was found that the message signal could be detected with a minimum of 0 dBm of carrier frequency input power and a 50% modulation depth for input power sweep testing. Similarly for modulation depth sweep testing, the minimum modulation depth for detection was about 15% with 11 dBm carrier frequency input power. Figure 2.36 and Figure 2.37 show the results from these experiments. These figures

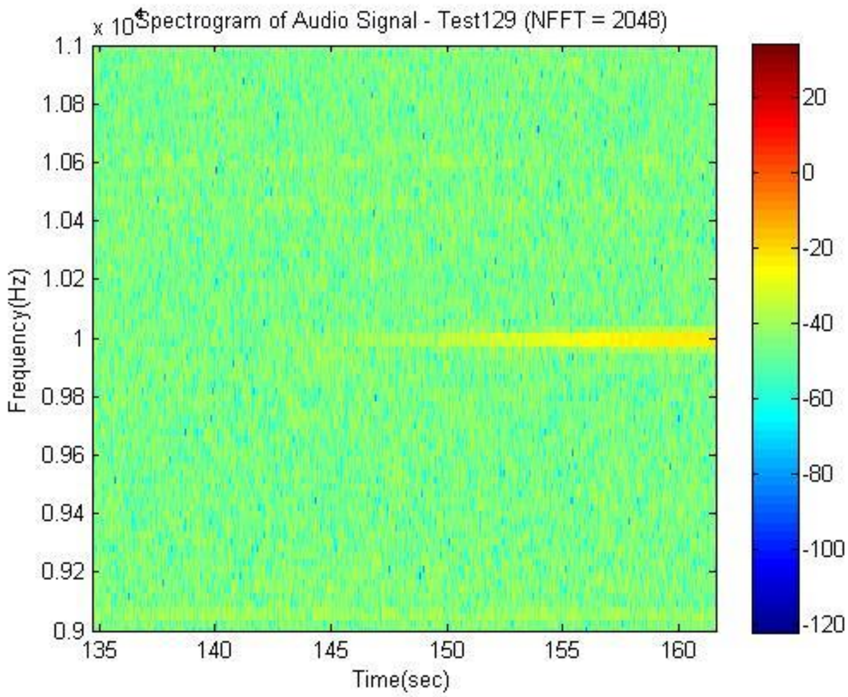

Figure 2.36. Computer Microphone: Carrier Frequency Input Power Sweep.

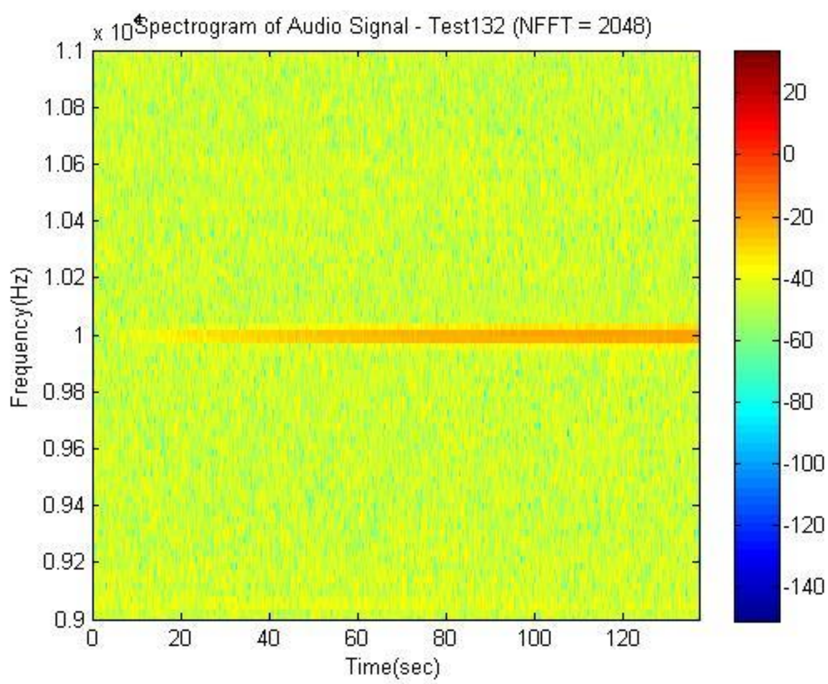

Figure 2.37. Computer Microphone: Modulation Depth Sweep.

show the general trend that as either the carrier frequency power or the percent modulation of the message signal becomes larger, the message couples better into the audio recordings. This increase in coupling is represented by the horizontal yellow (Figure 2.36) or red line (Figure 2.37) at 10 kHz that darkens in color over time.

To determine how the orientation of the computer microphone impacted testing, recordings were taken with turntable positions ranging from 0° to 355° at 5° increments while using a fixed coupling carrier frequency and message frequency. The recordings for each turntable position were nearly 20 seconds long. A PSD estimate was calculated for each recording, and the value at the message frequency was stored in a data array. This data array was then normalized with respect to the largest value and graphed in a polar plot as shown in Figure 2.38 and Figure 2.39. Message frequencies of 500 Hz, 10 kHz, and 22 kHz were tested in three separate sets of experiments. The polar plots generated for these messages were all similar in shape as verified by the additional plots in Appendix B.

Overall, coupled messages were fairly dependent on turntable position as shown in Figure 2.38 and Figure 2.39. The susceptibility pattern looks similar to a three leaf clover. For this set of tests, the most coupling occurred when the microphone was facing away from the antenna. It was found, however, that the susceptibility pattern of this device was extremely setup dependent. One extra susceptibility pattern test was taken in a different session of measurements. The results shown in Figure 2.40 and Figure 2.41 were generated from this measurement. The difference between these figures and Figure 2.38 and Figure 2.39 illustrate the sensitivity of the coupling pattern to the setup by the drastic change in shape of the coupling pattern.

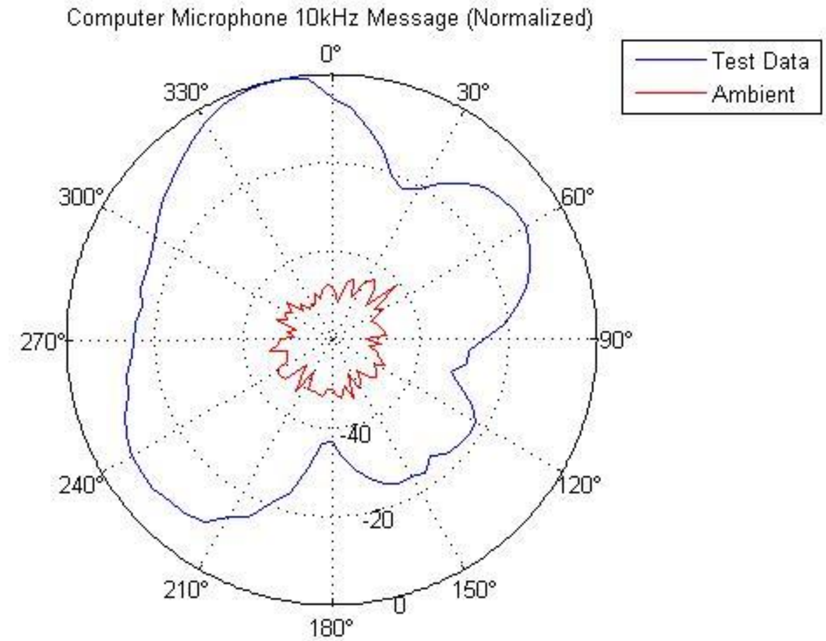

Figure 2.38. Computer Microphone: PSD Estimate Comparison Polar Plot for Message Frequency 10 kHz.

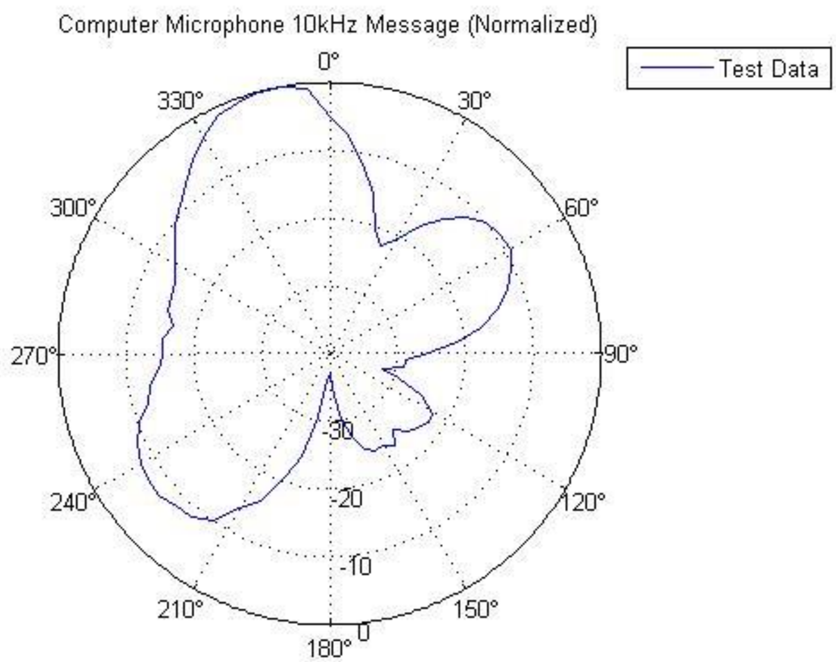

Figure 2.39. Computer Microphone: PSD Estimate Single Polar Plot for Message Frequency 10 kHz.

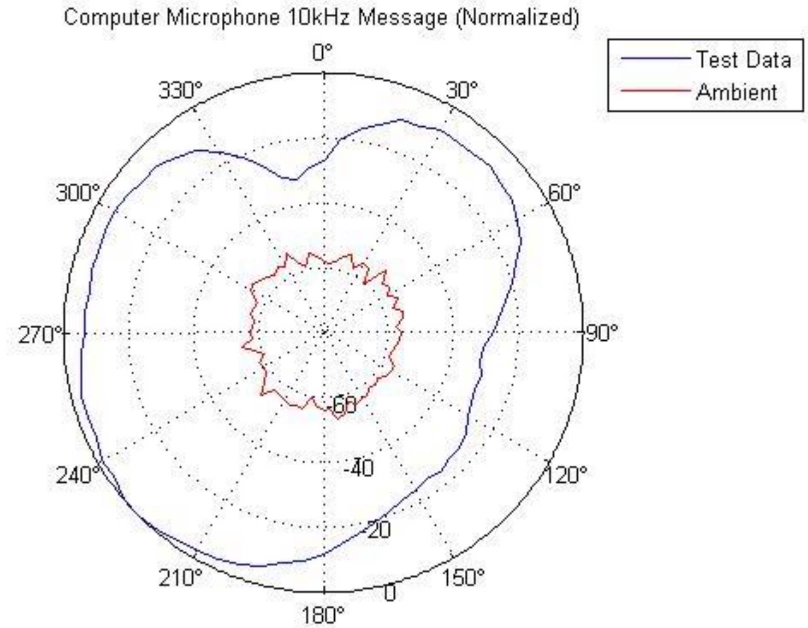

Figure 2.40. Computer Microphone: Additional PSD Estimate Comparison Polar Plot for Message Frequency 10 kHz.

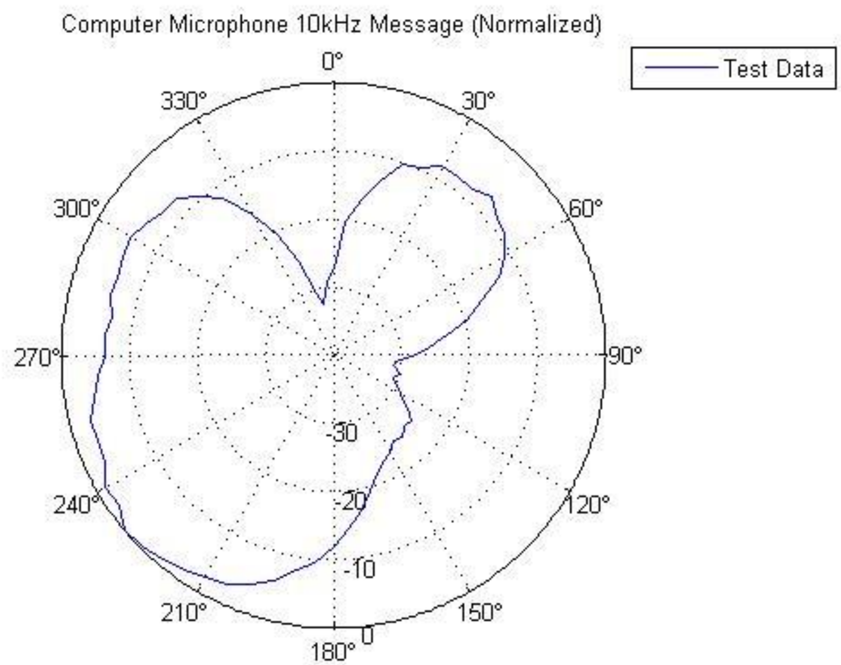

Figure 2.41. Computer Microphone: Additional PSD Estimate Single Polar Plot for Message Frequency 10 kHz.

2.2.3. Digital Video Camera

Figure 2.42 shows the testing setup for the digital video camera at a 0° turntable position.

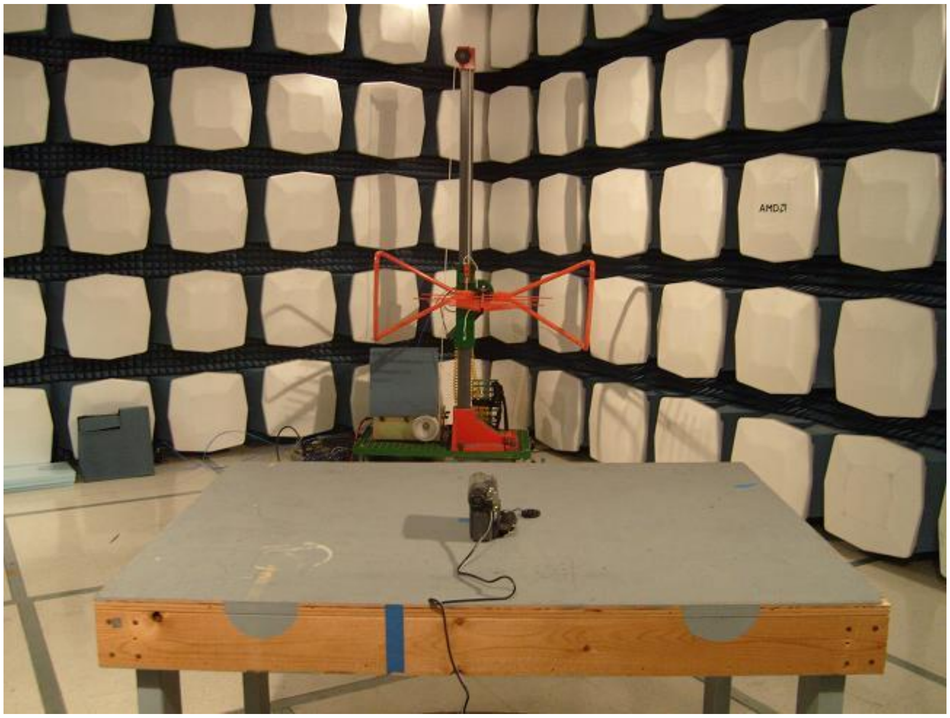

Figure 2.42. Digital Video Camera Chamber Testing Setup.

Although sweep tests were performed with a pure sine wave signal and with FM signals, these did not yield any coupled messages onto recordings with the digital video camera. Tests involving AM signals, however, did produce coupled messages in the recordings. Figures 2.43-2.45 show spectrogram plots produced under equivalent test conditions (same device orientation and antenna polarization) when a pure sine wave, an AM signal, and an FM signal was applied to the transmitting antenna.

The message coupling can be seen in Figure 2.44, represented by the vertical, dark red lines in the spectrogram plot. Due to the audio leveling properties of this device, the message signal is more difficult to identify in the spectrogram than for previously studied devices. The message signal was ramped over a two second interval from 440 Hz to 25 kHz. This ramped sweep can be seen in the plot shown in Figure 2.44. The lines are dotted because the message signal was swept discretely in frequency with a DC power supply. No lines representing the frequency ramping message appear in Figure 2.43 and Figure 2.45. The carrier frequency was ramping from 206 MHz to 228 MHz in the plots during the time interval shown.

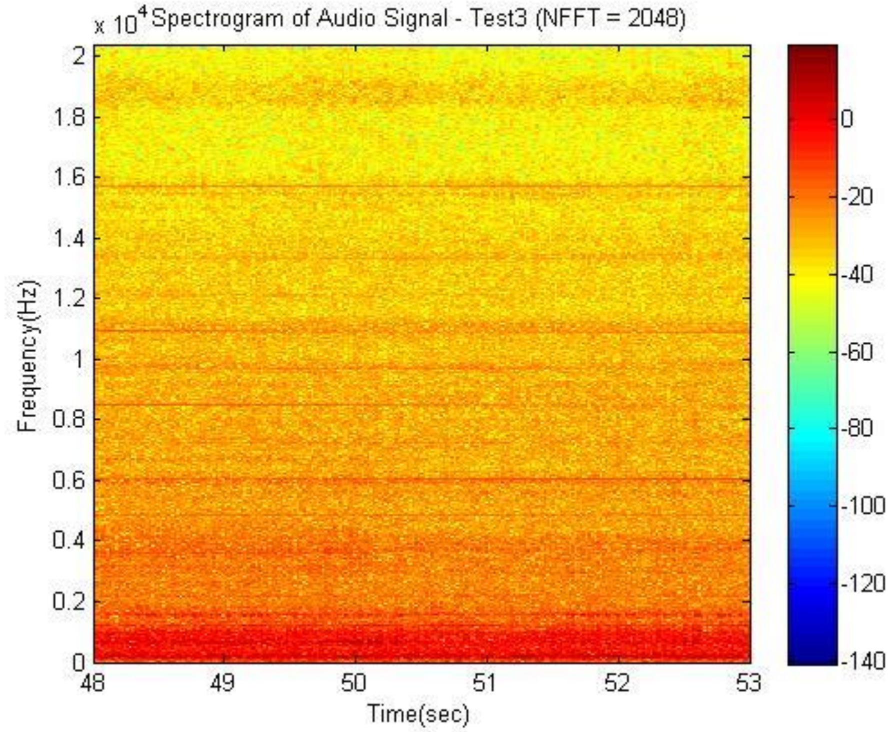

Figure 2.43. Digital Video Camera: Sine Wave Sweep.

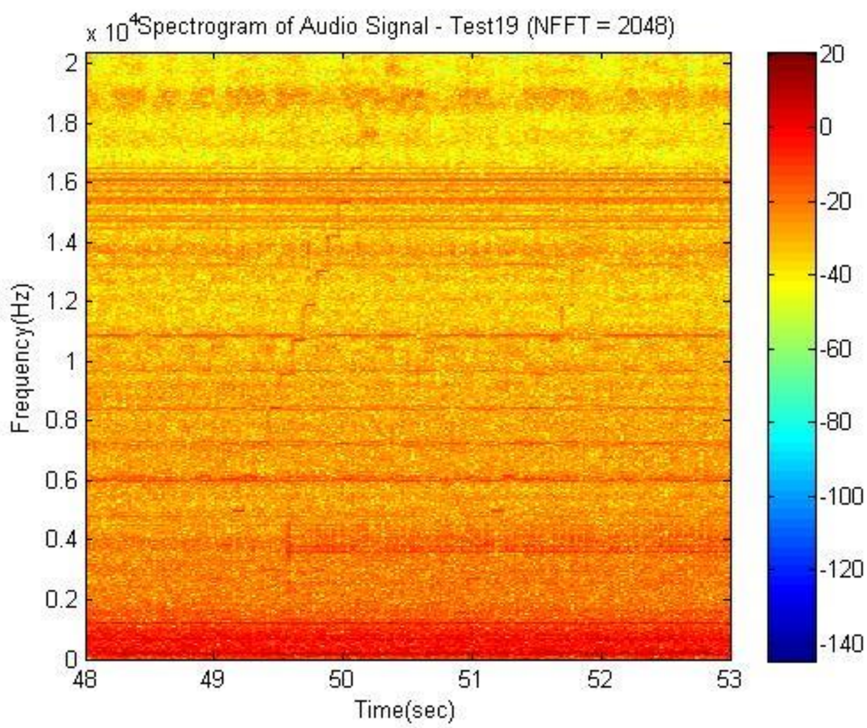

Figure 2.44. Digital Video Camera: AM with Simultaneous Carrier Sweep and Message Sweep.

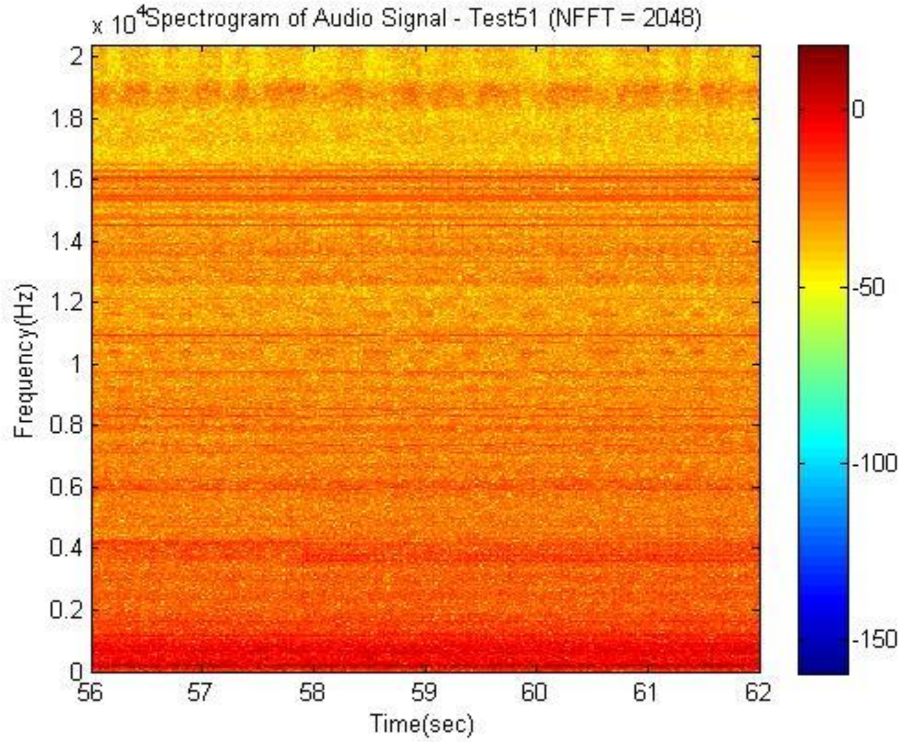

Figure 2.45. Digital Video Camera: FM with Simultaneous Carrier Sweep and Message Sweep.

Specific testing with this device found only one coupling carrier frequency range that produced measureable signals in the recordings: 202-218 MHz. Within this frequency range, the coupling was strongest for carrier frequencies from 208-213 MHz. Figure 2.46 shows an example of message coupling in the strongest carrier frequency range. This figure shows that when the carrier frequency was set to a frequency within the strong coupling range, the messages can easily be seen above the noise floor. To determine the message signal frequency limits, the carrier frequency was set to one strong coupling carrier frequency and the message signal was swept in frequency over the range 465 Hz-25 kHz in one instance, and 47 Hz-2 kHz in another. The message frequency limits for the digital video camera were approximately 1 kHz-20.4 kHz. The limits were not carrier frequency dependent as long as the carrier frequency was within the strong coupling range. Figure 2.47 and Figure 2.48 display the results from these experiments.

The upper message frequency limit as suggested by Figure 2.47 was around 20.4 kHz, which also represented the cutoff frequency above which signals were severely attenuated. This attenuation is represented in blue in Figure 2.47. The attenuation could be caused by a filter

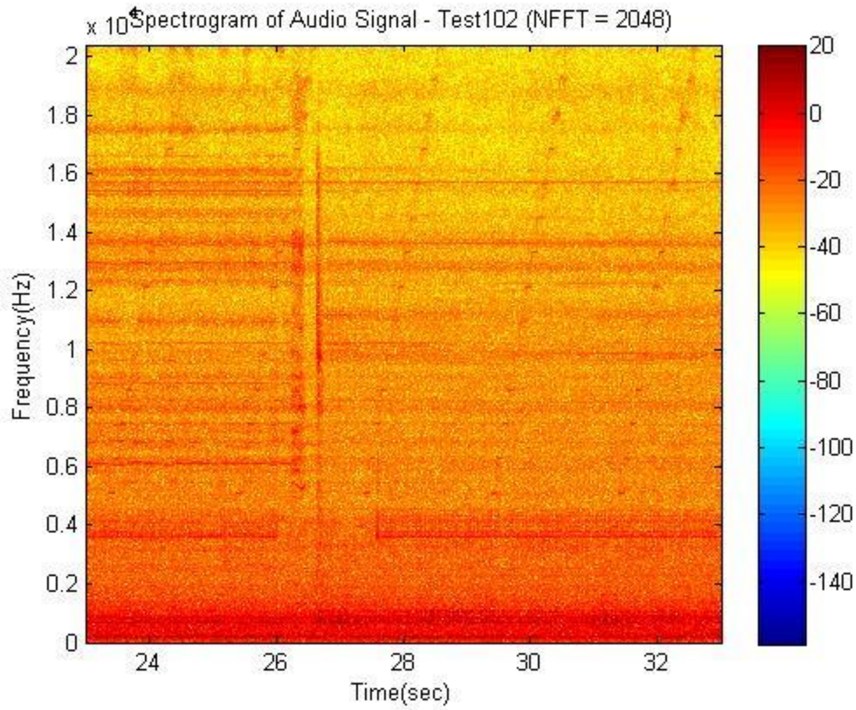

Figure 2.46. Digital Video Camera: Strong Coupling Range.

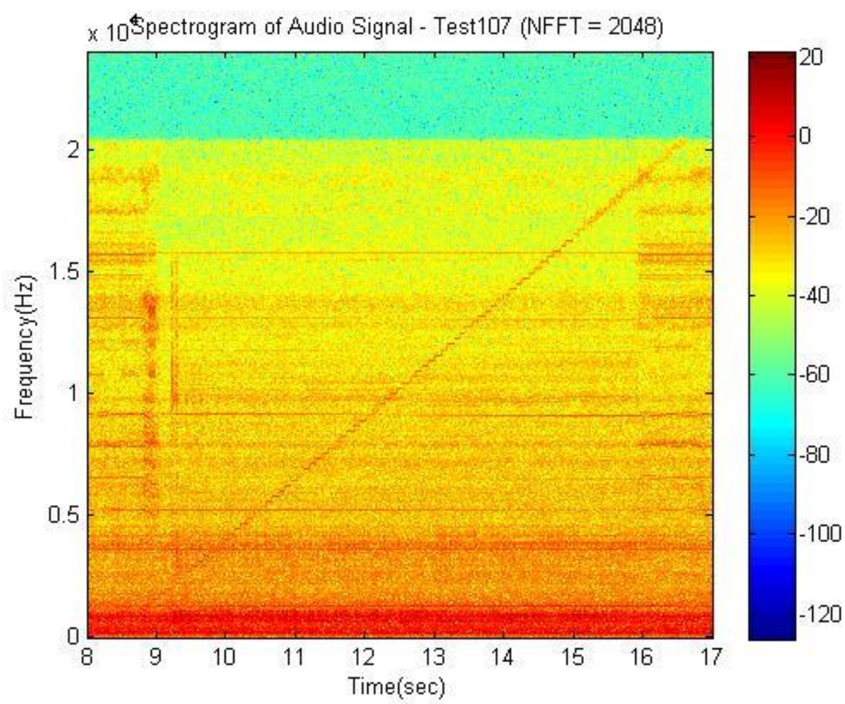

Figure 2.47. Digital Video Camera: Message Frequency Total Limits Testing with 211 MHz Carrier Frequency.

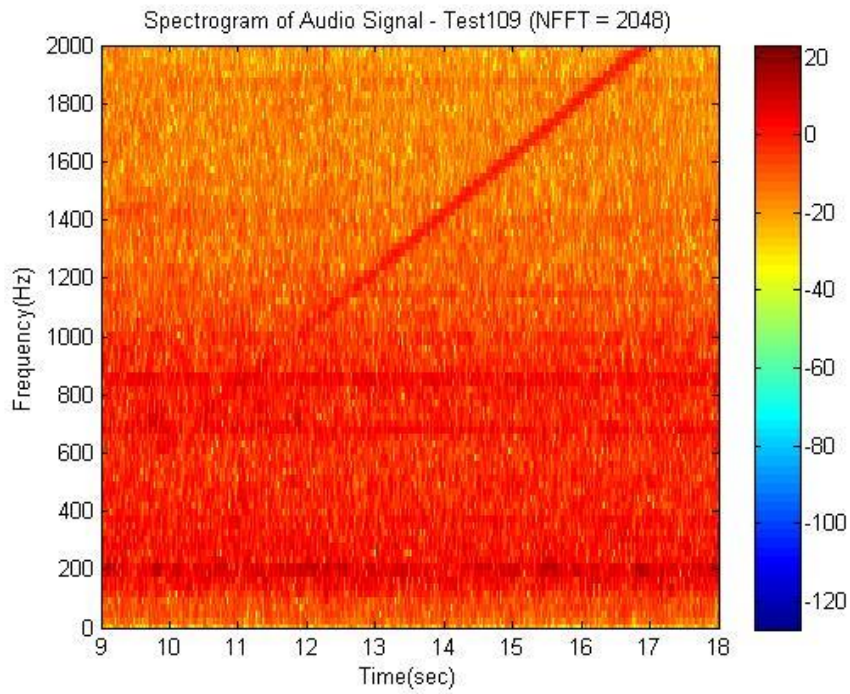

Figure 2.48. Digital Video Camera: Message Frequency Lower Limit Testing with 211 MHz Carrier Frequency.

present in the digital video camera, or a digital filter that was applied to the audio data when it was extracted by an audio editing program. Figure 2.48 shows that the lower limit for message coupling was around 1 kHz because it is at this frequency that the dark red line representing the swept frequency message vanishes.

Additional testing was performed to show that the coupled messages in the recordings were the same as the messages created by the signal generators. The carrier frequency was fixed, and messages were transmitted at a few fixed frequencies. The recordings were analyzed by creating a PSD estimate plot using Welch's method. Figures 2.49-2.52 show a few of the results from these experiments. Additional plots can also be found in Appendix B.

The message signal spikes in the PSD plots show a strong correlation between the messages seen on the recordings and the messages input to the modulation source. For example, for the data shown in Figure 2.51, a 10 kHz message was applied to the modulation source while a recording was made. Spectral analysis of the recording made under these test conditions revealed a coupled message at 10 kHz, showing that the coupled message was equivalent to the original message applied to the modulation source. Figure 2.49 provides a PSD plot of the full

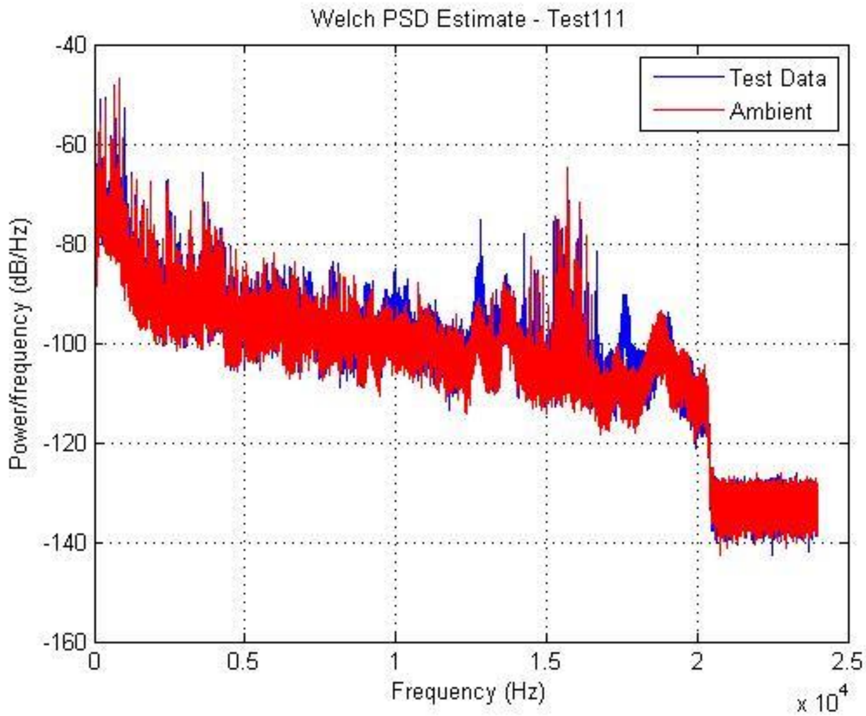

Figure 2.49. Digital Video Camera: PSD Estimate with 211 MHz Carrier Frequency and 1 kHz Message (Full Frequency Range).

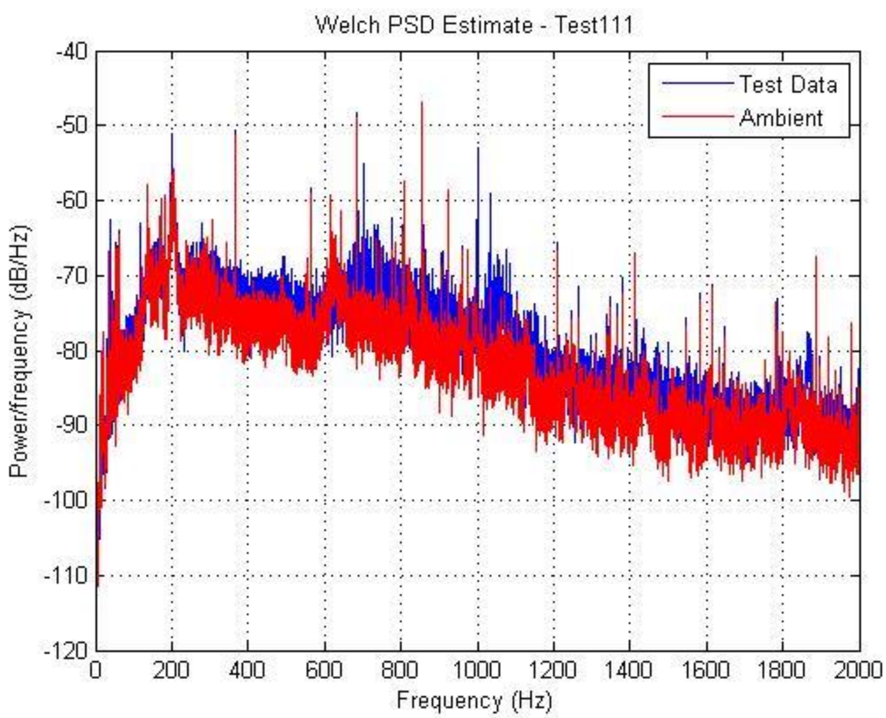

Figure 2.50. Digital Video Camera: PSD Estimate with 211 MHz Carrier Frequency and 1 kHz Message (Expanded Near 1 kHz).

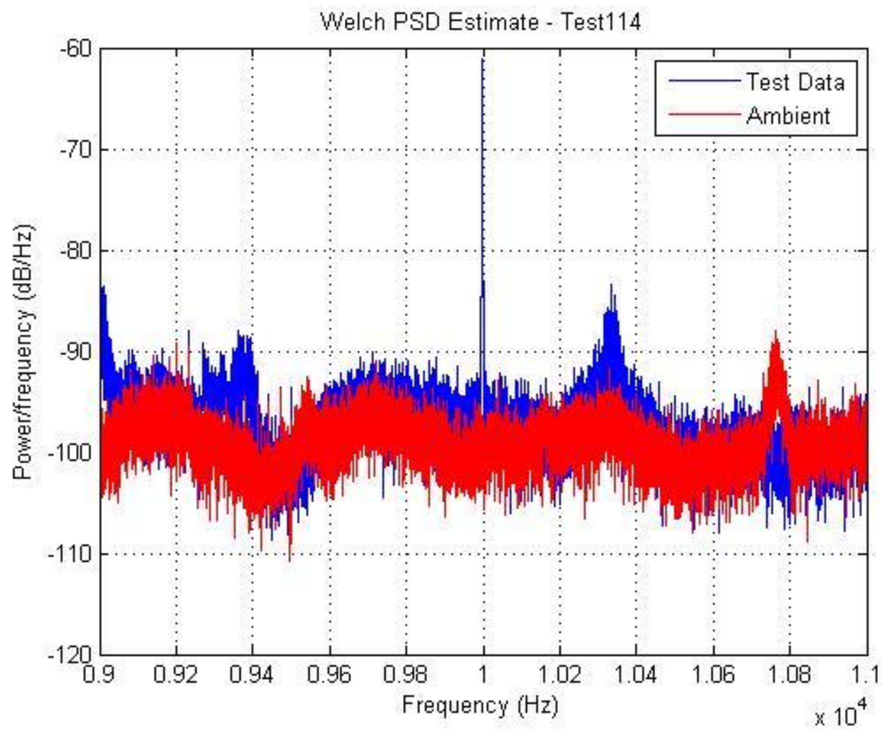

Figure 2.51. Digital Video Camera: PSD Estimate with 211 MHz Carrier Frequency and 10 kHz Message (Expanded Near 10 kHz).

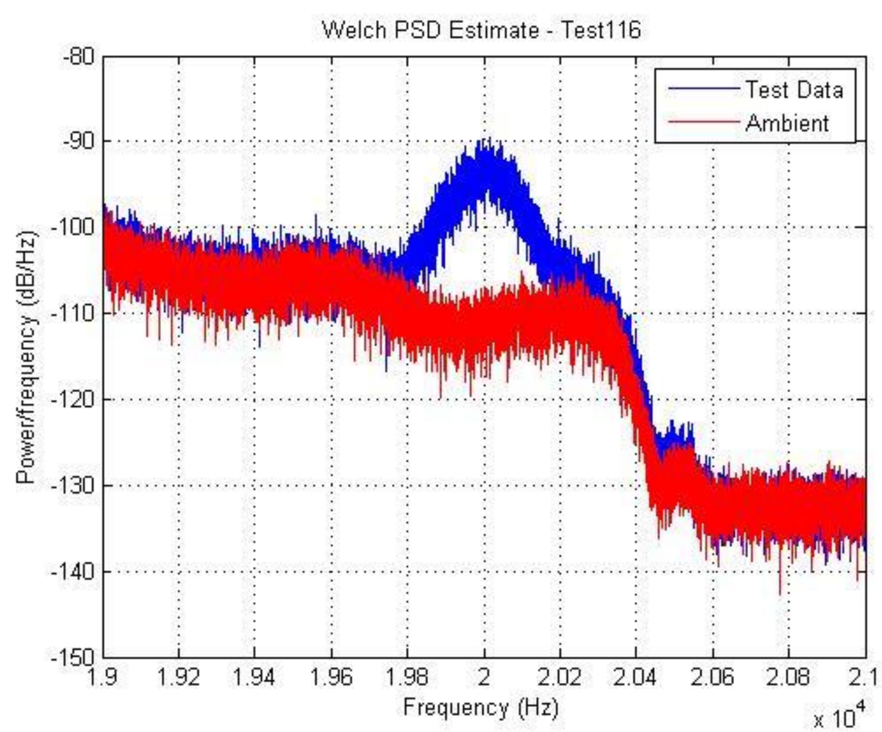

Figure 2.52. Digital Video Camera: PSD Estimate with 211 MHz Carrier Frequency and 20 kHz Message (Expanded Near 20 kHz).

frequency spectrum of an example recording so that it may be compared to previous spectrogram plots.

In order to couple a message into the digital video camera, the antenna polarization must be horizontally polarized with respect to the camera position in Figure 2.42. For tests with vertical antenna polarization, no detectable coupling occurred. Figure 2.44 and Figure 2.53 show results from two identical tests where the carrier frequency and message signals were swept, but the antenna polarizations were different. The message signal was ramping over a two second interval from 440 Hz to 25 kHz, and the carrier frequency was ramping from 206 MHz to 228 MHz. Recall that the message frequency limits for the digital video camera were approximately 1 kHz-20.4 kHz. The data shown in Figure 2.44 was taken with a horizontal antenna polarization. The data shown in Figure 2.53 was taken with a vertical antenna polarization. This figure illustrates that no coupling occurred for vertical antenna polarization by the lack of dark red vertical lines representing the swept frequency message signal. In contrast, Figure 2.44 shows message coupling with the presence of dark red vertical lines representing the swept frequency message signal.

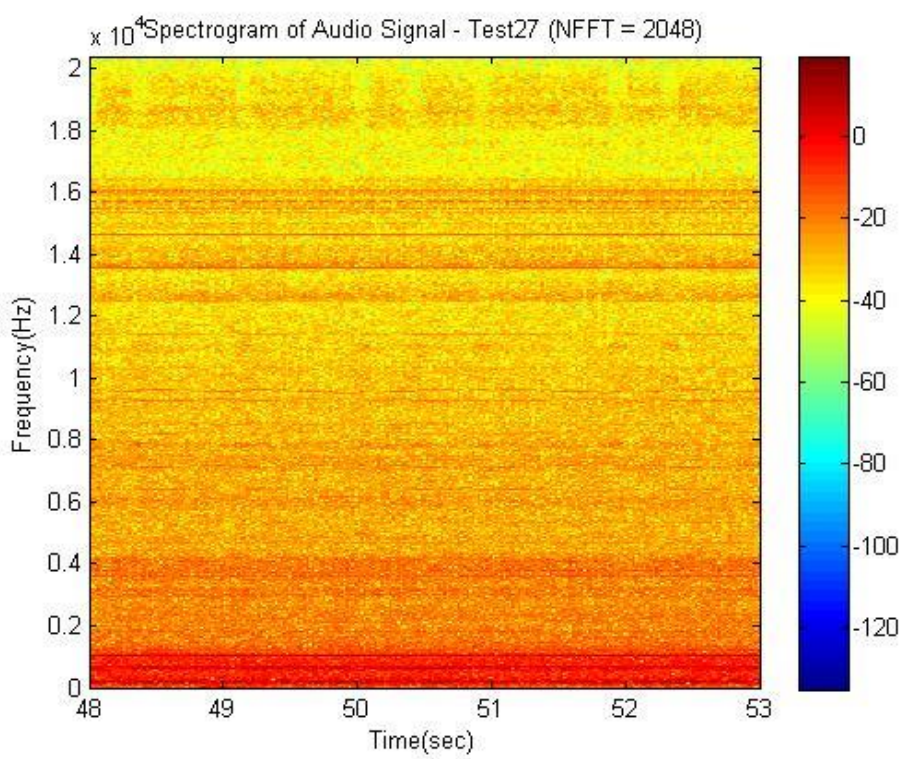

Figure 2.53. Digital Video Camera: Vertical Antenna Polarization.

Two tests were performed to determine the signal strength needed to produce a measureable message in the recording. In the first test, the carrier frequency and message frequency were fixed while the input power (-127 dBm to 13 dBm) into the transmitting antenna was varied. In the second test, the same signal frequencies were used while the percent modulation was varied (1-99%). The message frequency was fixed at 10 kHz. Without any additional signal processing than that used to generate the plots, it was found that the message signal could be detected with a minimum of 0 dBm of carrier frequency input power and a 50% modulation depth for input power sweep testing. Similarly for modulation depth sweep testing, the minimum modulation depth for detection was about 8% with 11 dBm carrier frequency input power. Figure 2.54 and Figure 2.55 show the results from these experiments. These figures show the general trend that as either the carrier frequency power or the percent modulation of the message signal becomes larger, the message couples better into the audio recordings. This increase in coupling is represented by the horizontal red line at 10 kHz that darkens in color over time.

To determine how the orientation of the digital video camera impacted testing, recordings were taken with turntable positions ranging from 0° to 355° at 5° increments while using a fixed coupling carrier frequency and message frequency. The recordings for each turntable position were nearly 20 seconds long. A PSD estimate was calculated for each recording, and the value at the message frequency was stored in a data array. This data array was then normalized with respect to the largest value and graphed in a polar plot as shown in Figure 2.56 and Figure 2.57. Message frequencies of 1 kHz, 10 kHz, and 20 kHz were tested in three separate sets of experiments. The polar plots generated for these messages were all similar in shape as verified by the additional plots in Appendix B.

Aside from two nulls in coupling that occurred at 0° and 180°, which correspond to when the digital video camera had the least surface area exposed, the susceptibility pattern of the digital video camera was fairly independent of turntable position. The susceptibility pattern looks similar to one of the cut planes of the radiation pattern for a dipole antenna [2].

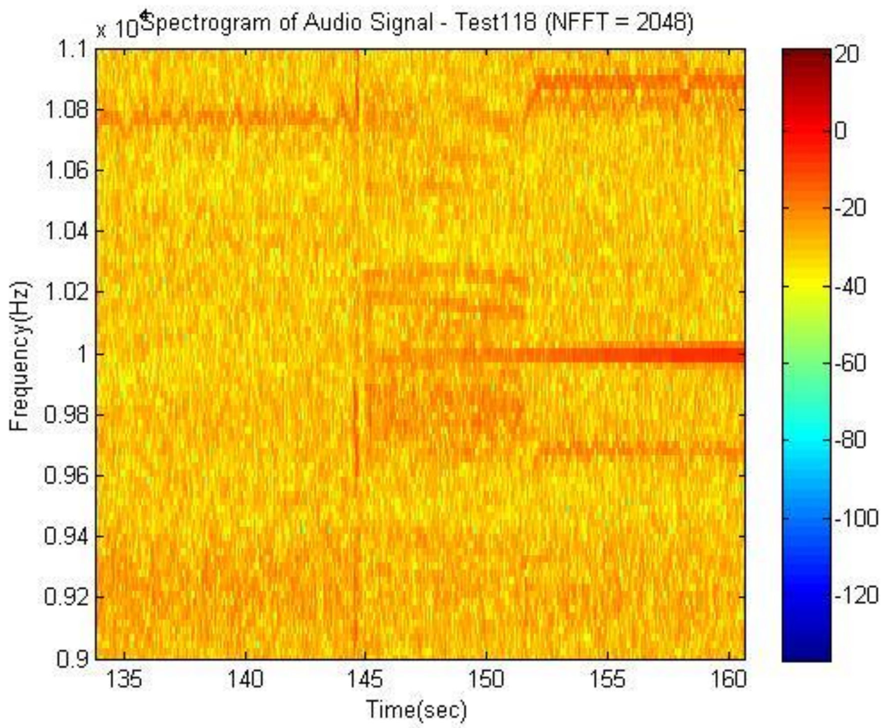

Figure 2.54. Digital Video Camera: Carrier Frequency Input Power Sweep.

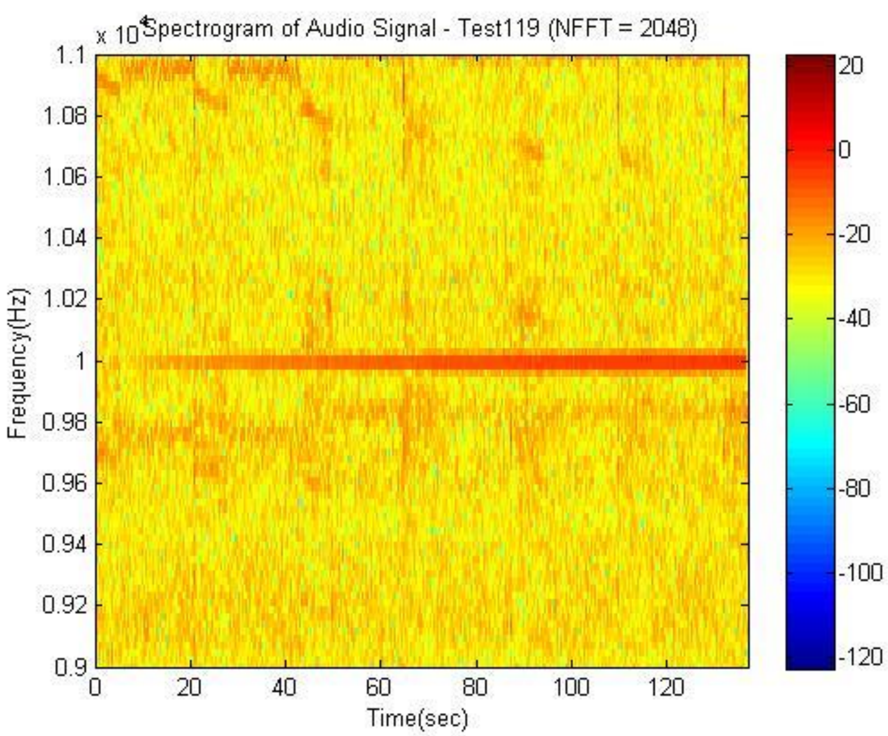

Figure 2.55. Digital Video Camera: Modulation Depth Sweep.

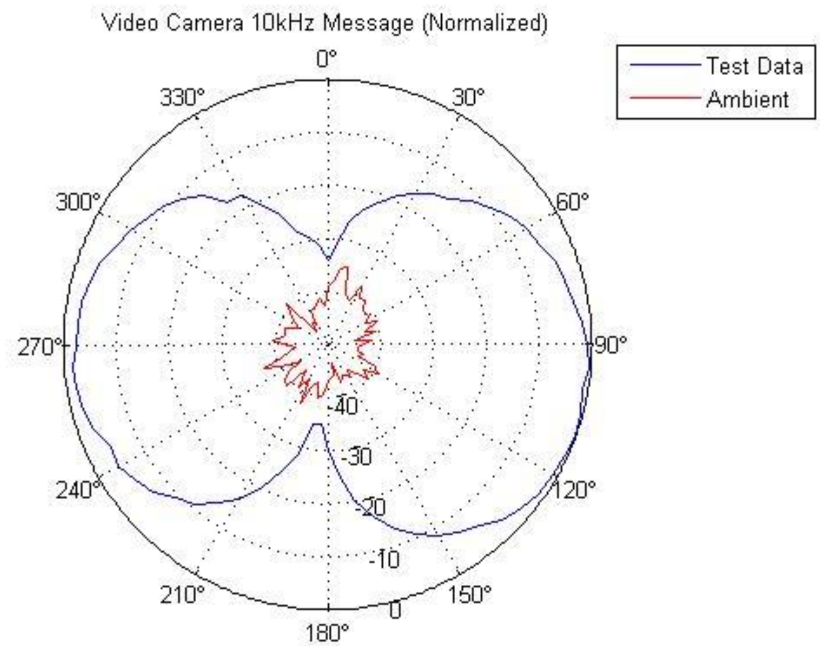

Figure 2.56. Digital Video Camera: PSD Estimate Comparison Polar Plot for Message Frequency 10 kHz.

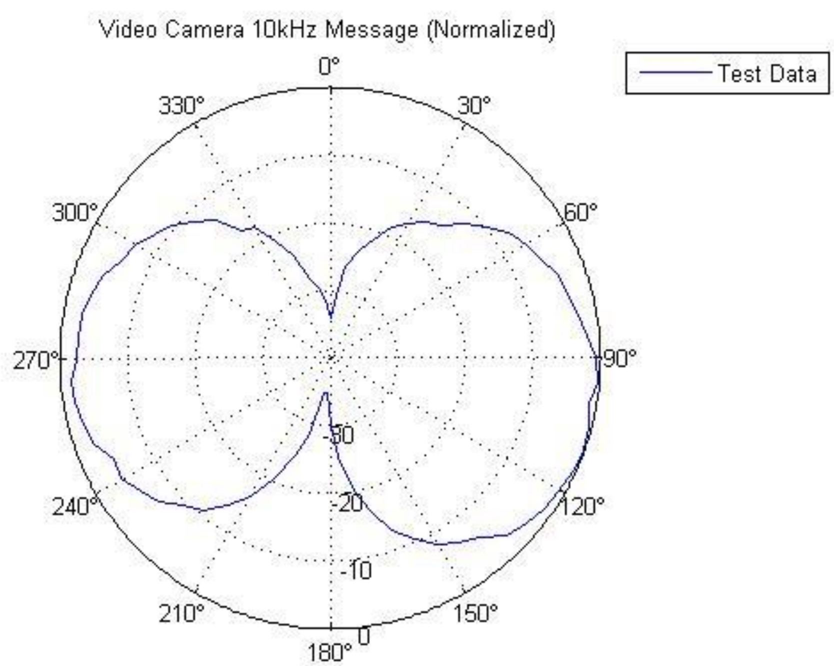

Figure 2.57. Digital Video Camera: PSD Estimate Single Polar Plot for Message Frequency 10 kHz.

2.2.4. Wireless Microphone System

Figure 2.58 shows the testing setup for the wireless microphone system at a 0° turntable position.

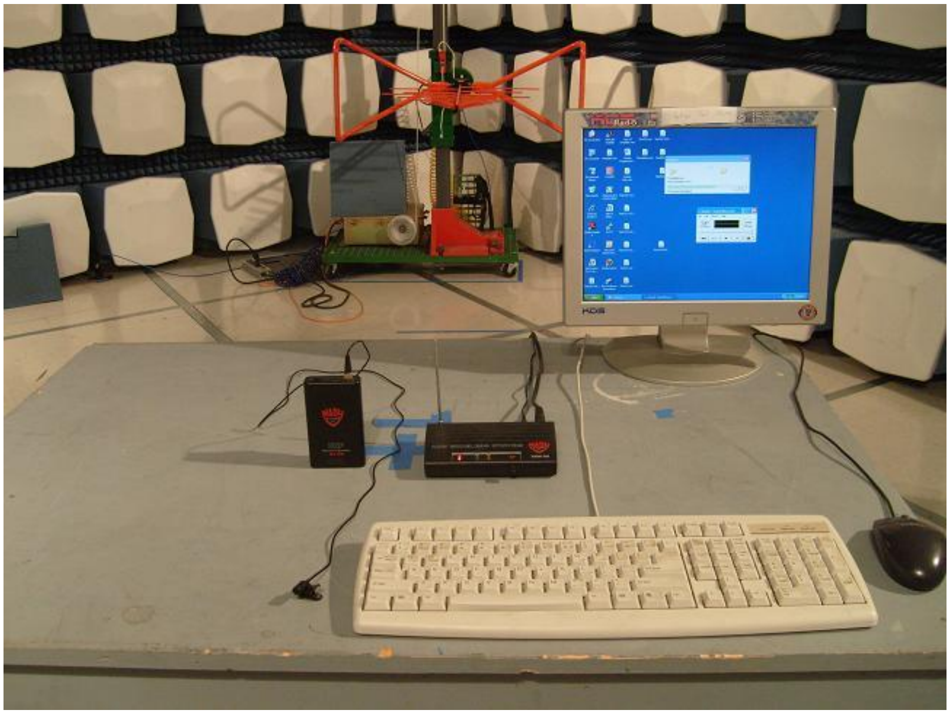

Figure 2.58. Wireless Microphone System Chamber Testing Setup.

Although sweep tests were performed with a pure sine wave signal and with FM signals, these did not yield any coupled messages onto recordings with the wireless microphone system. Tests involving AM signals, however, did produce coupled messages in the recordings. Figures 2.59-2.61 show spectrogram plots produced under equivalent test conditions (same device orientation and antenna polarization) when a pure sine wave, an AM signal, and an FM signal was applied to the transmitting antenna.

The message coupling can be seen in Figure 2.60, represented by the vertical, red and yellow lines in the spectrogram plot. In addition, the message coupling can easily be heard. The message signal was ramped over a two second interval from 440 Hz to 25 kHz. This ramped sweep can clearly be seen in the plot shown in Figure 2.60. The lines are dotted because the message signal was swept discretely in frequency with a DC power supply. No lines representing the frequency ramping message appear in Figure 2.59 and Figure 2.61. The carrier frequency was ramping from 304 MHz to 330 MHz in the plots during the time interval shown.

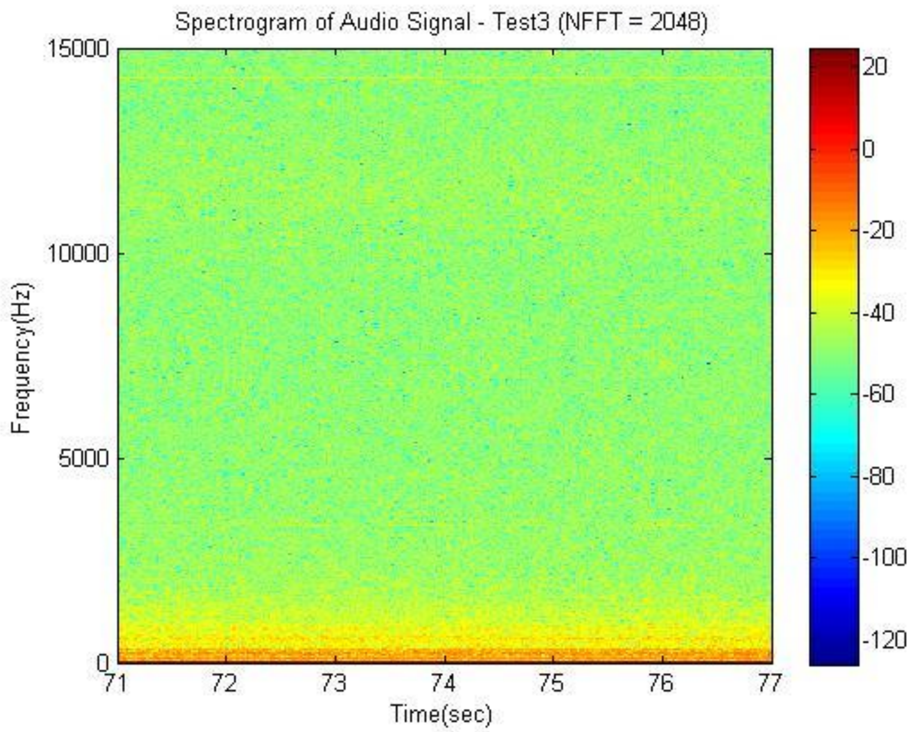

Figure 2.59. Wireless Microphone System: Sine Wave Sweep.

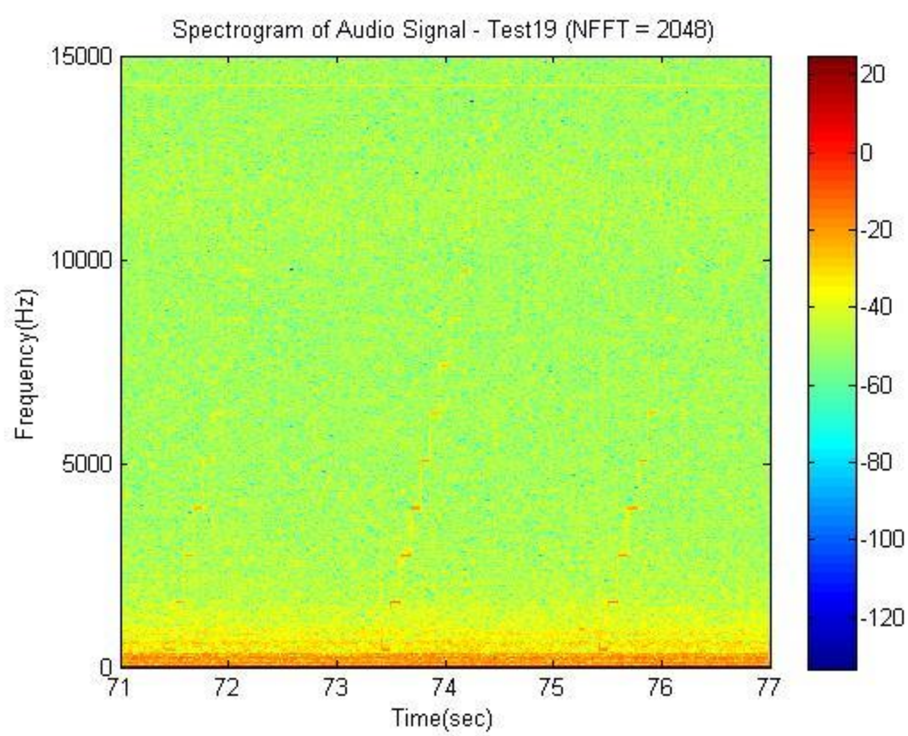

Figure 2.60. Wireless Microphone System: AM with Simultaneous Carrier Sweep and Message Sweep.

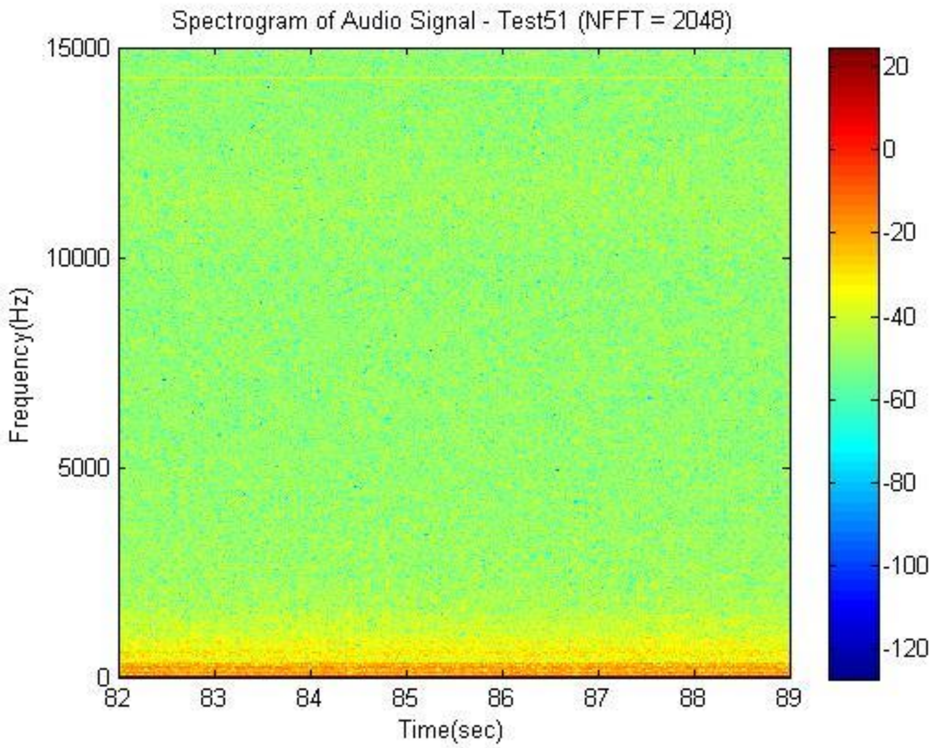

Figure 2.61. Wireless Microphone System: FM with Simultaneous Carrier Sweep and Message Sweep.

Specific testing with this device revealed the ability to couple a message at different carrier frequencies was highly dependent on the test setup. The coupling was sensitive to orientation and antenna polarization depending on the coupling frequency. With a different, but nearly identical setup than that used for the data shown in Figures 2.59-2.61, the coupling frequency range that produced the largest measureable signals in the recordings was 241-298 MHz. Within this frequency range, the coupling was strongest from 250-259 MHz. Figure 2.62 shows an example of message coupling in the strongest carrier frequency range. This figure shows that when the carrier frequency was set to a frequency within the strong coupling range, the messages can easily be seen above the noise floor.

To determine the message signal frequency limits, the carrier frequency was set to a strong coupling carrier frequency and the message signal was swept in frequency over the range 471 Hz-25 kHz in one instance, and 25 Hz-1.5 kHz in another. The message frequency limits for the wireless microphone system were approximately 25 Hz-24 kHz. The limits were not carrier frequency dependent as long as the carrier frequency was within the strong coupling range. For some of the lower frequency messages, the harmonics of the messages also coupled into the

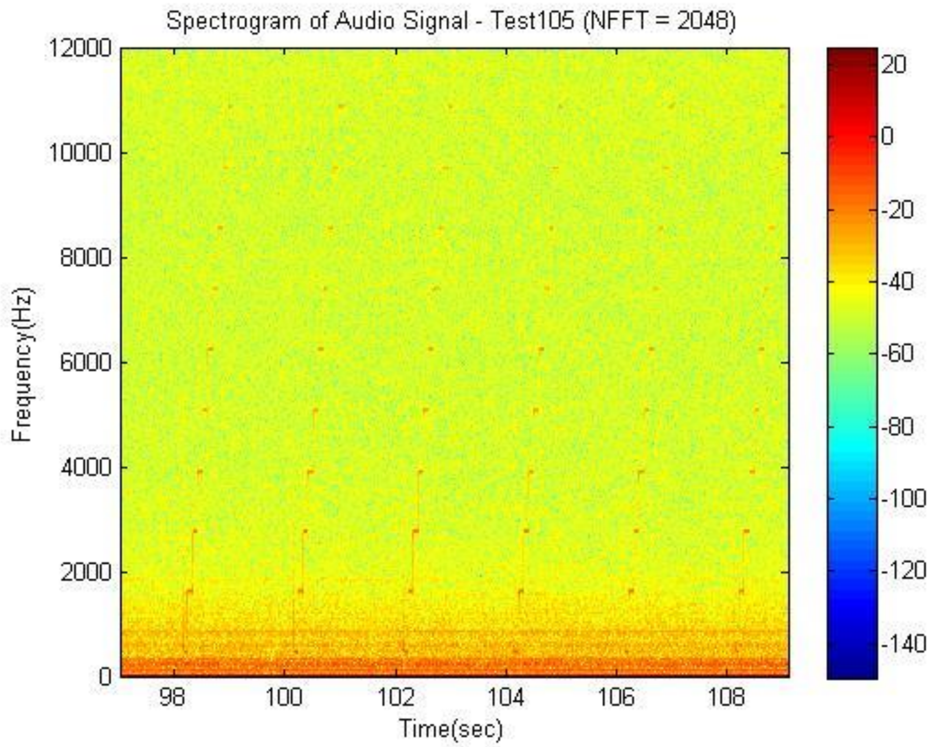

Figure 2.62. Wireless Microphone System: Strong Coupling Range.

recordings. Figure 2.63 and Figure 2.64 display the results from these experiments. The upper limit to message coupling was 24 kHz since Figure 2.63 shows the swept message signal without bound up to this frequency. Figure 2.64 shows that the lower limit for the message coupling was around 25 Hz because it is at this frequency that the red line representing the swept frequency message vanishes.

Additional testing was performed to show that the coupled messages in the recordings were the same as the messages created by the signal generators. The carrier frequency was fixed, and messages were transmitted at a few fixed frequencies. The recordings were analyzed by creating a PSD estimate plot using Welch's method. Figures 2.65-2.68 show the results from these experiments. Additional plots can also be found in Appendix B.

The message signal spikes in the PSD plots show a strong correlation between the messages seen in the recordings and the messages input to the modulation source. For example, for the data shown in Figure 2.66, a 200 Hz message was applied to the modulation source while a recording was made. Spectral analysis of the recording made under these test conditions revealed a coupled message at 200 Hz, showing that the coupled message was equivalent to the

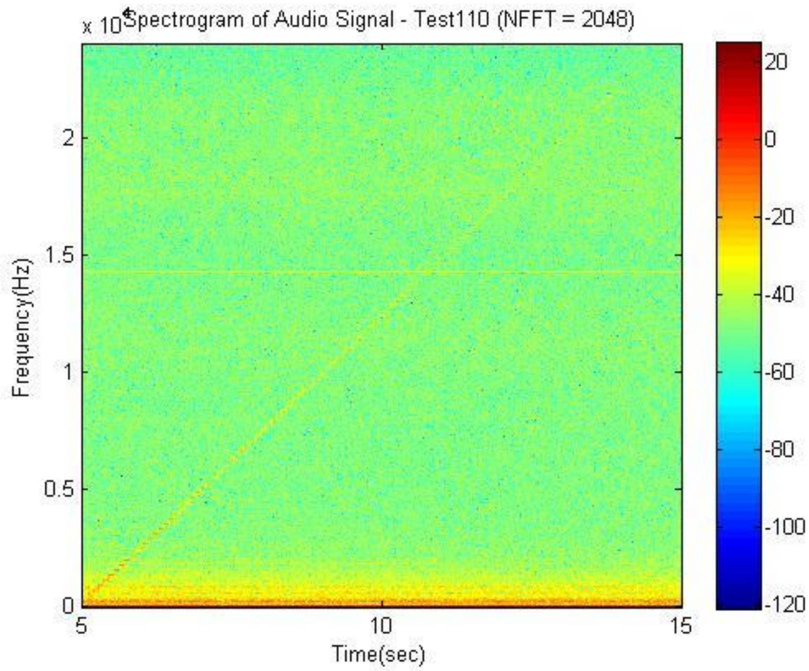

Figure 2.63. Wireless Microphone System: Message Frequency Total Limits Testing with 254 MHz Carrier Frequency.

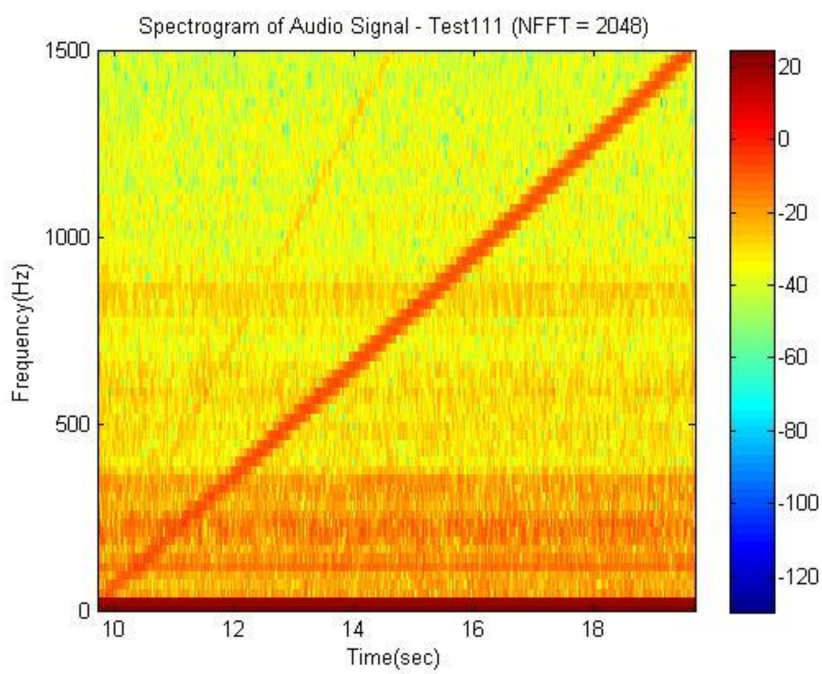

Figure 2.64. Wireless Microphone System: Message Frequency Lower Limit Testing with 254 MHz Carrier Frequency.

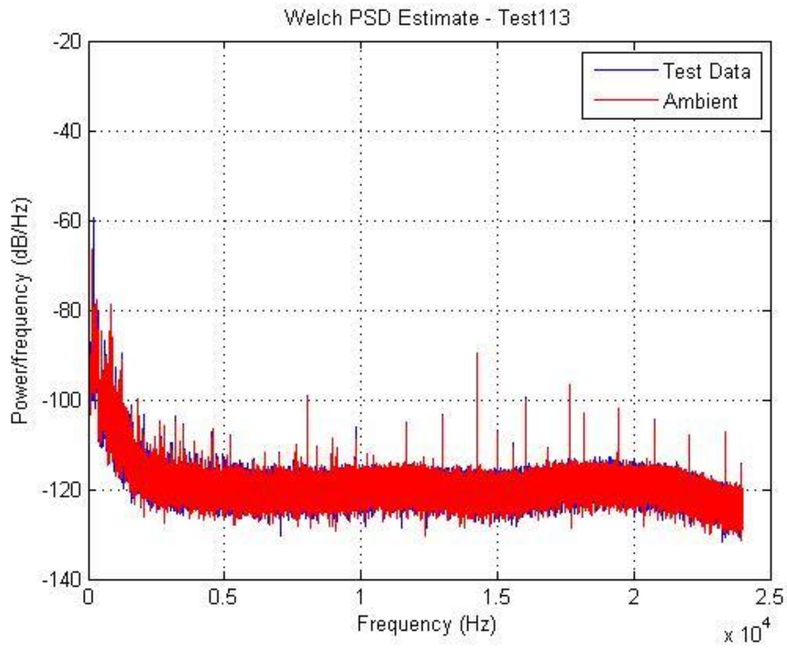

Figure 2.65. Wireless Microphone System: PSD Estimate with 254 MHz Carrier Frequency and 200 Hz Message (Full Frequency Range).

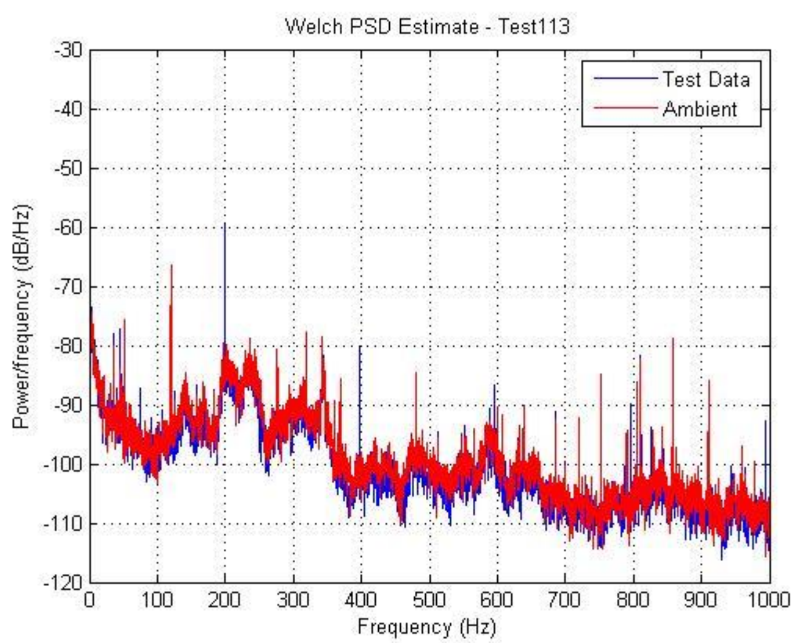

Figure 2.66. Wireless Microphone System: PSD Estimate with 254 MHz Carrier Frequency and 200 Hz Message (Expanded Near 200 Hz).

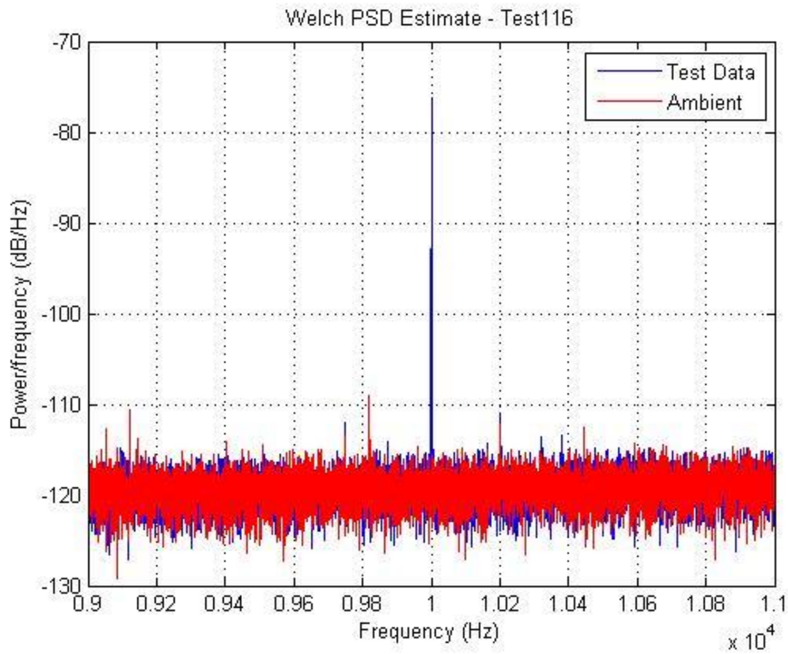

Figure 2.67. Wireless Microphone System: PSD Estimate with 254 MHz Carrier Frequency and 10 kHz Message (Expanded Near 10 kHz).

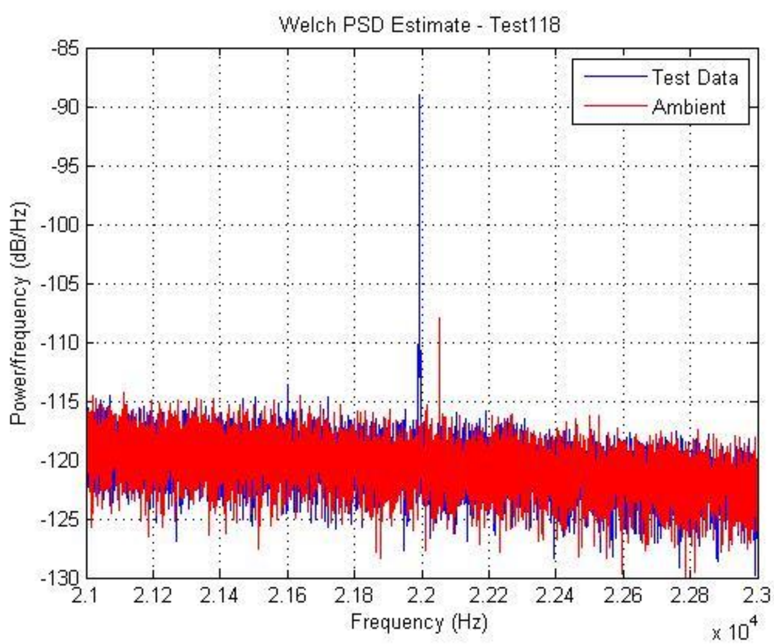

Figure 2.68. Wireless Microphone System: PSD Estimate with 254 MHz Carrier Frequency and 22 kHz Message (Expanded Near 22 kHz).

original message applied to the modulation source. Figure 2.65 provides a PSD plot of the full frequency spectrum of an example recording so that is may be compared to previous spectrogram plots.

In order to couple a message into the wireless microphone system, the antenna polarization could be horizontally or vertically polarized with respect to the microphone system position in Figure 2.58. Overall, stronger coupling occurred for the horizontal antenna polarization. Figure 2.60 shows results for an example case where there was a horizontal antenna polarization. The coupling with vertical antenna polarization was too weak to easily be seen on a spectrogram, and could barely be heard on the audio recordings when it occurred.

Two tests were performed to determine the signal strength needed to produce a measureable message in the recording. In the first test, the carrier frequency and message frequency were fixed while the input power (-127 dBm to 13 dBm) into the transmitting antenna was varied. In the second test, the same signal frequencies were used while the percent modulation was varied (1-99%). The message frequency was fixed at 2 kHz. Without any additional signal processing than that used to generate the plots, it was found that the message signal could be detected with a minimum of 0 dBm of carrier frequency input power and a 50% modulation depth for input power sweep testing. Similarly for modulation depth sweep testing, the minimum modulation depth for detection was about 5% with 11 dBm carrier frequency input power. Figure 2.69 and Figure 2.70 show the results from these experiments. These figures show the general trend that as either the carrier frequency power or the percent modulation of the message signal becomes larger, the message couples better into the audio recordings. This increase in coupling is represented by the horizontal red line at 2 kHz that darkens in color over time.

To determine how the orientation of the wireless microphone system impacted testing, recordings were taken with turntable positions ranging from 0° to 355° at 5° increments while using a fixed coupling carrier frequency and message frequency. The recordings for each turntable position were nearly 20 seconds long. A PSD estimate was calculated for each recording, and the value at the message frequency was stored in a data array. This data array was then normalized with respect to the largest value and graphed in a polar plot as shown in Figure 2.71 and Figure 2.72. Message frequencies of 200 Hz, 2 kHz, and 22 kHz were tested in three

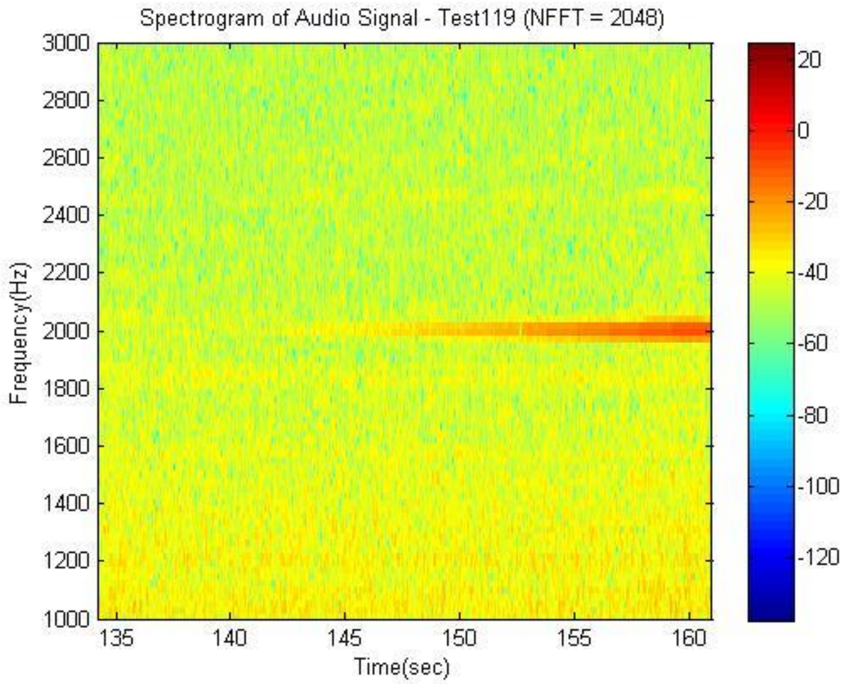

Figure 2.69. Wireless Microphone System: Carrier Frequency Input Power Sweep.

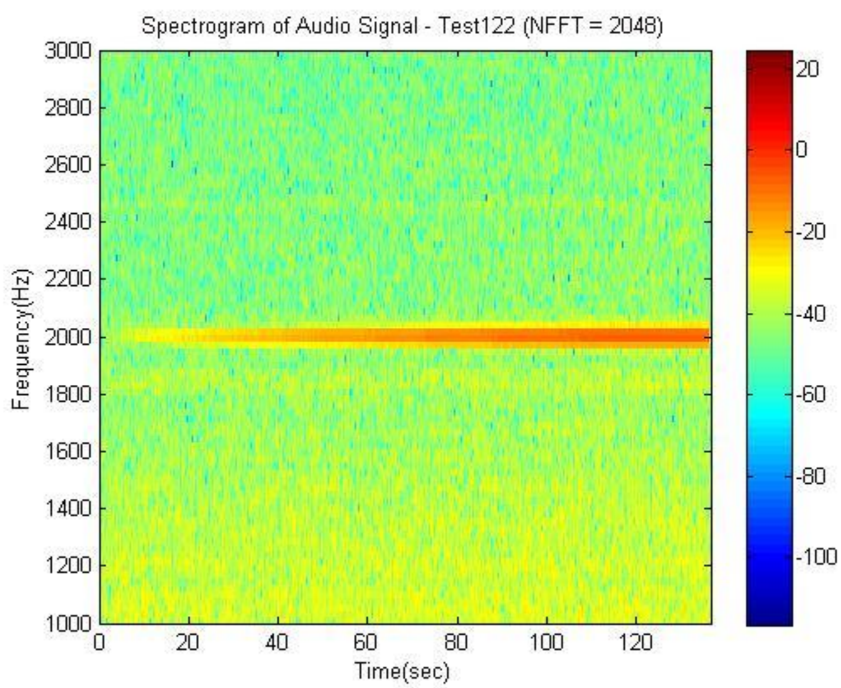

Figure 2.70. Wireless Microphone System: Modulation Depth Sweep.

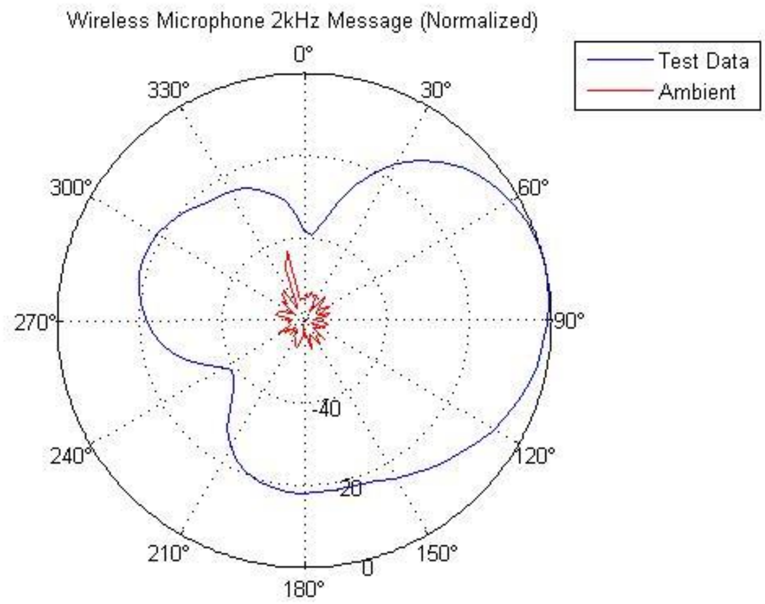

Figure 2.71. Wireless Microphone System: PSD Estimate Comparison Polar Plot for Message Frequency 2 kHz.

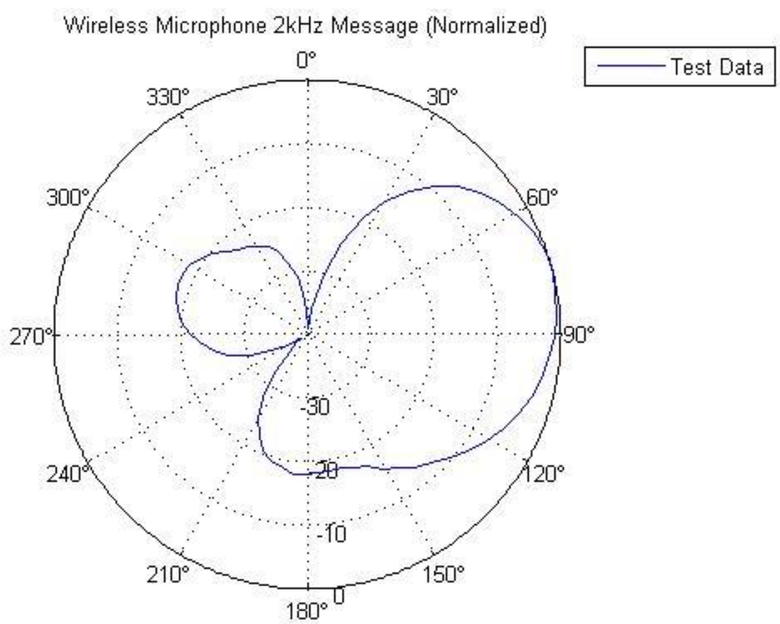

Figure 2.72. Wireless Microphone System: PSD Estimate Single Polar Plot for Message Frequency 2 kHz.

separate sets of experiments. The polar plots generated for these messages were all similar in shape as verified by the additional plots in Appendix B.

Overall, the coupled messages were fairly dependent on turntable position as shown by Figure 2.71 and Figure 2.72. For this set of tests, the most coupling occurred when the wireless microphone system was between 30° and 150°. Since the coupling parameters were highly dependent on the experimental setup, it is likely the position/orientation with greatest sensitivity will change from one setup to another.

2.3. Summary of Testing Results

Every device tested showed susceptibility to an external EM field. For most of the devices, little is known about the coupling path that allows messages in a transmitted electromagnetic signal to appear in the device recordings. For the analog tape recorder, a few possible coupling paths include coupling directly onto the microcassette tape or coupling onto the recording head. The digital video camera was the only device where significant information about the coupling path was available. A test was performed with strong coupling parameters, and the camera recorded the test under battery power. In this test no coupling occurred, showing that the coupling into the device was through the power cable. Since the coupled message did not seem to influence the sound auto-leveling function of the video recorder, the message was evidently not coupled in toward the front end of the audio circuitry (i.e. before the auto-leveling electronics). The experimental setup sensitivity for coupling parameters for the computer microphone and the wireless microphone systems suggests that the coupling path for these two devices was in the microphone cables or the microphone sensor. It should be noted that experiments with the wired microphone and the wireless microphone involved a computer to capture the audio recordings. It is possible that message coupling occurred inside the computer, but no distinction can be made if the coupling path was inside the computer or either audio recording device. Despite this coupling path uncertainty, even if the coupling was occurring inside the computer, a computer will always be needed to make an audio recording with both of these audio recording devices. Table 2.2 lists some of the possible coupling paths for the tested devices.

Table 2.2. Possible Audio Recording Coupling Paths

Audio Recorder	Possible Coupling Paths
Analog Tape Recorder	Directly onto the Tape, Recording Head
Digital Video Camera	Power Cable (Confirmed)
Computer Microphone	Microphone Sensor, Microphone Cable
Wireless Microphone	Microphone Sensor, Microphone Cable

The only stimulation signals that coupled effectively to all devices were AM signals. Coupling carrier frequencies and message frequencies were highly specific to each device. Table 2.3 and Figure 2.73 illustrate the strongest carrier frequencies that would couple to a recording and Table 2.4 and Figure 2.74 show the strongest message frequencies that would couple to each device.

Table 2.3. Coupling Carrier Frequency Ranges

Audio Recorder	Coupling Carrier Frequency Ranges
Analog Tape Recorder	510-600 MHz, Very Strong – 512-568 MHz 803-855 MHz, Very Strong – 823-845 MHz
Digital Video Camera	202-218 MHz, Very Strong – 208-213 MHz
Computer Microphone	215-227 MHz, Very Strong – 216-223 MHz 425-437 MHz, Very Strong – 427-434 MHz
Wireless Microphone	241-298 MHz, Very Strong – 250-259 MHz

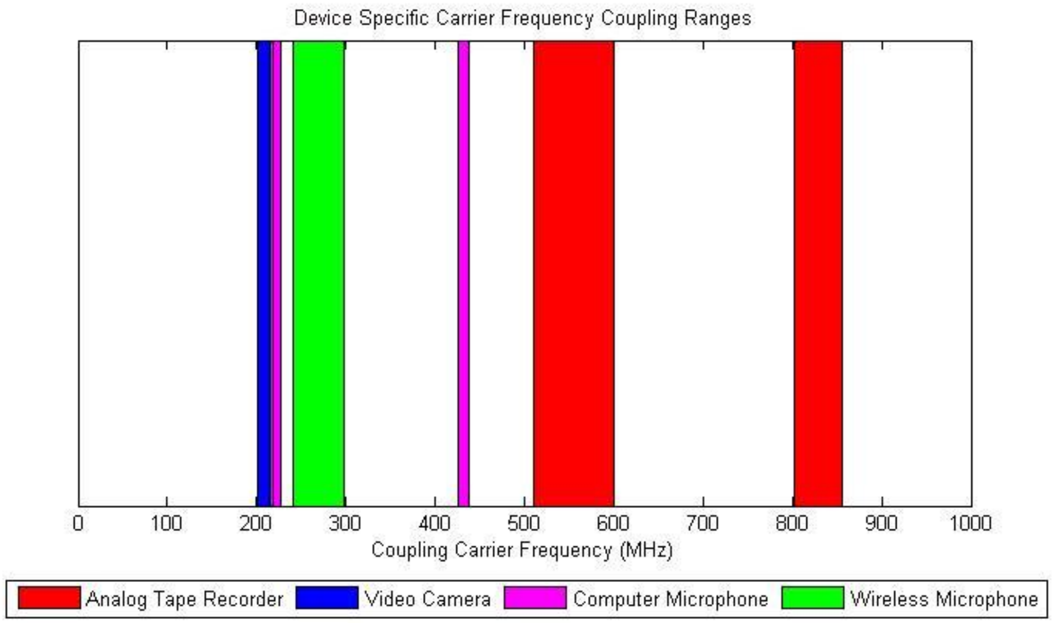

Figure 2.73. Coupling Carrier Frequency Ranges.

Table 2.4. Coupling Message Frequency Ranges

Audio Recorder	Coupling Message Frequency Ranges
Analog Tape Recorder	300 Hz-6 kHz
Digital Video Camera	1 kHz-20.4 kHz
Computer Microphone	400 Hz-24 kHz
Wireless Microphone	25 Hz-24 kHz

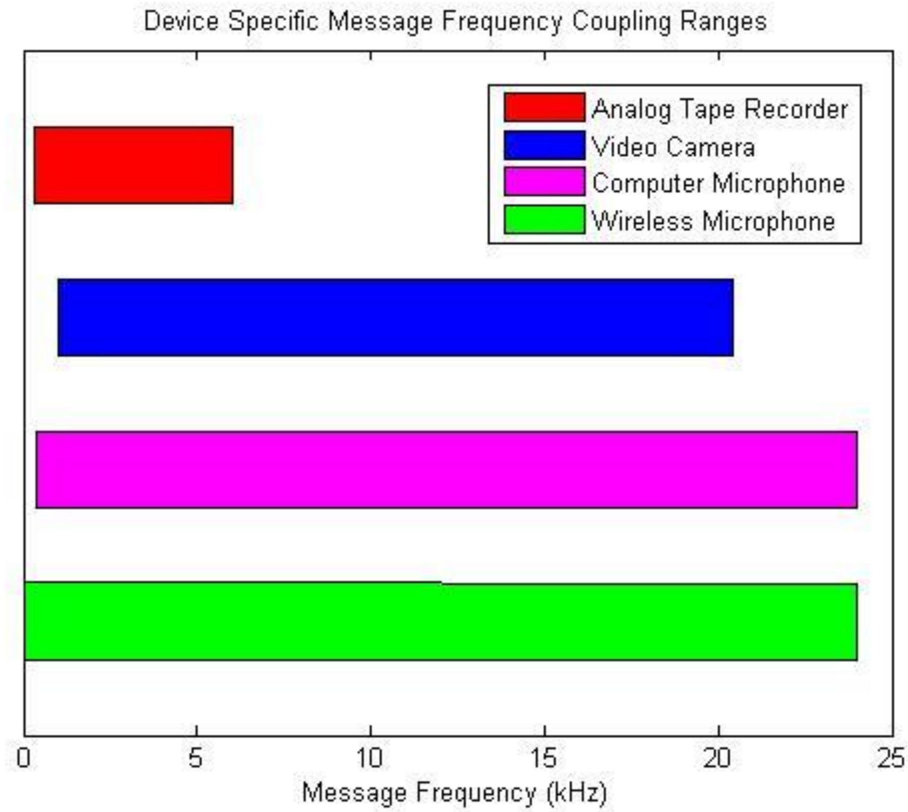

Figure 2.74. Coupling Message Frequency Ranges.

The bandwidths of the coupled messages were fairly consistent for carrier frequencies in the strong coupling range for each device and were roughly from a few hundred Hz to 20 kHz. As the carrier frequency moved out of a strong coupling range, the coupling message bandwidth tapered off uniquely for each device. In all devices, the coupled messages were equivalent to the modulated messages made by the signal generators. Table 2.5 shows the necessary antenna polarization for device message coupling.

Table 2.5. Antenna Polarization Required For Message Coupling

Audio Recorder	Antenna Polarization Required For Message Coupling
Analog Tape Recorder	Vertical Only
Digital Video Camera	Horizontal Only
Computer Microphone	Vertical (Strongest), Horizontal (Some Cases)
Wireless Microphone	Horizontal (Strongest), Vertical (Weak Coupling in Some Cases)

For all devices, higher input power to the transmitting antenna corresponded to stronger message coupling in the audio recordings. Table 2.6 shows the minimal carrier input power levels that a strong coupling message signal with a 50% modulation depth could be detected without any significant signal processing in the chamber experiments. These measurements, in terms of the power delivered to the antenna, will be converted to electric field strength in the next section.

Table 2.6. Minimal Carrier Frequency Power Needed For Message Detection

Audio Recorder	Carrier Frequency Power
Analog Tape Recorder	3 dBm
Digital Video Camera	0 dBm
Computer Microphone	0 dBm
Wireless Microphone	0 dBm

Greater modulation depth also correlated to greater message coupling for all recording devices. Table 2.7 lists the minimum modulation depth percentage that a strong coupling message signal could be detected without any significant signal processing in the chamber experiments when using a strong coupling carrier frequency fixed at an input power of 11 dBm.

Table 2.7. Minimal Modulation Depth Needed For Message Detection

Audio Recorder	Modulation Depth
Analog Tape Recorder	15%
Digital Video Camera	8%
Computer Microphone	15%
Wireless Microphone	5%

The susceptibility patterns were device specific. For devices without a fixed geometry, namely the computer microphone and the wireless microphone system that included many cables, the susceptibility patterns were highly variable due to their geometrical properties. Devices with a fixed geometry such as the digital video camera and analog tape recorder had consistent susceptibility patterns. Table 2.8 and Table 2.9 show typical susceptibility patterns for each device.

Table 2.8. Device Susceptibility Pattern Comparison With Ambient

Audio Recorder	Susceptibility Pattern
Analog Tape Recorder	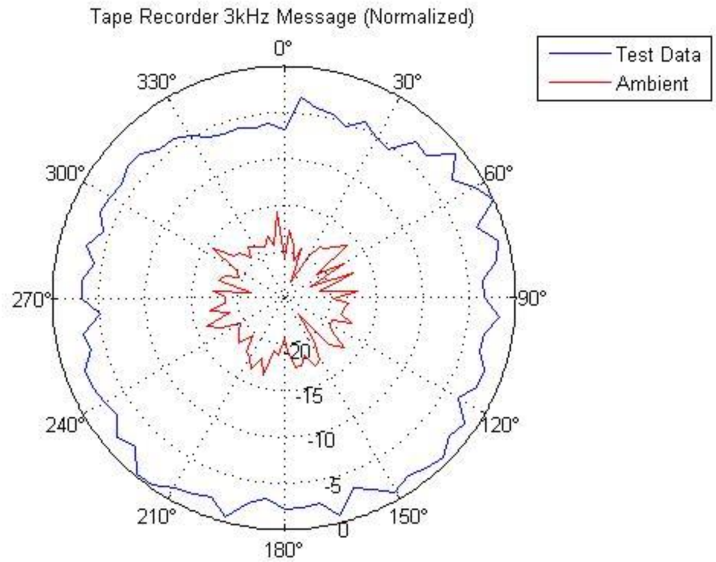
Digital Video Camera	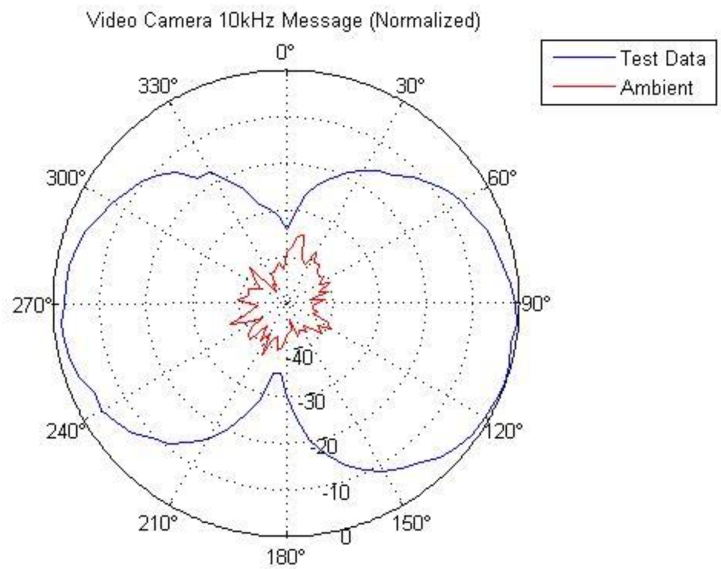

Table 2.8. (Continued)

Audio Recorder	Susceptibility Pattern
Computer Microphone	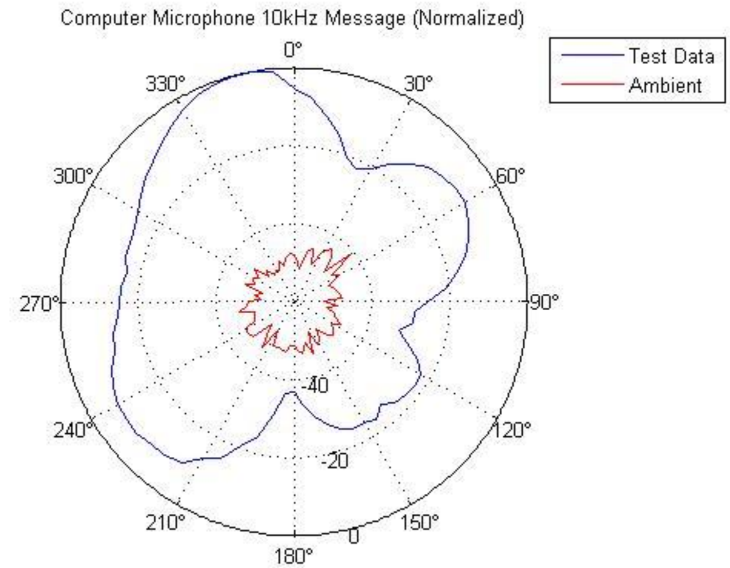
Wireless Microphone	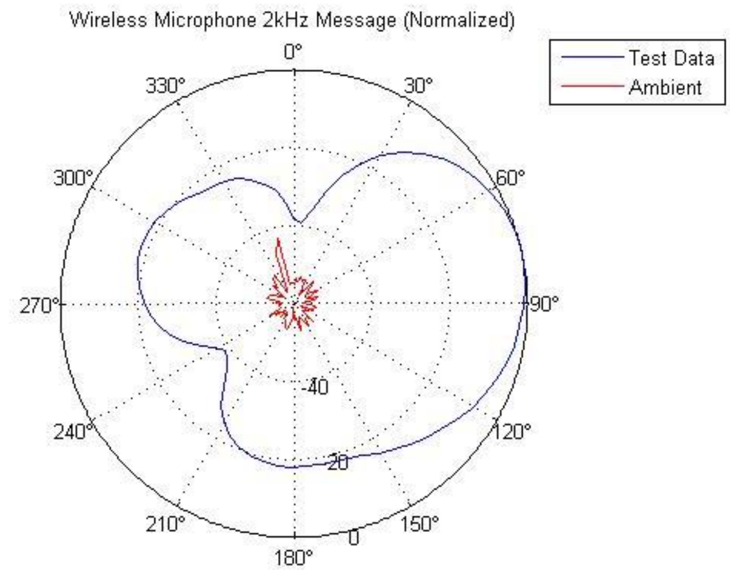

Table 2.9. Device Susceptibility Pattern Comparison Without Ambient

Audio Recorder	Susceptibility Pattern
Analog Tape Recorder	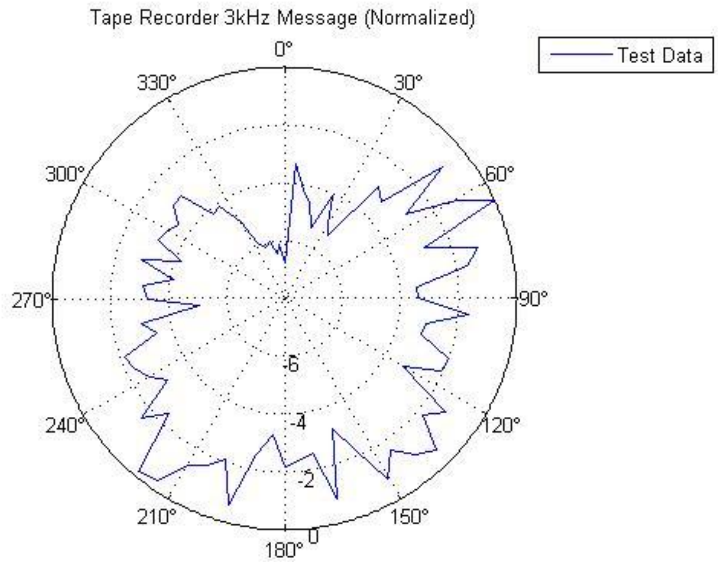
Digital Video Camera	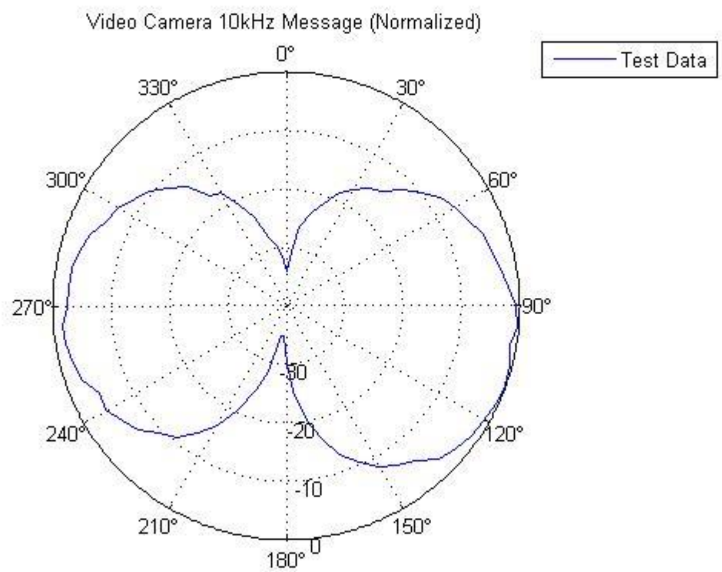

Table 2.9. (Continued)

Audio Recorder	Susceptibility Pattern
Computer Microphone	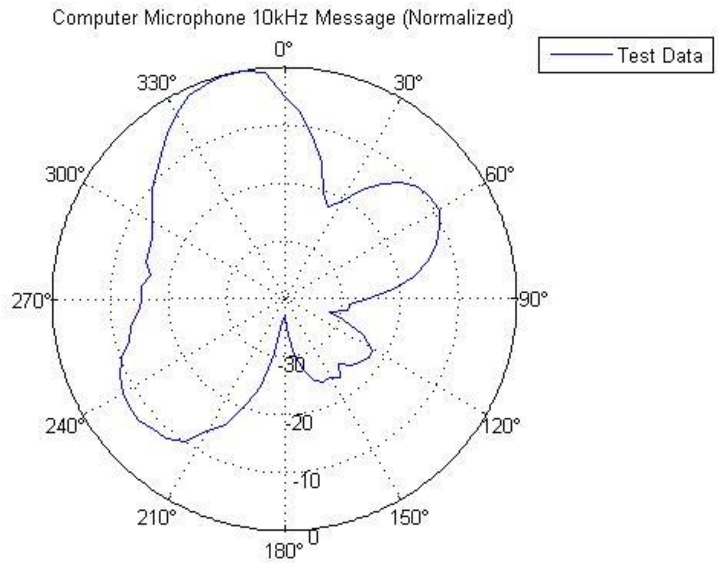
Wireless Microphone	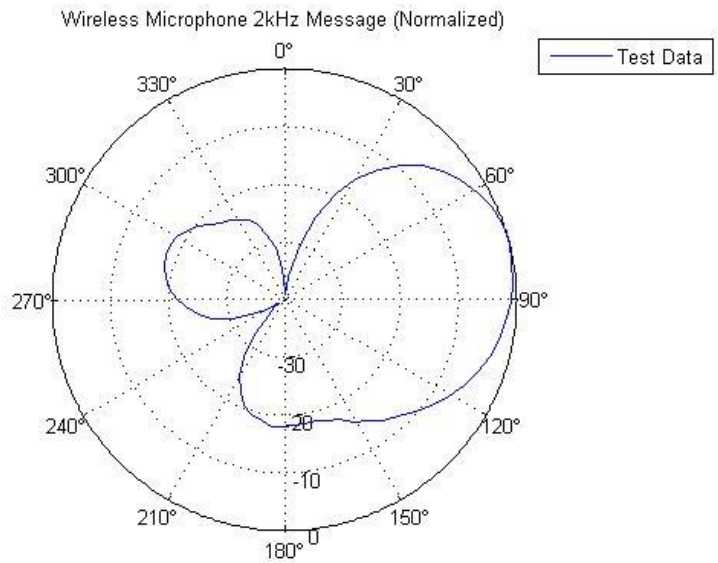

3. ANALYSIS OF RESULTS

3.1. Electric Field Analysis

To understand the message coupling properties of the tested audio recording devices, it is critical to know the electric field strength at the device during the test. Once the electric field strength is known and the test data has been analyzed, one could estimate how much coupling may occur in a real-world situation by correlating known electric field strength with the coupling characteristics of the device. This information would also allow for the prediction of the minimum field strength required for message coupling to a recording device in a realistic environment.

3.1.1. Electric Field Theory

To develop an equation for the electric field at a recording device under test (DUT), one must start with an expression of the signals present at the signal generator. Electrical phase is being disregarded in this derivation since the primary quantity of interest is the magnitude of the electric field. For coupled messages to appear in audio recordings, AM signals were applied to the transmitting antenna. In communications theory the voltage expression for amplitude modulation is given as shown in (1)-(4) [3].

$$x_c(t) = A_c[1 + am_n(t)]\,cos(2\pi f_c t) \qquad 0 \le a \le 1 \tag{1}$$

$$A_c = \sqrt{2 * 50 * \frac{10^{\frac{P_{in}}{10}}}{1000}} \tag{2}$$

$$a = \frac{mod.\ depth\,(\%)}{100\%} \tag{3}$$

$$m_n(t) = 2V_{pp} \tag{4}$$

where

A_c is the amplitude of the carrier signal without any modulation,

a is the modulation index (where (a x 100) is known as the percent modulation or modulation depth),

$m_n(t)$ is the normalized message signal

f_c is the carrier frequency, and

P_{in} is the input power in dBm to the transmit antenna.

Converting (1) from the time domain to frequency domain with linear systems theory results in (5) given below [3].

$$\begin{aligned} X_c(f) &= \tfrac{1}{2}A_c\delta(f-f_c) + \tfrac{1}{2}A_c\delta(f+f_c) + \tfrac{1}{2}A_c a M_n(f-f_c) + \tfrac{1}{2}A_c a M_n(f+f_c) \\ &= \tfrac{1}{2}A_c\{[\delta(f-f_c)+\delta(f+f_c)] + a[M_n(f-f_c)+M_n(f+f_c)]\} \end{aligned} \quad (5)$$

Taking into account cable losses and reflections caused by the transmitting antenna not being matched to a 50 Ω system, the voltage at the antenna terminals in the frequency domain is given by (6).

$$|X_c(f)| \approx \frac{1}{2}\frac{1-|\Gamma(f_c)|}{L(f_c)}A_c\{[\delta(f-f_c)+\delta(f+f_c)] + a[M_n(f-f_c)+M_n(f+f_c)]\} \quad (6)$$

where

Γ is the reflection coefficient and

L is the cable loss.

Equation (6) makes the assumption that the highest message frequency is much smaller than the carrier frequency. To find the electric field at the transmitting antenna, the voltage at the antenna terminals must be multiplied by an antenna factor as shown in (7) [1].

$$|E_{antenna}(f)| = \left(10^{\frac{AF_{dB}}{20}}\right)|X_c(f)| \quad (7)$$

where

AF_{dB} is the antenna factor for the transmitting antenna in dB.

To next find the electric field at the DUT, reflections from the chamber floor and field attenuation must be considered. Because the test was performed in a semi-anechoic chamber, the floor of the chamber reflects some of the electromagnetic waves as they propagate towards the DUT. Using image theory, these reflections would be equivalent to having a two antenna array separated by two times the antenna height [2]. The field propagation of a two element antenna array is given by (8)-(11) [2].

$$E_{total}(f) = E_{single\ element}(f) * [Array\ Factor] \tag{8}$$

$$Array\ Factor = 2\cos\left(\frac{2\pi}{\lambda} H\cos(\theta)\right) \tag{9}$$

$$\theta = tan^{-1}\left(\frac{R}{H}\right) \tag{10}$$

$$\lambda = \frac{c}{f} \tag{11}$$

where

H is the antenna height (m),
λ is the free-space wavelength,
f is the frequency of operation,
c is the speed of light, and
R is the distance from the transmitting antenna to the DUT.

In a practical application, the array factor would be approximately equal to two, because R would be much larger than H. The array factor is not necessarily equal to two in experimental data taken in the semi-anechoic chamber because R is about three meters and H is about one meter. This small ratio between the R and H terms makes the wavelength dependence in the array factor equation become significant.

Assuming that the DUT was placed in the far-field region it is known the electric field at a distance is inversely proportional to the separation distance as shown in (12)-(13) [2].

$$E_{DUT}(f) \propto \frac{1}{D} \tag{12}$$

$$D = \sqrt{R^2 + H^2} \tag{13}$$

In the chamber setup for message coupling experiments, carrier frequencies above 300 MHz would correspond to devices being in the far-field region, assuming the far-field is about three times the wavelength [1]. The frequency range for effective coupling to the digital video camera and the wireless microphone system do not correspond to these devices being in the far-field under this assumption. Despite being in the near-field, data from these two devices will be validated with the electric field far-field region equations, which should still be in close agreement to the test data. From (8)-(13), the expression for the peak value of the electric field at the DUT is given by (14).

$$|E_{DUT}(f)| = \left|\frac{1}{D}E_{antenna}(f) * \left[2\cos\left(\frac{2\pi}{\lambda}Hcos(\theta)\right)\right]\right|$$
$$|E_{DUT}(f)| = \left|\frac{cos\left(\frac{2\pi}{\lambda}Hcos\left(tan^{-1}\left(\frac{R}{H}\right)\right)\right)}{\sqrt{R^2+H^2}}\left(10^{\frac{AF_{dB}}{20}}\right)\sqrt{2 * 50 * \frac{10^{\frac{P_{in}}{10}}}{1000}\left(\frac{1-|\Gamma(f_c)|}{L(f_c)}\right)} * \left\{\delta(f-f_c)+\delta(f+f_c)+\frac{mod.depth\,(\%)}{100\%}[M_n(f-f_c)+M_n(f+f_c)]\right\}\right| \quad (14)$$

Equation (14) was formed under the assumption that only reflections of the electric field were caused by the floor of the chamber. Thus, it assumed that there were no other structures within the chamber that would reflect the electric field, and all of the fields that impinge upon the walls and ceiling of the chamber were absorbed by the foam and ferrite tiles. From (14), the induced voltage in an audio recording can also be predicted. It is known that the AM electric field at the DUT induced a voltage somewhere in the recording circuitry that was then demodulated through an envelope detector in the same circuitry [3]. This envelope detector could be formed by the parasitic circuit elements found in the electronic device. Thus, the magnitude of the message voltage at the DUT is given by (15) [3].

$$|X_{DUT}(f)| = \left|\frac{2}{D}cos\left(\frac{2\pi}{\lambda}Hcos(\theta)\right)\left(10^{\frac{AF_{dB}}{20}}\right)A_c\left(\frac{1-|\Gamma(f_c)|}{L(f_c)}\right)a[M_n(f)]\right| * \rho(\theta,\phi,polarization,f_c,f_m)$$
$$|X_{DUT}(f)| = \left|\frac{2}{\sqrt{R^2+H^2}}cos\left(\frac{2\pi}{\lambda}Hcos\left(tan^{-1}\left(\frac{R}{H}\right)\right)\right)\left(10^{\frac{AF_{dB}}{20}}\right)\sqrt{2 * 50 * \frac{10^{\frac{P_{in}}{10}}}{1000}\left(\frac{1-|\Gamma(f_c)|}{L(f_c)}\right)} * \frac{mod.\ depth\,(\%)}{100\%}[M_n(f)]\right|\rho(\theta,\phi,polarization,f_c,f_m) \quad (15)$$

where

ρ represents the coupling coefficient for a given DUT as a function of device orientation (θ, φ), antenna polarization (polarization), carrier frequency (f_c), and message frequency (f_m)

dependence. The unit on this coupling coefficient is meters. This coefficient is found empirically for each DUT.

Equation 15 makes the assumption that the coupled message signal plus the noise will not cause clipping in the recorded audio signal. To empirically find ρ with experimental data (16) should be used.

$$\rho = \frac{D|V_{DUT}(f_m)|}{2\cos\left(\frac{2\pi}{\lambda}H\cos(\theta)\right)\left(10^{\frac{AF_{dB}}{20}}\right)A_c\left(\frac{1-|\Gamma(f_c)|}{L(f_c)}\right)a|M_n(f_m)|} \tag{16}$$

where

V_{DUT} is the voltage amplitude at the message frequency of interest in a single-sided plot generated from a fast Fourier transform and

f_m is the message frequency of interest.

3.1.2. Electric Field Measurements

Field measurements were taken to validate the electric field equation for the fields in the semi-anechoic chamber, as represented by (14), to account for a strong uncertainty in the antenna factor for the transmitting biconilog antenna. Calibration data for this antenna was not available so typical values for the antenna factor had to be used for theoretical electric field strength predictions.

Since calibrated electric field probes were not available to measure the fields from the biconilog antenna in the chamber, a calibration was performed using two dipole antennas (EMCO 3121C-DB3 and EMCO 3121C-DB4). Calibration data was also not available for these antennas, so measurements were performed in a GTEM cell to roughly validate the manufacturer typical data for these dipole antennas. The first field measurement was performed with the smaller of the two dipole antennas. Figure 3.1 and Figure 3.2 show the GTEM cell experimental setup. While this experimental setup is not ideal, it was sufficient to show the manufacturer data was on the right order of magnitude.

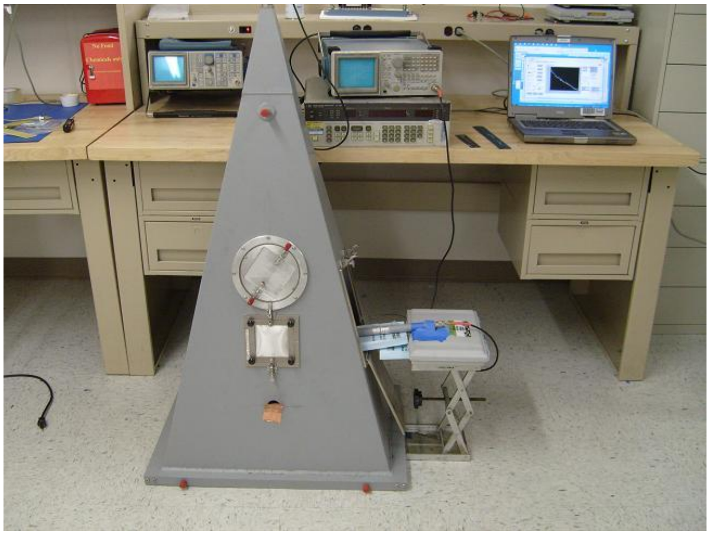

Figure 3.1. GTEM Cell Field Measurement View 1.

Figure 3.2. GTEM Cell Field Measurement View 2.

Using a special ruler provided by the manufacturer, the dipole antenna was tuned to 700 MHz, 800 MHz and 900 MHz. For each tuned frequency, the input power to the GTEM cell was swept from -70 dBm to 13 dBm, and an un-modulated sine wave was applied with the same tuned frequency. The dipole antenna was placed in the GTEM cell where the distance between the septum and the outer conductor was approximately 22.5 cm. The dipole antenna was connected to a spectrum analyzer where the power at the tuned frequency could be analyzed. The theoretical and measured electric field quantities were calculated with (17)-(18).

$$E_{GTEM\ Theoretical}(f) = \frac{\sqrt{\left(10^{\frac{P_{in}-L_{Cable}}{10}}\right)\left(\frac{50}{1000}\right)}}{D} \tag{17}$$

$$E_{GTEM\ Measured}(f) = \sqrt{\left(10^{\frac{P_{SA}+L_{Cable}}{10}}\right)\left(\frac{50}{1000}\right)}(AF) \tag{18}$$

where

P_{in} is the input power to the GTEM cell cable at the tuned frequency in dBm,

L_{cable} is the cable loss in dB at the tuned frequency (for the GTEM cell in (17) and the dipole antenna in (18)),

D is the distance between the septum and the outer conductor of the GTEM cell where the dipole antenna was placed (in meters),

P_{SA} is the power reading from the spectrum analyzer at the tuned frequency in dBm, and

AF is the dipole antenna factor that converts an antenna voltage to an electric field quantity. The antenna factor is provided by the manufacturer and has units of m^{-1}. The calibration data showing the antenna factor information was unavailable for the dipole antennas, so typical values were used as provided in the data sheet.

The cable losses for the cables attached to the GTEM cell and the dipole antenna are shown in Figure 3.3. The manufacturer's reported antenna factor for the dipole antennas is shown in Figure 3.4 and Figure 3.5. The electric field strengths estimated for the GTEM cell input and estimated from the dipole measurement (using the manufacturer's antenna factor) made in these experiments are shown in Figures 3.6-3.8 [4].

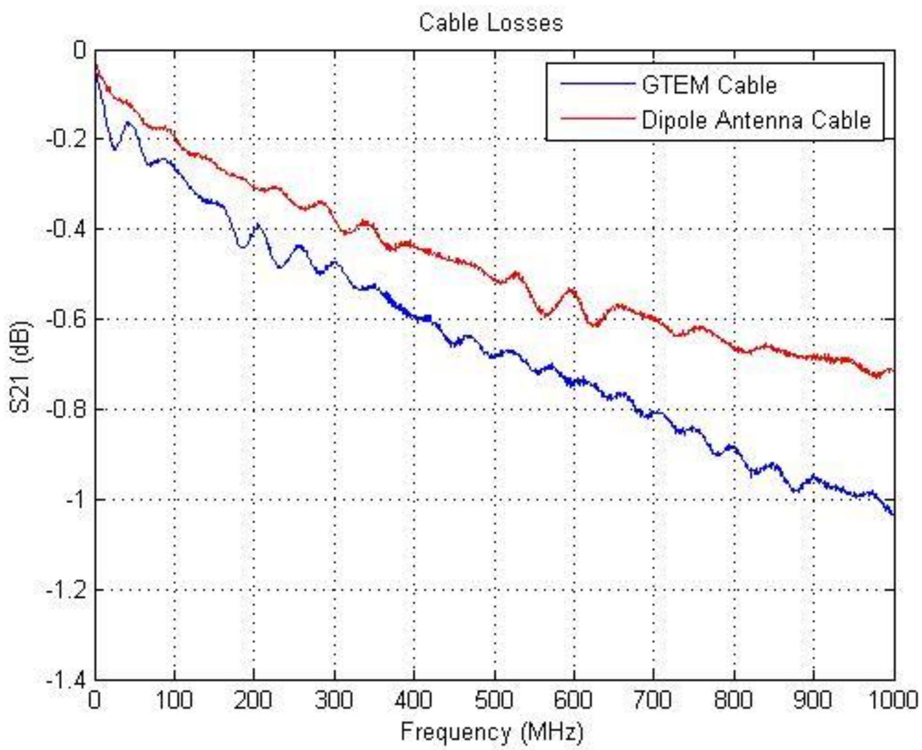

Figure 3.3. GTEM Experiment Cable Losses.

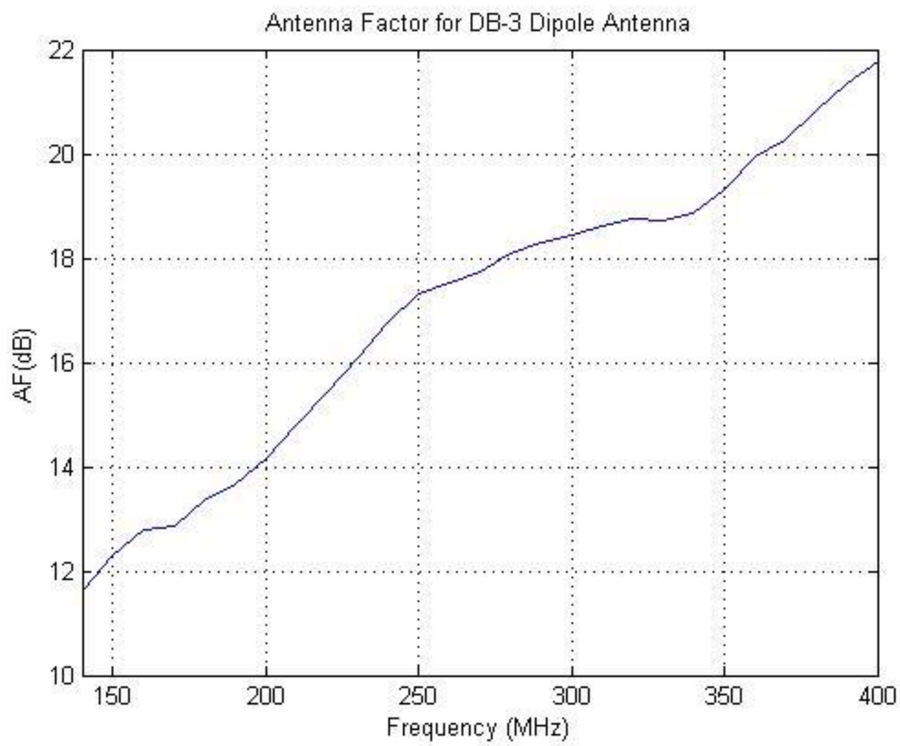

Figure 3.4. Dipole Antenna Factor For DB-3 Antenna.

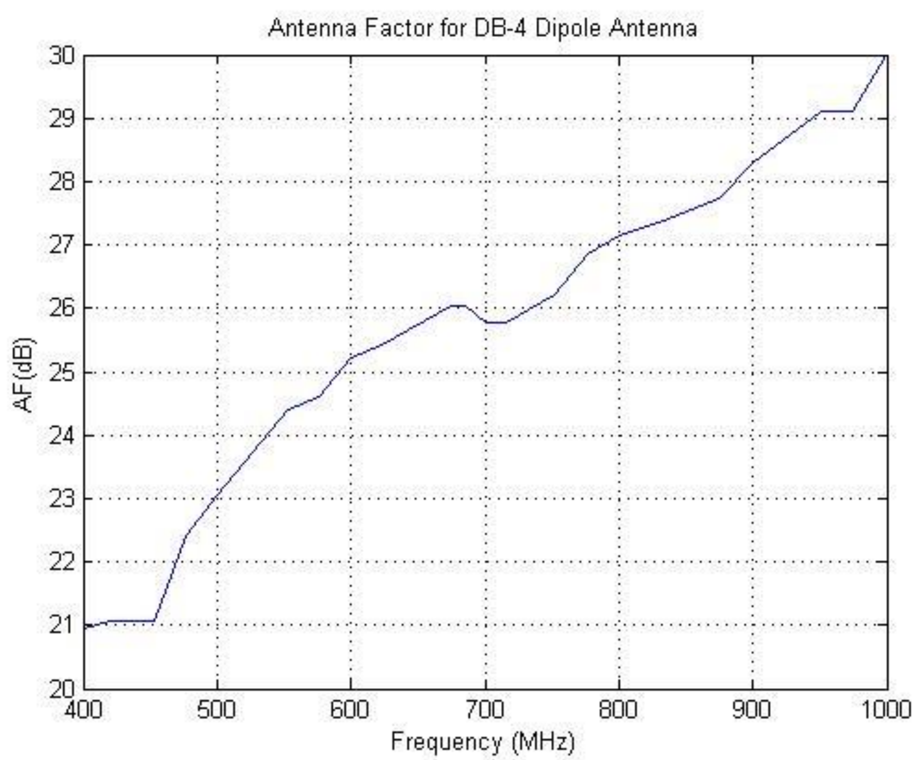

Figure 3.5. Dipole Antenna Factor For DB-4 Antenna.

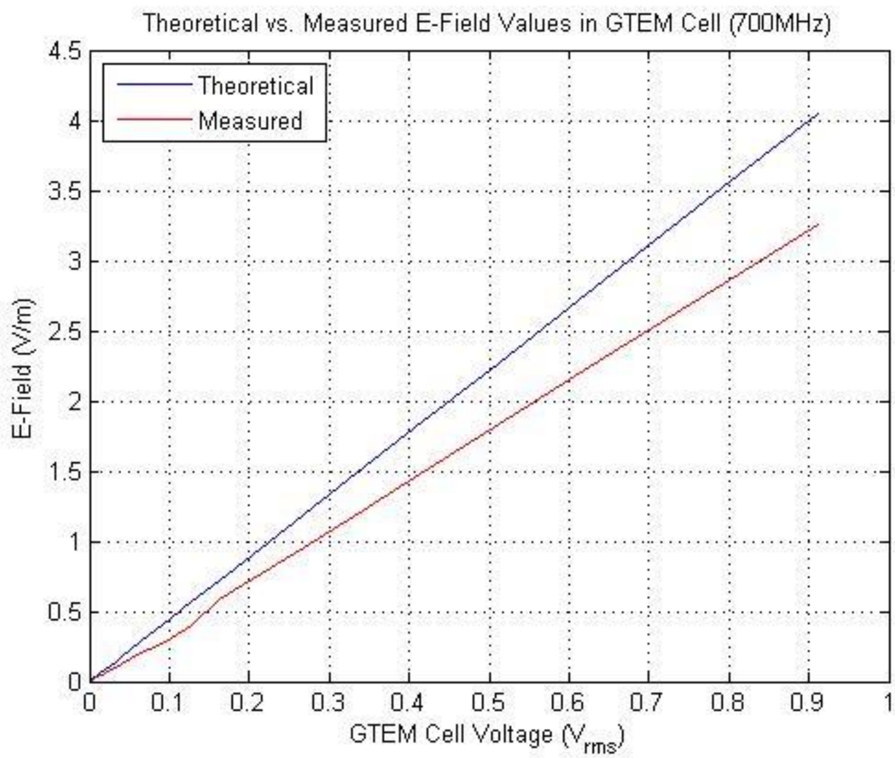

Figure 3.6. GTEM Cell Measurement with a 700 MHz Tuned Frequency.

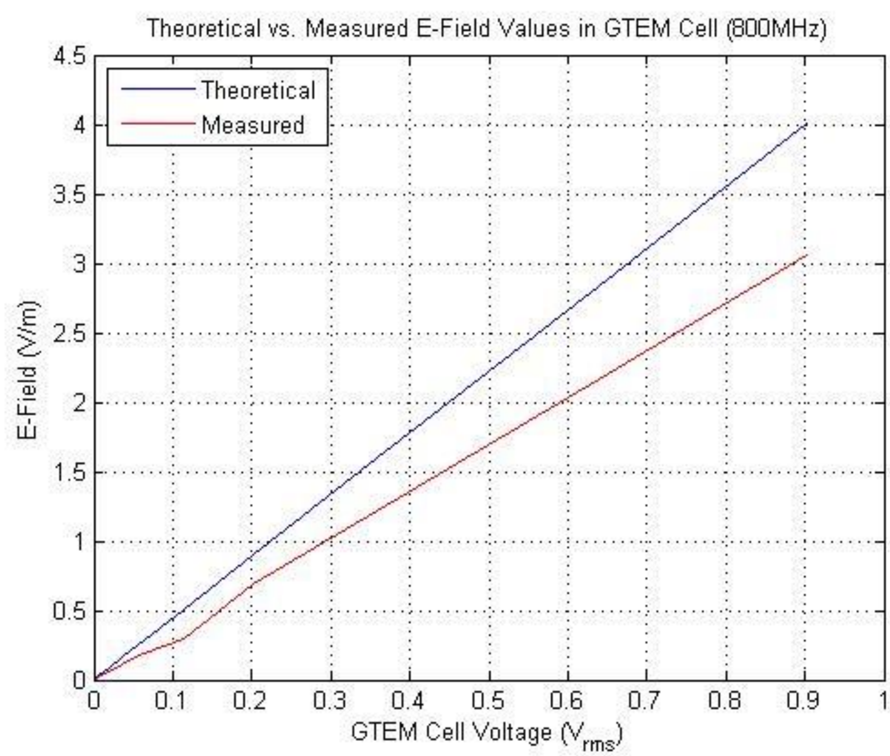

Figure 3.7. GTEM Cell Measurement with a 800 MHz Tuned Frequency.

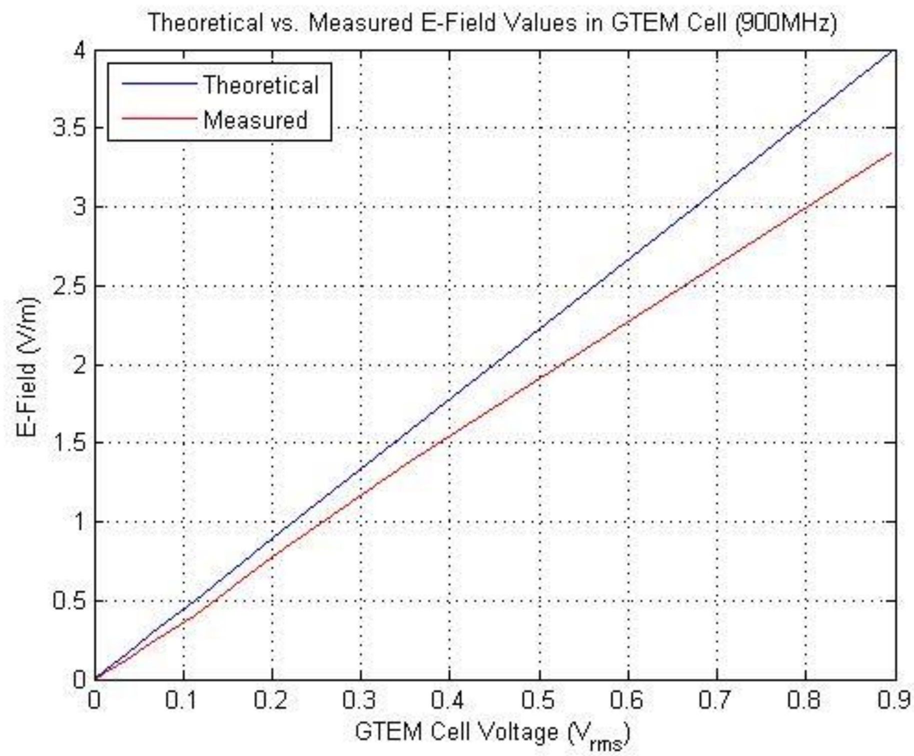

Figure 3.8. GTEM Cell Measurement with a 900 MHz Tuned Frequency.

Figures 3.6-3.8 show a reasonable agreement between theory and measured results, especially at lower field strengths. While this measurement with the dipole antennas is not ideal, it is sufficient to show the antennas respond roughly as expected and should be sufficient to justify using the dipole antennas to determine the approximate electric field strength generated by the biconilog antenna at the DUT.

With the dipole antenna characteristics roughly validated from the results in Figures 3.6-3.8, experiments were next performed in the chamber to measure the fields generated by the biconilog antenna. The chamber experimental setup is shown in Figure 3.9.

Figure 3.9. Chamber Field Measurement Setup.

Using a tape measure or a special ruler provided by the manufacturer, the dipole was tuned to 211 MHz, 220 MHz, 254 MHz, 430 MHz, 547 MHz, and 831 MHz. For each tuned frequency, the input power to the chamber antenna was swept from the lowest input power that could be detected by the receiving dipole antenna, which in most cases was about -70 dBm, to a maximum input power level of 13 dBm. Un-modulated sine waves with the same frequency the receiving dipole antenna was tuned were applied to the transmitting antenna in all cases. The dipole antenna was placed on a wooden table in the chamber. The distance between the dipole antenna and the biconilog antenna was about three meters. Both antennas were about one meter above the floor of the semi-anechoic chamber.

Equation 14 and (18) were used for theoretical and measured calculations. It should be noted that since this testing did not involve any modulation, the modulation depth in (14) should be set to zero. The manufacturer's typical values for antenna factor were used for the biconilog and dipole antennas. The cable losses for the chamber experiments are shown in Figure 3.10. The S_{11} measurement of the biconilog antenna is shown in Figure 3.11. The manufacturer's typical antenna factor for the biconilog antenna is shown in Figure 3.12. A comparison of the electric field strengths generated from the biconilog antenna as predicted using (14) in blue and the measured field strength by the dipole antenna using (18) in red are shown in Figure 3.13 and Figure 3.14 [5].

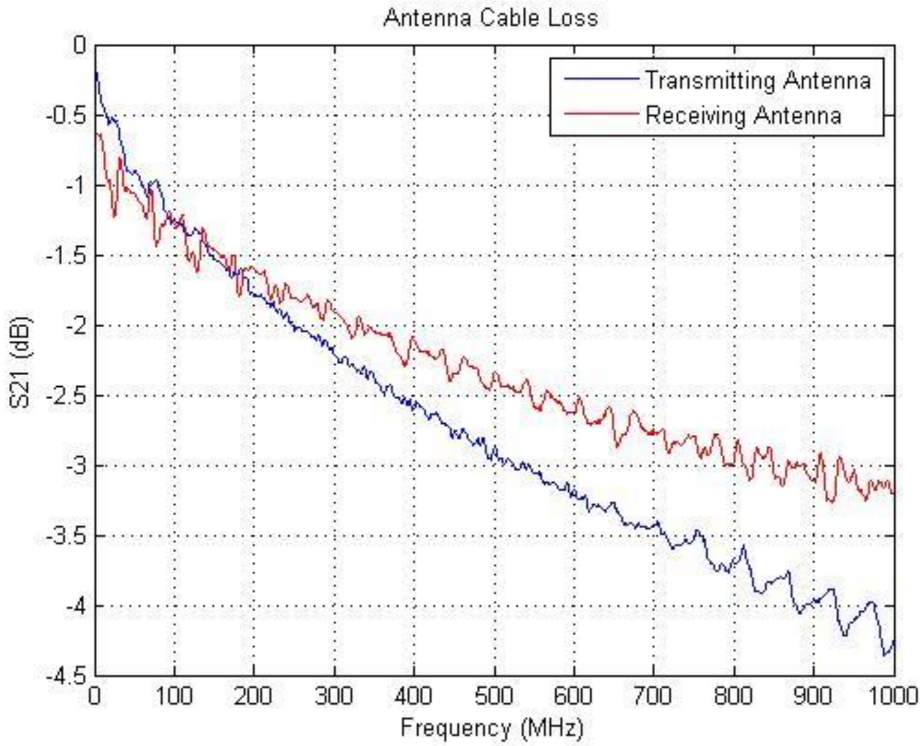

Figure 3.10. Chamber Experiment Cable Losses.

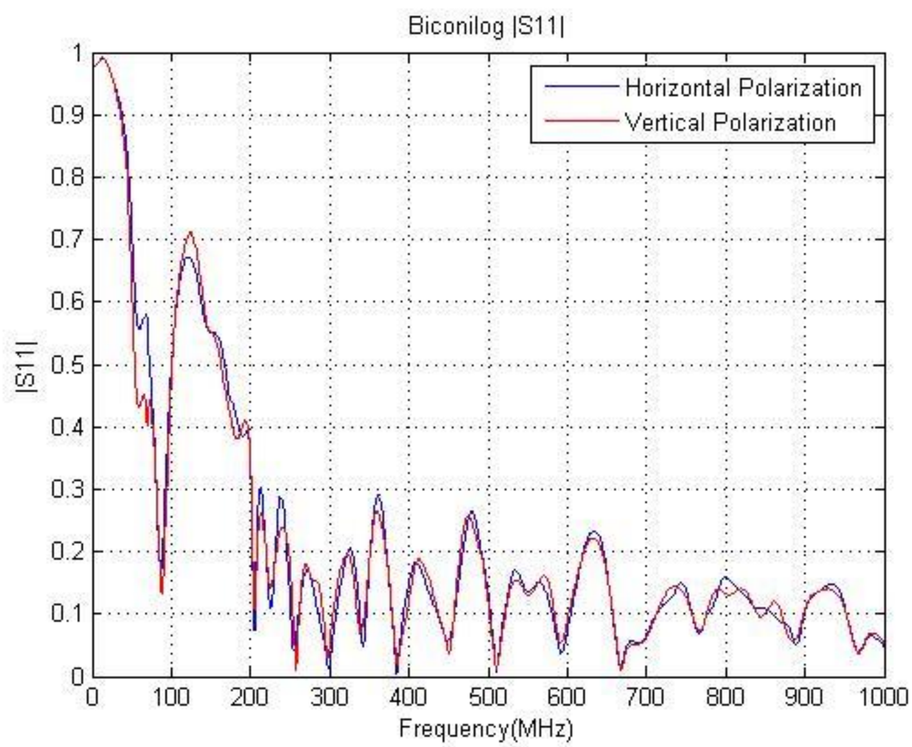

Figure 3.11. Biconilog Antenna S_{11} Measurement.

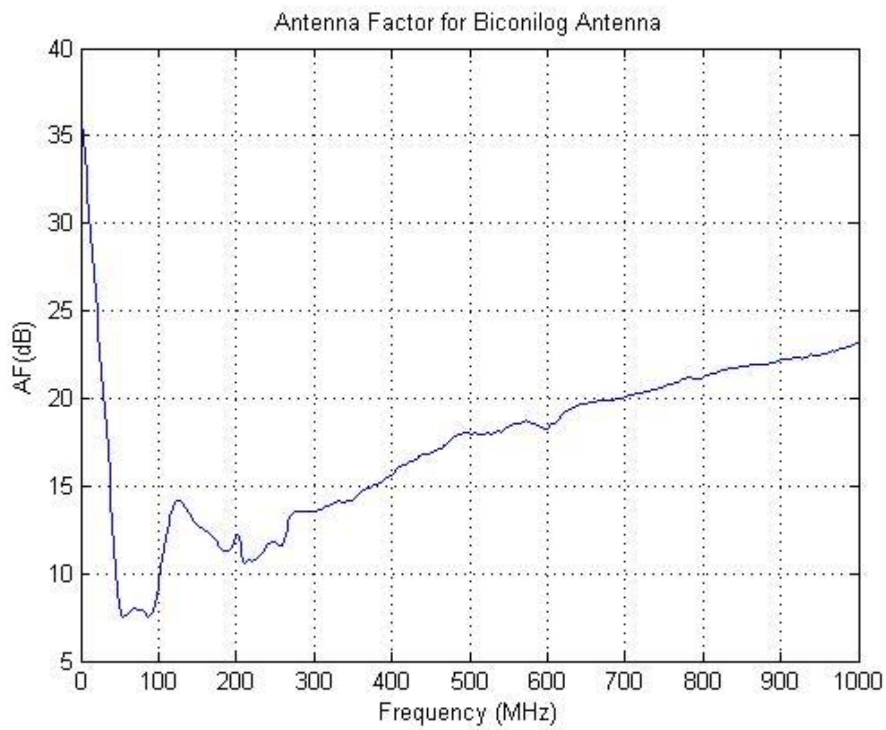

Figure 3.12. Biconilog Antenna Factor.

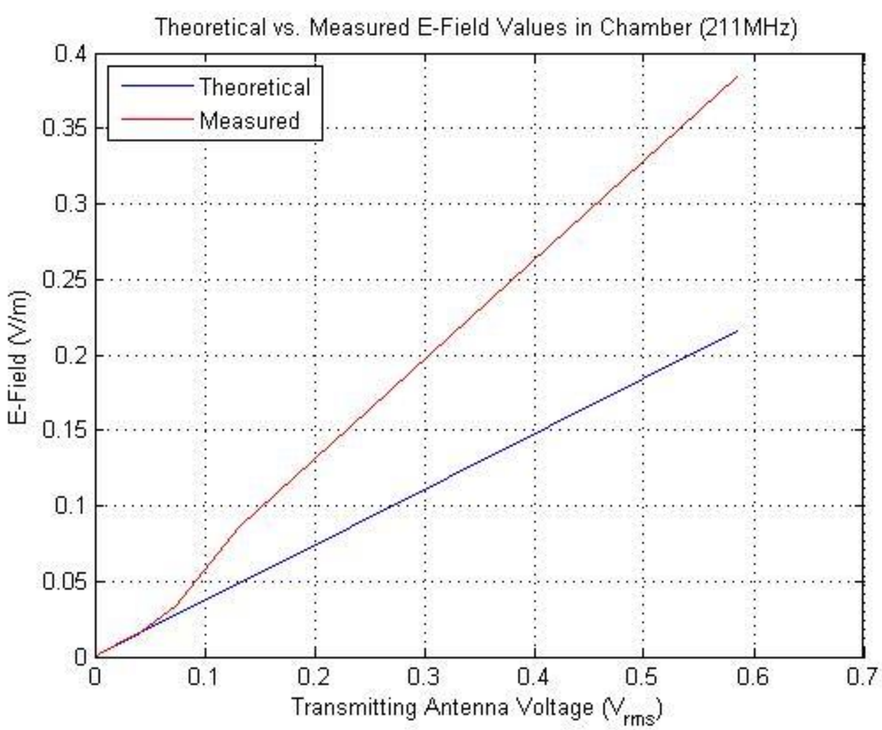

Figure 3.13. Electric Field Chamber Measurement with a 211 MHz Tuned Frequency.

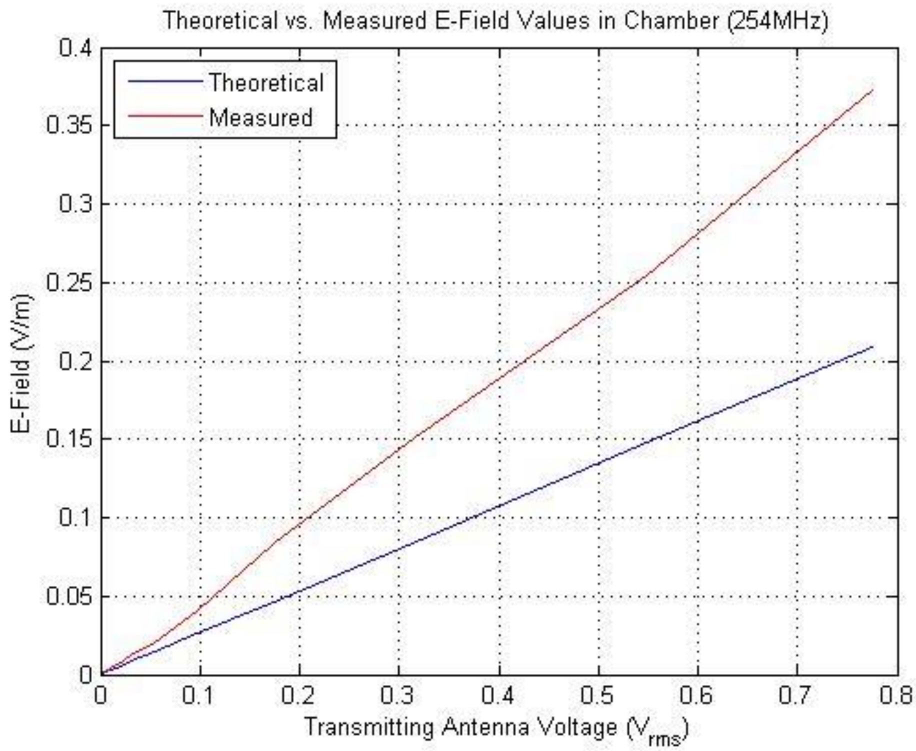

Figure 3.14. Electric Field Chamber Measurement with a 254 MHz Tuned Frequency.

Overall, the measured results did not match well with theoretical predictions. This mis-prediction could be caused by several factors. The dipole antenna was not truly in the far-field of the biconilog antenna, so the antenna factor data was not entirely valid. Because the dipole is not electrically small, it may also perturb the field and the resulting reading [6]. The dipole antennas themselves were not well calibrated, so their receiving characteristics are somewhat in question. While these experimental results are not perfect, they do provide a general measure to ensure that the theoretical and measured electric field values are on the same order of magnitude and roughly validate the theoretical electric field equation.

3.2. Message Coupling Analysis

3.2.1. Coupling Coefficient Analysis

As shown by (15), message coupling for all audio recording devices is dependent on the coupling coefficient (ρ). This variable is a function of several variables including device orientation, electric field polarization, carrier frequency, and message frequency. To optimally couple to a device, test conditions must be optimized to obtain a maximum coupling coefficient. Poor test conditions can result in no message coupling. Figures 3.15-3.18 illustrate some of the dependencies for this variable.

To generate the plots shown in Figures 3.15-3.18, the fast Fourier transform was computed for audio recordings at each turntable position, and then (16) was applied. The results are based on the theoretical formula for the electric field at the DUT, not the electric field measurements shown in the previous section. In general, it can be seen that the lower frequency messages coupled more strongly than higher frequency messages. The noise floor for the low frequency messages, however, was higher than the high frequency messages forcing the coupling coefficient to zero in several cases when a message could not be seen above the noise floor. In addition to device orientation impacting the coupling coefficient, the carrier frequency and antenna polarization can also cause a significant impact as well. Sufficient data is not available to generate similar plots to those shown in Figures 3.15-3.18, but based on the general testing and specific testing performed on each recording device, the carrier frequency and antenna polarization should be set as outlined in Table 2.3 and Table 2.5 to maximize the coupling coefficient.

Given that the coupling parameters for all of the recording devices in this susceptibility study have been defined, it is possible to find both the minimum field strength required for message coupling and the maximum distance a device can be from a theoretical transmitter operating at a known power level. To explore these two parameters of interest, an ideal, theoretical testing scenario must be considered. To simplify calculations it is assumed that there is a matched, isotropic source, with negligible cable losses, on a piece of land that is perfectly flat and without any other structures [7]. The soil surrounding the isotropic source is assumed to be conductive and can be modeled as a perfect electric conductor. An amplitude modulated signal is applied to the source with 100% modulation depth. Lastly, the curvature of the earth and reflections from the atmosphere are ignored [2].

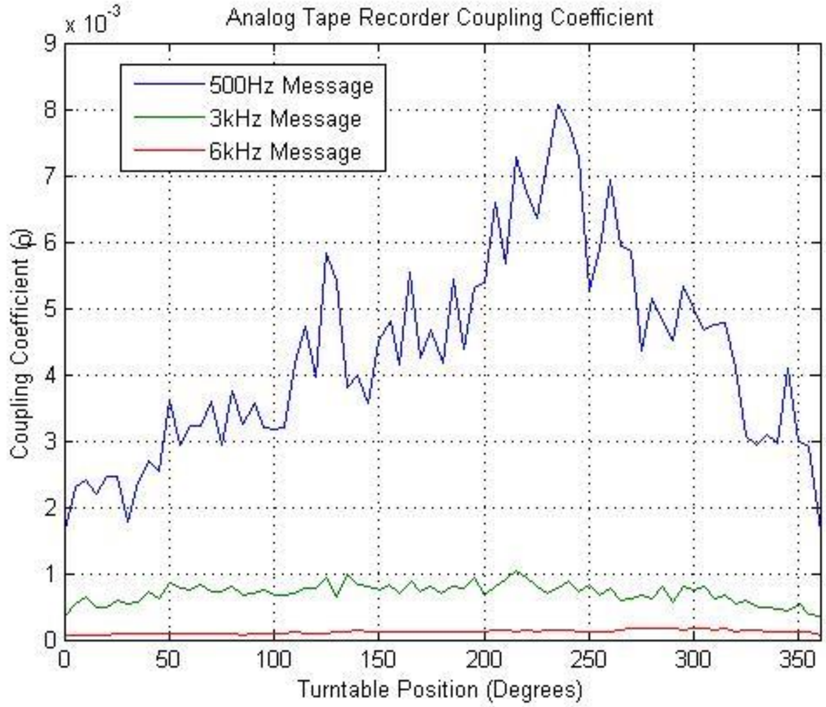

Figure 3.15. Analog Tape Recorder Coupling Coefficient as a Function of Turntable Position and Message Frequency.

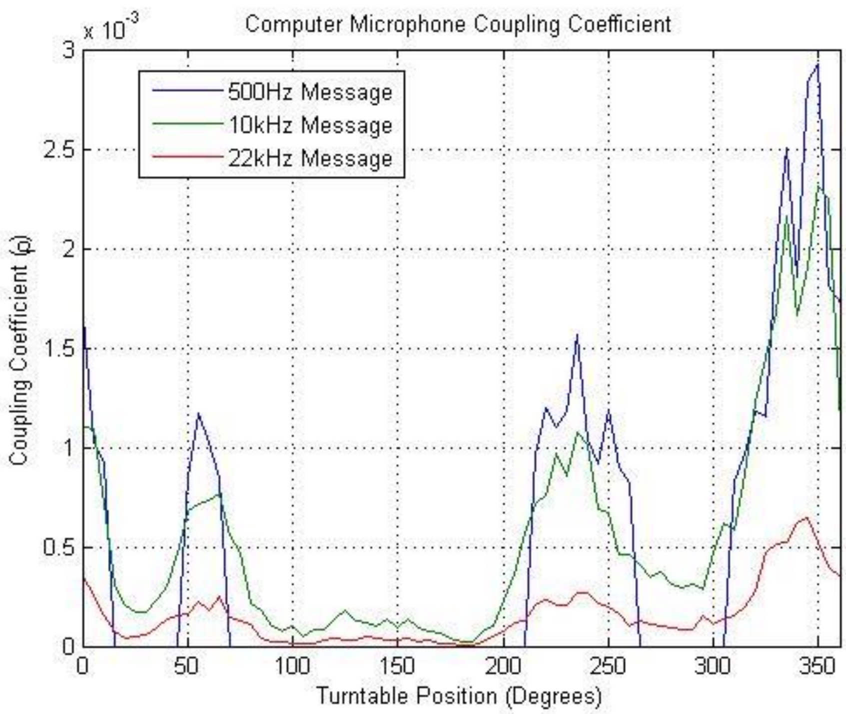

Figure 3.16. Computer Microphone Coupling Coefficient as a Function of Turntable Position and Message Frequency.

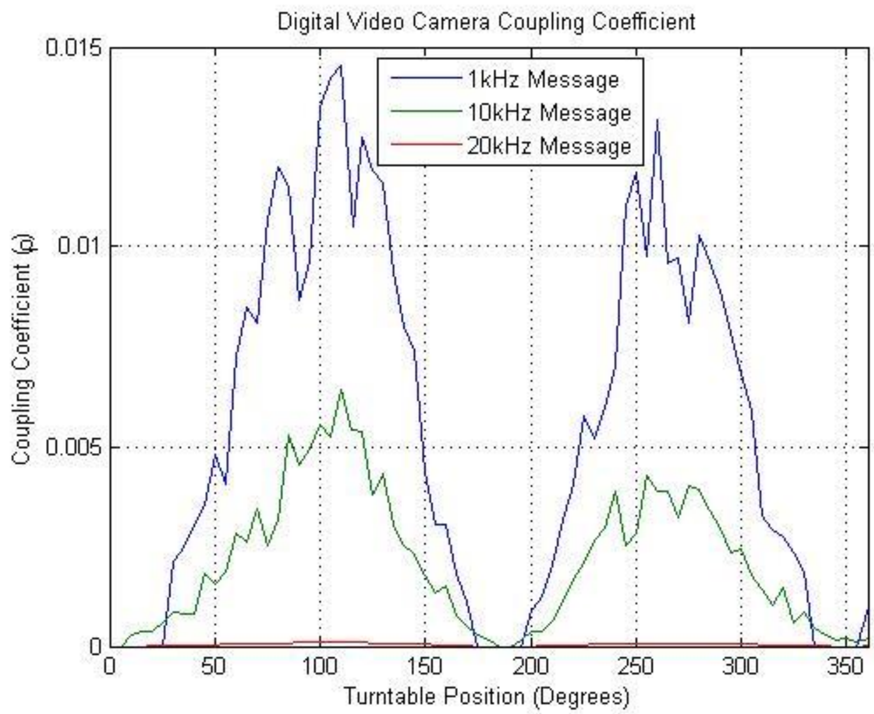

Figure 3.17. Digital Video Camera Coupling Coefficient as a Function of Turntable Position and Message Frequency.

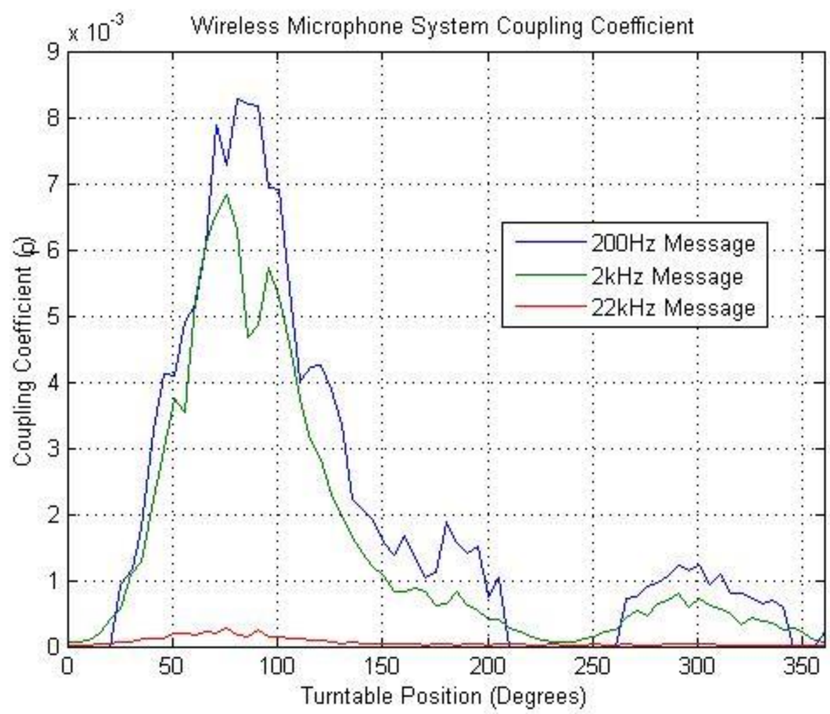

Figure 3.18. Wireless Microphone System Coupling Coefficient as a Function of Turntable Position and Message Frequency.

From these test conditions, the expression for the induced signal on a recording for a single frequency message can be represented by (19), which is a simplified form of (15).

$$|X_{DUT}(f)| = \frac{2}{R} A_c \rho \tag{19}$$

Assuming signal processing is not being used, the minimum threshold for message signal detection is at the noise floor. Thus (19) can be re-written as shown in (20) to find the maximum allowable distance from the recording device to the source for message coupling detection, where V_{noise} is a peak voltage.

$$R_{max} = \frac{2A_c \rho}{V_{noise}} \tag{20}$$

Using (14) and (15), the minimum field strength in V_{RMS} at the lower or upper side band of the modulated signal can be found with (21).

$$E_{min} = \frac{V_{noise}}{2\sqrt{2}\rho} \tag{21}$$

Using the coupling coefficient results shown in Figures 3.15-3.18, the minimum field strength at the device under test and the maximum distance assuming a 1 kW transmitter required to produce a signal above the noise floor are given below in Tables 3.1-3.4. The results in these tables represent a worst case scenario for coupling to the recording devices. The coupling coefficient for each device is assumed to be at their maximum values from Figures 3.15-3.18. It should be noted that these results came from ideal conditions, and in practice the maximum distance and minimum field strength values will need to be larger for coupling to occur. These results are also ideal in the sense that measurements were taken in an environment that was acoustically and electromagnetically "quiet", so no other interference existed. Given the approximations used to estimate these quantities, results are not expected to be more accurate than within a factor of two. Nonetheless, results suggest that messages may realistically be coupled to these devices at reasonable distances from the antenna, even under non-ideal conditions.

Table 3.1. Analog Tape Recorder Ideal Coupling Results

Message Frequency	ρ_{max}	V_{noise} (Vp)	R_{max}	E_{min} (mV_{RMS}/m)
500 Hz	.0081	.001 V	3.2 miles	43.65 mV/m
3 kHz	.001	.0003 V	1.3 miles	106.07 mV/m
6 kHz	1.7779×10^{-4}	.0001 V	0.7 miles	196.42 mV/m

Table 3.2. Computer Microphone Ideal Coupling Results

Message Frequency	ρ_{max}	V_{noise} (Vp)	R_{max}	E_{min} (mV_{RMS}/m)
500 Hz	.0029	1×10^{-5} V	114.0 miles	1.22 mV/m
10 kHz	.0023	1×10^{-6} V	903.9 miles	0.15 mV/m
22 kHz	6.4204×10^{-4}	5×10^{-7} V	503.0 miles	0.28 mV/m

Table 3.3. Digital Video Camera Ideal Coupling Results

Message Frequency	ρ_{max}	V_{noise} (Vp)	R_{max}	E_{min} (mV_{RMS}/m)
1 kHz	.0146	1×10^{-4} V	57.4 miles	2.42 mV/m
10 kHz	.0064	8×10^{-6} V	314.4 miles	0.44 mV/m
20 kHz	1.1744×10^{-4}	2.5×10^{-6} V	18.9 miles	7.37 mV/m

Table 3.4. Wireless Microphone System Ideal Coupling Results

Message Frequency	ρ_{max}	V_{noise} (Vp)	R_{max}	E_{min} (mV_{RMS}/m)
200 Hz	.0083	0.5×10^{-4} V	65.2 miles	2.13 mV/m
2 kHz	.0068	1.5×10^{-6} V	1781.6 miles	0.08 mV/m
22 kHz	2.7955×10^{-4}	0.5×10^{-6} V	220.1 miles	0.63 mV/m

3.2.2. Signal Processing Considerations

In some applications, signal processing could be used to determine if a coupled message signal was present in an audio recording. Recording device susceptibility analysis can be improved with signal processing techniques because these methods can potentially detect the presence of some signals even when they fall below the noise floor. In contrast, without signal processing, signals must be above the noise floor for detection.

One of the simplest methods to detect a known signal is to cross-correlate a recorded audio signal from an audio device with the message signal that was applied during test. If the message is present in the recording, a large spike can be found in the cross-correlation result, at the point where the input message and coupled message align. The peak in the cross-correlation could be compared to a threshold value, and a decision made about a coupled message signal's presence.

To better understand the impact of this method of signal processing, an analysis of the statistical variation of the peak cross-correlation result and the "noise" at off-peak locations was performed. Let the recorded audio signal by a device be represented by (22).

$$Y_i = \begin{cases} N_i & i \leq 0 \\ X_i + N_i & 0 < i \leq A \\ N_i & A < i \leq B \end{cases} \tag{22}$$

where

X_i is a random variable representing the message signal at a sample i,
N_i is a random variable representing noise,
Y_i is the recorded audio signal,
A is the length of the message signal (in number of samples), and
B is the length of the recorded audio signal (in number of samples).

Next, assume that the message signal and the noise are zero mean random variables and each sample of the message signal and noise are independent. In addition, assume samples of the noise and the message signal are independent from each other (that is, the expected value of X_i and X_j is zero for $i \neq j$). To determine if the message signal is present in the recorded audio signal, a cross-correlation is performed with X_i and Y_i. The maximum value of the cross-correlation, denoted by the variable m, will occur when the message signal intersects the portion of the recorded signal that has the message signal plus the noise and is defined by (23) [8].

$$\begin{aligned} m &= \frac{1}{A}\sum_{i=1}^{A}(X_i + N_i)X_i \\ m &= \frac{1}{A}\sum_{i=1}^{A}(X_i^2 + N_iX_i) \\ m &= \frac{1}{A}\sum_{i=1}^{A}X_i^2 + \frac{1}{A}\sum_{i=1}^{A}N_iX_i \end{aligned} \tag{23}$$

In most cases, for optimal signal detection, a signal-to-noise ratio (SNR) must be maximized. To find the conditions for optimal signal detection such as signal length, first let the SNR be represented by (24)-(26), where (25) and (26) represent the "signal" and "noise" within the variable m.

$$SNR \triangleq \frac{E(G^2)}{E(P^2)} \tag{24}$$

$$G \triangleq \frac{1}{A}\sum_{i=1}^{A} X_i^2 \tag{25}$$

$$P \triangleq \frac{1}{A}\sum_{i=1}^{A} N_i X_i \tag{26}$$

where

G is defined as the signal and

P is defined as the noise.

The variance of (25) and (26) can be found in (27) and (28) [8], [9].

$$\begin{aligned}
E(G^2) &= E\left[\left\{\frac{1}{A}\sum_{i=1}^{A} X_i^2\right\}^2\right] \\
E(G^2) &= \frac{1}{A^2}E[\{\sum_{i=1}^{A} X_i^2\}^2] \\
E(G^2) &= \frac{1}{A^2}E[\{X_1^2 + X_2^2 + \cdots + X_A^2\}^2] \\
E(G^2) &= \frac{1}{A^2}[A(3\sigma_X^4) + (A^2 - A)\sigma_X^4] \\
E(G^2) &= \frac{1}{A}[3\sigma_X^4 + (A-1)\sigma_X^4]
\end{aligned} \tag{27}$$

$$\begin{aligned}
E(P^2) &= E\left[\left\{\frac{1}{A}\sum_{i=1}^{A} N_i X_i\right\}^2\right] \\
E(P^2) &= \frac{1}{A^2}E[\{\sum_{i=1}^{A} N_i X_i\}^2] \\
E(P^2) &= \frac{1}{A^2}E[\{N_1X_1 + N_2X_2 + \cdots + N_AX_A\}^2] \\
E(P^2) &= \frac{1}{A^2}E[\sum_{i=1}^{A} N_i^2 X_i^2] \\
E(P^2) &= \frac{1}{A^2}E[N_1^2X_1^2 + N_2^2X_2^2 + \cdots + N_A^2X_A^2] \\
E(P^2) &= \frac{1}{A^2}[\sigma_N^2\sigma_X^2 + \sigma_N^2\sigma_X^2 + \cdots + \sigma_N^2\sigma_X^2] \\
E(P^2) &= \frac{\sigma_N^2\sigma_X^2}{A}
\end{aligned} \tag{28}$$

From (27) and (28), the SNR as defined by (24) can be solved as shown in (29).

$$SNR = \frac{E(G^2)}{E(P^2)}$$

$$SNR = \frac{\frac{1}{A}\left[3\sigma_X^4 + (A-1)\sigma_X^4\right]}{\frac{\sigma_N^2\sigma_X^2}{A}}$$

$$SNR = \frac{(2+A)\sigma_X^2}{\sigma_N^2} \qquad (29)$$

The SNR within the peak cross-correlation value is a multiple of the SNR of the recording before cross-correlation and is dependent on the number of samples. To validate the expression given in (29), a simulation was performed where samples of X and samples of N were randomly generated by a Matlab script. The standard deviation of X was equal to three and the standard deviation of N was equal to two. The signal length (A) was varied from 10 to 1000 samples and vectors for the random variables G and P, represented by (25) and (26), were computed for each signal length. The vectors for G and P were 10000 samples long for each signal length (A). The total simulated recording length (B) was 10000 samples long. The signal to noise ratio as given by (24), was calculated from the variance of the G and P vectors. The results from this simulation can be seen in Figure 3.19. In general the simulated results closely follow the theoretical formula for the SNR as in (29). As the signal length becomes larger the SNR increases, indicating for optimal SNR the message signal should be made as large as possible.

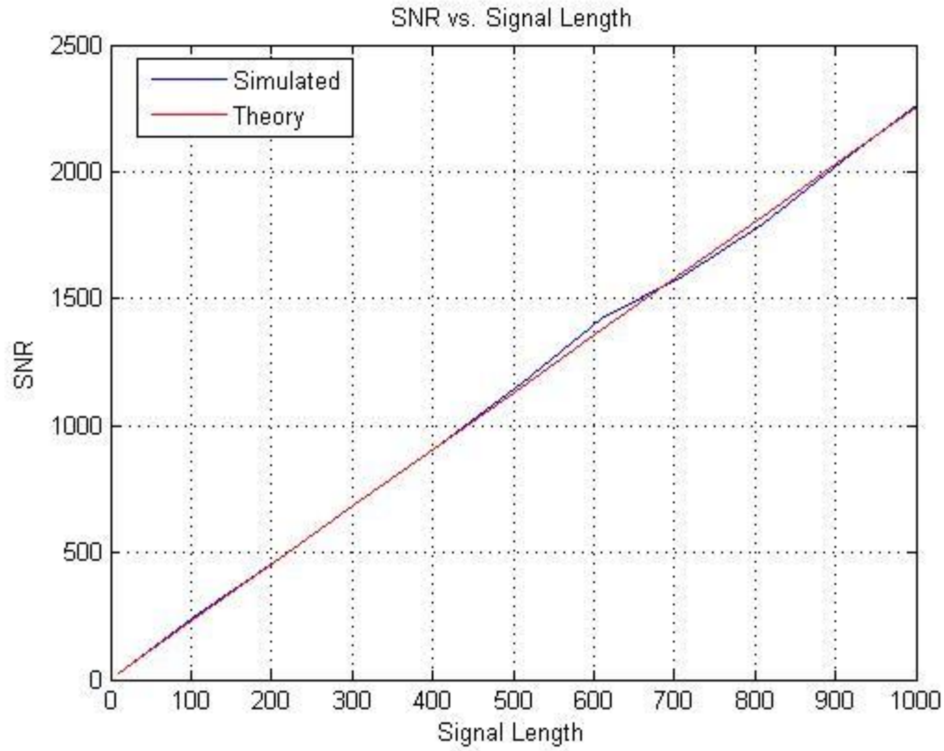

Figure 3.19. SNR Validation Plot.

Although it provides some statistical insight into the point m, (29) does not provide information about how the value of point m changes with respect to the values of other points around m. The definition of SNR in (29) only predicts the change in the peak value of the correlation, independent of the correlation at points around the peak. Since detection is often performed based on the ability to find a strong peak in the cross-correlation, a more useful calculation of SNR may be to compare how the second moment of the point m as defined by (23) changes with the second moment at other points in the cross-correlation vector. An alternative definition for the SNR is explored in more detail in Appendix C.

Another way to determine the signal length for optimal detection is to analyze the probability of message signal detection versus the probability of false alarm for a fixed threshold. The threshold must be fixed at a level between the value m as given by (23) and off-peak values represented by (30) [8].

$$d = \frac{1}{A}\left[\sum_{z=1+|\Delta|}^{A}\left(X_z + N_{z-|\Delta|}\right)X_{z-|\Delta|} + \sum_{z=A+1}^{A+|\Delta|} N_z X_z\right]$$
$$d = \frac{1}{A}\left[\sum_{z=1+|\Delta|}^{A}\left(X_z X_{z-|\Delta|} + N_{z-|\Delta|}X_{z-|\Delta|}\right) + \sum_{z=A+1}^{A+|\Delta|} N_z X_z\right]$$
$$d = \frac{1}{A}\left[\sum_{z=1+|\Delta|}^{A} X_z X_{z-|\Delta|} + \sum_{z=1+|\Delta|}^{A} N_{z-|\Delta|}X_{z-|\Delta|} + \sum_{z=A+1}^{A+|\Delta|} N_z X_z\right]$$
$$d = \frac{1}{A}\sum_{z=1+|\Delta|}^{A} X_z X_{z-|\Delta|} + \frac{1}{A}\sum_{z=1+|\Delta|}^{A} N_{z-|\Delta|}X_{z-|\Delta|} + \frac{1}{A}\sum_{z=A+1}^{A+|\Delta|} N_z X_z \tag{30}$$

where

Δ is the sample offset from point m (at the peak) and is assumed to have a value between zero and the signal length A.

To find a reasonable threshold, it is helpful to look at the mean of the desired peak and off-peak values. The expected values for (23) and (30) are given below in (31) and (32).

$$E[m] = E\left[\frac{1}{A}\sum_{i=1}^{A} X_i^2 + \frac{1}{A}\sum_{i=1}^{A} N_i X_i\right]$$
$$E[m] = \sigma_X^2 \tag{31}$$

$$E[d] = E\left[\frac{1}{A}\sum_{z=1+|\Delta|}^{A} X_z X_{z-|\Delta|} + \frac{1}{A}\sum_{z=1+|\Delta|}^{A} N_{z-|\Delta|}X_{z-|\Delta|} + \frac{1}{A}\sum_{z=A+1}^{A+|\Delta|} N_z X_z\right]$$
$$E[d] = 0 \tag{32}$$

From (31) and (32) a reasonable threshold would be any value greater than 0, but less than the variance of the message signal. The probability of message detection is given in (33) for a threshold equal to half the message variance.

$$P_{Detection} = P\left(\frac{1}{A}\sum_{i=1}^{A} X_i^2 + \frac{1}{A}\sum_{i=1}^{A} N_i X_i \geq \frac{\sigma_X^2}{2}\right)$$
$$P_{Detection} = 1 - P\left(\frac{1}{A}[X_1^2 + X_1 N_1] + \frac{1}{A}[X_2^2 + X_2 N_2] + \cdots + \frac{1}{A}[X_A^2 + X_A N_A] \leq \frac{\sigma_X^2}{2}\right)$$
$$P_{Detection} = 1 - P\left(H_1 + H_2 + \cdots + H_A \leq \frac{\sigma_X^2}{2}\right)$$
$$P_{Detection} \approx 1 - P\left(Z_n \leq \frac{\frac{\sigma_X^2}{2} - A * E[H_1]}{\sigma_{H_1}\sqrt{A}}\right)$$

$$E[H_1] = E\left[\frac{1}{A}(X_1^2 + X_1 N_1)\right]$$
$$E[H_1] = \frac{1}{A}E[X_1^2] + \frac{1}{A}E[X_1]E[N_1]$$
$$E[H_1] = \frac{1}{A}\sigma_X^2$$

$$VAR[H_1] = E\left[\left\{\frac{1}{A}(X_1^2 + X_1N_1)\right\}^2\right] - \left(E\left[\frac{1}{A}(X_1^2 + X_1N_1)\right]\right)^2$$
$$VAR[H_1] = \frac{1}{A^2}E[X_1^4 + 2X_1^3N_1 + X_1^2N_1^2] - \frac{1}{A^2}\sigma_X^4$$
$$VAR[H_1] = \frac{1}{A^2}E[X_1^4] + \frac{1}{A^2}\sigma_X^2\sigma_N^2 - \frac{1}{A^2}\sigma_X^4$$
$$VAR[H_1] = \frac{3}{A^2}\sigma_X^4 + \frac{1}{A^2}\sigma_X^2\sigma_N^2 - \frac{1}{A^2}\sigma_X^4$$
$$VAR[H_1] = \frac{2}{A^2}\sigma_X^4 + \frac{1}{A^2}\sigma_X^2\sigma_N^2$$

$$P_{Detection} \approx 1 - P\left(Z_n \leq \frac{\frac{\sigma_X^2}{2} - A * \frac{1}{A}\sigma_X^2}{\sqrt{\frac{2}{A^2}\sigma_X^4 + \frac{1}{A^2}\sigma_X^2\sigma_N^2}\sqrt{A}}\right)$$
$$P_{Detection} \approx 1 - P\left(Z_n \leq \frac{A\left(\frac{\sigma_X^2}{2} - \sigma_X^2\right)}{\sigma_X\sqrt{2\sigma_X^2 + \sigma_N^2}\sqrt{A}}\right)$$
$$P_{Detection} \approx P\left(Z_n \geq \frac{\sigma_X\sqrt{A}}{2\sqrt{2\sigma_X^2 + \sigma_N^2}}\right) \quad (33)$$

where

Z_n is a Gaussian random variable with zero mean and unit variance according to the Central Limit Theorem [8].

Equation (33) shows the relation that as the message signal becomes longer, the probability of detection increases as expected. To verify this relation, a simulation was performed where the standard deviation of X was equal to three, and the standard deviation of N was equal to two. The signal length (A) was varied from 2 to 50 samples. A vector for the random variable m, represented by (23), was computed for each signal length. The vector for m was 10000 samples long for each signal length (A). The probability of detection was then calculated with sampled values of m for each signal length. The result from this simulation is shown in Figure 3.20. Because the standard deviation of X is relatively large, it does not take many samples for the probability of detection to approach the value of one.

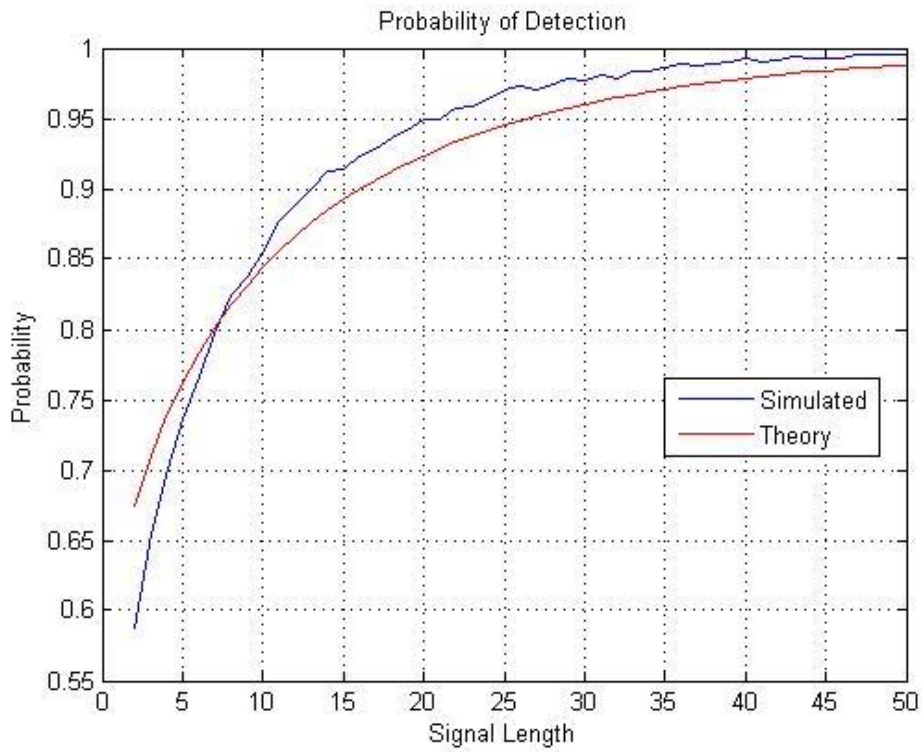

Figure 3.20. Probability of Message Detection for Standard Deviation of X Equal to Three and Standard Deviation of N Equal to Two.

Another important quantity is the probability of false alarm. This probability determines the likelihood that values of d, given in (30), and other off-peak values will be larger than a set threshold. To ease computational complexity, the probability of false alarm can be split up into two regions. Region one will be the off-peak points in the cross-correlation vector where the message signal is correlated with noise. Region two will be the off-peak points where the message signal is correlated with a delayed message plus noise. The total probability of false alarm could be calculated by finding the probability that points in either region one or region two will be larger than the threshold value. The calculation of total false alarm probability is cumbersome due to probabilistic dependencies among points in regions one and two. To simplify the false alarm probability analysis, the probability of false alarm in either region will be analyzed separately. The points in region one can be represented by s, shown below in (34).

$$s = \frac{1}{A}\sum_{i=1}^{A} N_i X_i \qquad (34)$$

Region two can be represented by the points in d, given in (30). The calculation for the probability of false alarm in region one is shown below in (35) for a threshold equal to half the message variance.

$$P_{False\ Alarm} = P\left(\frac{1}{A}\sum_{i=1}^{A} N_i X_i \geq \frac{\sigma_X^2}{2}\right)$$
$$P_{False\ Alarm} = 1 - P\left(\frac{1}{A}[N_1 X_1] + \frac{1}{A}[N_2 X_2] + \cdots + \frac{1}{A}[N_A X_A] \leq \frac{\sigma_X^2}{2}\right)$$
$$P_{False\ Alarm} = 1 - P\left(I_1 + I_2 + \cdots + I_A \leq \frac{\sigma_X^2}{2}\right)$$
$$P_{False\ Alarm} \approx 1 - P\left(Z_n \leq \frac{\frac{\sigma_X^2}{2} - A * E[I_1]}{\sigma_{I_1}\sqrt{A}}\right)$$

$$E[I_1] = E\left[\frac{1}{A}(N_1 X_1)\right]$$
$$E[I_1] = 0$$

$$VAR[I_1] = E\left[\left\{\frac{1}{A}(N_1 X_1)\right\}^2\right] - \left(E\left[\frac{1}{A}(N_1 X_1)\right]\right)^2$$
$$VAR[I_1] = \frac{1}{A^2}E[N_1^2 X_1^2]$$
$$VAR[I_1] = \frac{1}{A^2}\sigma_N^2 \sigma_X^2$$

$$P_{False\ Alarm} \approx 1 - P\left(Z_n \leq \frac{\frac{\sigma_X^2}{2}\sqrt{A}}{\sigma_N \sigma_X}\right)$$
$$P_{False\ Alarm} \approx 1 - P\left(Z_n \leq \frac{\sigma_X \sqrt{A}}{2\sigma_N}\right) \quad (35)$$

where

Z_n is a Gaussian random variable with zero mean and unit variance according to the Central Limit Theorem [8].

Equation (35) shows that as a message signal becomes larger, the probability of false alarm becomes smaller as expected. To verify this relation, a simulation was performed where the standard deviation of X was equal to three, and the standard deviation of N was equal to two. The signal length (A) was varied from 2 to 50 samples. A vector for the random variable s, represented by (34), was computed for each signal length. The vector for s was 10000 samples long for each signal length (A). The probability of false alarm was then calculated with sampled values of s for each signal length. The result from this simulation is shown in Figure 3.21.

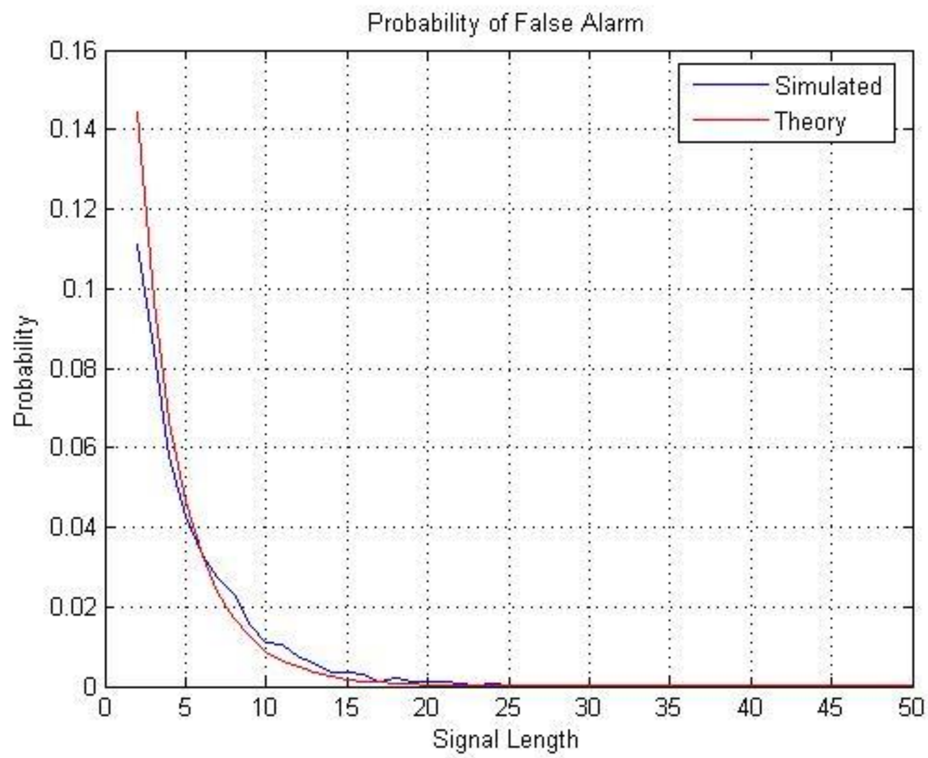

Figure 3.21. Probability of False Alarm in Region One for Standard Deviation of X Equal to Three and Standard Deviation of N Equal to Two.

Because the standard deviation of X is relatively large, it does not take many samples for the probability of false alarm in region one to approach zero.

A similar derivation can be applied for the probability of false alarm in region two, but due to computational complexity it will not be shown. Instead, to find the probability of false alarm in region two, a simulation was performed where the standard deviation of X was equal to three, and the standard deviation of N was equal to two. The signal length (A) was varied from 2 to 50 samples. A vector for the random variable d, represented by (30), was computed for each signal length and for each possible sample offset (Δ). The total vector for d was variable due to variability of the sample offset range for each sample length. The total vector for d was 10000 samples long for the signal length of two, and was 500000 samples long for the signal length of 50. The probability of false alarm was calculated with sampled values of d for each signal length. The result from this simulation is shown in Figure 3.22. Because the standard deviation of X is relatively large, it does not take many samples for the probability of false alarm in region two to approach zero.

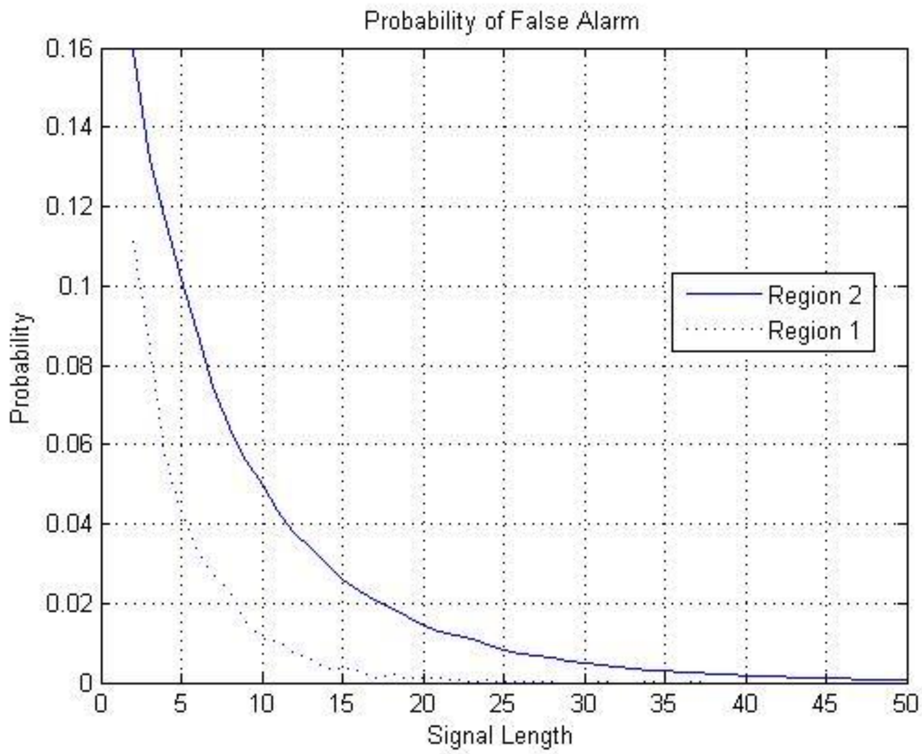

Figure 3.22. Probability of False Alarm in Region Two for Standard Deviation of X Equal to Three and Standard Deviation of N Equal to Two.

To understand the impacts of the noise and signal variances on the detection and false alarm probabilities, a simulation was performed with different variances. The theoretical formula for the detection probability and false alarm probability in region one was used in the simulation. In a separate simulation, the cross-correlation was computed for sample cases with the same variances. The threshold value was set to half the message variance. Simulated values of the probability of false alarm in region one and the probability of detection with the signal sample length are shown in Figure 3.23. Example cross-correlations between the message and the "measured signal" are shown in Figures 3.24-3.26.

Figure 3.23 shows that detecting a weak message signal (a signal with a small standard deviation relative to the standard deviation for noise) requires a message signal to be as long as possible to maximize detection probability and minimize false alarm probability. This result indicates that even weakly coupled signals can be detected given a sufficient number of samples in the message signal.

Figures 3.24-3.26 illustrate how the peak value of the cross-correlation improves as the signal energy goes up relative to the noise energy. Figure 3.24 illustrates an example case were the probability of detection is low and the probability of false alarm is high. In this data set the intended peak (m) would not be detected, and other peaks would trigger false alarms. Figure 3.25 shows an example case where both the detection and false alarm probabilities are moderate. The intended peak would be detected, but another peak to the right of m would trigger a false alarm. Figure 3.26 shows the best example case where the probability of detection is high and the probability of false alarm is low. In this data set the peak is obvious. The intended peak would be detected, and no false alarms would occur.

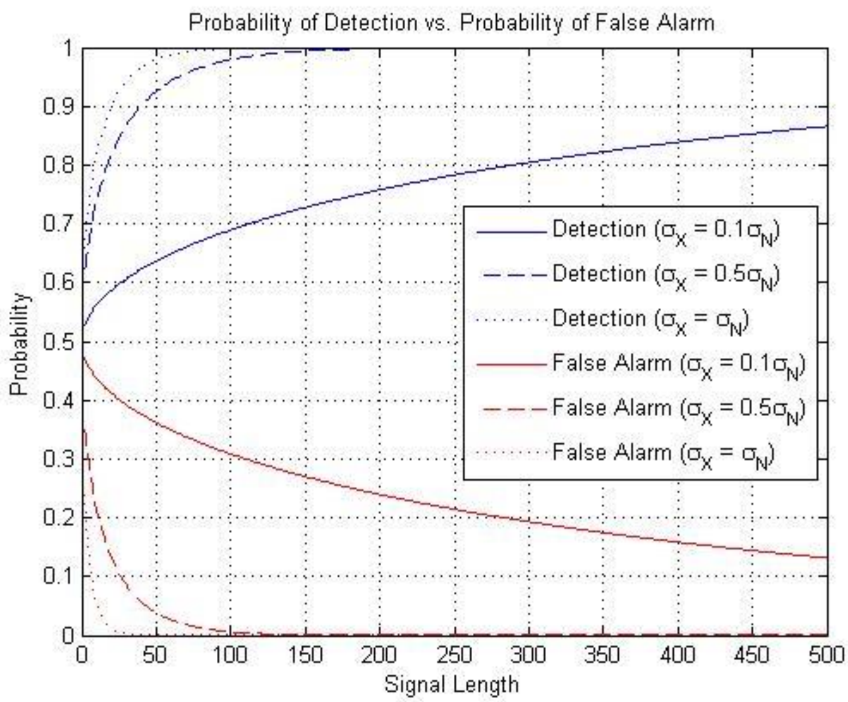

Figure 3.23. Probability of Detection versus Probability of False Alarm.

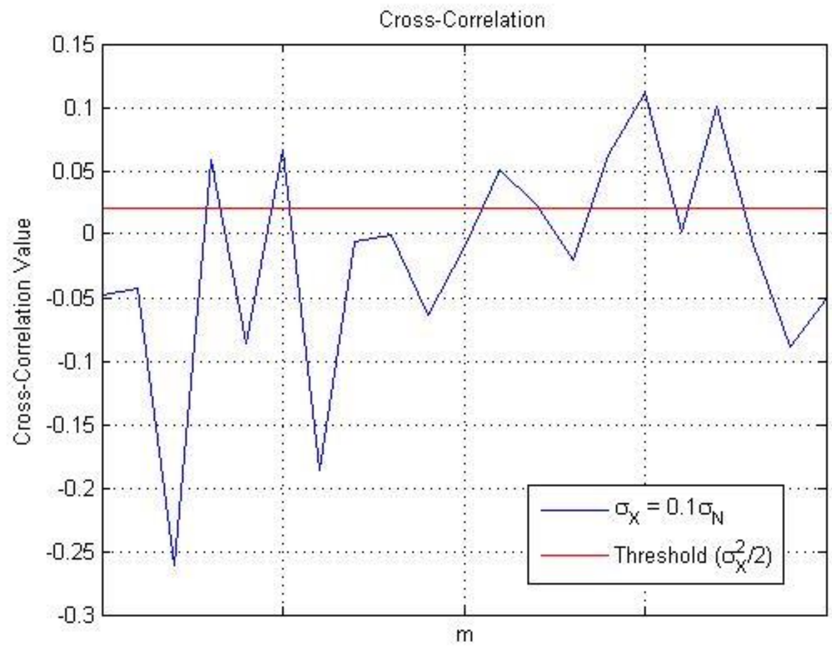

Figure 3.24. Cross-Correlation with Low Probability of Detection.

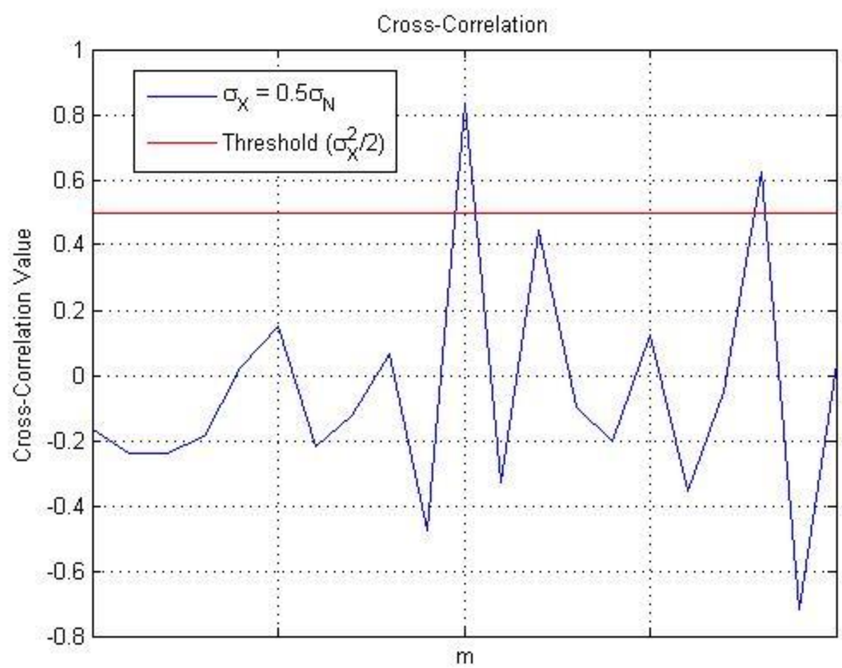

Figure 3.25. Cross-Correlation with Moderate Probability of Detection.

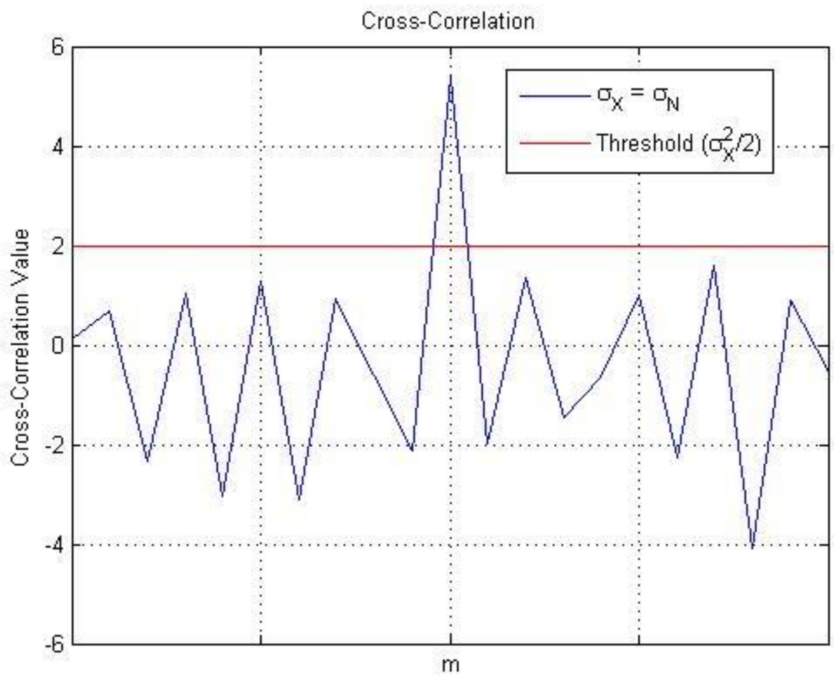

Figure 3.26. Cross-Correlation with High Probability of Detection.

Another simulation was performed to show the impact of message signal length on the probability of detection and the probability of false alarm based on the analysis of one data set from a cross-correlation. To illustrate that long message signals are needed for optimal detection of weak message signals, the standard deviation of the message was set to 0.1 times the standard deviation of the noise. The noise standard deviation was set to two. Figures 3.27-3.29 show the results from this simulation.

Figure 3.27 illustrates an example case were the probability of detection is low and the probability of false alarm is high. In this data set the intended peak (m) would not be detected, and other peaks would trigger false alarms. Figure 3.28 shows an example case where both the detection and false alarm probabilities are moderate. The intended peak would be detected, but other peaks would trigger a false alarm. Figure 3.29 shows the best example case where the probability of detection is high and the probability of false alarm is low. In this data set the peak is obvious and is an ideal case for signal detection. With the long message signal the intended peak would be detected, and no false alarms would occur.

It should be noted that in the above derivations it was assumed that the message signal in the recording, X, and the message signal being used for cross-correlation (also X) were of the same magnitude. In reality, these two signals will have a different magnitude due to the unknown coupling coefficient, ρ, as given in (16) and other transmitter properties as shown in (15). These parameters will alter the value of the signal variance, σ_X^2, to a fractional value of the variance in (29), (33), and (35). The basic result, however, is the same.

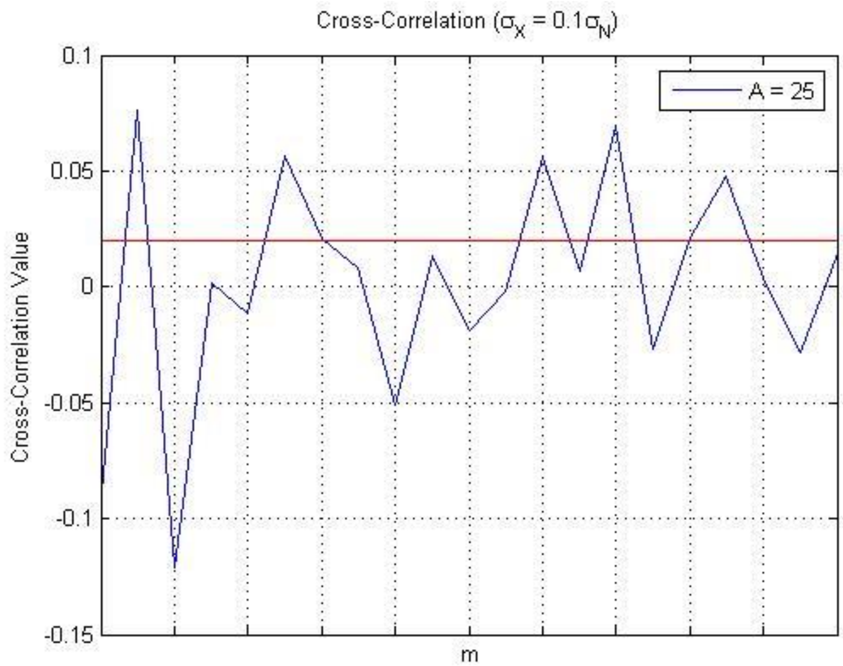

Figure 3.27. Cross-Correlation with a Short Message.

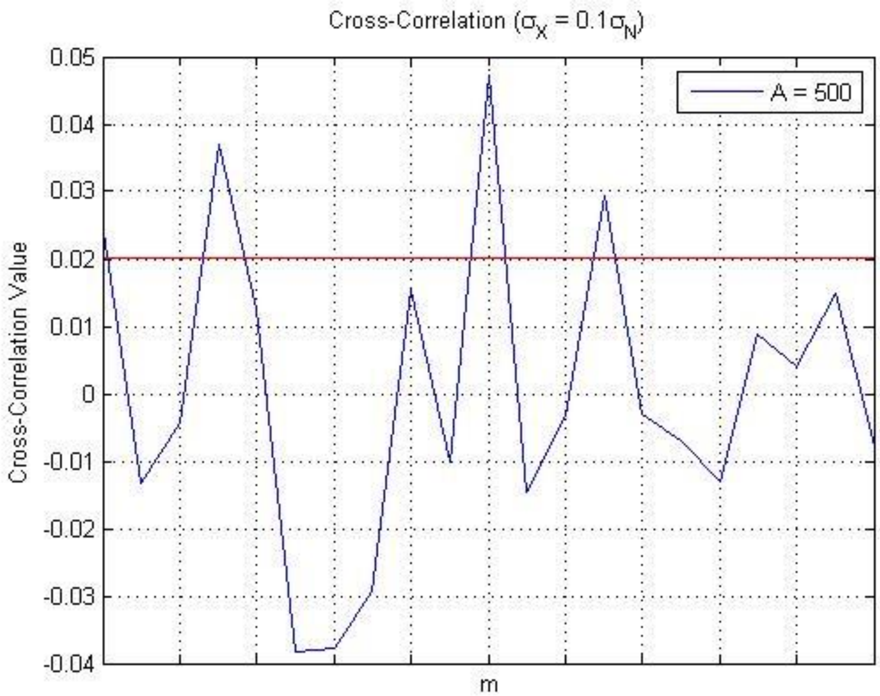

Figure 3.28. Cross-Correlation with a Moderate Length Message.

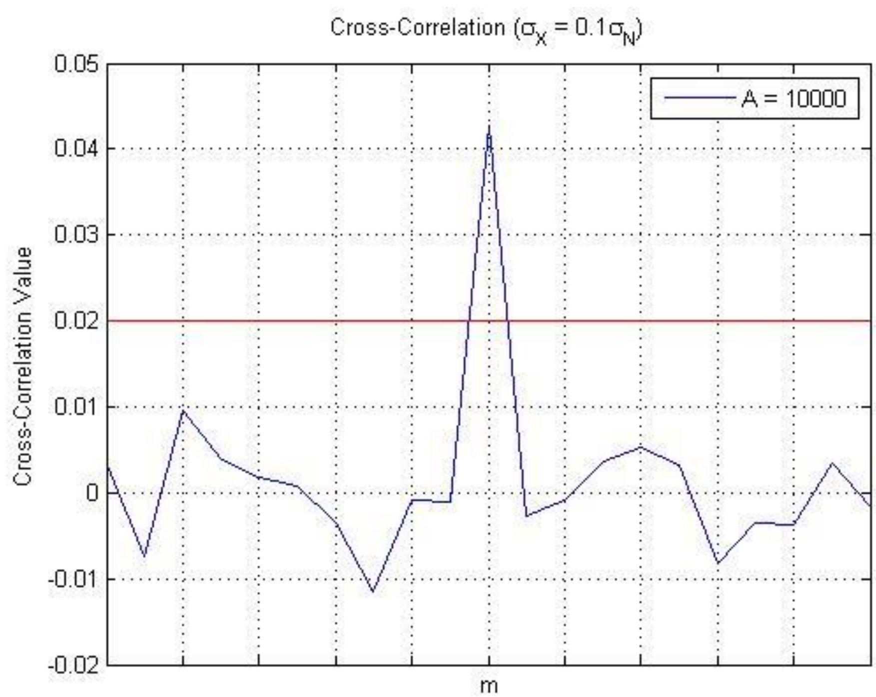

Figure 3.29. Cross-Correlation with a Long Message.

4. CONCLUSION

An electromagnetic susceptibility study of an analog tape recorder, a digital video camera, a wired computer microphone, and a wireless microphone system with a variety of signals in a semi-anechoic chamber was performed. It was found that all devices were susceptible to amplitude modulated signals, and modulated message signals were demodulated within each recording device. Coupling parameters such as carrier frequency ranges, message frequency ranges, device orientation, and field polarization were highly specific to each device. After performing electric field and message coupling analysis, it was found that the minimum field strength required for coupling in a worst-case scenario was not unreasonable for possible detection under realistic conditions.

In the worst-case scenario, message coupling could occur for all devices within one mile from a 1 kW transmitter, assuming optimal coupling parameters (coupling carrier and message frequencies, field polarization, and device orientation). For three of the four devices, significant coupling could be achieved at distances of more than 50 miles. The worst-case scenario considered a relatively small transmitting antenna, and in practice many of these antennas are fed with much greater power levels [10]. It is likely that a more powerful transmitter could overcome many of the field losses not considered in the worst-case scenario as well as sub-optimal coupling parameters. For example, a device may not be oriented for worst-case coupling relative to the antenna, but reflections from the surrounding may provide adequate energy at the coupled level. The reflections may not be as strong as the source, but may be sufficient to allow detection at reasonable distances from the antenna (e.g. at 10 miles from an antenna when the ideal maximum were 50 miles). Coupled with some basic signal processing as discussed in the previous section, message coupling at the calculated maximum distances could still be achieved, especially if the messages were long. Even if the coupled messages were weak, the long messages would allow the probability of detection to approach one.

There are many avenues for future work in this susceptibility study of recording devices. One possible path would be to study how messages couple to devices with carrier frequencies above 990 MHz. Another possible study would investigate more expensive audio equipment which may be used more often in “professional” recordings than the devices studied in this research. Rather than only studying audio signals, video signals could also be studied in the case of the digital video recorder to see how the video is impacted by electromagnetic signals.

5. REFERENCES

[1] C. R. Paul, *Introduction to Electromagnetic Compatibility*, 2nd ed. Hoboken, NJ: John Wiley & Sons, 2006, pp. 81, 423, 456-460.

[2] C. A. Balanis, *Antenna Theory: Analysis and Design*, 3rd ed. Hoboken, NJ: John Wiley & Sons, 2005, pp. 174, 151-160, 184-189, 208-214, 284-286, 774.

[3] R. E. Ziemer and W. H. Tranter, *Principles of Communications: Systems, Modulation, and Noise*, 5th ed. New York: John Wiley & Sons, 2002, pp. 106-110, 620-621.

[4] "Model 3121C Tuned Dipole," [Online]. Available: http://www.ets-lindgren.com/pdf/ant5.pdf [Accessed: March 15, 2010].

[5] "Broadband EMC Test Antennas: 30 MHz – 6 GHz," [Online]. Available: http://www.sunolsciences.com/pdf/JB%20Antennas%20w-patterns.pdf [Accessed: March 15, 2010].

[6] D. M. Pozar, *Microwave Engineering*, 3rd ed. Hoboken, NJ: John Wiley & Sons, 2005, pp. 298.

[7] Federal Communications Commission, "AM Station Classes: Clear, Regional, and Local Channels," [Online]. Available: http://www.fcc.gov/mb/audio/amclasses.html [Accessed: March 21, 2010].

[8] A. Leon-Garcia, *Probability, Statistics, and Random Processes for Electrical Engineering*, 3rd ed. Upper Saddle River, NJ: Pearson Prentice Hall, 2008, pp. 109-110, 283, 369-373, 416-419, 442, 496-497.

[9] J. G. Proakis, *Digital Communications*, 2nd ed. New York: McGraw-Hill, 1989, pp. 55.

[10] Federal Communications Commission, "Frequency Allocation Table," [Online]. Available: http://www.fcc.gov/oet/spectrum/table/Welcome.html [Accessed: March 21, 2010].

APPENDIX A: TESTING TABLES

Below is more information about the generalized testing that was performed for each of the devices. Table A.1 and Table A.2 specifies the most pertinent test conditions for the generalized testing.

Table A.1. Generalized Testing Details for All Recording Devices

Antenna Polarization	Test Type	Turntable Position	Test Numbers
Horizontal	No Modulation	0	1,2
		90	3,4
		180	5,6
		270	7,8
Vertical	No Modulation	0	9,10
		90	11,12
		180	13, 14
		270	15, 16
Horizontal	AM1	0	17, 18
		90	19, 20
		180	21, 22
		270	23, 24
Vertical	AM1	0	25, 26
		90	27, 28
		180	29, 30
		270	31, 32
Horizontal	AM2	0	33, 34
		90	35, 36
		180	37, 38
		270	39, 40
Vertical	AM2	0	41, 42
		90	43, 44
		180	45, 46
		270	47, 48
Horizontal	FM1	0	49, 50
		90	51, 52
		180	53, 54
		270	55, 56
Vertical	FM1	0	57, 58
		90	59, 60
		180	61, 62
		270	63, 64

Table A.2. General Testing Test Type Description

Test Type	Test Details
No Modulation	Carrier Frequency Sweep 1-990 MHz, Carrier Frequency Step 1 MHz, 13 dBm Output Power
AM1	Carrier Frequency Sweep 1-990 MHz, Carrier Frequency Step 1 MHz, Message Sweep 440 Hz-25 kHz, 2 Second Message Ramp, 50% Modulation Depth, 13 dBm Output Power
AM2	Carrier Frequency Sweep 1-990 MHz, Carrier Frequency Step 1 MHz, Message Sweep 45 Hz-15.5 kHz, 2 Second Message Ramp, 50% Modulation Depth, 13 dBm Output Power
FM1	Carrier Frequency Sweep 1-990 MHz, Carrier Frequency Step 1 MHz, Message Sweep 440 Hz-25 kHz, 2 Second Message Ramp, 25 kHz Peak Deviation Frequency, 13 dBm Output Power

Below is more information about the specific testing that was performed for each device. Tables A.3-A.6 specify the most pertinent test conditions for the device specific testing.

Table A.3. Specific Testing For Analog Tape Recorder

Test Numbers	Test Purpose	Test Conditions
101, 102	Determine Exact Coupling Carrier Frequencies	AM, Carrier Frequency Sweep 510-600 MHz, Carrier Frequency Step 1 MHz, Message Sweep 450 Hz-25 kHz, 2 Second Message Ramp, 50% Modulation Depth, 13 dBm Output Power, Vertical Antenna Polarization, 180° Turntable Position
103, 104	Determine Exact Coupling Carrier Frequencies	AM, Carrier Frequency Sweep 770-855 MHz, Carrier Frequency Step 1 MHz, Message Sweep 450 Hz-25 kHz, 2 Second Message Ramp, 50% Modulation Depth, 13 dBm Output Power, Vertical Antenna Polarization, 180° Turntable Position
105, 106	Determine General Message Coupling Limitations	AM, Carrier Frequency 547 MHz, Message Sweep 45 Hz-15 kHz, 10 Second Message Ramp, 50% Modulation Depth, 13 dBm Output Power, Vertical Antenna Polarization, 180° Turntable Position

Table A.3. (Continued)

Test Numbers	Test Purpose	Test Conditions
107, 108	Determine General Message Coupling Limitations	AM, Carrier Frequency 547 MHz, Message Sweep 432 Hz-25 kHz, 10 Second Message Ramp, 50% Modulation Depth, 13 dBm Output Power, Vertical Antenna Polarization, 180° Turntable Position
109, 110	Determine General Message Coupling Limitations	AM, Carrier Frequency 831 MHz, Message Sweep 45 Hz-15 kHz, 10 Second Message Ramp, 50% Modulation Depth, 13 dBm Output Power, Vertical Antenna Polarization, 180° Turntable Position
111, 112	Determine General Message Coupling Limitations	AM, Carrier Frequency 831 MHz, Message Sweep 432 Hz-25 kHz, 10 Second Message Ramp, 50% Modulation Depth, 13 dBm Output Power, Vertical Antenna Polarization, 180° Turntable Position
113, 114	Determine Message Coupling Lower Limit	AM, Carrier Frequency 547 MHz, Message Sweep 25 Hz-500 Hz, 10 Second Message Ramp, 50% Modulation Depth, 13 dBm Output Power, Vertical Antenna Polarization, 180° Turntable Position
115, 116	Determine Message Coupling Lower Limit	AM, Carrier Frequency 831 MHz, Message Sweep 25 Hz-500 Hz, 10 Second Message Ramp, 50% Modulation Depth, 13 dBm Output Power, Vertical Antenna Polarization, 180° Turntable Position
Ambient1, 117-122	Establish Input Message and Coupled Message Correlation	AM, Carrier Frequency 547 MHz, 50% Modulation Depth, 13 dBm Output Power, Vertical Antenna Polarization, 180° Turntable Position Message Frequencies: Ambient1 – No Message & No Carrier, Test117 – 300 Hz, Test118 – 500 Hz, Test119 – 1 kHz, Test120 – 2 kHz, Test121 – 5 kHz, Test122 – 7 kHz

Table A.3. (Continued)

Test Numbers	Test Purpose	Test Conditions
Ambient2, 123-128	Establish Input Message and Coupled Message Correlation	AM, Carrier Frequency 831 MHz, 50% Modulation Depth, 13 dBm Output Power, Vertical Antenna Polarization, 180° Turntable Position Message Frequencies: Ambient2 – No Message & No Carrier, Test123 – 300 Hz, Test124 – 500 Hz, Test125 – 1 kHz, Test126 – 2 kHz, Test127 – 5 kHz, Test128 – 7 kHz
129, 130	Determine Minimum Carrier Power Needed For Message Detection	AM, Carrier Frequency 547 MHz, Message 1 kHz, 50% Modulation Depth, Output Power Sweep -127 dBm to 13 dBm, Output Power Step 1 dBm, Vertical Antenna Polarization, 180° Turntable Position
131, 132	Determine Minimum Modulation Depth Needed For Message Detection	AM, Carrier Frequency 547 MHz, Message 1 kHz, Modulation Depth Sweep 1-99%, Modulation Depth Step 1%, 11 dBm Output Power, Vertical Antenna Polarization, 180° Turntable Position
STestAmb, STest1-STest4	Determine Device Orientation Impact on Message Coupling	AM, Carrier Frequency 547 MHz, 50% Modulation Depth, 13 dBm Output Power, Vertical Antenna Polarization, Turntable Position Sweep 0-355°, Turntable Position Interval 5° Message Frequencies: STestAmb – No Message & No Carrier, STest1 – 500 Hz, STest2 – 3 kHz, STest3 – 6 kHz

Table A.4. Specific Testing For Computer Microphone

Test Numbers	Test Purpose	Test Conditions
101, 102	Determine Exact Coupling Carrier Frequencies	AM, Carrier Frequency Sweep 200-240 MHz, Carrier Frequency Step 1 MHz, Message Sweep 469 Hz-25 kHz, 2 Second Message Ramp, 50% Modulation Depth, 13 dBm Output Power, Vertical Antenna Polarization, 0° Turntable Position
103, 104	Determine Exact Coupling Carrier Frequencies	AM, Carrier Frequency Sweep 415-445 MHz, Carrier Frequency Step 1 MHz, Message Sweep 469 Hz-25 kHz, 2 Second Message Ramp, 50% Modulation Depth, 13 dBm Output Power, Vertical Antenna Polarization, 180° Turntable Position
105, 106	Determine General Message Coupling Limitations	AM, Carrier Frequency 220 MHz, Message Sweep 48 Hz-15.512 kHz, 10 Second Message Ramp, 50% Modulation Depth, 13 dBm Output Power, Vertical Antenna Polarization, 0° Turntable Position
107, 108	Determine General Message Coupling Limitations	AM, Carrier Frequency 220 MHz, Message Sweep 470 Hz-25 kHz, 10 Second Message Ramp, 50% Modulation Depth, 13 dBm Output Power, Vertical Antenna Polarization, 0° Turntable Position
109, 110	Determine General Message Coupling Limitations	AM, Carrier Frequency 430 MHz, Message Sweep 48 Hz-15.512 kHz, 10 Second Message Ramp, 50% Modulation Depth, 13 dBm Output Power, Vertical Antenna Polarization, 180° Turntable Position
111, 112	Determine General Message Coupling Limitations	AM, Carrier Frequency 430 MHz, Message Sweep 470 Hz-25 kHz, 10 Second Message Ramp, 50% Modulation Depth, 13 dBm Output Power, Vertical Antenna Polarization, 180° Turntable Position

Table A.4. (Continued)

Test Numbers	Test Purpose	Test Conditions
113, 114	Determine Message Coupling Lower Limit	AM, Carrier Frequency 220 MHz, Message Sweep 25 Hz-1.501 kHz, 10 Second Message Ramp, 50% Modulation Depth, 13 dBm Output Power, Vertical Antenna Polarization, 0° Turntable Position
115, 116	Determine Message Coupling Lower Limit	AM, Carrier Frequency 430 MHz, Message Sweep 25 Hz-1.501 kHz, 10 Second Message Ramp, 50% Modulation Depth, 13 dBm Output Power, Vertical Antenna Polarization, 180° Turntable Position
Ambient1, 117-122	Establish Input Message and Coupled Message Correlation	AM, Carrier Frequency 220 MHz, 50% Modulation Depth, 13 dBm Output Power, Vertical Antenna Polarization, 0° Turntable Position Message Frequencies: Ambient1 – No Message & No Carrier, Test117 – 500 Hz, Test118 – 2 kHz, Test119 – 5 kHz, Test120 – 10 kHz, Test121 – 15 kHz, Test122 – 22 kHz
Ambient2, 123-128	Establish Input Message and Coupled Message Correlation	AM, Carrier Frequency 430 MHz, 50% Modulation Depth, 13 dBm Output Power, Vertical Antenna Polarization, 180° Turntable Position Message Frequencies: Ambient2 – No Message & No Carrier, Test123 – 500 Hz, Test124 – 2 kHz, Test125 – 5 kHz, Test126 – 10 kHz, Test127 – 15 kHz, Test128 – 22 kHz
129, 130	Determine Minimum Carrier Power Needed For Message Detection	AM, Carrier Frequency 220 MHz, Message 10 kHz, 50% Modulation Depth, Output Power Sweep -127 dBm to 13 dBm, Output Power Step 1 dBm, Vertical Antenna Polarization, 0° Turntable Position

Table A.4. (Continued)

Test Numbers	Test Purpose	Test Conditions
131, 132	Determine Minimum Modulation Depth Needed For Message Detection	AM, Carrier Frequency 220 MHz, Message 10 kHz, Modulation Depth Sweep 1-99%, Modulation Depth Step 1%, 11 dBm Output Power, Vertical Antenna Polarization, 0° Turntable Position
STestAmb, STest1-STest4	Determine Device Orientation Impact on Message Coupling	AM, Carrier Frequency 220 MHz, 50% Modulation Depth, 13 dBm Output Power, Vertical Antenna Polarization, Turntable Position Sweep 0-355°, Turntable Position Interval 5° Message Frequencies: STestAmb – No Message & No Carrier, STest1 – 500 Hz, STest2 – 10 kHz, STest3 – 22 kHz

Table A.5. Specific Testing For Digital Video Camera

Test Numbers	Test Purpose	Test Conditions
101, 102	Determine Exact Coupling Carrier Frequencies	AM, Carrier Frequency Sweep 200-240 MHz, Carrier Frequency Step 1 MHz, Message Sweep 471 Hz-25 kHz, 2 Second Message Ramp, 50% Modulation Depth, 13 dBm Output Power, Horizontal Antenna Polarization, 90° Turntable Position
103, 104	Determine Exact Coupling Carrier Frequencies	AM, Carrier Frequency Sweep 340-390 MHz, Carrier Frequency Step 1 MHz, Message Sweep 471 Hz-25 kHz, 2 Second Message Ramp, 50% Modulation Depth, 13 dBm Output Power, Horizontal Antenna Polarization, 90° Turntable Position

Table A.5. (Continued)

Test Numbers	Test Purpose	Test Conditions
105, 106	Determine General Message Coupling Limitations	AM, Carrier Frequency 211 MHz, Message Sweep 48 Hz-15 kHz, 10 Second Message Ramp, 50% Modulation Depth, 13 dBm Output Power, Horizontal Antenna Polarization, 90° Turntable Position
107, 108	Determine General Message Coupling Limitations	AM, Carrier Frequency 211 MHz, Message Sweep 465 Hz-25 kHz, 10 Second Message Ramp, 50% Modulation Depth, 13 dBm Output Power, Horizontal Antenna Polarization, 90° Turntable Position
109, 110	Determine Message Coupling Lower Limit	AM, Carrier Frequency 211 MHz, Message Sweep 47 Hz-2 kHz, 10 Second Message Ramp, 50% Modulation Depth, 13 dBm Output Power, Horizontal Antenna Polarization, 90° Turntable Position
Ambient1, 111-116	Establish Input Message and Coupled Message Correlation	AM, Carrier Frequency 211 MHz, 50% Modulation Depth, 13 dBm Output Power, Horizontal Antenna Polarization, 90° Turntable Position Message Frequencies: Ambient1 – No Message & No Carrier, Test111 – 1 kHz, Test112 – 2 kHz, Test113 – 5 kHz, Test114 – 10 kHz, Test115 – 15 kHz, Test116 – 20 kHz
117, 118	Determine Minimum Carrier Power Needed For Message Detection	AM, Carrier Frequency 211 MHz, Message 10 kHz, 50% Modulation Depth, Output Power Sweep -127 dBm to 13 dBm, Output Power Step 1 dBm, Horizontal Antenna Polarization, 90° Turntable Position

Table A.5. (Continued)

Test Numbers	Test Purpose	Test Conditions
119, 120	Determine Minimum Modulation Depth Needed For Message Detection	AM, Carrier Frequency 211 MHz, Message 10 kHz, Modulation Depth Sweep 1-99%, Modulation Depth Step 1%, 11 dBm Output Power, Horizontal Antenna Polarization, 90° Turntable Position
STestAmb, STest1-STest4	Determine Device Orientation Impact on Message Coupling	AM, Carrier Frequency 211 MHz, 50% Modulation Depth, 13 dBm Output Power, Horizontal Antenna Polarization, Turntable Position Sweep 0-355°, Turntable Position Interval 5° Message Frequencies: STestAmb – No Message & No Carrier, STest1 – 1 kHz, STest2 – 10 kHz, STest3 – 20 kHz
121, 122	Determine Possible Coupling Path	AM, Carrier Frequency 211 MHz, Message Sweep 470 Hz-25 kHz, 10 Second Message Ramp, 50% Modulation Depth, 13 dBm Output Power, Horizontal Antenna Polarization, 90° Turntable Position, Camera Operating on Battery Power

Table A.6. Specific Testing For Wireless Microphone System

Test Numbers	Test Purpose	Test Conditions
101, 102	Determine Unusual Coupling Carrier Frequencies	No Modulation, Sine Wave Sweep 35-60 MHz, Sine Wave Step 1 MHz, 13 dBm Output Power, Vertical Antenna Polarization, 90° Turntable Position

Table A.6. (Continued)

Test Numbers	Test Purpose	Test Conditions
103, 104	Determine General Coupling Carrier Frequencies	AM, Carrier Frequency Sweep 1-990 MHz, Carrier Frequency Step 1 MHz, Message Sweep 471 Hz-25 kHz, 2 Second Message Ramp, 50% Modulation Depth, 13 dBm Output Power, Horizontal Antenna Polarization, 90° Turntable Position
105, 106	Determine Exact Coupling Carrier Frequencies	AM, Carrier Frequency Sweep 225-300 MHz, Carrier Frequency Step 1 MHz, Message Sweep 471 Hz-25 kHz, 2 Second Message Ramp, 50% Modulation Depth, 13 dBm Output Power, Horizontal Antenna Polarization, 90° Turntable Position
107, 108	Determine General Message Coupling Limitations	AM, Carrier Frequency 254 MHz, Message Sweep 48 Hz-15.522 kHz, 10 Second Message Ramp, 50% Modulation Depth, 13 dBm Output Power, Horizontal Antenna Polarization, 90° Turntable Position
109, 110	Determine General Message Coupling Limitations	AM, Carrier Frequency 254 MHz, Message Sweep 471 Hz-25 kHz, 10 Second Message Ramp, 50% Modulation Depth, 13 dBm Output Power, Horizontal Antenna Polarization, 90° Turntable Position
111, 112	Determine Message Coupling Lower Limit	AM, Carrier Frequency 254 MHz, Message Sweep 25 Hz-1.497 kHz, 10 Second Message Ramp, 50% Modulation Depth, 13 dBm Output Power, Horizontal Antenna Polarization, 90° Turntable Position

Table A.6. (Continued)

Test Numbers	Test Purpose	Test Conditions
Ambient1, 113-118	Establish Input Message and Coupled Message Correlation	AM, Carrier Frequency 254 MHz, 50% Modulation Depth, 13 dBm Output Power, Horizontal Antenna Polarization, 90° Turntable Position Message Frequencies: Ambient1 – No Message & No Carrier, Test113 – 200 Hz, Test114 – 2 kHz, Test115 – 5 kHz, Test116 – 10 kHz, Test117 – 15 kHz, Test118 – 22 kHz
119, 120	Determine Minimum Carrier Power Needed For Message Detection	AM, Carrier Frequency 254 MHz, Message 2 kHz, 50% Modulation Depth, Output Power Sweep -127 dBm to 13 dBm, Output Power Step 1 dBm, Horizontal Antenna Polarization, 90° Turntable Position
121, 122	Determine Minimum Modulation Depth Needed For Message Detection	AM, Carrier Frequency 254 MHz, Message 2 kHz, Modulation Depth Sweep 1-99%, Modulation Depth Step 1%, 11 dBm Output Power, Horizontal Antenna Polarization, 90° Turntable Position
STestAmb, STest1-STest4	Determine Device Orientation Impact on Message Coupling	AM, Carrier Frequency 254 MHz, 50% Modulation Depth, 13 dBm Output Power, Horizontal Antenna Polarization, Turntable Position Sweep 0-355°, Turntable Position Interval 5° Message Frequencies: STestAmb – No Message & No Carrier, STest1 – 200 Hz, STest2 – 2 kHz, STest3 – 22 kHz

APPENDIX B: ADDITIONAL PLOTS

The following section contains additional plots that further characterize the electromagnetic coupling characteristics of each device. For each device there are two main types of plots that will be shown in this section. The first class of plots show additional evidence there was a 1-1 correlation between coupled messages in each device to the messages input to the modulation source in the experimental setup. The second class of plots illustrates coupling characteristics as a function of angular position for each device in the spin tests.

B.1. Analog Tape Recorder

Testing was performed to show that the coupled messages in the recordings were the same as the messages created by the signal generators. The carrier frequency was fixed, and the messages were transmitted at a few fixed frequencies. The recordings were analyzed by creating a PSD estimate plot using Welch's method. Figures B.1-B.2 show a few additional results from these experiments. The message signal spikes in the PSD plots show a strong correlation between the messages seen on the recordings and the messages input to the modulation source.

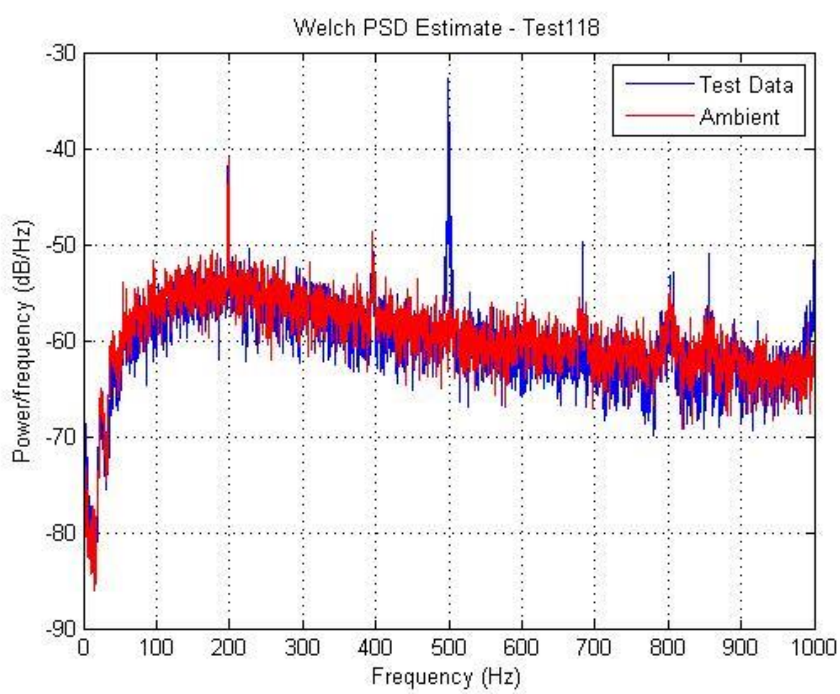

Figure B.1. Analog Tape Recorder: PSD Estimate with 547 MHz Carrier Frequency and 500 Hz Message.

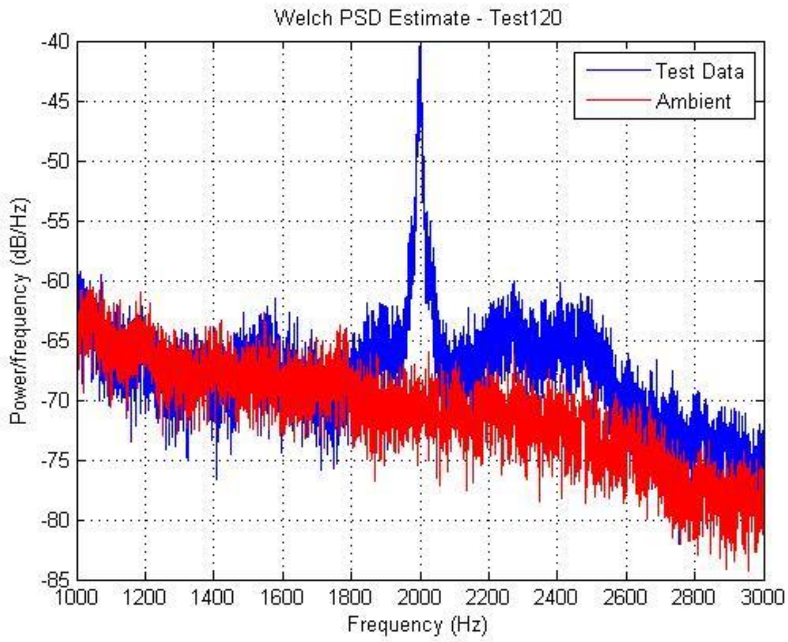

Figure B.2. Analog Tape Recorder: PSD Estimate with 547 MHz Carrier Frequency and 2 kHz Message.

To determine how the orientation of the tape recorder impacted testing, recordings were taken with turntable positions ranging from 0° to 355° at 5° increments while using a fixed coupling carrier frequency and message frequency. The recordings for each turntable position were nearly 10 seconds long. A PSD estimate was calculated for each recording, and the value at the message frequency was stored in a data array. This data array was then normalized with respect to the largest value and graphed in a polar plot. Message frequencies of 500 Hz, 3 kHz, and 5 kHz were tested in three separate sets of experiments.

Figure B.3 and Figure B.4 show the PSD estimate for a 500 Hz message where maximum and minimum coupling occur due to the angular position of the tape recorder. Figure B.5 and Figure B.6 illustrate the coupling as a function of angular position for a 3 kHz message signal in a polar plot. Figure B.7 and Figure B.8 show the PSD estimate for a 3 kHz message where maximum and minimum coupling occur due to the angular position of the tape recorder. Figure B.9 and Figure B.10 illustrate the coupling as a function of angular position for a 6 kHz message signal in a polar plot. Figure B.11 and Figure B.12 show the PSD estimate for a 6 kHz message where maximum and minimum coupling occur due to the angular position of the tape recorder. It can be seen from the polar plots in Figure B.5 and Figure B.9 that the susceptibility pattern of the analog tape recorder was relatively independent of the message frequency.

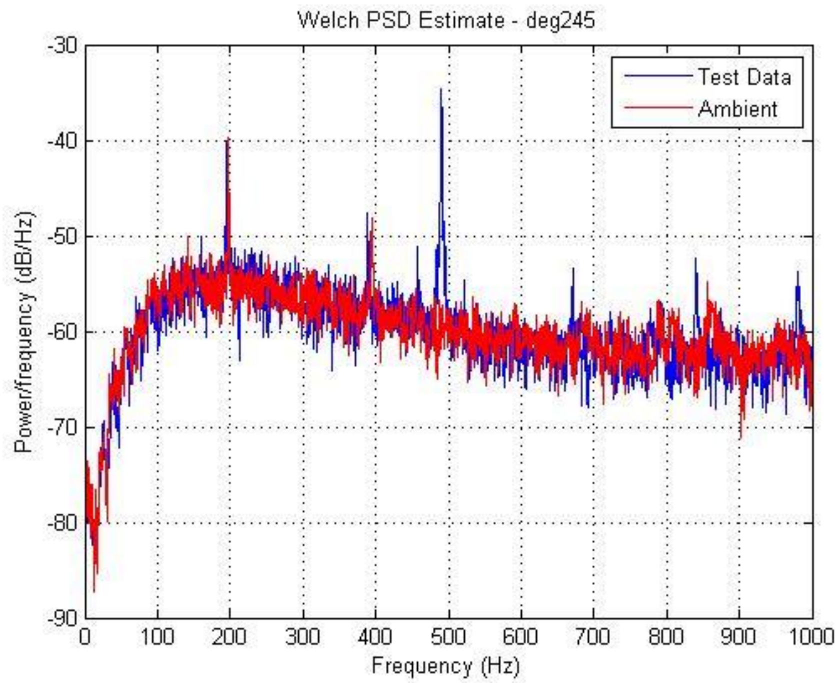

Figure B.3. Analog Tape Recorder: PSD Estimate with 547 MHz Carrier Frequency, 500 Hz Message, and 245° Turntable Position for Maximum Coupling.

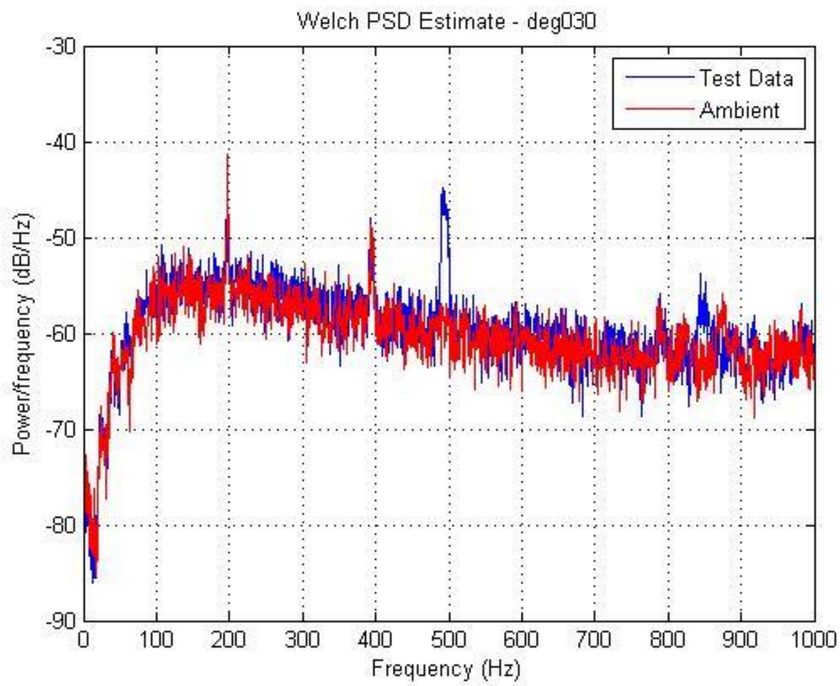

Figure B.4. Analog Tape Recorder: PSD Estimate with 547 MHz Carrier Frequency, 500 Hz Message, and 30° Turntable Position for Minimum Coupling.

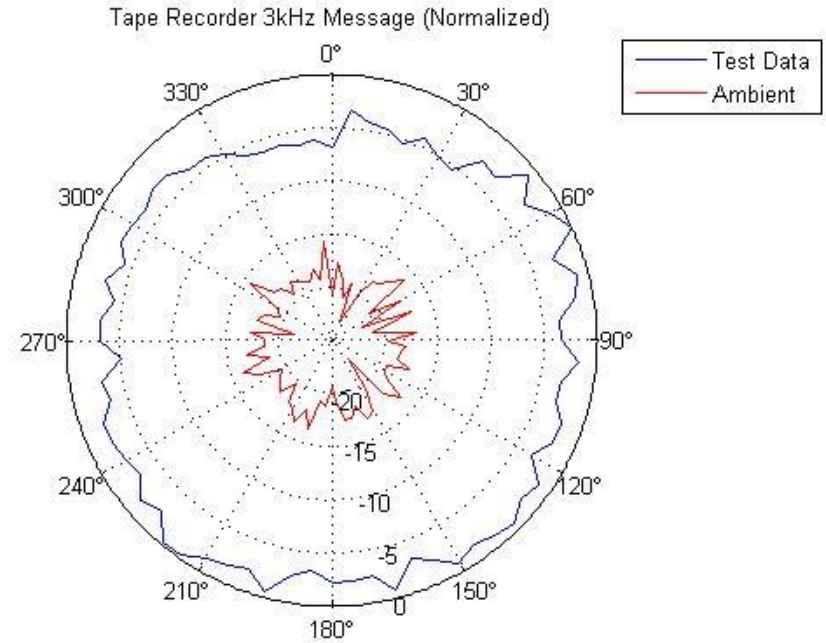

Figure B.5. Analog Tape Recorder: PSD Estimate Comparison Polar Plot for Message Frequency 3 kHz.

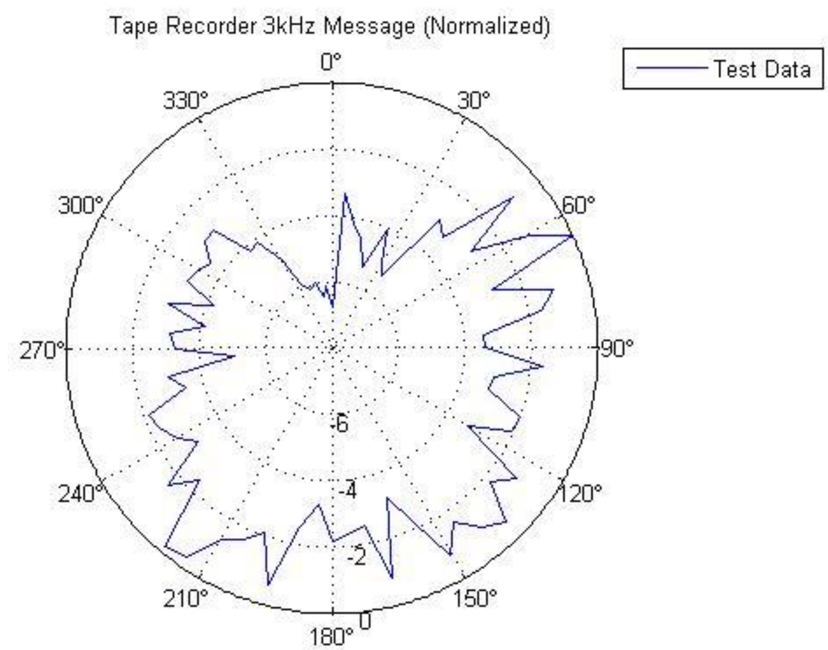

Figure B.6. Analog Tape Recorder: PSD Estimate Single Polar Plot for Message Frequency 3 kHz.

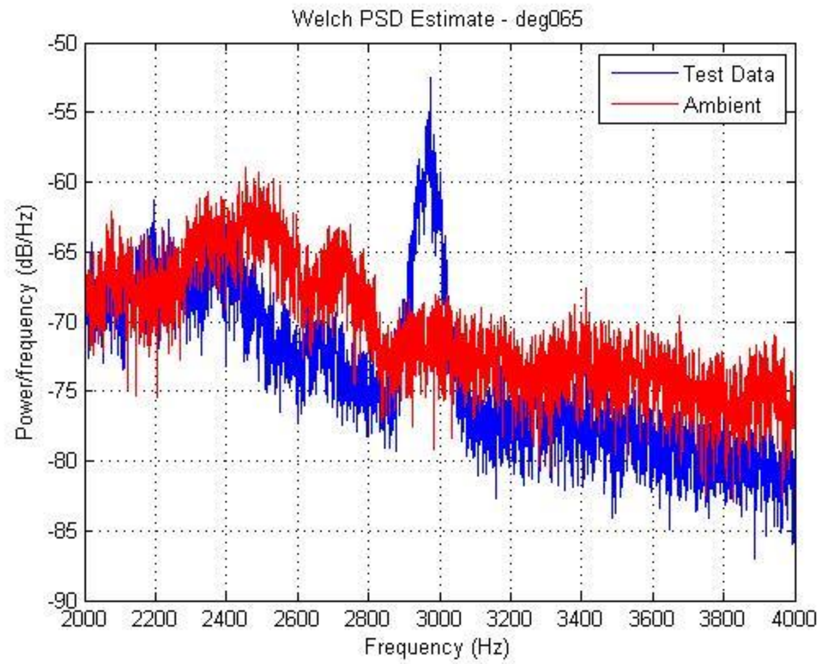

Figure B.7. Analog Tape Recorder: PSD Estimate with 547 MHz Carrier Frequency, 3 kHz Message, and 65° Turntable Position for Maximum Coupling.

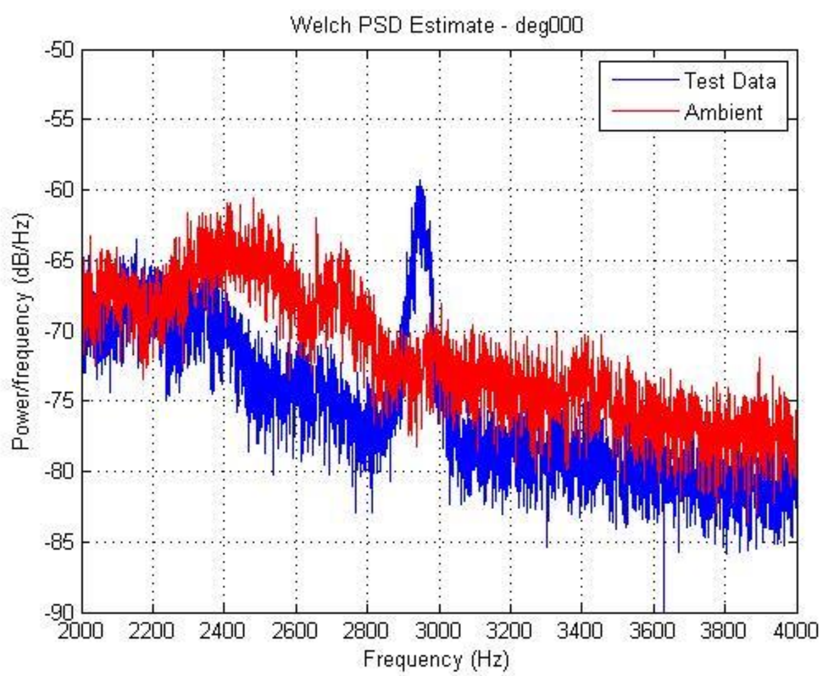

Figure B.8. Analog Tape Recorder: PSD Estimate with 547 MHz Carrier Frequency, 3 kHz Message, and 65° Turntable Position for Minimum Coupling.

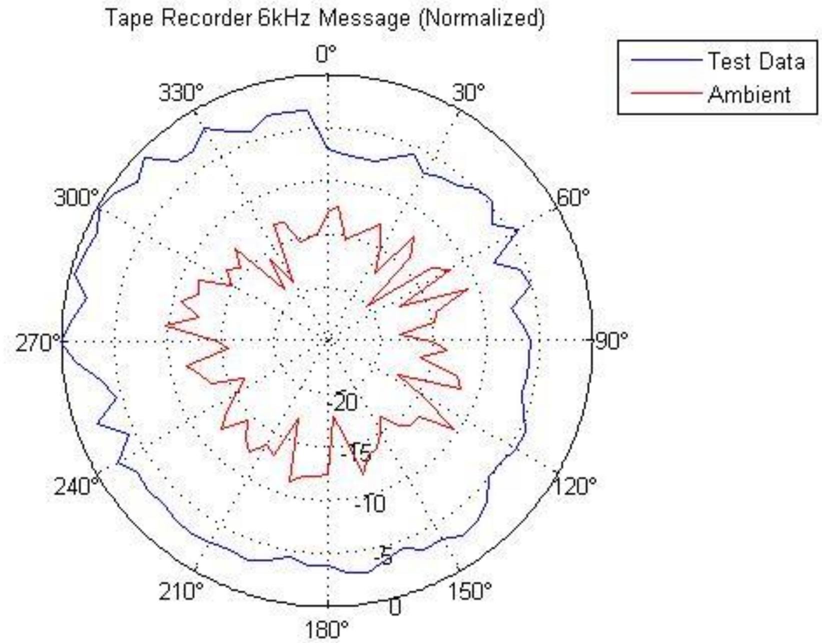

Figure B.9. Analog Tape Recorder: PSD Estimate Comparison Polar Plot for Message Frequency 6 kHz.

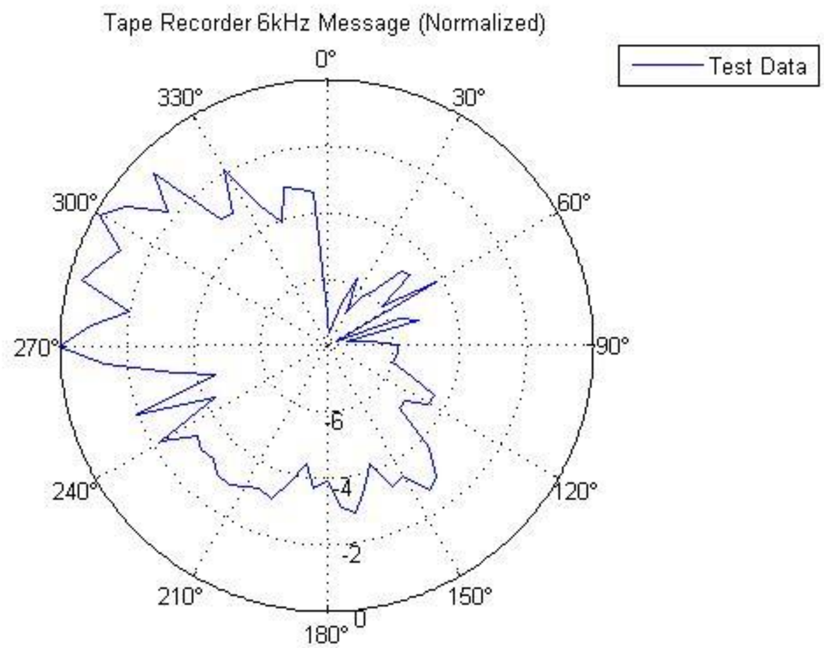

Figure B.10. Analog Tape Recorder: PSD Estimate Single Polar Plot for Message Frequency 6 kHz.

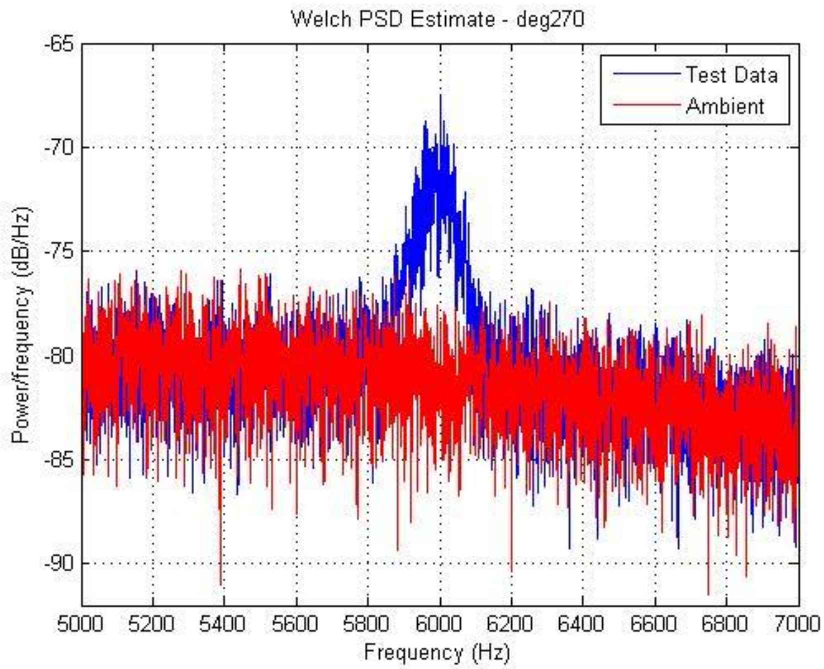

Figure B.11. Analog Tape Recorder: PSD Estimate with 547 MHz Carrier Frequency, 6 kHz Message, and 270° Turntable Position for Maximum Coupling.

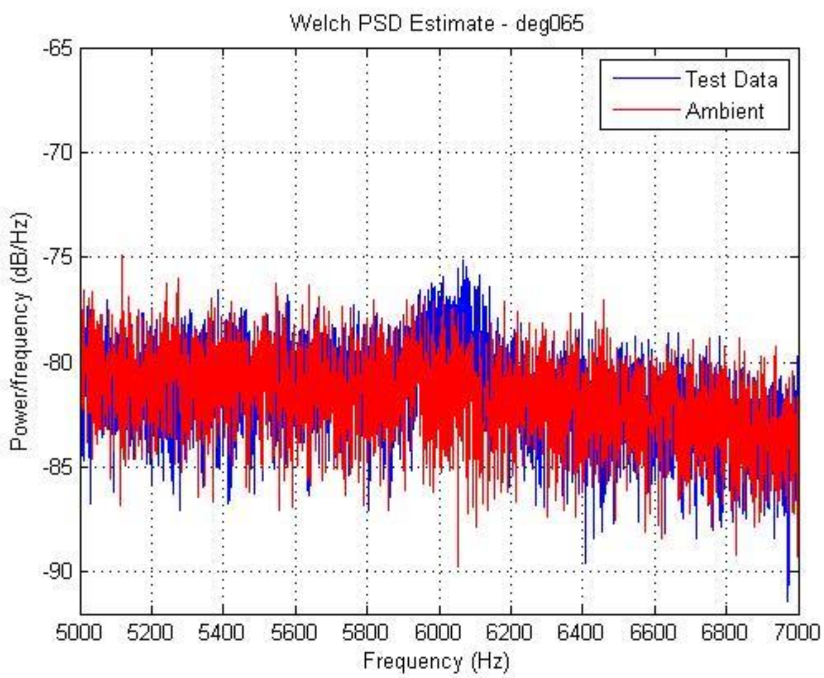

Figure B.12. Analog Tape Recorder: PSD Estimate with 547 MHz Carrier Frequency, 6 kHz Message, and 270° Turntable Position for Minimum Coupling.

B.2. Computer Microphone

Testing was performed to show that the coupled messages in the recordings were the same as the messages created by the signal generators. The carrier frequency was fixed, and the messages were transmitted at a few fixed frequencies. The recordings were analyzed by creating a PSD estimate plot using Welch's method. Figures B.13-B.15 show a few additional results from these experiments. The message signal spikes in the PSD plots show a strong correlation between the messages seen on the recordings and the messages input to the modulation source.

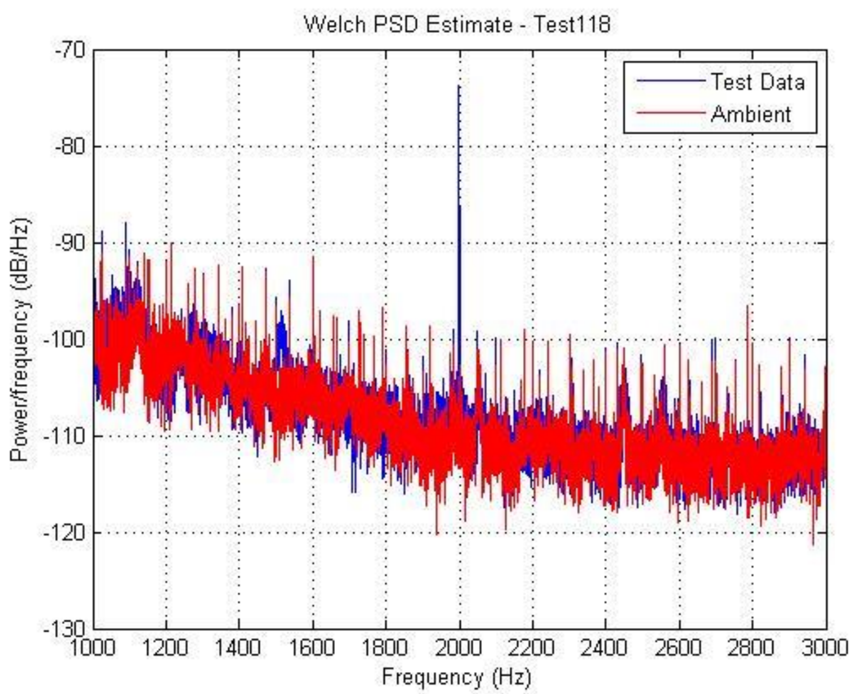

Figure B.13. Computer Microphone: PSD Estimate with 220 MHz Carrier Frequency and 2 kHz Message.

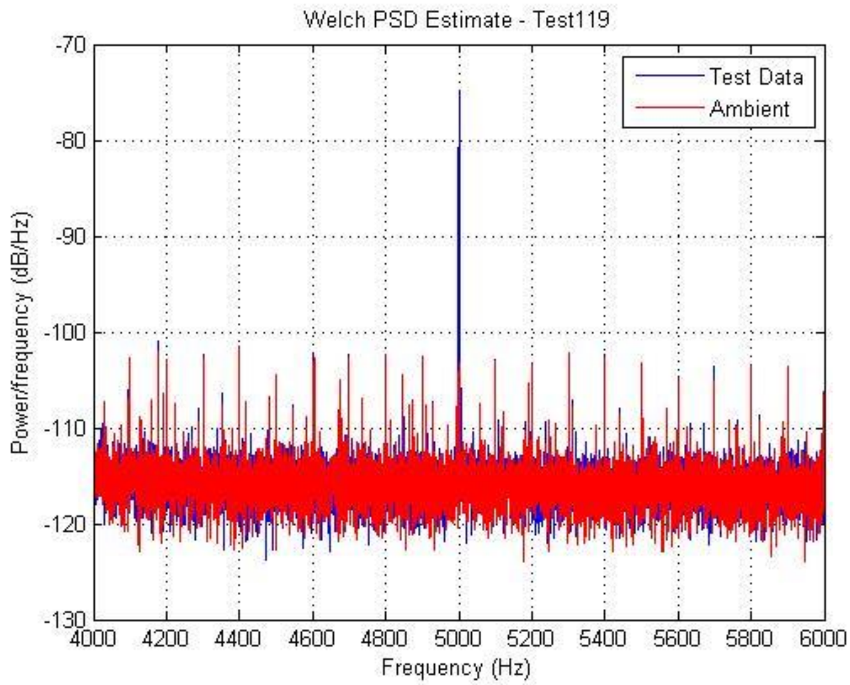

Figure B.14. Computer Microphone: PSD Estimate with 220 MHz Carrier Frequency and 5 kHz Message.

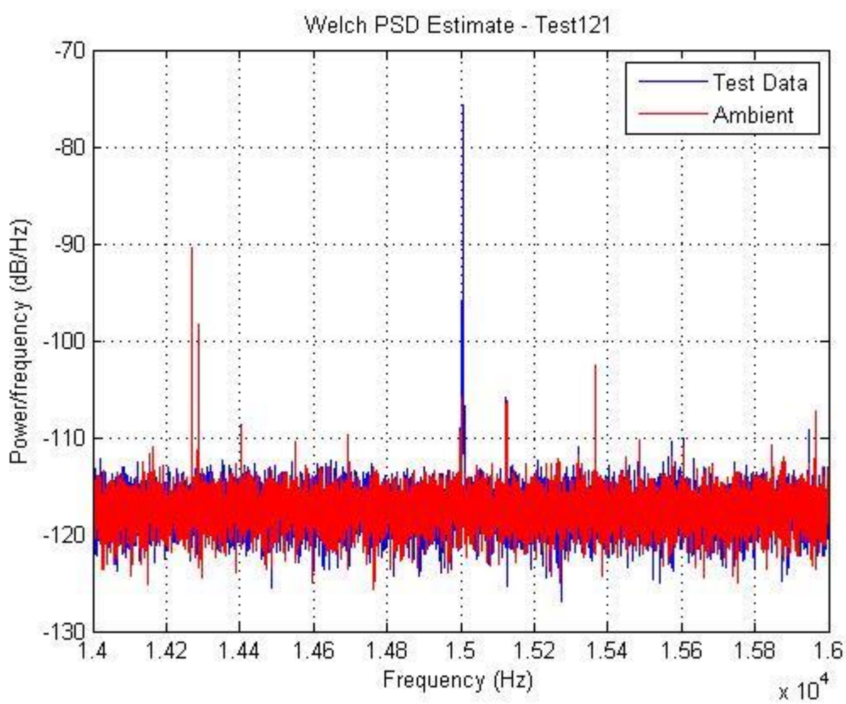

Figure B.15. Computer Microphone: PSD Estimate with 220 MHz Carrier Frequency and 15 kHz Message.

To determine how the orientation of the computer microphone impacted testing, recordings were taken with turntable positions ranging from 0° to 355° at 5° increments while using a fixed coupling carrier frequency and message frequency. The recordings for each turntable position were nearly 20 seconds long. A PSD estimate was calculated for each recording, and the value at the message frequency was stored in a data array. This data array was then normalized with respect to the largest value. Message frequencies of 500 Hz, 10 kHz, and 22 kHz were tested in three separate sets of experiments.

Figure B.16 and Figure B.17 show the PSD estimate for a 10 kHz message where maximum and minimum coupling occur due to the angular position of the computer microphone. Figure B.18 and Figure B.19 illustrate the coupling as a function of angular position for a 500 Hz message signal in a polar plot. Figure B.20 and Figure B.21 show the PSD estimate for a 500 Hz message where maximum and minimum coupling occur due to the angular position of the computer microphone. Figure B.22 and Figure B.23 illustrate the coupling as a function of angular position for a 22 kHz message signal in a polar plot. Figure B.24 and Figure B.25 show the PSD estimate for a 22 kHz message where maximum and minimum coupling occur due to the angular position of the computer microphone. It can be seen from the polar plots in Figure B.19 and Figure B.23 that the susceptibility pattern of the computer microphone was similar among the message frequencies that couple well into the device. Overall, coupled messages were fairly dependent on turntable position.

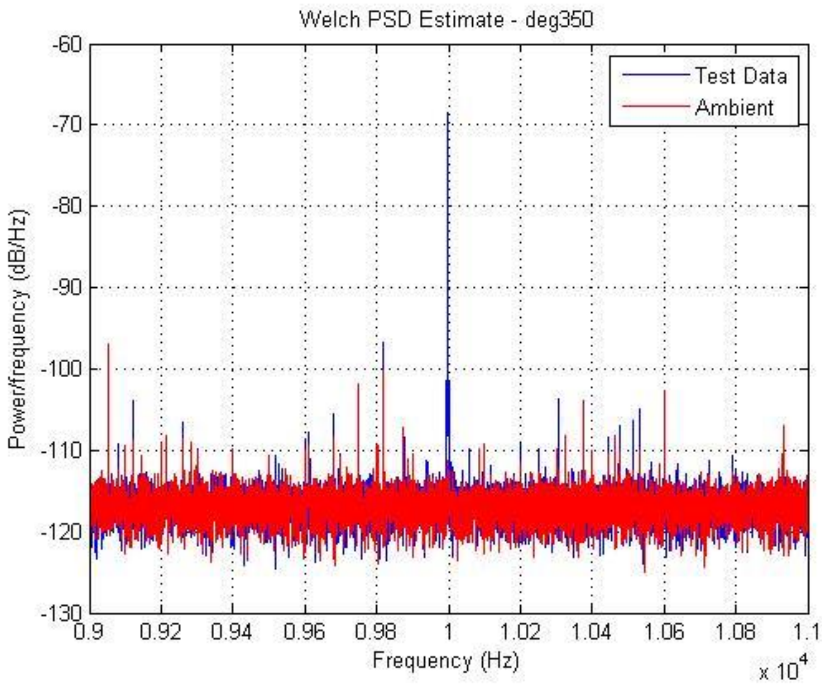

Figure B.16. Computer Microphone: PSD Estimate with 220 MHz Carrier Frequency, 10 kHz Message, and 350° Turntable Position for Maximum Coupling.

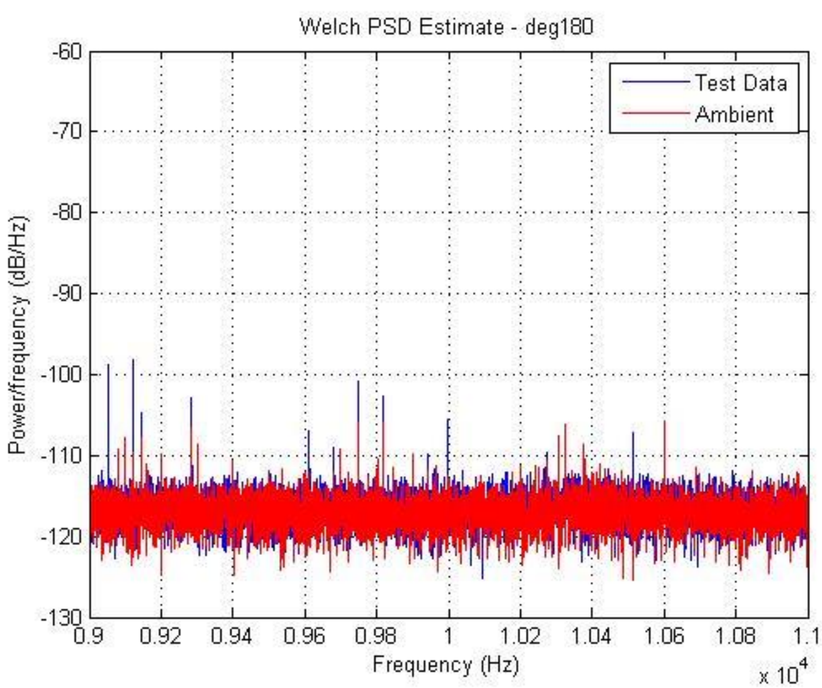

Figure B.17. Computer Microphone: PSD Estimate with 220 MHz Carrier Frequency, 10 kHz Message, and 350° Turntable Position for Minimum Coupling.

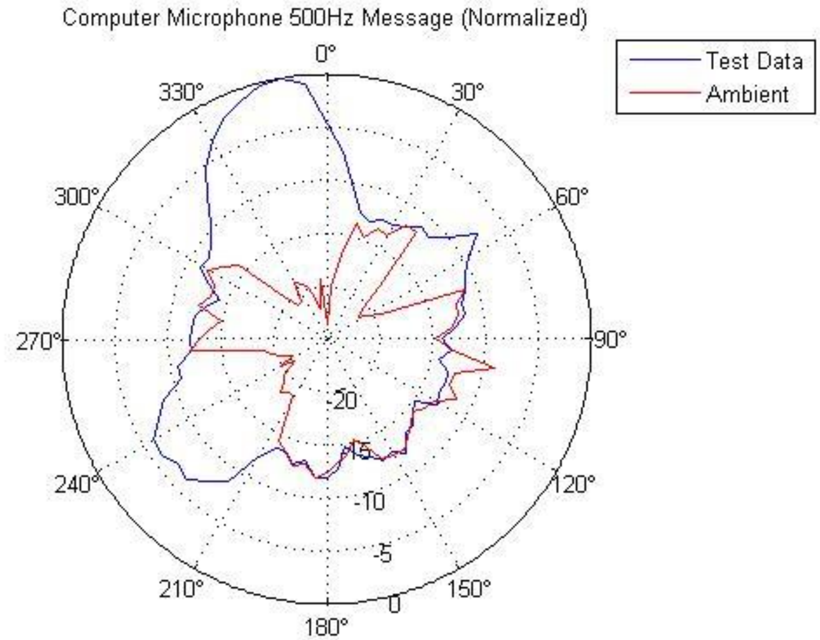

Figure B.18. Computer Microphone: PSD Estimate Comparison Polar Plot for Message Frequency 500 Hz.

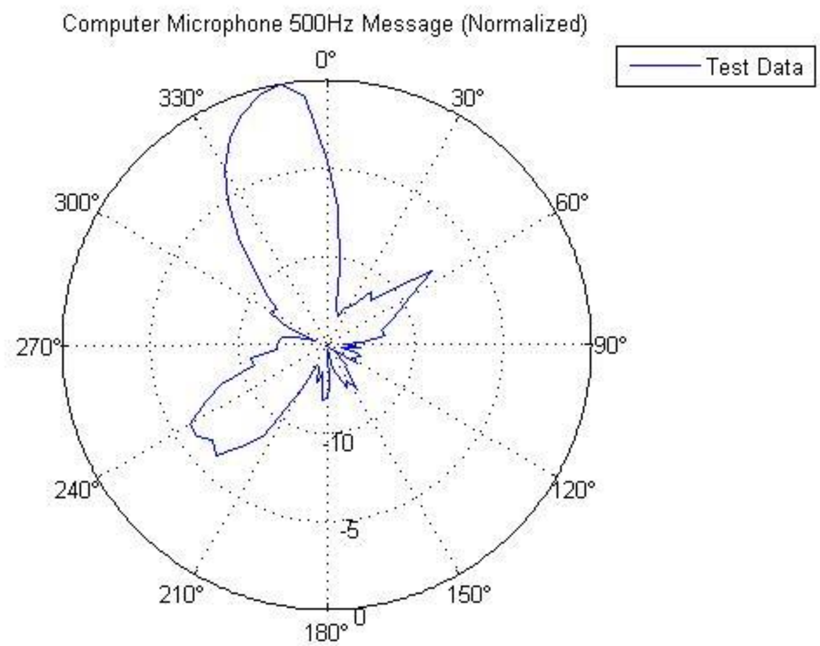

Figure B.19. Computer Microphone: PSD Estimate Single Polar Plot for Message Frequency 500 Hz.

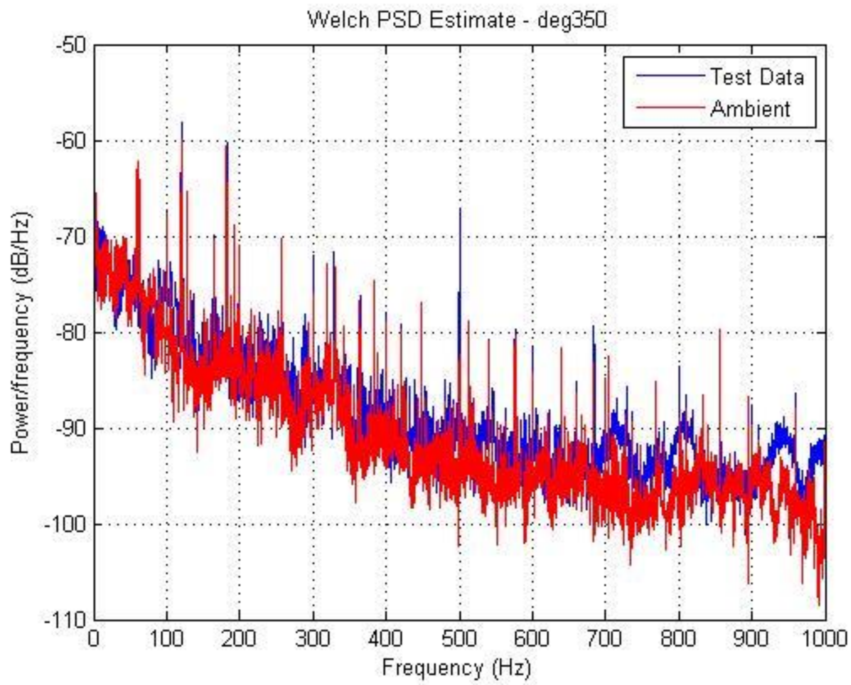

Figure B.20. Computer Microphone: PSD Estimate with 220 MHz Carrier Frequency, 500 Hz Message, and 350° Turntable Position for Maximum Coupling.

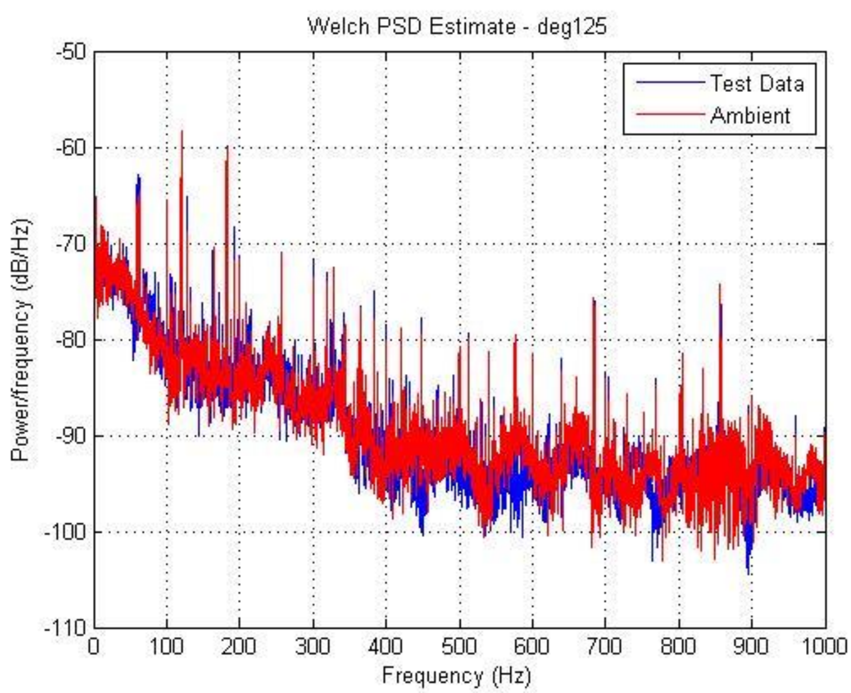

Figure B.21. Computer Microphone: PSD Estimate with 220 MHz Carrier Frequency, 500 Hz Message, and 125° Turntable Position for Minimum Coupling.

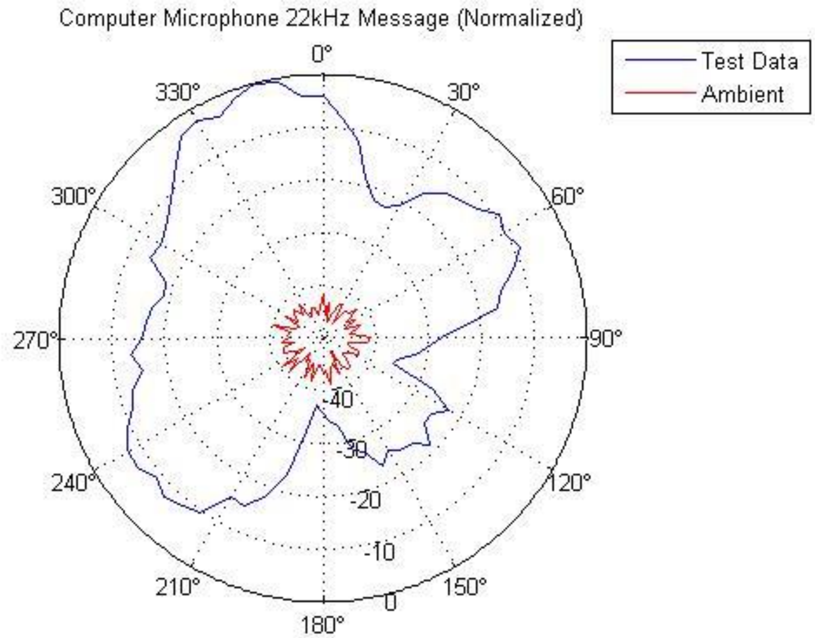

Figure B.22. Computer Microphone: PSD Estimate Comparison Polar Plot for Message Frequency 22 kHz.

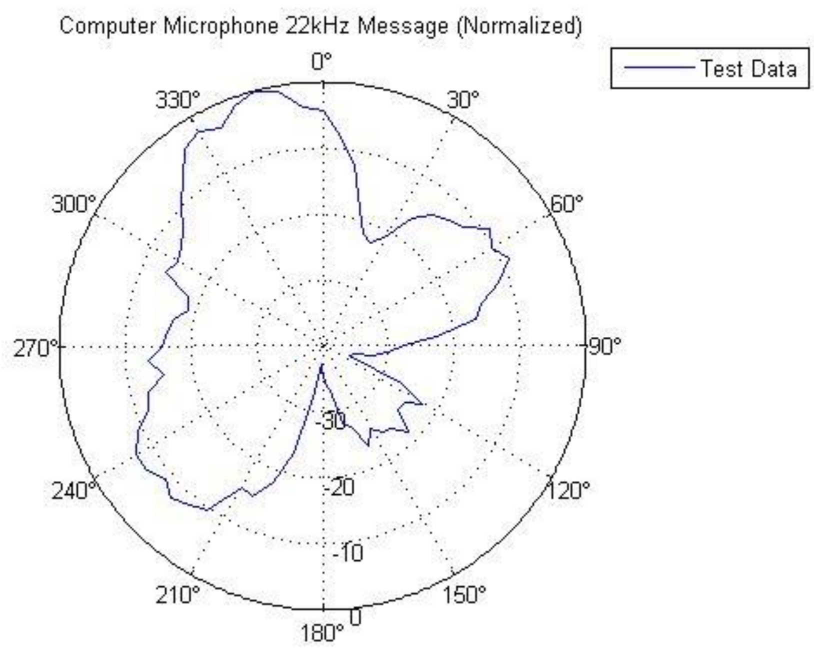

Figure B.23. Computer Microphone: PSD Estimate Single Polar Plot for Message Frequency 22 kHz.

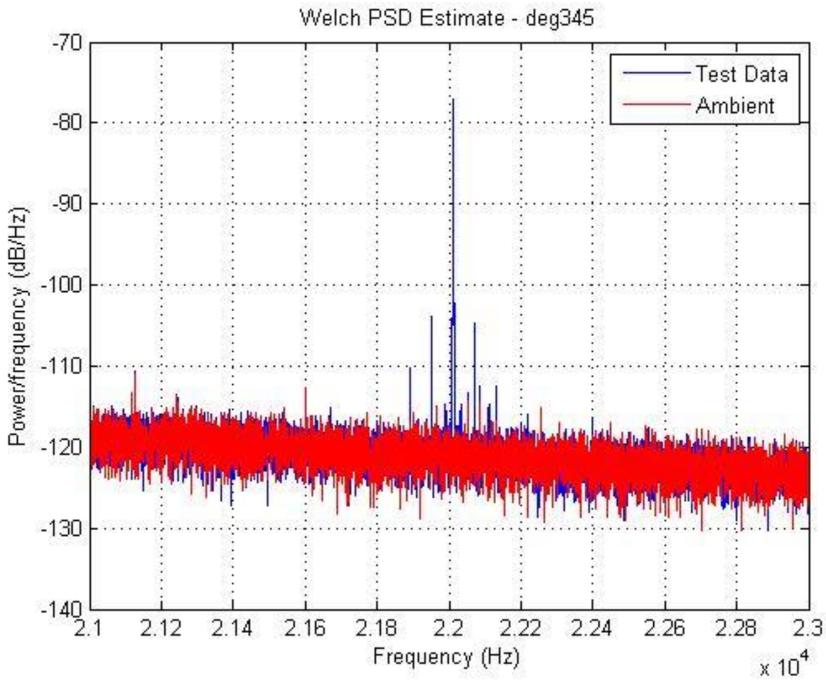

Figure B.24. Computer Microphone: PSD Estimate with 220 MHz Carrier Frequency, 22 kHz Message, and 345° Turntable Position for Maximum Coupling.

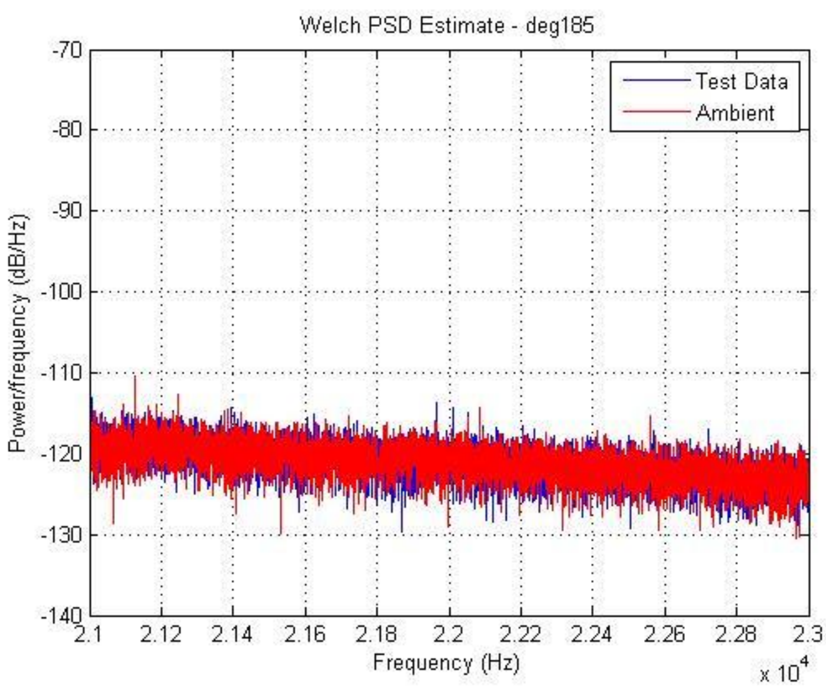

Figure B.25. Computer Microphone: PSD Estimate with 220 MHz Carrier Frequency, 22 kHz Message, and 185° Turntable Position for Minimum Coupling.

One extra susceptibility pattern test was taken in a different session of measurements. In this test the coupling properties of the computer microphone were studied for a 10 kHz message frequency. The resulting susceptibility pattern was significantly different from those shown in Figures B.18-B.19 and Figures B.22-B.23. The PSD estimate for the recording at the maximum and minimum coupling angles are shown in Figure B.26 and Figure B.27, respectively.

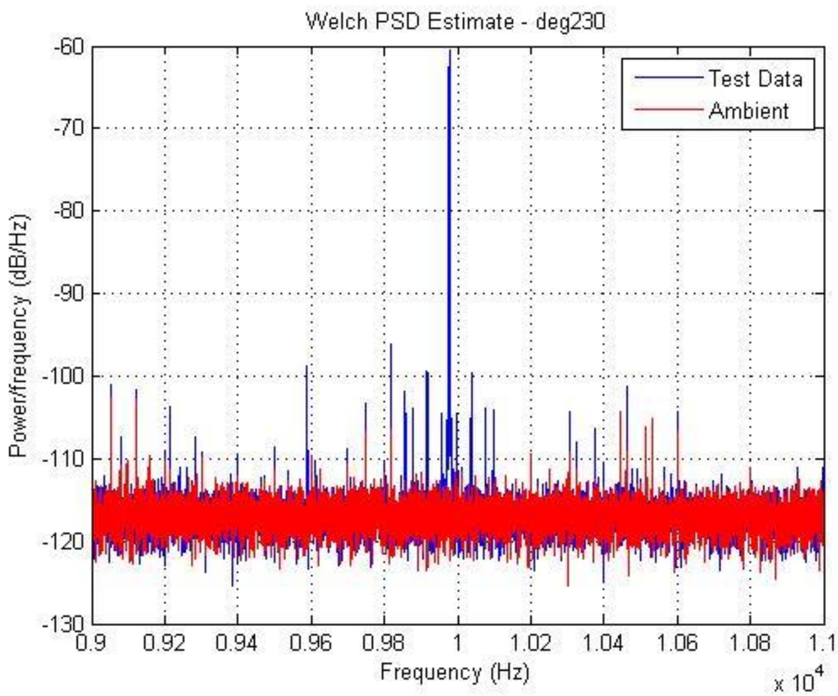

Figure B.26. Computer Microphone: PSD Estimate with 220 MHz Carrier Frequency, 10 kHz Message, and 230° Turntable Position for Maximum Coupling (Extra Test).

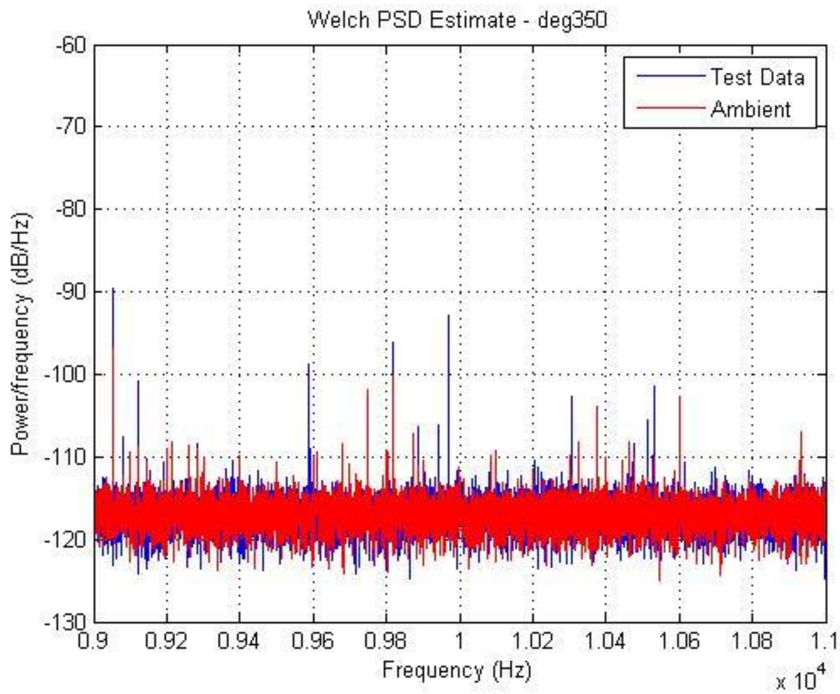

Figure B.27. Computer Microphone: PSD Estimate with 220 MHz Carrier Frequency, 10 kHz Message, and 350° Turntable Position for Minimum Coupling (Extra Test).

B.3. Digital Video Camera

Testing was performed to show that the coupled messages in the recordings were the same as the messages created by the signal generators. The carrier frequency was fixed, and the messages were transmitted at a few fixed frequencies. The recordings were analyzed by creating a PSD estimate plot using Welch's method. Figures B.28-B.30 show a few additional results from these experiments. The message signal spikes in the PSD plots show a strong correlation between the messages seen on the recordings and the messages input to the modulation source.

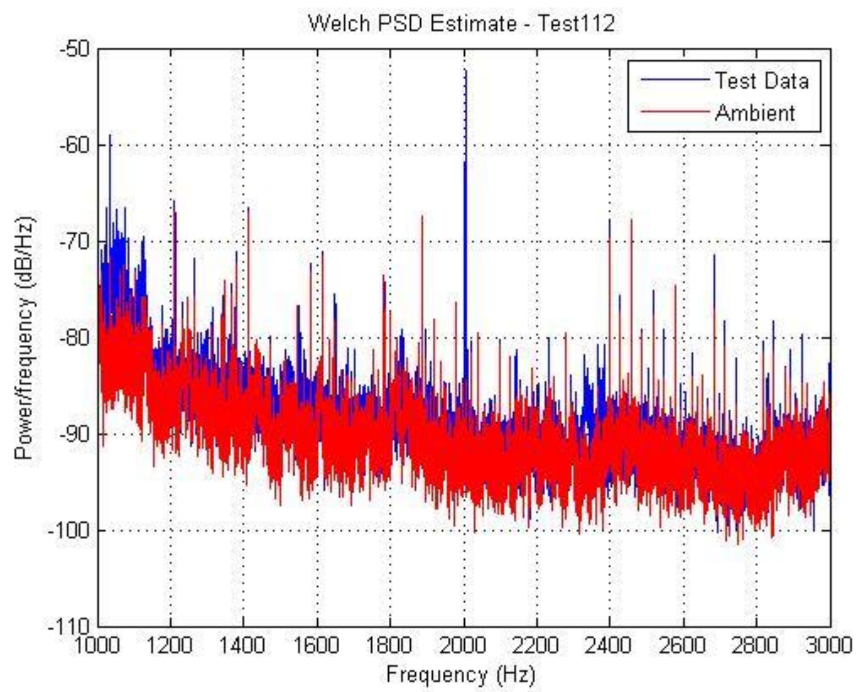

Figure B.28. Digital Video Camera: PSD Estimate with 211 MHz Carrier Frequency and 2 kHz Message.

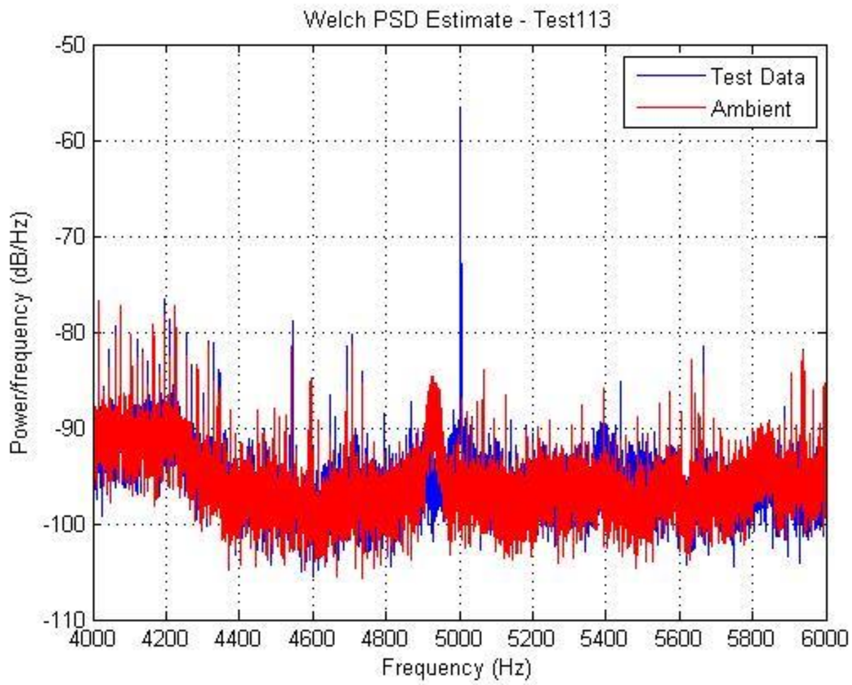

Figure B.29. Digital Video Camera: PSD Estimate with 211 MHz Carrier Frequency and 5 kHz Message.

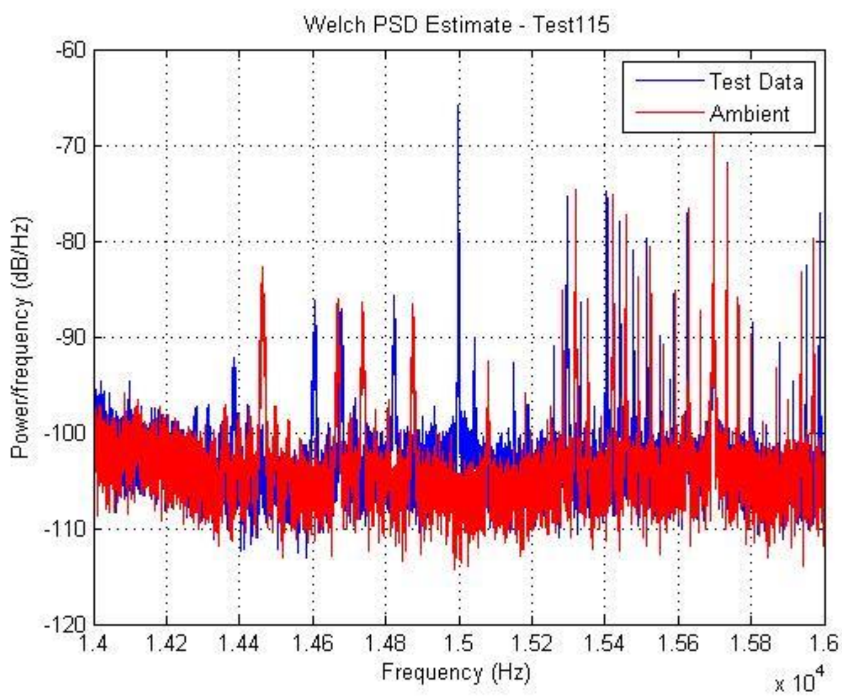

Figure B.30. Digital Video Camera: PSD Estimate with 211 MHz Carrier Frequency and 15 kHz Message.

To determine how the orientation of the digital video camera impacted testing, recordings were taken with turntable positions ranging from 0° to 355° at 5° increments while using a fixed coupling carrier frequency and message frequency. The recordings for each turntable position were nearly 20 seconds long. A PSD estimate was calculated for each recording, and the value at the message frequency was stored in a data array. This data array was then normalized with respect to the largest value and graphed in a polar plot. Message frequencies of 1 kHz, 10 kHz, and 20 kHz were tested in three separate sets of experiments.

Figure B.31 and Figure B.32 show the PSD estimate for a 10 kHz message where maximum and minimum coupling occur due to the angular position of the digital video camera. Figure B.33 and Figure B.34 illustrate the coupling as a function of angular position for a 1 kHz message signal in a polar plot. Figure B.35 and Figure B.36 show the PSD estimate for a 1 kHz message where maximum and minimum coupling occur due to the angular position of the digital video camera. Figure B.37 and Figure B.38 illustrate the coupling as a function of angular position for a 20 kHz message signal in a polar plot. Figure B.39 and Figure B.40 show the PSD estimate for a 20 kHz message where maximum and minimum coupling occur due to the angular position of the digital video camera. It can be seen from the polar plots in Figure B.34 and Figure B.38 that the susceptibility pattern of the digital video camera was relatively independent of the message frequency. Aside from two nulls in coupling that occurred at 0° and 180°, which correspond to when the digital video camera had the least surface area exposed, the susceptibility pattern of the digital video camera was fairly independent of turntable position.

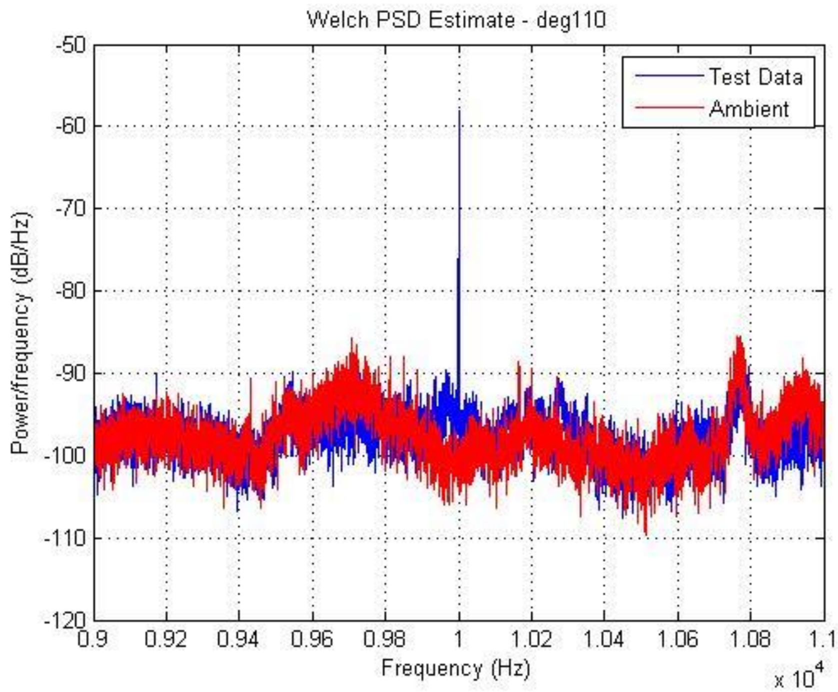

Figure B.31. Digital Video Camera: PSD Estimate with 211 MHz Carrier Frequency, 10 kHz Message, and 110° Turntable Position for Maximum Coupling.

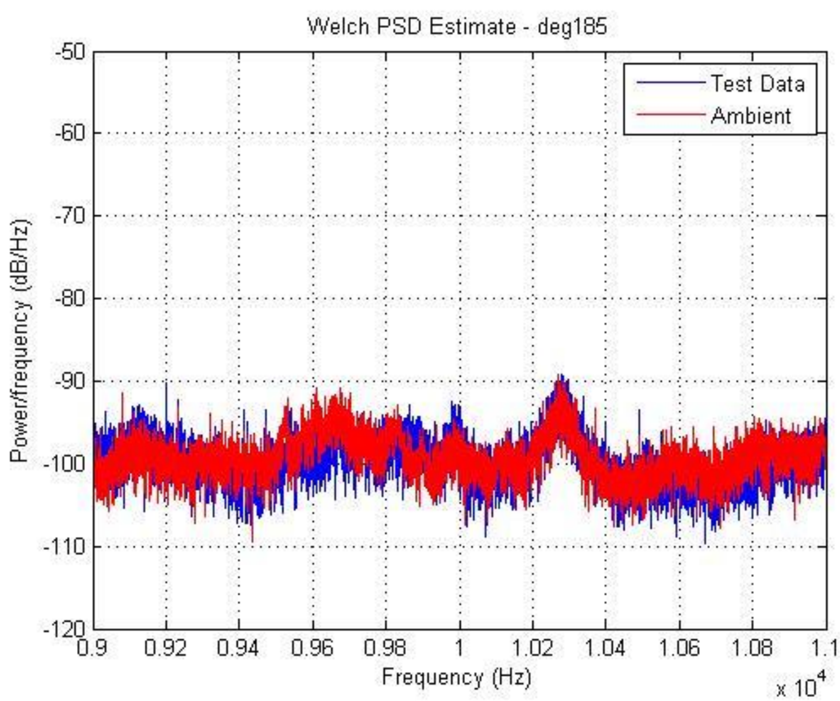

Figure B.32. Digital Video Camera: PSD Estimate with 211 MHz Carrier Frequency, 10 kHz Message, and 185° Turntable Position for Minimum Coupling.

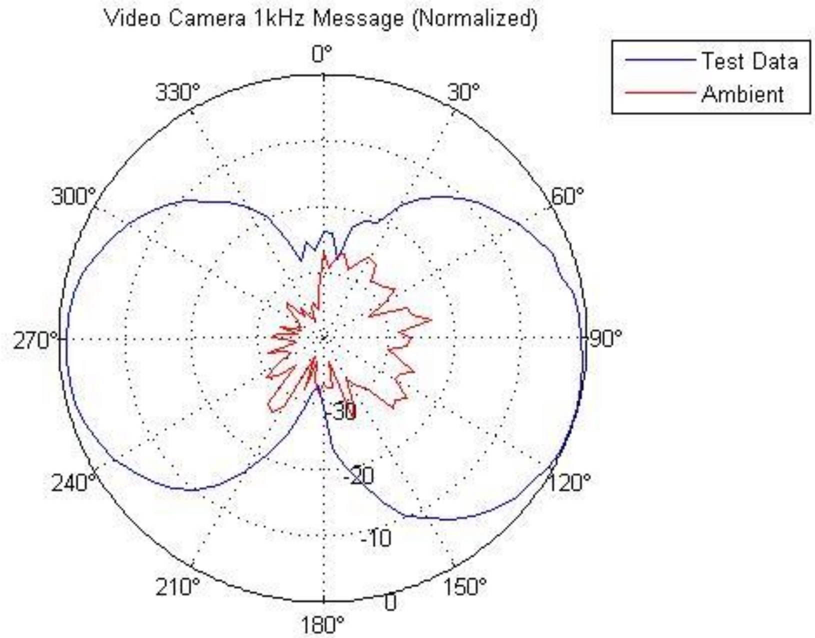

Figure B.33. Digital Video Camera: PSD Estimate Comparison Polar Plot for Message Frequency 1 kHz.

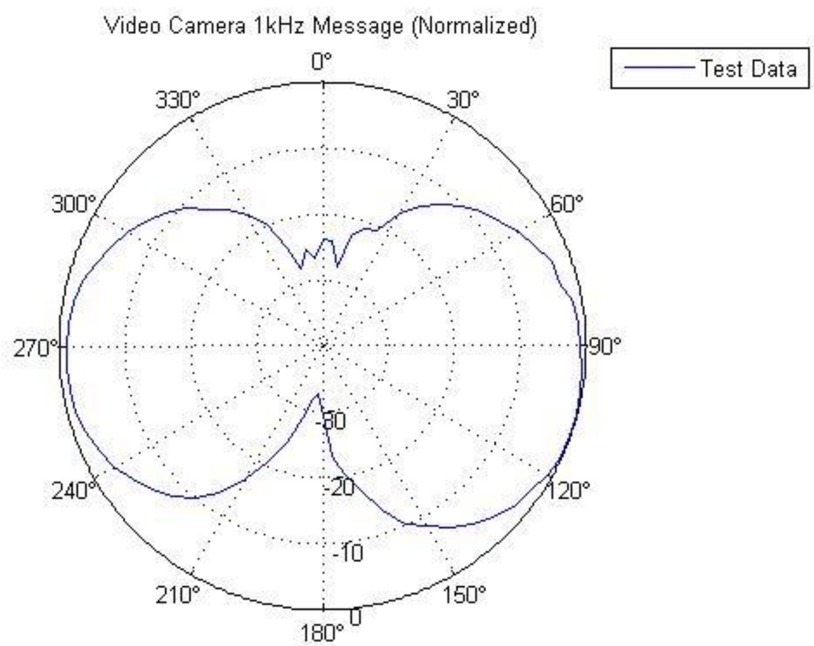

Figure B.34. Digital Video Camera: PSD Estimate Single Polar Plot for Message Frequency 1 kHz.

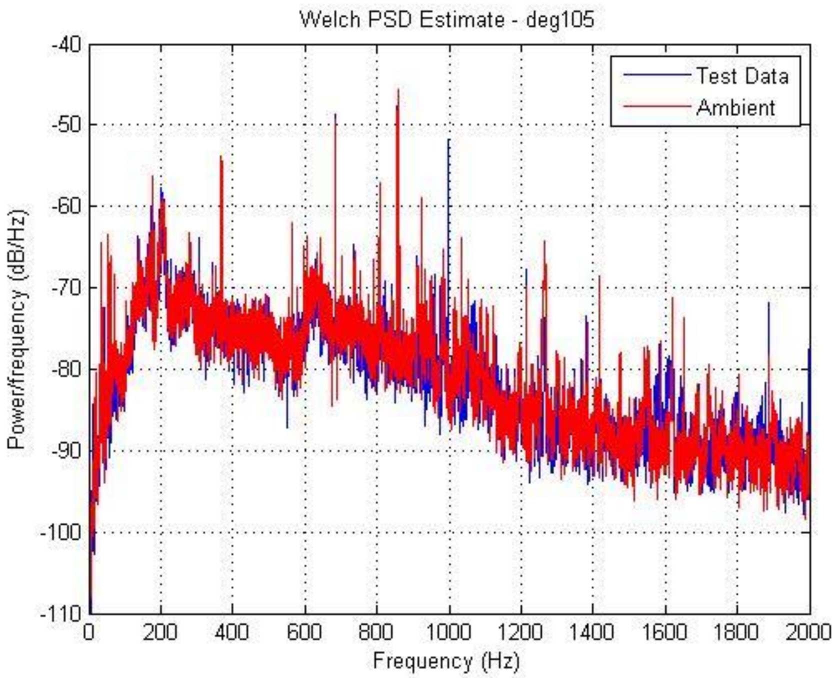

Figure B.35. Digital Video Camera: PSD Estimate with 211 MHz Carrier Frequency, 1 kHz Message, and 105° Turntable Position for Maximum Coupling.

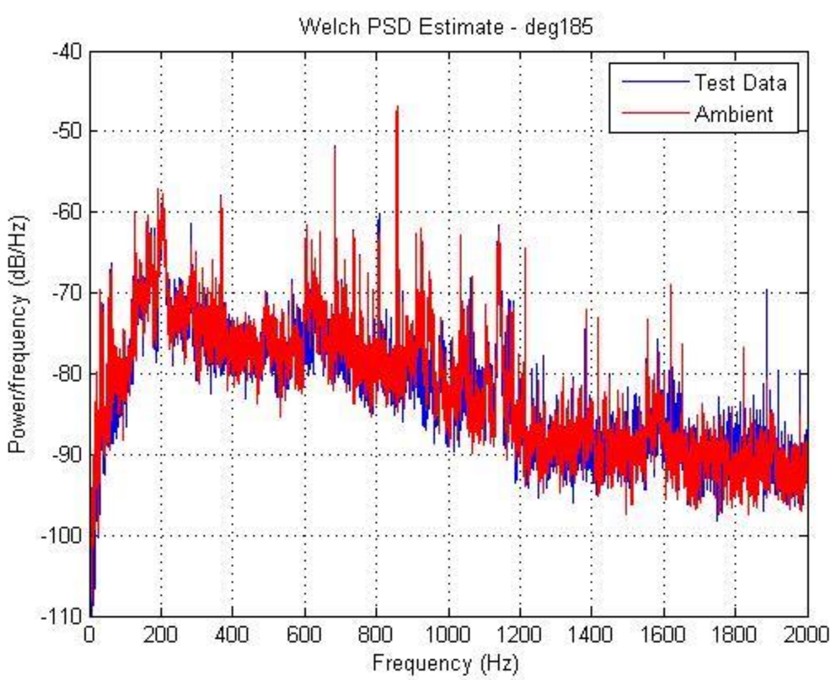

Figure B.36. Digital Video Camera: PSD Estimate with 211 MHz Carrier Frequency, 1 kHz Message, and 185° Turntable Position for Minimum Coupling.

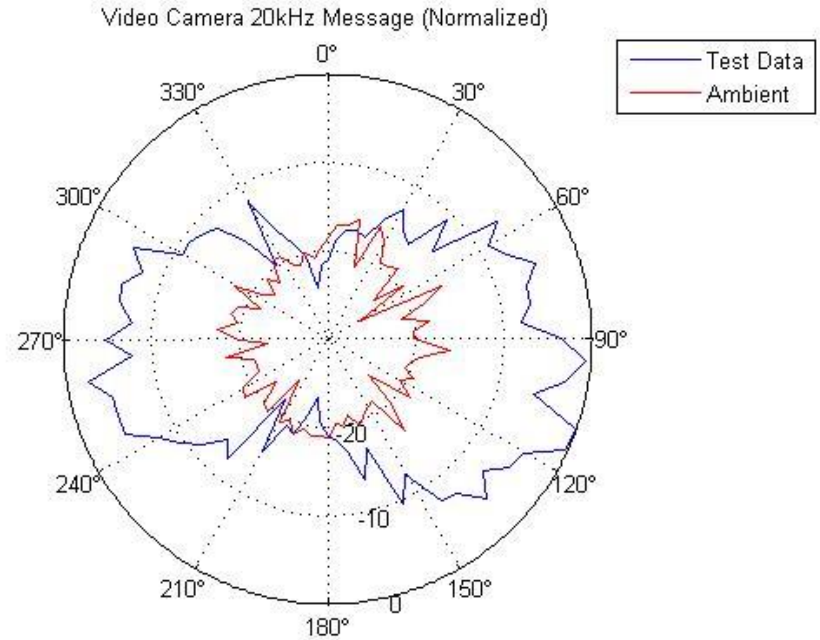

Figure B.37. Digital Video Camera: PSD Estimate Comparison Polar Plot for Message Frequency 20 kHz.

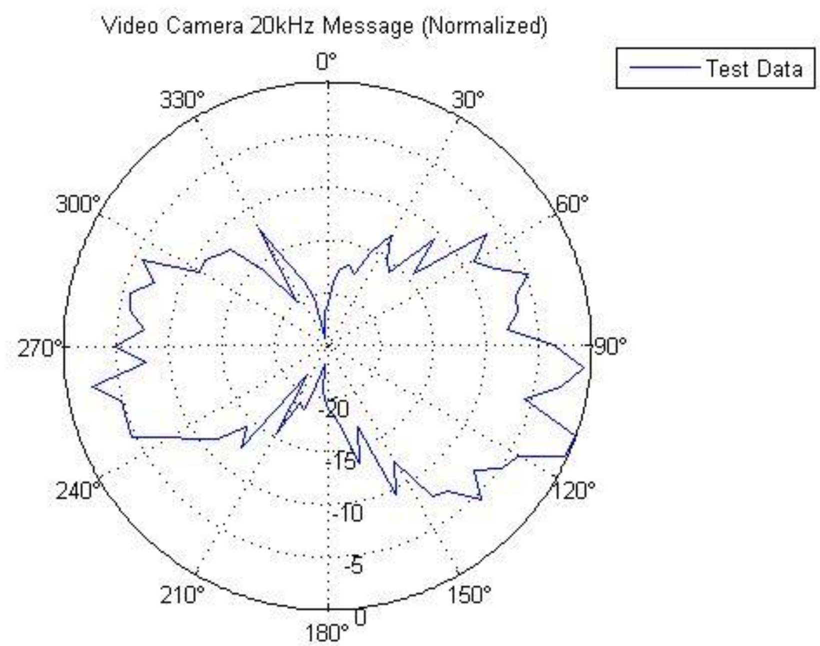

Figure B.38. Digital Video Camera: PSD Estimate Single Polar Plot for Message Frequency 20 kHz.

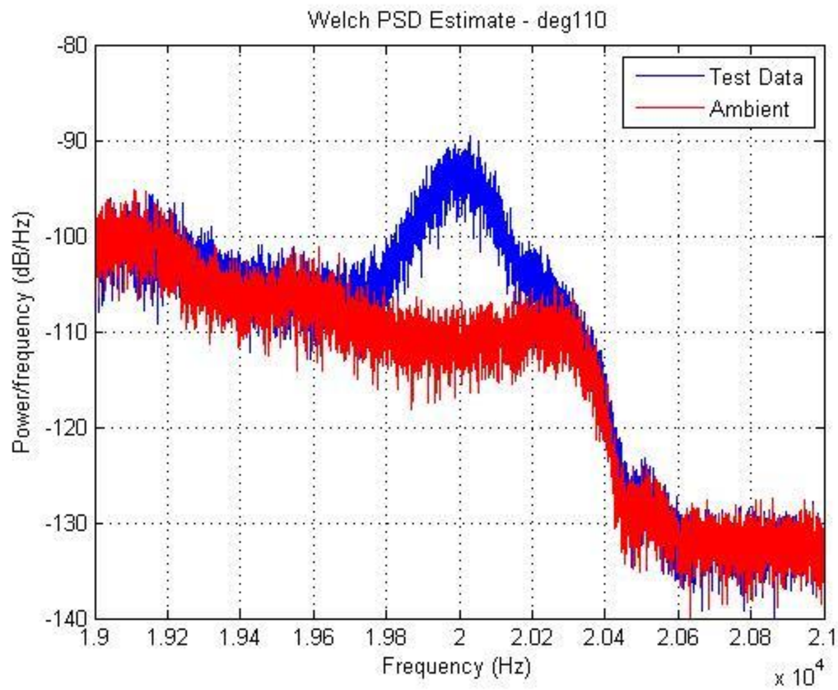

Figure B.39. Digital Video Camera: PSD Estimate with 211 MHz Carrier Frequency, 20 kHz Message, and 110° Turntable Position for Maximum Coupling.

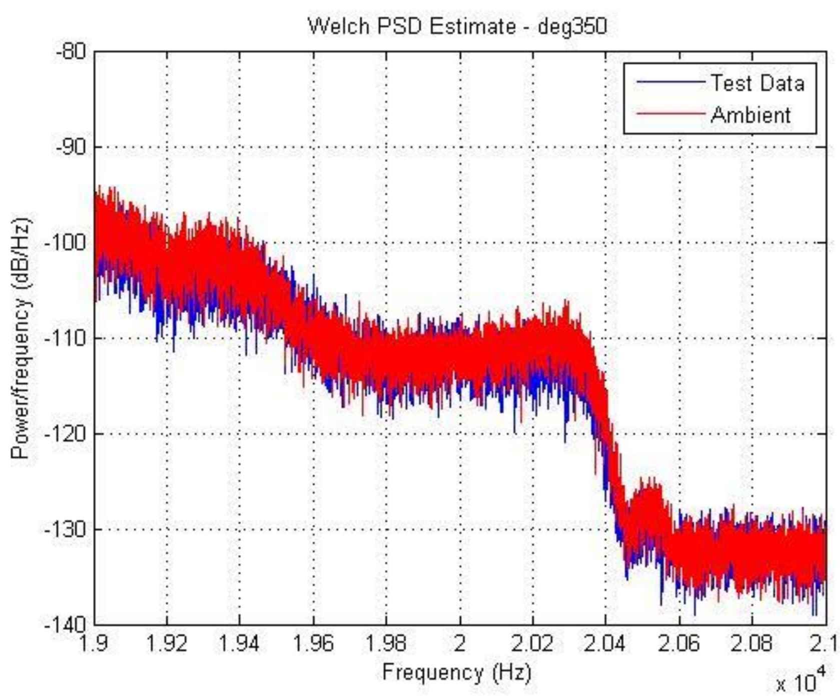

Figure B.40. Digital Video Camera: PSD Estimate with 211 MHz Carrier Frequency, 20 kHz Message, and 350° Turntable Position for Minimum Coupling.

B.4. Wireless Microphone System

Testing was performed to show that the coupled messages in the recordings were the same as the messages created by the signal generators. The carrier frequency was fixed, and the messages were transmitted at a few fixed frequencies. The recordings were analyzed by creating a PSD estimate plot using Welch's method. Figures B.41-B.43 show a few additional results from these experiments. The message signal spikes in the PSD plots show a strong correlation between the messages seen on the recordings and the messages input to the modulation source.

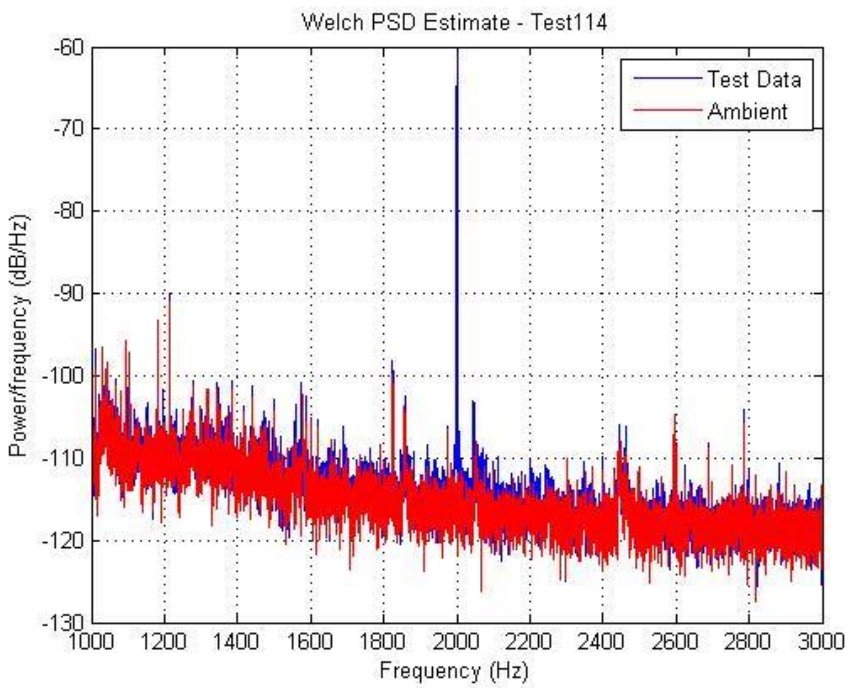

Figure B.41. Wireless Microphone System: PSD Estimate with 254 MHz Carrier Frequency and 2 kHz Message.

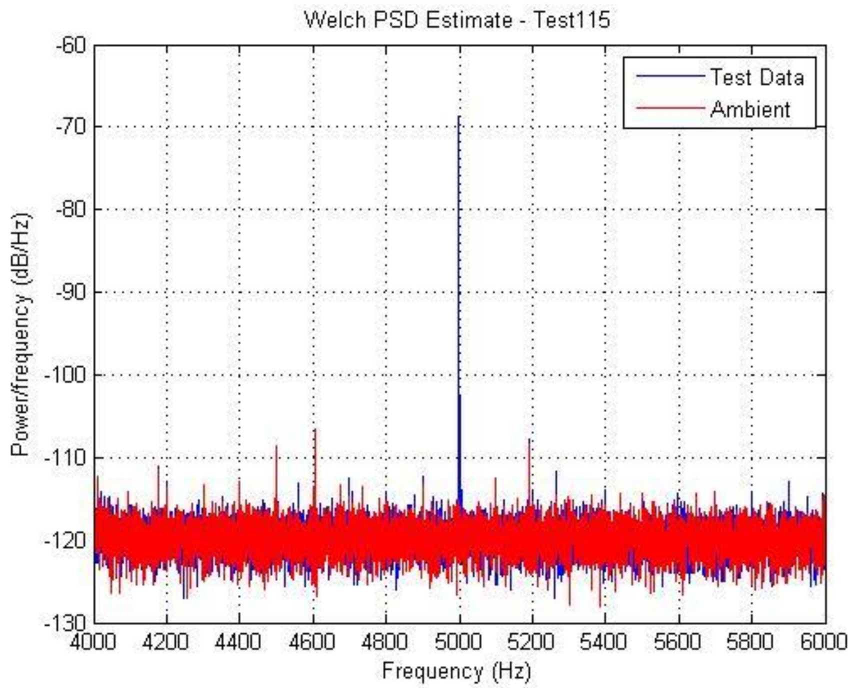

Figure B.42. Wireless Microphone System: PSD Estimate with 254 MHz Carrier Frequency and 5 kHz Message.

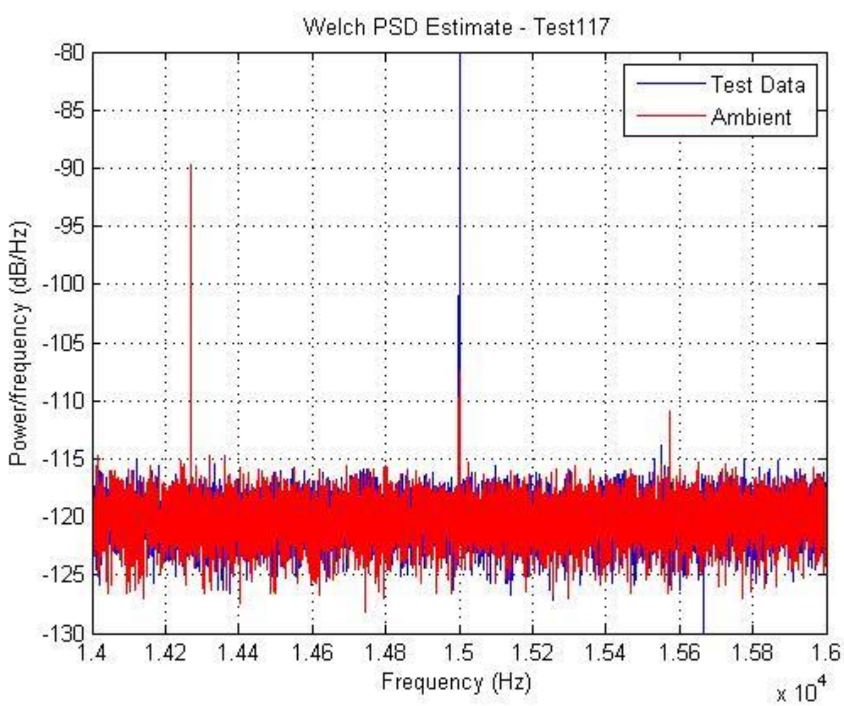

Figure B.43. Wireless Microphone System: PSD Estimate with 254 MHz Carrier Frequency and 15 kHz Message.

To determine how the orientation of the wireless microphone system impacted testing, recordings were taken with turntable positions ranging from 0° to 355° at 5° increments while using a fixed coupling carrier frequency and message frequency. The recordings for each turntable position were nearly 20 seconds long. A PSD estimate was calculated for each recording, and the value at the message frequency was stored in a data array. This data array was then normalized with respect to the largest value and graphed in a polar plot. Message frequencies of 200 Hz, 2 kHz, and 22 kHz were tested in three separate sets of experiments.

Figure B.44 and Figure B.45 show the PSD estimate for a 2 kHz message where maximum and minimum coupling occur due to the angular position of the wireless microphone system. Figure B.46 and Figure B.47 illustrate the coupling as a function of angular position for a 200 Hz message signal in a polar plot. Figure B.48 and Figure B.49 show the PSD estimate for a 200 Hz message where maximum and minimum coupling occur due to the angular position of the wireless microphone system. Figure B.50 and Figure B.51 illustrate the coupling as a function of angular position for a 22 kHz message signal in a polar plot. Figure B.52 and Figure B.53 show the PSD estimate for a 22 kHz message where maximum and minimum coupling occur due to the angular position of the wireless microphone system. It can be seen from the polar plots in Figure B.47 and Figure B.51 that the susceptibility pattern of the computer microphone was similar among the message frequencies that couple well into the device. Overall, coupled messages were fairly dependent on turntable position.

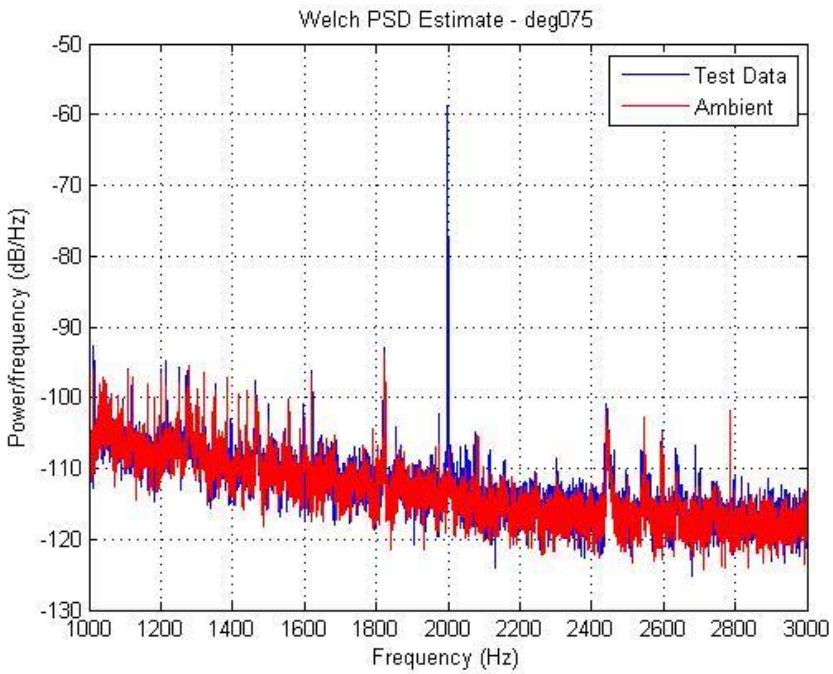

Figure B.44. Wireless Microphone System: PSD Estimate with 254 MHz Carrier Frequency, 2 kHz Message, and 75° Turntable Position for Maximum Coupling.

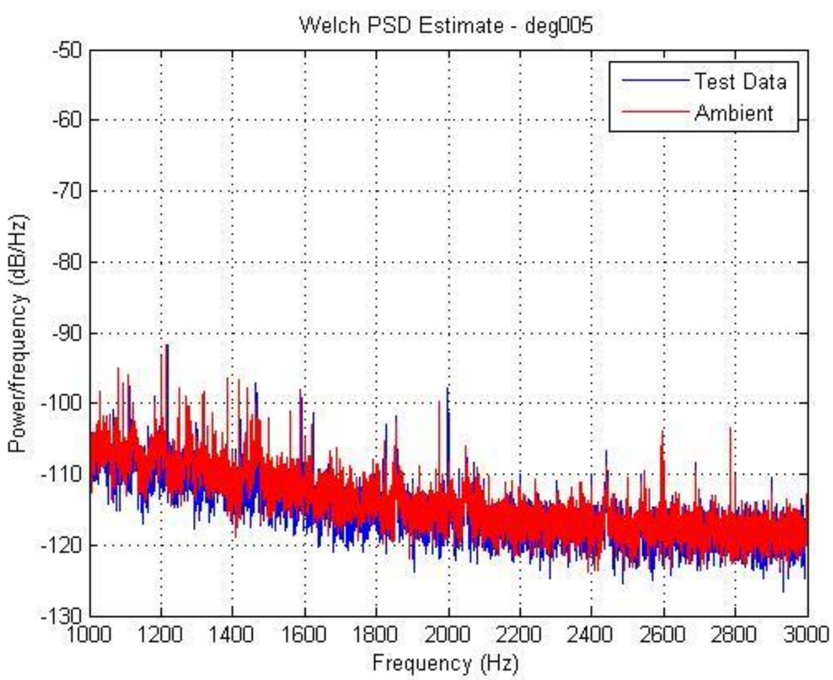

Figure B.45. Wireless Microphone System: PSD Estimate with 254 MHz Carrier Frequency, 2 kHz Message, and 5° Turntable Position for Minimum Coupling.

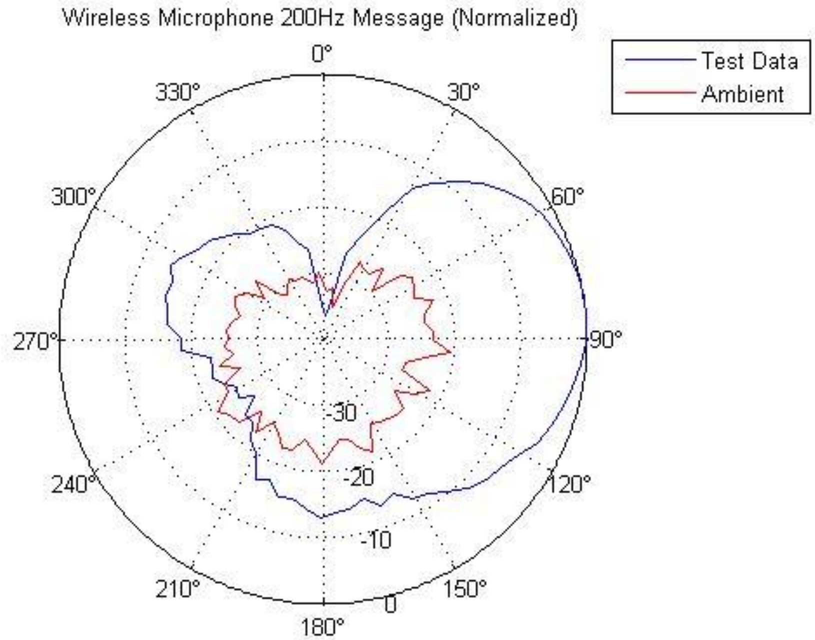

Figure B.46. Wireless Microphone System: PSD Estimate Comparison Polar Plot for Message Frequency 200 Hz.

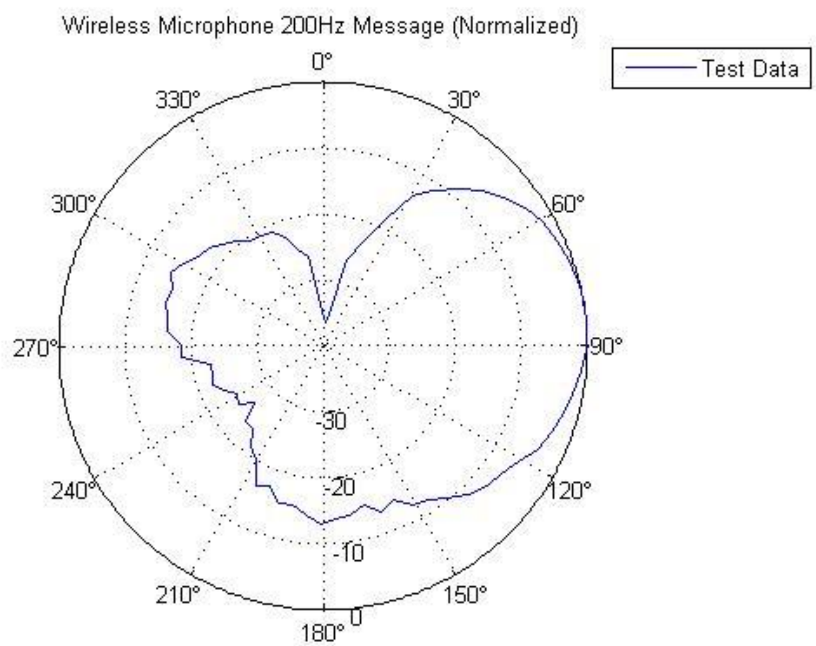

Figure B.47. Wireless Microphone System: PSD Estimate Single Polar Plot for Message Frequency 200 Hz.

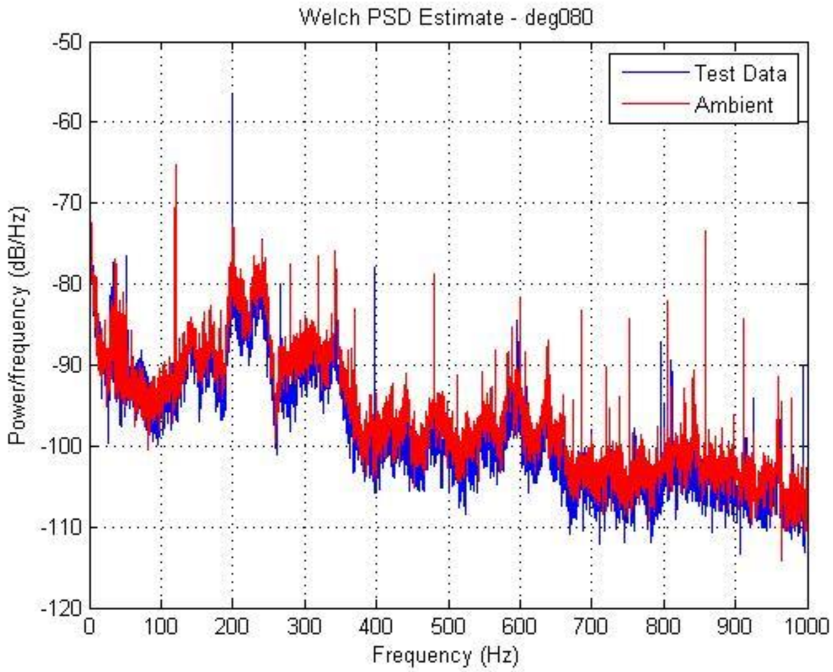

Figure B.48. Wireless Microphone System: PSD Estimate with 254 MHz Carrier Frequency, 200 Hz Message, and 80° Turntable Position for Maximum Coupling.

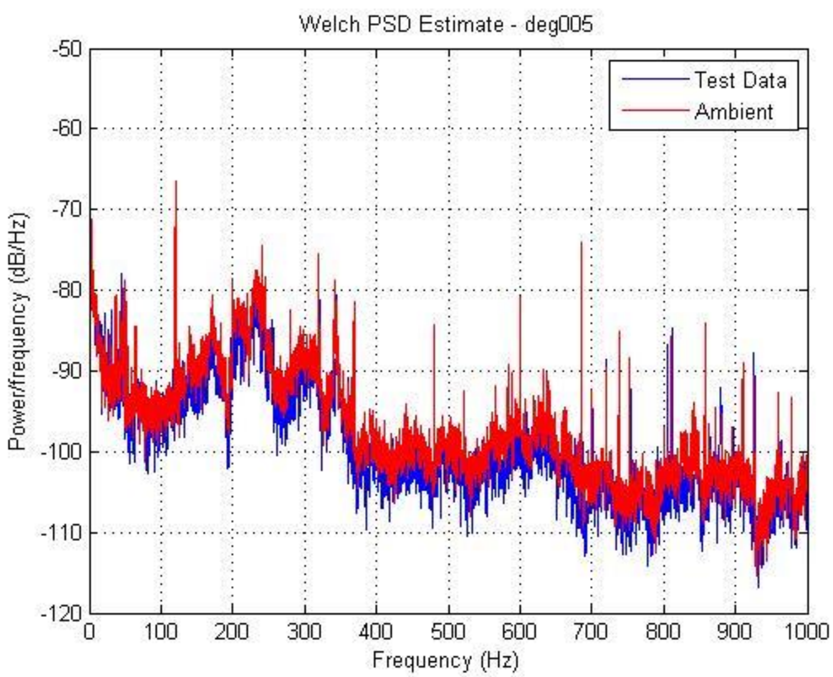

Figure B.49. Wireless Microphone System: PSD Estimate with 254 MHz Carrier Frequency, 200 Hz Message, and 5° Turntable Position for Minimum Coupling.

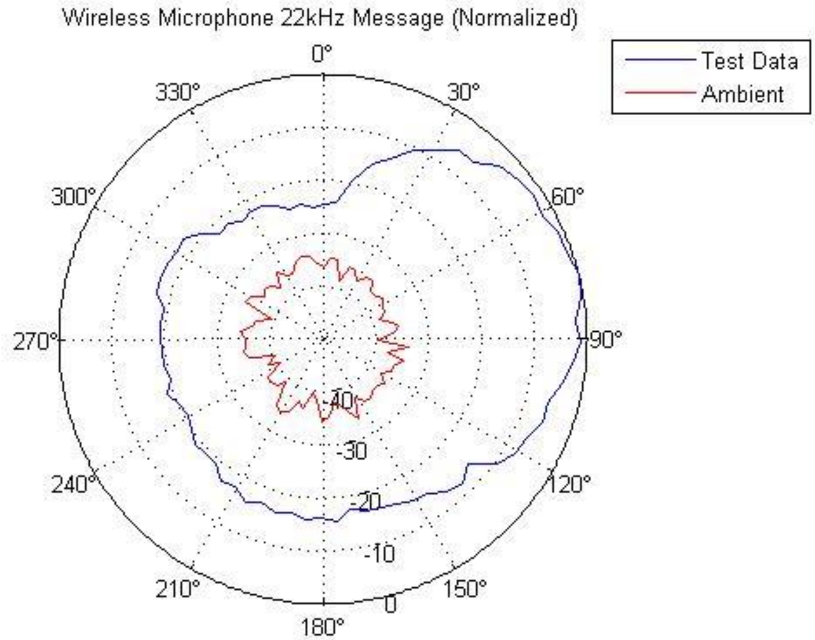

Figure B.50. Wireless Microphone System: PSD Estimate Comparison Polar Plot for Message Frequency 22 kHz.

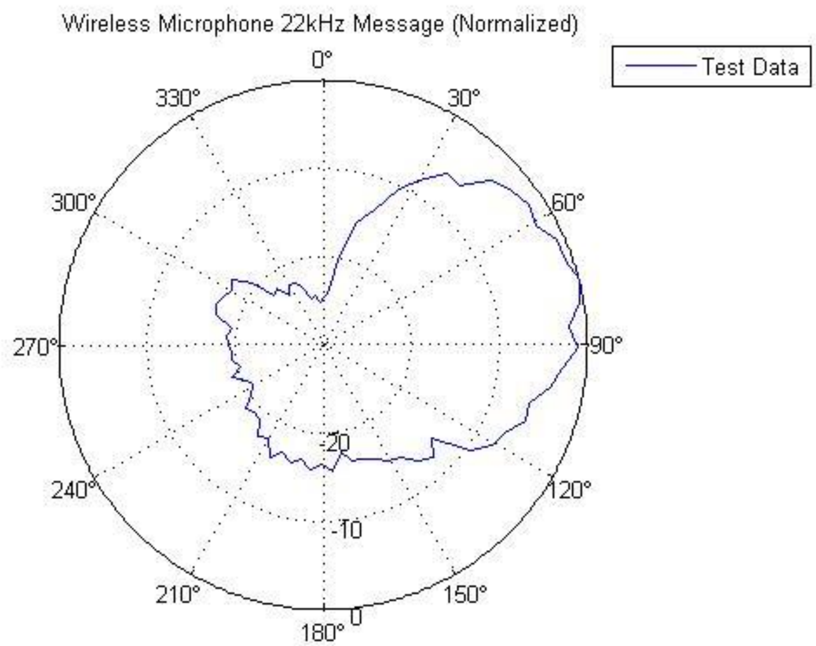

Figure B.51. Wireless Microphone System: PSD Estimate Single Polar Plot for Message Frequency 22 kHz.

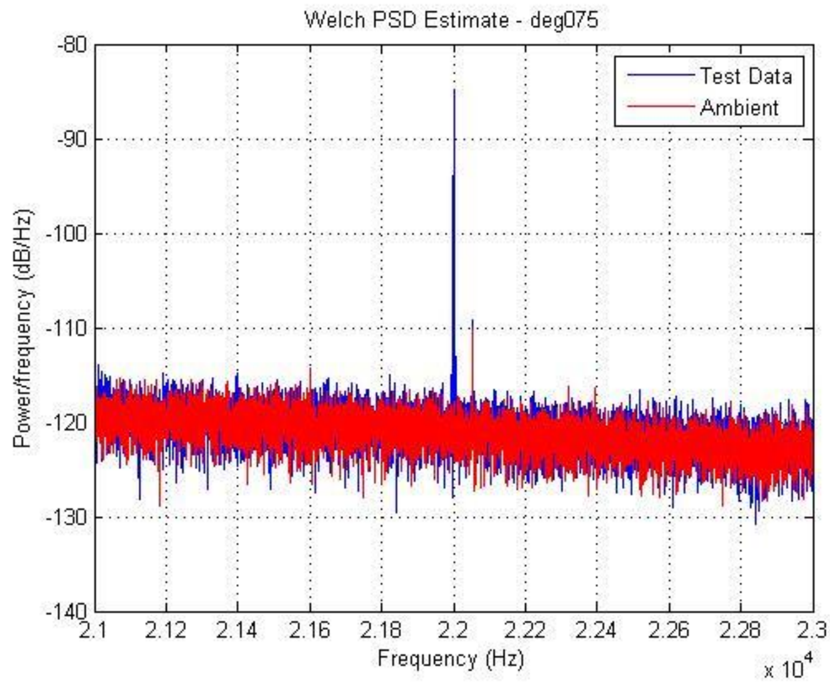

Figure B.52. Wireless Microphone System: PSD Estimate with 254 MHz Carrier Frequency, 22 kHz Message, and 75° Turntable Position for Maximum Coupling.

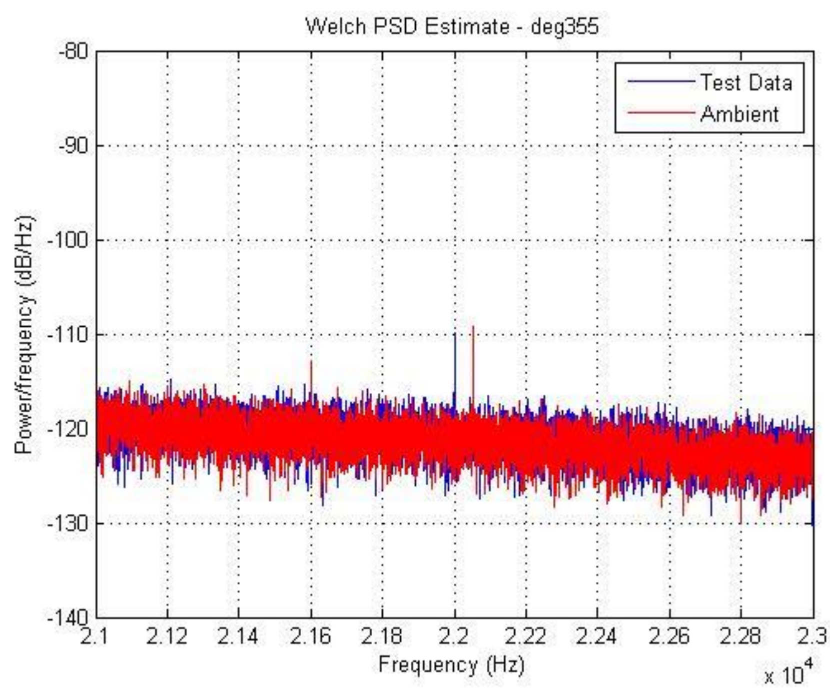

Figure B.53. Wireless Microphone System: PSD Estimate with 254 MHz Carrier Frequency, 22 kHz Message, and 355° Turntable Position for Minimum Coupling.

APPENDIX C: ALTERNATE SNR DEFINITION

The variable d will be defined as the noise, and the variable m represented by (23) will be defined as the signal. The SNR can then be defined as shown in (36) [C1].

$$SNR \triangleq \frac{E\left(m^2\right)}{E(d^2)} \tag{36}$$

The variances shown in (36) are given in (37) and (38) below [C1], [C2].

$$\begin{aligned}
E(m^2) &= E\left[\left\{\tfrac{1}{A}\textstyle\sum_{i=1}^{A} X_i^2 + \tfrac{1}{A}\sum_{i=1}^{A} N_i X_i\right\}^2\right] \\
E(m^2) &= \tfrac{1}{A^2} E[\{\textstyle\sum_{i=1}^{A} X_i^2 + \sum_{i=1}^{A} N_i X_i\}^2] \\
E(m^2) &= \tfrac{1}{A^2} E[\{X_1^2 + X_2^2 + \cdots + X_A^2 + N_1X_1 + N_2X_2 + \cdots + N_AX_A\}^2] \\
E(m^2) &= \tfrac{1}{A^2}\{A(3\sigma_X^4) + (A^2 - A)\sigma_X^4 + E[\textstyle\sum_{i=1}^{A} N_i^2 X_i^2]\} \\
E(m^2) &= \tfrac{1}{A^2}\{A(3\sigma_X^4) + (A^2 - A)\sigma_X^4 + A\sigma_N^2\sigma_X^2\} \\
E(m^2) &= \tfrac{1}{A}\{(3\sigma_X^4) + (A - 1)\sigma_X^4 + \sigma_N^2\sigma_X^2\} \\
E(m^2) &= \tfrac{1}{A}\{(2 + A)\sigma_X^4 + \sigma_N^2\sigma_X^2\}
\end{aligned} \tag{37}$$

$$\begin{aligned}
E(d^2) &= E\left[\left\{\tfrac{1}{A}\textstyle\sum_{z=1+|\Delta|}^{A} X_z X_{z-|\Delta|} + \tfrac{1}{A}\sum_{z=1+|\Delta|}^{A} N_{z-|\Delta|}X_{z-|\Delta|} + \tfrac{1}{A}\sum_{z=A+1}^{A+|\Delta|} N_z X_z\right\}^2\right] \\
E(d^2) &= \tfrac{1}{A^2} E\left[\left\{\textstyle\sum_{z=1+|\Delta|}^{A} X_z X_{z-|\Delta|} + \sum_{z=1+|\Delta|}^{A} N_{z-|\Delta|}X_{z-|\Delta|} + \sum_{z=A+1}^{A+|\Delta|} N_z X_z\right\}^2\right] \\
E(d^2) &= \tfrac{1}{A^2} E\left[\left\{\begin{matrix} X_{1+|\Delta|}X_1 + X_{2+|\Delta|}X_2 + \cdots + X_A X_{A-|\Delta|} \\ +N_1X_1 + N_2X_2 + \cdots + N_{A-|\Delta|}X_{A-|\Delta|} \\ +N_{A+1}X_{A+1} + N_{A+2}X_{A+2} + N_{A+|\Delta|}X_{A+|\Delta|} \end{matrix}\right\}^2\right] \\
E(d^2) &= \tfrac{1}{A^2}[(A - |\Delta|)\sigma_X^4 + (A - |\Delta|)\sigma_N^2\sigma_X^2 + |\Delta|\sigma_N^2\sigma_X^2] \\
E(d^2) &= \tfrac{1}{A^2}[(A - |\Delta|)\sigma_X^4 + A\sigma_N^2\sigma_X^2] \\
E(d^2) &= \tfrac{1}{A}\left[\sigma_X^4 - \tfrac{1}{A}|\Delta|\sigma_X^4 + \sigma_N^2\sigma_X^2\right] \\
E(d^2) &= \tfrac{1}{A}\left[\sigma_X^4 - \tfrac{1}{A}|\Delta|\sigma_X^4 + \sigma_N^2\sigma_X^2\right], \quad 1 \le |\Delta| \le A - 1, \quad A \ge 2
\end{aligned} \tag{38}$$

From (37) and (38), the SNR as defined by (36) can be solved as shown in (39).

$$\begin{aligned}
SNR &= \frac{E\left(m^2\right)}{E(d^2)} \\
SNR &= \frac{\frac{1}{A}\left\{(2+A)\sigma_X^4 + \sigma_N^2\sigma_X^2\right\}}{\frac{1}{A}\left(\sigma_X^4 - \frac{1}{A}|\Delta|\sigma_X^4 + \sigma_N^2\sigma_X^2\right)} \\
SNR &= \frac{(2+A)\sigma_X^4 + \sigma_N^2\sigma_X^2}{\sigma_X^4 - \frac{1}{A}|\Delta|\sigma_X^4 + \sigma_N^2\sigma_X^2}, \quad 1 \le |\Delta| \le A - 1, \quad A \ge 2
\end{aligned} \tag{39}$$

Equation 39 shows the relation that as the signal length becomes larger, the SNR increases. To validate the expression given in (39), a simulation was performed where the standard deviation of X was equal to three, and the standard deviation of N was equal to two. The signal length (A) was varied from 10 to 200 samples. Vectors for the random variables m and d, represented by (23) and (30), were computed for each signal length. The vectors for m and d were 10000 samples long for each signal length (A). The total simulated recording length (B) was 2000 samples long. The signal to noise ratio as given by (36), was calculated from the variance of the m and d vectors. The sample offset (Δ) was set equal to 1. The result from this simulation is shown below in Figure C.1.

To optimize the SNR as defined by (39), a message signal should be as long as possible. Although optimizing the SNR is important for message detection, it is not the only factor to consider. Optimizing the SNR in this manner will decrease the message detection error also if a threshold detector is used with few cross-correlation data sets [C1]. Figure C.2 below shows the cross-correlation for two variables that are independent from each other.

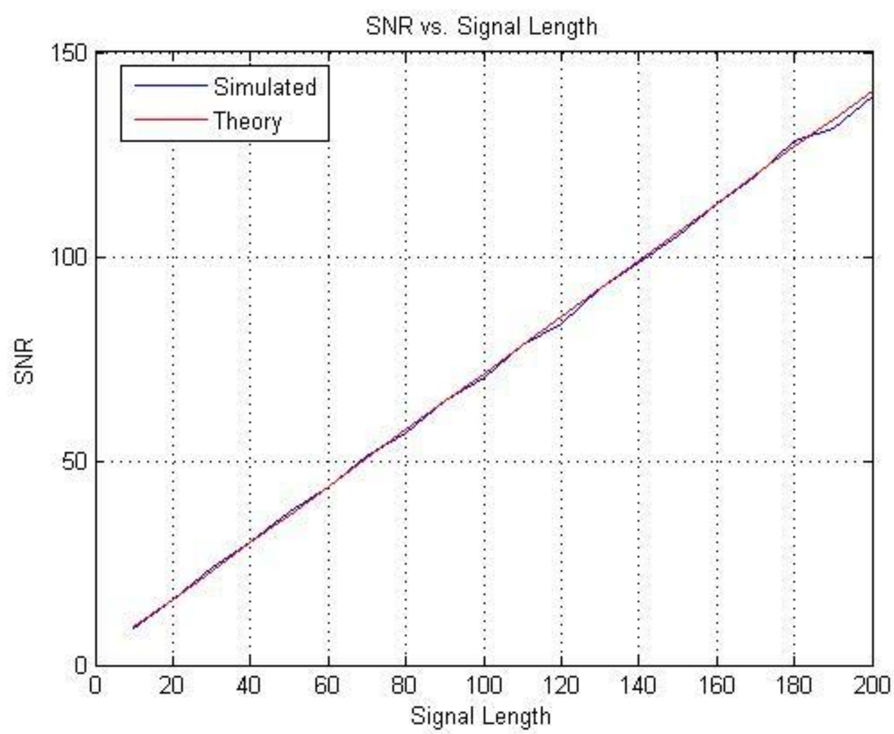

Figure C.1. Validation of SNR Equation (40) (A = 10 to 200).

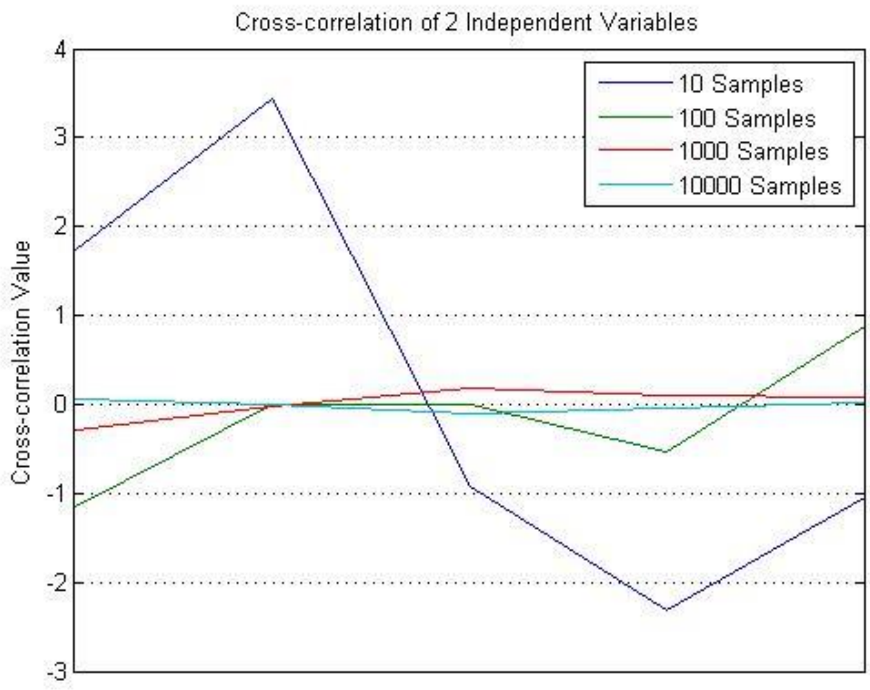

Figure C.2. Cross-correlation of Two Independent Variables.

Figure C.2 shows how the cross-correlation improves as a function of the number of samples for a given message signal. Ideally the cross-correlation between two independent variables should be equal to zero. As the number of samples increase for the two signals, the cross-correlation approaches this value. For the tested data, where both signals were 10 samples long, it is likely that this resulting cross-correlation would have triggered a false alarm for message detection with a threshold detector applied to the cross-correlation. Thus, optimizing signal detection involves using message signals that are as long as possible to maximize SNR and minimize message detection error.

APPENDIX C REFERENCES

[C1] A. Leon-Garcia, *Probability, Statistics, and Random Processes for Electrical Engineering*, 3rd ed. Upper Saddle River, NJ: Pearson Prentice Hall, 2008, pp. 109-110, 283, 369-373, 416-419, 442, 496-497.

[C2] J. G. Proakis, *Digital Communications*, 2nd ed. New York: McGraw-Hill, 1989, pp. 55.

DISTRIBUTION

1 Daryl Beetner
4000 Enterprise Dr.
Rolla, Mo 65401

1 Steve Grant
228 Emerson Electric Co. Hall
301 West 16th Street
Rolla, Mo 65409

1	MS0402	Matthew Halligan	5762
1	MS0899	Technical Library	9536 (electronic copy)

Sandia National Laboratories